XENON DIFLUORIDE ETCHING AND MOLECULAR OXYGEN OXIDATION OF SILICON BY REACTIVE SCATTERING

by

DANIEL WALTER ROWLANDS

B.S. CHEMISTRY
CALIFORNIA INSTITUTE OF TECHNOLOGY, 2009

SUBMITTED TO THE DEPARTMENT OF CHEMISTRY
IN PARTIAL FULMILLMENT OF THE REQUIREMENTS

FOR THE DEGREE OF
MASTER OF SCIENCE IN CHEMISTRY

at the

MASSACHUSETTS INSTITUTE OF TECHNOLOGY

SEPTEMBER 2015

Signature of Author: ______________ Signature redacted
Department of Chemistry
28 August 2015

Certified by: ______________________ Signature redacted
Sylvia T. Ceyer
John C. Sheehan Professor of Chemistry
Thesis Supervisor

Accepted by: ______________________ Signature redacted
Robert W. Field
Robert T. Haslam and Bradley Dewey Professor of Chemistry
Chairman, Departmental Committee on Graduate Students

Xenon Difluoride Etching and Molecular Oxygen Oxidation of Silicon by Reactive Scattering

by Daniel Walter Rowlands

Submitted to the Department of Chemistry on 28 August 2015
in Partial Fulfillment of the Requirements for the Degree of
Master of Science in Chemistry

Abstract

While both molecular fluorine (F_2) and xenon difluoride (XeF_2) fluorinate Si(100)2x1 surfaces at coverages up to one monolayer, fluorine is unable to cleave Si-Si bonds that ultimately leads to etching silicon at coverages above one monolayer (reaction probability 9×10^{-4}) while XeF_2 does so readily (reaction probability 0.6). Previous studies have demonstrated that both fluorine and xenon difluoride react with silicon via atom-abstraction mechanisms at low coverages, and that the XeF radicals produced by atom abstraction from xenon difluoride dissociate in the gas phase, producing a source of F radicals that may contribute to Si-Si bond cleavage by formation of multiple F-Si bonds. In addition, it has been shown that van der Waals clusters of F_2 with a Xe atom and with a Kr atom have reaction probabilities with silicon at one monolayer of fluorine coverage of roughly 0.9 and 0.04, respectively, suggesting that the effect of mass of the incident gas molecules is important in activating the cleavage of silicon-silicon bonds through a multiple collision process.

A model based on a classical harmonic oscillator linked via a variable damping term to the thermal energy of the lattice is proposed to test the importance of the mass of the gas molecules to energy transfer and the duration of the vibrational excitation of the silicon-silicon lattice bonds. Computer simulations using this model suggest that the mass of the gas molecule does not affect the overall energy transferred to the silicon. However, the heavy mass and the resulting multiple collisions do extend the duration of the silicon excitation and the duration during which the gas molecule is in contact with the vibrationally excited silicon lattice.

The techniques that have been used to study the reactivity of fluorine compounds with silicon are potentially of use to the study of another problem: why triplet molecular oxygen (O_2) is able to dissociatively chemisorb across singlet silicon-silicon dimer bonds to form the singlet Si-O product. Several mechanisms, including atom abstraction and non-adiabatic ladder climbing of $(O_2)_2$ van der Waals dimers are suggested to explain this reaction and a series of experiments to test the hypothesized mechanisms are proposed.

In addition, a detailed account of the ultra-high-vacuum molecular beam surface scattering apparatus used for these studies is provided, including a detailed description of its operation and maintenance procedures.

Thesis Supervisor: Sylvia T. Ceyer
Title: J.C. Sheehan Professor of Chemistry and Head, Department of Chemistry

Παλλάδ' Ἀθηναίην ἐρυσίπτολιν ἄρχομ' ἀείδειν,
δεινήν, ᾗ σὺν Ἄρηι μέλει πολεμήια ἔργα
περθόμεναί τε πόληες ἀϋτή τε πτόλεμοί τε,
καί τ' ἐρρύσατο λαὸν ἰόντα τε νισσόμενόν τε.

Χαῖρε, θεά, δὸς δ' ἄμμι τύχην εὐδαιμονίην τε.

-- 11th Homeric Hymn, "To Athena"

Acknowledgements

It is hard to believe that my time at MIT is finally coming to an end. When I first arrived here, I thought that the Green Line extension to Somerville would open before I graduated. Problems with the Big Machine delayed my thesis much more than I expected in those naive days as a first-year, but not as much as the MBTA's construction was delayed. I suppose I'll have to come back to ride it when it eventually opens. Though, with all the friends I've made in Boston, I expect that I'll be back a number of times before then.

My first thanks need to go to Professor Sylvia Ceyer: without Sylvia's guidance and encouragement, I would have given up years ago. She is a wonderful chemist but—perhaps more importantly for this project—she is a wonderful engineer. She's the only chemist I've ever met who keeps a drafting table in her office, and she never minds getting her hands dirty examining failed parts even when she's busy with administrative work. Furthermore, she has an amazing ability to be inspiring and encouraging, even when the Machine is misbehaving and it seems like data is nothing but a distant dream.

Along with Sylvia, my teachers on the Big Machine were Mike Blair and Dr. Jae-Gook Lee. I only shared the Machine with Jae-Gook for a few months, but he helped me get an initial footing in surface science and work with ultra-high vacuum equipment. I worked with Mike for longer, and he played a major role in shaping my understanding of the Machine and of silicon surfaces. He was always a source of interesting and different perspectives.

Equally essential to my success were the help of Dr. Gang Liu in the Chemistry Electronics Shop, Dennis Nagle in the Chemistry Student Machine Shop, and Andy Gallant and Scott Spence in the MIT Central Machine Shop. Gang was a wizard at repairing the many bizarre electronics problems we came to him with, and Dennis always had helpful advice for fixing mechanical problems, as well as a lot of interesting stories from his past working as a technician for the Navy. Without Andy and Scott's willingness to attempt—and achieve—the impossible for us, we would have been lost, especially when the lower weld in the lid cryostat flange opened up. I still find it a bit hard to believe that they were able to get a replacement flange installed without damaging the alignment and without having to remove the whole lid.

Although I only worked with him for a couple of weeks, I really appreciate Dr. Alexandros Anastasopoulos's willingness to learn to take over the Big Machine just as I was leaving. Although I know it is a daunting job, I'm impressed by how much progress he has already made and I wish him all the best with it.

I didn't work directly with the Little Machine people—Dr. Christopher Leon, Beth Hocking, and Qing Liu—but they were wonderful co-workers. Chris, in particular, was a great source of advice and an inspiration to work with. I wish I had half his drive, confidence, and scientific knowledge. Beth played a big role in keeping me sane when the Machine was doing its best to drive me out of my mind. It was wonderful having another Medievalist in the lab: I hope our expositions on Christological heresies, the Medieval Church, and English history didn't confuse everyone else too much. It amuses me to realize that one of my longest-lasting contributions to

MIT may well be the new Chemistry Department logo that we designed together one night at dinner at Cinderella's.

It is traditional for grad students to joke about research being their life and lab being their identity—when worrying about how to dress for the Gordon Conference two years ago, we considered asking Sylvia if there was lab livery she'd like us to wear—but I have done a pretty good job of having a life at MIT that extended beyond the Ceyer Lab and the Chemistry Department.

In my first year here, the MIT Science Fiction Society gave me a ready-formed social group, as well as a chance to procrastinate on my fights with the Big Machine by fighting with the army of books that was trying to devour us all. I really enjoyed my time as a Keyholder and my five years on the Star Chamber. Paul Weaver, Kendra Beckler, Lee Fuchs, Bram Sterling, Susan Shepherd, Margaret Gentile, Naomi Hinchen, and Miss Katie Ray were particularly important in helping me get settled in at MIT, and I appreciate their help in introducing me to experiences and opportunities I otherwise wouldn't have had as an MIT grad student. More recently, I really enjoyed working with Karl Ramm, Cathy Zhang, Ben Kaduk, Bill Starr, Laura McKnight, and Alex Westbrook in running and reorganizing the library. I'm particularly proud of my and Cathy's work at rearranging and rationalizing the whole collection during the two parts of the Great Merge. And I have great confidence in my successor as Skinner, Cathleen Nalezyty: she has the combination of enthusiasm, knowledge of the library, and skepticism about traditions she'll need to keep the books at bay.

My other major student group commitment at MIT was my time on the executive board of the Association of Student Activities. I only spent two years on the ASA—one as student member at large and one as the ASA Treasurer—but they were an important part of my time here, and played a big role in my transition from feeling like an outsider to believing that I was a part of MIT. Kendra recruited me for the ASA and was my predecessor and mentor as treasurer, but the incomparable Rachel Meyer, who was ASA President during my first year on the Board, was a huge influence as well, and it was an honor to serve under her. In addition, I'd like to thank Emily Moberg and Cory Hernandez for their efforts to keep the ASA running after I left, and Jenny (Jiwon) Kim for stepping up to take over as ASA Treasurer at the start of her sophomore year when my handpicked successor flaked out.

Although it wasn't an official student group, starting a branch of the Caltech Polish Food Club here in the North-East Frontier Province is something I'm quite proud of as well. I really appreciated all the people who helped cook and taught me new recipes, especially Cathy Douglass, Veronica Hanus, Fangfei Shen, Tegan Sutherland, Kelly Alioth Drinkwater, Laura McKnight and Lilly Chin. That Polish cooking allowed me to be on a winning MIT Mystery Hunt team and participate in the runaround as a cook for "One Fish Two Fish Random Fish Blue Fish" in 2014 and again for the writing team in 2015 was a wonderful bonus: my thanks to all the skilled puzzle-solvers who made that happen.

Cathy and Veronica weren't my only supportive Caltech friends in Cambridge: Andrew Lai and Andy Dubin were incredibly important to my time here as well. Andrew has been very helpful in encouraging me to persevere through bad situations in lab, just like he helped me persevere through Ph 125—graduate quantum mechanics—as an undergrad at Caltech. Andy was a great support in personal struggles as well as being my comrade in student government and chair of the GSC Housing and Community Affairs Committee—the "Committee on Depressing Things"—when I served on it.

Some of my biggest sources of emotional support—and my biggest sources of social interaction—while in grad school were actually long-distance friends. Three in particular stick out in this respect: Sir Grace Chen, Deepthi Gopal, and Shulin Ye. Sir Grace was my closest friend in high school and I've really appreciated her efforts to stay in touch even as our lives have diverged in many ways. Deepthi, my closest friend from Caltech, has become an older brother figure to me and has been incredibly supportive when I've felt lost and broken, as well as a wonderful source of advice, even though we haven't lived on the same continent for most of my time here. And while we only met less than two years ago, Shulin has come to be one of my most frequent correspondents and a trusted confidant.

Jamie Jackson, Alex Malz, and Glenn Wagner from Caltech have been great friends as well, even if we haven't managed to stay in touch as regularly, and I really appreciated Glenn's invitations to stay with his family for the Fourth of July and Thanksgiving so I wouldn't spent the holidays in lab. His parents are wonderful people, and it was very amusing to discover that his dad, Dr. Fred Wagner, was Professor Ceyer's labmate at Berkeley. Annelise Beck—whom I met on a prospective grad student visiting weekend at the University of Chicago and then traded coasts with (she was an undergrad at MIT)—has been a great correspondent as well as we've completed our physical chemistry studies on opposite sides of the country.

Finally, I'd like to thank the people without whose help I would never have made it to MIT. My parents have been incredibly supportive throughout my education, from helping me with homework and putting up with me checking fifty books out of the library at a time when I was in elementary school right up to inviting me over for dinner a lot when writing this thesis was making me too busy to cook.

Among my former teachers, Professor Mitchio Okumura, my academic advisor as an undergraduate at Caltech, has been a continuing important influence on my life as a chemist. I really appreciate his willingness to provide advice and support to a former student who graduate half a decade ago, as well as his continuing confidence in me. Going back even further, Jane Hemelt, Rocco Mennella, and Michael Samordic at Eleanor Roosevelt High School have continued to support me throughout my time at Caltech and MIT.

Table of Contents

List of Tables and Figures

Chapter I

Chapter II

Chapter III

Chapter IV

Chapter I: The Etching of Silicon by Fluorine Compounds

Modern technology depends heavily on silicon components, and the ability to control silicon surface chemistry is essential to the manufacture of a variety of devices. One industrially important procedure involving silicon surface chemistry is surface etching of silicon, required for microchip manufacture. For some systems, such as those where mechanical components are integrated with electronics—known as microelectromechanical systems (MEMS)—it is preferable to use dry, vapor-phase etchants, which are less damaging to other structures present on a chip than the immersion, stirring, and heating required for the use of wet etchants, to remove sacrificial layers during the production of these components. Neutral, non-plasma etchants are preferred as well, since plasma etchants pose a risk of inadvertently doping the semiconductor with ions. XeF_2 is a particularly useful vapor-phase etchant for these systems, since it selectively reacts with silicon and is unreactive with SiO_2, allowing the latter to be used to bound the area to be etched.[1]

The details of *how* XeF_2 reacts with silicon, however, are somewhat more obscure. In particular, why does XeF_2 rapidly etch silicon while the same reaction with F_2—which should be 22 kcal/mol more energetic—has a 10^3 to 10^4 times lower reaction probability? Despite this difference in etching reactivity, however, XeF_2 and F_2 show very similar reactivity when fluorinating a clean silicon surface. It is only after the surface is fully fluorinated that divergent behavior is observed.[2,3,4,5,6]

Over the last twenty years, the Ceyer lab has studied the mechanism by which this etching occurs using the ultra-high vacuum molecular beam scattering apparatus discussed in Chapter IV of this thesis. These experiments have shown that F_2 reacts with dangling bonds on a clean silicon surface by atom abstraction.[7,8,9] Unlike classical dissociative chemisorption, in which the bond in a diatomic molecule is broken and both atoms form bonds to the surface, atom abstraction involves breaking one bond in a molecule with one of the atoms forming a bond with the surface while the complementary fragment is scattered into the gas phase. At fluorine coverages of less than one monolayer, the reaction of a single F atom with a Si dangling bond provides the needed energy to break a F-F or F-Xe bond, allowing the remaining F or XeF radical to scatter. Helium diffraction shows that the surface retains its 2×1 unit cell, with buckled surface Si-Si dimers, after a monolayer of fluorine has been added, indicating that fluorine only reacts with the dangling bonds and that the lattice is not disordered by the reaction exothermicity.[8,10] Further reaction with a fully fluorinated surface can be induced by translational excitation of the F_2 molecules to above 3.8 kcal/mol. However, even above this barrier, the reaction probability of F_2 with silicon grows linearly and only reaches 3.6×10^{-3} at 13 kcal/mol, indicating a late transition barrier as the limiting factor to reactivity.[11]

Additional experiments demonstrated that XeF_2 also reacts with a clean silicon surface via atom abstraction and reacts solely with dangling bonds at a fluorine coverage of less than one monolayer, and only begins to react with lattice Si-Si bonds once all dangling bonds are occupied.[10] Furthermore, the XeF radical released by abstraction of a fluorine atom from XeF_2 can dissociate due to reaction exothermicity from the abstraction being channeled to the vibrational mode of the XeF product, supplying a F radical that can itself react with a silicon dangling bond.[12,13,14]

Most recently, research has focused on the problem of why XeF_2 etches silicon so much more effectively than F_2. The use of van der Waals clusters of noble gas atoms with F_2—$Xe(F_2)$ and $Kr(F_2)$—has allowed mass effects to be disentangled from other chemical differences between F_2 and XeF_2. These clusters have essentially the same chemistry as F_2, since they consist of molecular fluorine bound to a noble gas by a weak van der Waals interaction, but their masses are either equivalent to that of XeF_2 (167 amu) or heavier than that of F_2 (38 amu). This mass difference has proven to be significant, with both dimers showing significantly greater reactivity with a silicon surface than F_2,[15,16] suggesting a role for collisional energy transfer seen in the etching of silicon by XeF_2 and in other reactions, such as the "chemistry with a hammer" dissociative chemisorption of methane on nickel.[17,18]

I.1 Overview of F_2 and XeF_2 Reactivity with Silicon

I.1.a The Si(100)2x1 Surface

To understand the reactivity of gas molecules on silicon surfaces, we must begin by understanding the structure of the surface itself. Silicon has a diamond-like tetrahedral crystal structure; when it is cut across the 100 crystallographic surface, each atom in the exposed top layer is left with two radical sites pointing into space where bonds were broken. This surface, with two radical sites per surface atom, is unstable and reconstructs to reduce the number of dangling bonds, and thus its surface free energy. In the resulting 2x1 reconstruction, neighboring Si atoms pair up into dimers, lowering the overall lattice energy at the expense of slightly distorting the tetrahedral structure of the top several bulk layers.[19]

One of the two dangling bonds on each Si atom is eliminated by the formation of the Si-Si dimer σ bond. The other dangling bond engages in a very weak π-bonding interaction with the other Si atom in the dimer. Because of the weakness of this interaction, the reactivity of this dangling bond has been calculated to be similar to that of a free-radical electron.[20] The presence of these free-radical sites means that the Si(100)2x1 surface is very reactive up to the addition of one monolayer of F atoms. However, once a coverage of one monolayer has been reached, the surface is passivated, since any further addition of F atoms will require the breaking of Si-Si bonds.

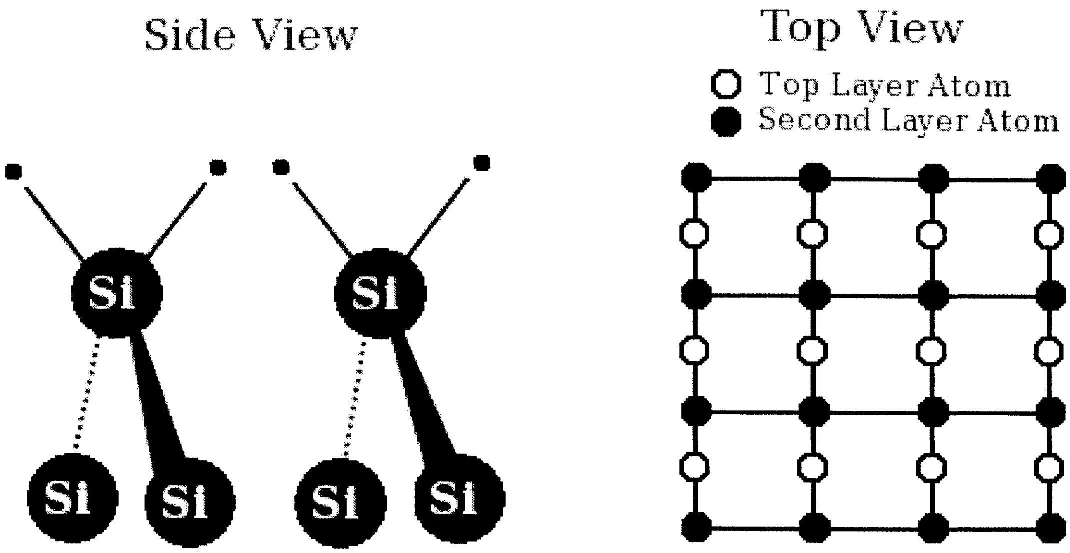

Figure I-1: The Unreconstructed Si(100) Surface

When a silicon crystal is cut across the 100 crystallographic surface, the top layer of exposed atoms has two radical sites per atom pointing into space where bonds were broken.

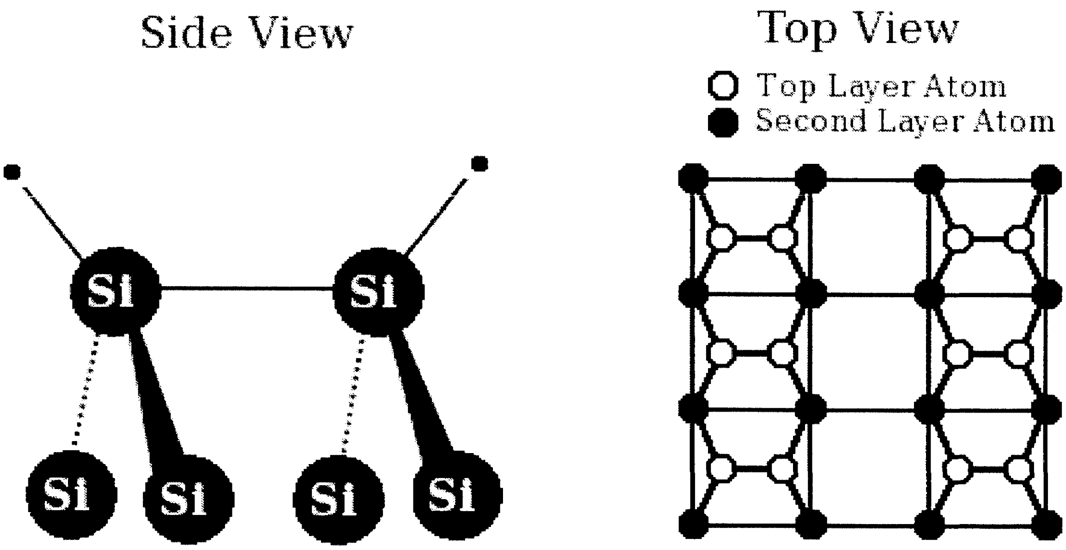

Figure I-2: Surface Dimers in the Reconstructed Si(100)2x1 Surface

When annealed, the Si(100) surface returns to a 2x1 reconstruction consisting of a surface layer of Si-Si dimers. Each Si atom in the top layer is bound to its dimer partner and two Si atoms in the next layer down. The remaining dangling bonds on the two Si atoms in the dimer form a very weak π bond but are highly reactive and can effectively regarded as radical sites.

I.1.b Observations of the Reactivity of F_2 and XeF_2

At coverages below one monolayer, both F_2 and XeF_2 react readily with Si(100)2x1 surfaces. The reaction probabilities for both gases are between 0.5 and 1, consistent with the high reactivity of the dangling bonds on the Si surface below one monolayer. Helium diffraction data confirm that both F_2 and XeF_2 react exclusively with dangling bonds at low coverages. As seen in Figure 1-3, exposure to either gas reduces the surface order until a coverage of roughly half a monolayer is reached. At this point, surface order increases until the original order is achieved. This result suggests that random dangling bonds on the surface are being fluorinated, decreasing the surface order until a minimum is reached when every dangling bond site has a fifty-percent chance of having a fluorine atom bound to it. The surface order is restored as additional fluorine atoms are added until every surface Si atom has a F atom bound to it. Furthermore, the half-order diffraction peak follows the same pattern as the specular peak, indicating that the dimer bonds and 2x1 structure of the surface remain present after the addition of a monolayer of F atoms. This restoration of surface order is possible because the F atoms have only reacted with the dangling bonds and have not broken Si-Si bonds.[7,10]

Above one monolayer, however, the reactivities of F_2 and XeF_2 diverge. Further exposure of the surface to low-energy F_2 molecules does not result in fluorination of the surface above one monolayer. At translational energies above 3.8 kcal/mol, the reaction probability rises linearly up to 3.6×10^{-3} at a translational energy of 13 kcal/mol. It appears that high-energy F_2 molecules react indiscriminately with both Si-Si dimer bonds and Si-Si lattice bonds. The changes in the specular, first-order, and second-order He diffraction features due to reaction with high-energy F_2 molecules at coverages above one monolayer have been found to be similar to the changes produced by sputtering the surface with 2 kV Ar^+ ions, which have a much higher energy than the Si-Si bonds and so should cleave all Si-Si bounds indiscriminately.[11]

While a barrier of 3.8 kcal/mol exists for the reaction of F_2 beyond one monolayer, no such barrier exists for the reaction of XeF_2. At a kinetic energy of 1.46 kcal/mol—less than half the energy needed to make F_2 react above one monolayer—the XeF_2 reaction probability is about 0.6 and only weakly dependent on coverage above one monolayer. Instead of ceasing to react when all dangling bonds are occupied, XeF_2 cleaves Si-Si dimer and lattice bonds, producing SiF_2 and SiF_4 etch products.[10]

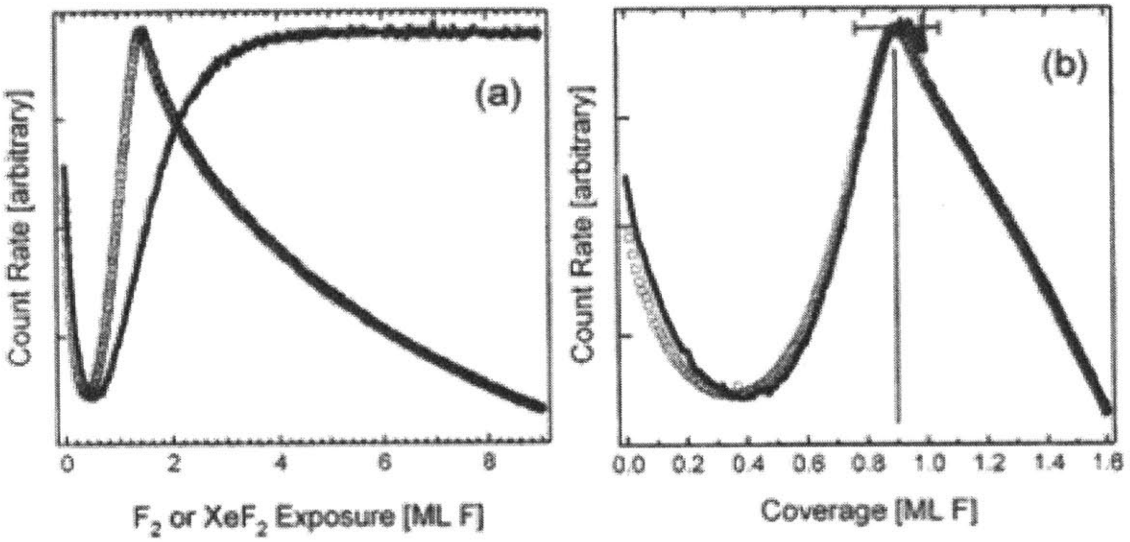

Figure I-3: He Diffraction Measurements of Surface Order During F_2 and XeF_2 Exposure

The effect of reaction with F_2 and XeF_2 on the order of an Si(100)2x1 surface can be measured by the intensity of the specular He diffraction peak. Exposure to F_2 is indicated by filled circles and exposure to XeF_2 is indicated by empty circles. In (a), the intensity is plotted against to exposure; in (b) it is plotted against the coverage. The line in (b) marks the coverage at which the scattered He signal is at its maximum. This figure is taken from Holt, Hefty, Tate, and Ceyer, 2002.[10]

I.1.c Thermodynamics of F_2 and XeF_2 Reactions with Silicon

While it is clear that XeF_2 is much more able to cleave Si-Si bonds than F_2, it is much less clear why this should be. The formation of a Si-F bond releases 151 kcal/mol of energy, while breaking a Si-Si bond requires 55 kcal/mol. Breaking the F-F bond in F_2 requires only 39 kcal/mol, while breaking a Xe-F bond in XeF_2 requires 61 kcal/mol, so F_2 should release 57 kcal/mol by reacting with a Si-Si bond while XeF_2 should release only 35 kcal/mol in the same reaction. Yet the reaction with XeF_2 has a reaction probability near unity at low kinetic energies, while the reaction with F_2 requires significant translational activation to achieve a reaction probability several orders of magnitude lower.[7,8,10,20] Why?

One traditional explanation for the etching of Si by XeF_2 is that the exothermicity of XeF_2's initial reactions with dangling bonds on the Si surface produces defects and disorder needed for the onset of Si-Si bond cleavage and etching.[21,22] However, this notion is questionable given that F_2's reaction with dangling bonds should be more exothermic than XeF_2's, and the experimental evidence that both F_2 and XeF_2 fully fluorinate the dangling bonds without damaging the surface order essentially puts this idea to rest.[10]

Another possible answer is that reactions with the Si-Si bonds are activated by vibrational excitations resulting from the collision of the gas molecules with the surface. A XeF_2 molecule is four times as massive as a F_2 molecule and at the same translational energy, it has half the velocity. Unlike collisions between two gas molecules, where the maximum kinetic energy transfer is usually achieved when the two molecules have the same mass, the collision of a gas molecule with a surface transfers the most energy when the gas molecule is much more massive than the unit of the surface with which it collides. Gas-surface collisions transfer the most energy when the gas molecule is much more massive than the surface unit because multiple collisions occur, as a result of the failure of the momentum of a heavier gas particle to be reversed upon the initial collision. Since a Si atom is roughly the same mass as a F_2 molecule and roughly a quarter the mass of a XeF_2 molecule, XeF_2 should transfer much more energy into the surface than F_2.[15]

I.2 F_2 Reactivity with the Si(100)2x1 Surface by Atom Abstraction

I.2.a Identifying Atom Abstraction via the TOF Distribution of Partner F Atoms

Closer study of the mechanism by which F_2 reacts with Si(100)2x1 surfaces has shown that the reaction proceeds by atom abstraction rather than classical dissociative chemisorption. In classical dissociative chemisorption, the bond between two atoms in a gas molecule on a surface is cleaved at the same time as bonds are formed between the atoms and sites on the surface in one four-centered reaction. The simultaneous breaking and formation of bonds allows both of the new bonds to contribute to the energy needed to cleave the bond between the atoms in the gas molecule. In atom abstraction, on the other hand, only one atom from the gas molecule binds to a surface site while the remainder of the molecule is scattered back into the gas phase. Because only one atom from the gas molecule binds to a surface site, atom abstraction reactions are only possible when the formation of a single bond to the surface will provide enough energy to cleave the gas molecule. The clean Si(100)2x1 surface is a good candidate for atom abstraction, since the dangling bonds act as free radical sites and the formation of a Si-F bond on one of them will release 151 kcal/mol.[8]

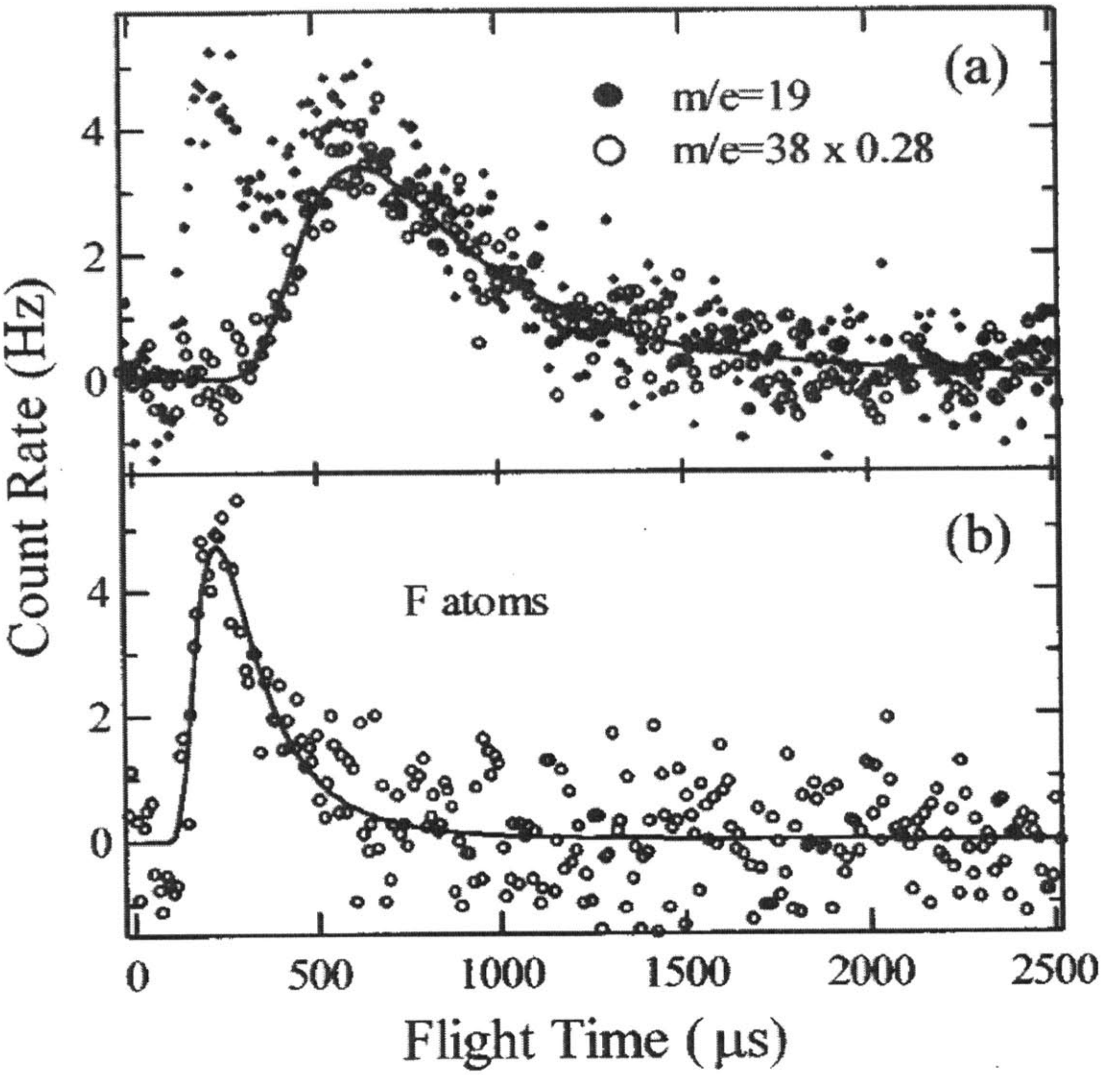

Figure I-4: Subtraction to Remove the Background from Ionizer Cracking of F_2

(a) TOF spectra at m/e = 38 multiplied by F_2 cracking ratio and at m/e = 19 measured with the molecular beam normal to the crystal, the detector 35° from normal, and the crystal at 250K. (b) Net scattered F atom TOF spectrum obtained by point-by-point subtraction of the m/e = 38 signal multiplied by the cracking ratio from the m/e = 19 signal. Solid lines show least-squares fit Maxwell-Boltzmann function for the number density. This figure is taken from Tate, Gosalvez-Blanco, Pullman, Tsekouras, Li, Yang, Laughlin, Eckman, Bertino, and Ceyer, 1999.[8]

Since atom abstraction differs from classical dissociative chemisorption in the release of part of the gas molecule back into the gas phase, the characteristic signal of atom abstraction from F_2 molecules is a population of F atoms scattered from the surface. In principle, these atoms should be detectable by mass spectrometry. However, the situation is complicated by the fact that F_2 molecules that do not react will also be scattered from the surface, and some of these molecules will crack in the mass spectrometer ionizer to produce a background of F atoms.

To demonstrate that atom abstraction is occurring, the background of F atoms produced by ionizer cracking must be removed to reveal the population of F atoms produced by atom abstraction. The removal of the cracking background is possible because some of the roughly 120 kcal/mol exothermicity of the atom abstraction reaction will be channeled into the F atoms, translationally heating them, while F atoms produced by ionizer cracking should have the same velocity distribution as the elastically scattered F_2 molecules they are produced from. These two populations can be separated by time-of-flight mass spectrometry, as shown in Figure 1-4. The cracking ratio—the fraction of F_2 molecules that will be broken into F atoms in the ionizer—can be measured to be 0.28 without interference from surface reactions by measuring the ratio of the signals at m/e = 38 and m/e = 19 in a molecular beam fired directly into the mass spectrometer ionizer. The time-of-flight distributions at m/e = 19 and m/e = 38 are then simultaneously collected for gas scattered off the Si crystal. The expected background of F atoms produced by cracking can then be determined by multiplying the signal at m/e = 38 by the 0.28 cracking ratio. A point-by-point subtraction of this signal from the observed m/e = 19 signal reveals a second population of F atoms with a shorter flight time and thus higher translational energy: the signature of atom abstraction.[8]

I.2.b Exothermicity of Atom Abstraction

When an incident beam of F_2 with a velocity of 395 m/s was reacted with the Si surface, the scattered F_2 signal had an average velocity of 440±20 m/s, while the population of scattered F atoms produced by atom abstraction had an average velocity of 1195±57 m/s. While the difference in velocities is sufficient to unambiguously show that the F atoms are translationally heated, it is interesting to note that the increase in velocity only corresponds to about 3% of the expected 103 kcal/mol exothermicity of the reaction. The remainder of the reaction exothermicity, presumably, is dissipated into the lattice. This low translational energy is consistent with an "attractive potential" or "early barrier" potential energy surface of the type proposed by Evans and Polanyi for gas-phase reactions. This sort of potential energy surface generally produces low translational energies and high vibrational excitations in the products of a reaction. Here, of course, F atoms cannot be vibrationally excited, so the vibrational excitation is presumably channeled into the surface.[8,23]

I.2.c Coverage Dependence and Two-Atom Abstraction

By measuring the signal of F atoms produced by atom abstraction as a function of F_2 exposure on a clean Si crystal, it is possible to determine the coverage dependence of the atom abstraction reaction. The signal has been found to be low but nonzero at zero exposure, to reach a maximum at intermediate exposure, and to decay to zero at long exposure. This exposure-dependence is identical at all scattering angles, which shows that it is the probability of atom abstraction and not just the scattering angle that is varying with exposure. The use of thermal desorption spectroscopy to determine the amount of fluorine on the surface allows the exposure dependence to be converted to a coverage dependence, demonstrating that atom abstraction ceases when a coverage of one monolayer is attained.[8]

Knowing both the fluorine coverage of the surface and the amount of scattered F atoms produced by atom abstraction as a function of F_2 exposure allows the probabilities of one and two F atoms being deposited by a single F_2 molecule to be determined. The deposition of two F atoms has its maximum probability, 0.8, on a clean crystal; its probability falls to 0.3 at a coverage of a half monolayer and to zero at a coverage of a monolayer. The deposition of one F atom, on the other hand, has a probability of about 0.1 on a clean crystal, rising to a maximum of 0.3 at a coverage of half a monolayer and then falling to zero at a coverage of a monolayer. The high probability of two-atom adsorption on clean surfaces is likely due to a two-atom atom abstraction mechanism in which the scattered atom produced by atom abstraction reacts with a nearby dangling bond before escaping the surface. The probability of two-atom abstraction decreases as the coverage increases and less dangling bonds are available, resulting in an increased probability of single-atom atom abstraction producing F atoms that successfully escape to the gas phase and can be detected.[8] A statistical model has shown that this combination of one-atom and two-atom abstraction explains the experimental results, and suggests that the reaction cross-section of an unoccupied dangling bond in a dimer where the other dangling bond is occupied by a F atom is twice the reaction cross-section of an unoccupied dangling bond in a fully unoccupied dimer. This difference in reactivity is expected, since the presence of a F atom bound to the other Si atom in the dimer disrupts the weak π-bonding interaction between the dangling bonds and leaves the unoccupied dangling bond with a greater free-radical character.[9]

I.3 XeF_2 Reactivity with the Si(100)2x1 Surface by Atom Abstraction

I.3.a Single-Atom Abstraction Producing XeF Radicals

As discussed in Section I.1.b , the reactivities of F_2 and XeF_2 with Si(100)2x1 surfaces are very similar at F coverages of less than one monolayer. Thus, it comes as no surprise that, like F_2, XeF_2 reacts with the Si surface via atom abstraction. The presence of XeF_2 atom abstraction can be demonstrated by the same technique that F_2 atom abstraction was observed. The XeF^+/XeF_2^+ cracking ratio is measured in a direct molecular beam and is used to subtract the contribution of XeF from ionizer dissociation of XeF_2 in a time-of-flight spectrum of the XeF scattered from the crystal. A separate population of XeF, translationally excited compared to the scattered XeF_2 and cracking-produced XeF, is observed, confirming the presence of atom abstraction.[12]

The angular and energy distributions of scattered XeF radicals are largely independent of the incident angle and energy of the XeF_2 molecules, suggesting that the strong chemical forces on the surface associated with the atom abstraction reaction erase the molecule's memory of its original trajectory. However, the translational energies of the scattered XeF radicals—between 8.4 and 11.6 kcal/mol—are much higher than the $2k_BT = 0.6$ kcal/mol translational energy that would be expected if the radicals had remained on and equilibrated with the surface before escaping.[13]

Interestingly, F atoms are also observed scattered from the surface, suggesting that some of the XeF radicals produced by atom abstraction dissociate before reaching the detector. Such dissociation is likely, given that the XeF radical has a bond strength of only 3 kcal/mol and the abstraction reaction has an exothermicity of 81 kcal/mol. Unfortunately, the F^+/XeF^+ cracking ratio cannot be directly measured without a beam of XeF radicals, so we cannot use the same procedure to subtract off the contribution of F atoms produced by ionizer cracking of XeF radicals. However, a modified procedure does allow us to put a lower bound on the population of F atoms produced by dissociation of XeF radicals before reaching the detector.[12]

Time-of-flight spectra were measured at eight coverages between zero and one-and-a-quarter monolayers and at three scattering angles to produce spectra with different F atom signals. Since the cracking ratio is necessarily the same for all coverages and scattering angles—it only depends on the ionizer conditions—the upper bound for the cracking ratio is the ratio that would indicate that all F atoms in the spectrum with the lowest ratio of F atoms to XeF radicals are produced by cracking. This technique gave a upper bound of 0.4 for the cracking ratio and confirmed that, at least at some coverages and scattering angles, XeF does dissociate before reaching the detector.[12]

I.3.b Gas-Phase Dissociation of XeF Radicals and Two-Atom Abstraction

The existence of a population of F atoms not produced by cracking in the ionizer demonstrates that some XeF radicals are dissociating before reaching the ionizer. It is not, however, sufficient to determine whether they are dissociating on the surface or in the gas phase after escaping the surface. If they are dissociating in the gas phase after leaving the surface's influence, though, then the trajectories of the XeF radicals before dissociation and the Xe and F atoms after dissociation must obey Newtonian conservation of energy and momentum.

Trajectories that conserve energy and momentum are most easily found in the frame of reference of the center of mass of the Xe-F system. However, they need to be converted to the lab frame, as shown in Figure I-5, to be experimentally validated. In addition, it is necessary to know the detector's relative sensitivity to Xe and F atoms to be able to meaningfully compare their distributions, requiring a measurement of the ratio of the transmission probabilities of Xe and F through the quadrupole. The ratio of transmission probabilities can be measured by measuring the observed flux of effusive beams, where the ideal gas law predicts that the ratio of their absolute fluxes is the ratio of their masses to the negative-half power. Since a beam of F atoms is not available, but transmission probability varies negligibly with a change in m/e ratio of 1, the ratio of transmission probabilities is measured for Xe and Ne instead.[8]

Modeling the dissociation of the XeF radical as a gas-phase process produced results consistent with the observed velocity and angular distributions of intact XeF radicals and Xe and F atoms produced by the dissociation of XeF. Given that the exothermicity of the atom abstraction reaction is channeled into the translational and robovibrational energy states of the ground state of the XeF radical, the dissociation is due to vibrational excitation and so must occur within one vibrational period. The XeF vibrational frequency is 225.40 cm^{-1} and the measured average velocity of the XeF radicals is 775 m/s, so dissociation must occur within 2 Å of the surface. Although many of the F atom radicals released by gas-phase dissociation eventually scatter from the surface, roughly 9% of them will collide with the surface again. At low coverage, they will react with dangling bonds, but it is possible that at higher coverages they cleave Si-Si bonds and contribute to XeF_2's ability to etch silicon.[13]

A second source of scattered Xe atoms, besides gas-phase dissociation, is two-atom abstraction. Unlike the addition of a second F atom that collides with the surface after a gas-phase dissociation, two-atom abstraction occurs when the XeF radical fails to escape to the gas phase and is pulled back in by the surface's attractive potential, allowing a second dangling bond to abstract its remaining F atom.[13]

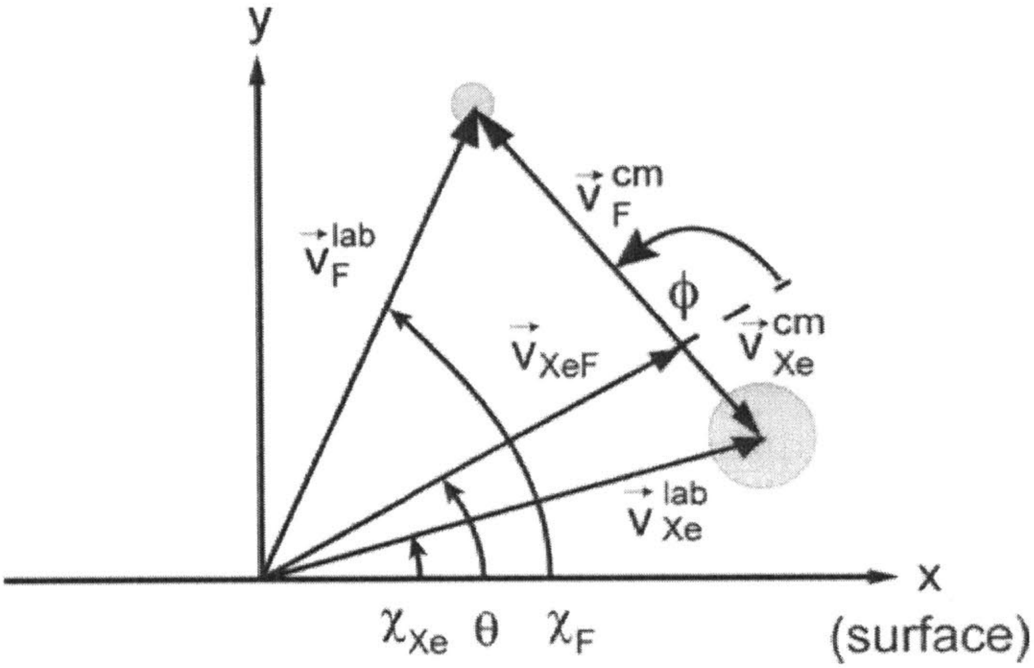

Figure I-5: Newton Diagram for Gas-Phase Dissociation of XeF Radicals

Using conservation of momentum, the angular distributions of intact XeF radicals and Xe and F atoms produced by gas-phase dissociation can be related. This figure is taken from Hefty, Holt, Tate, and Ceyer, 2008.[13]

I.3.c Atom Abstraction at High Fluorine Coverages

It has been established that at fluorine coverages below one monolayer, XeF_2—like F_2—only reacts with dangling bonds and not Si-Si dimer or lattice bonds, thus preserving surface order. However, unlike F_2—which ceases to react with Si when all dangling bond sites are occupied at a coverage of one monolayer—XeF_2 begins to cleave Si-Si bonds when the dangling bond sites are exhausted. Since the thermodynamics of cleaving Si-Si bonds are rather less favorable than the kinetics of reacting with dangling bonds that are effectively radical sites, it is not immediately obvious whether atom abstraction continues to be the mechanism for XeF_2 reactivity with Si at coverages above one monolayer. After all, F_2, which also reacts via atom abstraction, ceases its reactivity with Si once all dangling bonds are occupied.[10,12]

Additional experiments done at higher coverages, varying from zero to one-and-a-quarter monolayers have demonstrated that, in fact, atom abstraction is still a major mechanism for the reaction of XeF_2 with Si when dangling bond sites are no longer available. The ratio of single atom abstraction to double atom abstraction increases at higher coverages, probably because the surface becomes less attractive, making it easier for XeF radicals to escape the surface. The fraction of scattered XeF radicals that dissociates in the gas phase remains the same, and it is possible that the radical F atoms released by them that collide with the surface play a role in cleaving Si-Si bonds once there are no available dangling bonds.[14]

I.4 The Effect of Mass and Velocity on F_2 and XeF_2 Etching of Si Surfaces

I.4.a Varying in F_2 Velocity to Promote Etching

Since the chemical and thermodynamic properties of F_2 and XeF_2 do not appear to explain why XeF_2 etches Si surfaces while F_2 does not, a logical next step is to consider the mechanical properties of the molecules. XeF_2 has a mass over four times that of F_2 and so, at the same kinetic energy, has half the velocity of F_2. Is it possible that this difference in mass and velocity is responsible for their different reactivities?

One possibility is that the longer interaction time at the surface that results from XeF_2's lower incident velocity is the deciding factor. Perhaps the longer interaction time significantly increases the probability of Si-Si bond cleavage. If so, we would expect that slowing F_2 molecules would increase their effectiveness at etching Si.

A beam of low-velocity F_2 molecules can be produced by anti-seeding 1% F_2 in 99% Xe. Seeding is a technique in which the energy of molecules in a supersonic expansion is increased by mixing them with a large quantity of very light, fast molecules, usually He atoms. Since a supersonic expansion equalizes the velocities rather than the translational energies of its constituent molecules, much of the kinetic energy of the He atoms will be transferred to the molecules of interest. Anti-seeding is just the reverse of this procedure: the molecules of interest are diluted in a large quantity of very heavy Xe atoms, to which they will transfer most of their energy, creating a beam of inert Xe and slow-moving F_2 molecules.

The F_2/Xe anti-seeded beam, expanded through a room-temperature nozzle at 200 Torr, produced F_2 molecules with an average velocity of 398±10 m/s, intermediate between the measured velocities of pure XeF_2, 256±1 m/s, and pure F_2, 590±1 m/s. While this is higher than the velocity of the pure F_2 beams used to study its reaction with Si, XeF_2 has been observed to etch Si rapidly at velocities up to 559 m/s, so if long interaction time is the deciding factor for reactivity here, a 398 m/s F_2 beam would be expected to etch Si at a similar rate to XeF_2. However, He diffraction data and time-of-flight spectra of the molecules scattered from the surface show that the slow F_2 beam reacts with the surface identically to normal F_2: it reacts rapidly with dangling bonds up to a coverage of one monolayer and then ceases to react rather than cleaving Si-Si bonds as XeF_2 does.[15]

Evidently, increasing the interaction time between F_2 and the Si surface is insufficient to produce etching. In fact, the opposite is true: increasing the beam energy and velocity by seeding can induce F_2 to etch Si, albeit with a reaction probability several orders of magnitude lower than that of XeF_2.[11]

I.4.b Using van der Waals Dimers to Probe Etching

Neither raising the translational kinetic energy of F_2 nor lengthening its interaction time on the surface is sufficient to produce Si etching with reaction probabilities similar to those easily obtained with XeF_2. Unfortunately, the low mass of F_2 molecules means that we have a choice of high energy (and short interaction times) or long interaction times (and low energy), but not both. It would be convenient if we could attach inert weights to a F_2 molecule to slow it down without reducing its kinetic energy. Perhaps by producing F_2 molecules with the same energy and velocity as XeF_2, we would produce a combination of interaction time and energy transfer into the surface that would reproduce XeF_2's ability to etch Si.

Surprisingly, nature actually does give us just this ability. Seeding and anti-seeding are not the only possible results of producing a supersonic expansion from a mixture of F_2 molecules and noble gas atoms. In a supersonic expansion of a mixture of the two molecules, clusters held together by van der Waals dispersion forces can be formed. Since the van der Waals interaction has a bond energy of less than 1 kcal/mol, it has a minimal effect on the electronic structure of the F_2 molecule and, since the noble gas atom in the cluster is chemically inert, such a cluster should have identical chemistry to an F_2 molecule. Only the mass—and so the relationship between velocity and translational kinetic energy—is different.

The most obvious noble gas to use in producing van der Waals molecules to probe F_2 reactivity with Si is Xe: $Xe(F_2)$ clusters will have exactly the same mass as XeF_2 molecules, while being chemically identical to F_2 molecules. $Kr(F_2)$ clusters are also a logical choice, since they have about three-quarters the mass of XeF_2 molecules. An additional benefit of $Kr(F_2)$ clusters is that, unlike XeF_2, the formation of KrF_2 is not catalyzed by Ni, eliminating the possibility that the reactivity of the clusters is really due to XeF_2 (or KrF_2) contaminants produced in the Ni nozzle. Continuing on this path, if $Kr(F_2)$ clusters etch silicon, one might want to use $Ar(F_2)$ or $Ne(F_2)$ clusters as well to determine the minimum mass needed for effective etching. However, the strength of van der Waals interactions falls off with molecular radius, and it is much harder to produce substantial concentrations of clusters with lighter noble gases. At present, experiments have only been performed with $Xe(F_2)$ and $Kr(F_2)$ beams.[15,16]

One danger of producing supersonic beams from mixtures of F_2 and Xe is the possibility that molecular XeF_2 will be produced. XeF_2 cannot, of course, be directly distinguished from $Xe(F_2)$ by mass spectroscopy, since they have the same molecular masses. However, they can be distinguished by their cracking ratios. The cracking ratio of XeF_2 to XeF in the mass spectrometer ionizer is known to be roughly 1:2 from the atom abstraction experiments discussed in Section 1.3 . The exact cracking ratio for $Xe(F_2)$ is not known, but it is expected to be much smaller, since the Xe atom and F_2 molecule are held together by a very weak van der Waals interaction while the F_2 molecule is held together by a strong covalent bond in $Xe(F_2)$ clusters, while molecular XeF_2 consists of two F atoms each bound directly to an Xe atom by covalent bonds with no direct interaction between the F atoms, which are on directly opposite sides of the Xe atom. Using cracking ratio as a proxy, it has been confirmed that, while molecular beams produced by expanding an Xe/F_2 mixture through a hot nozzle do contain substantial XeF_2, cooling the nozzle to –60°C causes an increase in the production of $Xe(F_2)$ and a decrease in the production of XeF_2.[15]

I.4.c Si Etching by $Xe(F_2)$

To test the ability of $Xe(F_2)$ to etch Si surfaces, a 5% F_2 / 95% Xe mixture was expanded through a –50°C nozzle with a stagnation pressure of 150 Torr. The $Xe(F_2)$ flux in this beam was calculated to be about 1.4% of the total F_2 and $Xe(F_2)$ flux, although this percentage is likely an underestimate as Xe^+ and XeF^+ ions produced by ionizer cracking of $Xe(F_2)$ were neglected in the analysis leading to this value.[15]

As in the F_2 and XeF_2 atom abstraction experiments discussed above, the intensity of the He diffraction specular peak was measured as a function of exposure to this beam. As in those experiments, the specular intensity decreases to a minimum at a coverage of about half a monolayer and then returns to a maximum at a coverage of about a monolayer, as dangling bond sites are preferentially filled. After a coverage of one monolayer, the specular intensity decays faster than with F_2, but still quite slowly. That the decay of specular intensity is faster than with F_2 suggests that $Xe(F_2)$ may indeed be able to cleave Si-Si bonds, although the low concentration of $Xe(F_2)$ in the beam and the relatively non-quantitative nature of this measurement of reactivity makes it hard to determine the importance of this effect.[15]

Thermal desorption spectra were also taken of the Si surface to determine the F coverage attained after long-term exposure to the cluster beam. The results here were similar to those with

He diffraction: the coverage attained with the cluster beam was slightly higher than with a pure F_2 beam, but only by a minimal margin (0.94 monolayers for F_2 versus 1.03±0.01 monolayers for the cluster beam). Accounting for the low number of $Xe(F_2)$ clusters in the beam, the reaction probability of $Xe(F_2)$ with Si at coverages above one monolayer has been estimated to be 0.9 based on the thermal desorption data, three orders of magnitude larger than the 9×10^{-4} probability that has been measured for F_2.[15]

An attempt was also made to observe scattered products from the reaction of the cluster beam with the Si crystal at F coverages above one monolayer. Neither SiF_4 nor XeF was observed in the scattered beam, which is strong evidence that the cluster beam does not contain molecular XeF_2, since those species are the main two products of its reaction with Si at high coverage. However, it also proved impossible to produce F atoms produced by atom abstraction at coverages above one monolayer. This fact may be due to the very small amount of $Xe(F_2)$ in the cluster beam and the difficulty in distinguishing the small population of F atoms produced by it from the much larger population of F atoms produced by ionizer cracking of F_2.[15]

I.4.d Si Etching by $Kr(F_2)$

Etching experiments have also been performed using a beam containing $Kr(F_2)$ clusters. This beam was produced by expanding a 75% F_2 / 25% Kr mixture through a –75°C nozzle with a stagnation pressure of 300 Torr. The $Kr(F_2)$ flux in this beam was calculated to be approximately 0.21% of the total F_2 and $Kr(F_2)$ flux in the beam. As with the $Xe(F_2)$ cluster beam discussed above, the contributions from ionizer cracking of $Kr(F_2)$ to produce KrF^+ and Kr^+ ions were neglected. Furthermore, the F_2 flux used in this calculation was determined from the same measurements used for the $Xe(F_2)$ experiments, although these measurements were a decade old at the time the $Kr(F_2)$ experiments were conducted.[16]

Thermal desorption spectroscopy experiments were conducted using the $Kr(F_2)$ cluster beam on a fully fluorinated Si surface. These experiments indicated that the reaction probability of $Kr(F_2)$ was between 0.04 and 0.045, with a possible minimum of 0.01. While more work, and a new measurement of the F_2 flux, are needed to determine the exact value, these results are consistent with the hypothesis that the ability of XeF_2 to cleave Si-Si bonds is due to its mass, since they fall well in between the 9×10^{-4} reaction probability of F_2 and the 0.6 reaction probability of XeF_2. [16]

I.5 Conclusions and Future Work

I.5.a Conclusions

The Ceyer lab's study of the reaction of fluorine compounds with silicon surfaces over the last twenty-five years has resulted in a much-improved understanding of the mechanism by which these compounds react fluorinate and etch Si. They have included the first observations of atom abstraction from a gas molecule by a solid surface and of gas-phase dissociation of a scattered product from such an atom abstraction reaction. It is now clear that the fluorination of Si by both F_2 and XeF_2 proceeds by atom abstraction at coverages of less than one monolayer, and that the XeF radicals produced by atom abstraction from XeF_2 can themselves dissociate in the gas phase, producing F radicals some of which react with the surface.[8,12]

The matters of reactivity at coverages of more than one monolayer, the mechanism by which XeF_2 cleaves Si-Si bonds to etch Si, and the reason that it is able to do so while F_2 is not are less clear. However, strong evidence has been collected that the hypothesis that the reactivity difference is due to the increased ability of heavier molecules to transfer translational kinetic energy into the Si surface, stretching and compressing the Si-Si bonds and providing the activation energy needed to cleave them. While lowering the velocity of F_2 molecules does not enable them to etch Si, and raising their velocity significantly has only a minor effect on their ability to do so, increasing their mass by attaching them to heavy noble gas atoms in van der Waals clusters appears to have a significant effect on their ability to react with Si at F coverages above one monolayer, as shown by the results in Table I-1. Additional work with $Xe(F_2)$ and $Kr(F_2)$ clusters is needed to better quantify this effect. In addition, theoretical work is needed to better understand the relationship between mass and kinetic energy transfer to the surface lattice vibrations. An initial model and simulation for this purpose is discussed in the following chapter.[11,15,16]

Table I-1: Reaction Probabilities on Si at 1 ML F Coverage

Species	Absorption Probability
F_2	9×10^{-4}
XeF_2	6×10^{-1}
$Xe(F_2)$	9×10^{-1}
$Kr(F_2)$	4×10^{-2}

A comparison of the reaction probabilities for F_2, XeF_2, $Xe(F_2)$, and $Kr(F_2)$ reacting with a Si(100)2x1 surface at a coverage of one monolayer of F based on thermal desorption spectroscopy. The values for $Xe(F_2)$ and $Kr(F_2)$ are preliminary.[8,13,15,16]

I.5.b Increasing $Xe(F_2)$ Production via Improved Nozzle Cooling

The experiments performed with the $Xe(F_2)$ cluster beam described in Section I.4.c were limited by the low concentration of $Xe(F_2)$ present in the beam, as well as by concerns that some molecular XeF_2 might have been produced in the nozzle. Both of these issues could be alleviated by a lower nozzle temperature, but at the time those experiments were conducted, the nozzle set-up did not allow temperatures lower than –50°C, although the liquid He cold head used to cool the nozzle reaches a minimum temperature of –210°C. This difference in minimum temperatures was partly attributed to the high thermal conductivity of the copper block attached to the wall of the source chamber that was used to hold the nozzle in position. To rectify this problem, a new nozzle holder made of polyetheretherketone (PEEK), which has a thermal conductivity three orders of magnitude lower than that of copper, has been installed. Using the new nozzle holder, the nozzle can be cooled to –75°C for several hours, which should allow for a greater production of $Xe(F_2)$, as well as diminishing the possibility that XeF_2 is present in the beam. It would be worthwhile to repeat the $Xe(F_2)$ etching experiments using the improved cluster beam possible with a –75°C nozzle.[16]

I.5.c Additional $Kr(F_2)$ Experiments

While thermal desorption spectroscopy experiments have been performed with a $Kr(F_2)$ cluster beam using the lower nozzle temperature possible because of the modifications described in the previous section, the usefulness of the results is limited by the absence of recent measurements of the absolute F_2 flux in the F_2/Kr cluster beam and of the ratio of the quadrupole transmission functions for F_2 and $Kr(F_2)$. The absolute F_2 flux and ratio of transmission functions are needed in order to calculate the absolute $Kr(F_2)$ flux, which is needed to accurately determine the number of clusters to which the surface was exposed, and thus to determine a reaction probability from the coverages observed by TDS. Measuring the absolute flux for F_2 is a somewhat complicated, multi-step process involving measurements of a F_2 seeded in Ar. The latter is used because absolute flux measurements require that a seeded monoenergetic beam not exhibit Mach number focusing.[15,19]

The absolute flux, I_{in}, of a pure Ar beam produced with a given nozzle temperature and stagnation pressure can be measured via the pressure increase it causes when it introduced into the main chamber. The flux of the beam at the crystal times the area of the beam spot is equal to the time derivative of the number of molecules in the main chamber:

$$I_{in}A_{spot} = \dot{N} = \frac{d}{dt}\left(\frac{P_{actual}V}{k_B T}\right).$$

Under steady-state conditions, the pressure, P_{actual}, chamber volume, V, and beam temperature, T, are constant so the number of particles in the chamber actually varies with the pumping speed, S_P. In addition, to determine the actual main chamber pressure from the ion gauge reading, we must use a gas-specific correction factor, C_F, such that $P_{actual} = P_{obs}C_F$, where P_{obs} is the ion gauge reading. This substitution gives us the equation

$$I_{in} = \frac{P_{obs}C_F S_P}{k_B T_{beam} A_{spot}}$$

for the Ar flux. The flux for an F_2 beam produced with the same nozzle conditions should differ from the Ar beam flux only by the ratio of their root-mean-square velocities, which can be accounted for by a factor of the square roots of their molecular masses:

$$I_{in,F_2} = \frac{\sqrt{m_{Ar}}}{\sqrt{m_{F_2}}} I_{in,Ar}.$$

Determining the absolute flux of F_2 in the 75% F_2 / 25% Kr is not as simple as considering the ratio of gases in the stagnant mixture used to generate the beam because Mach number focusing causes heavier species to be more concentrated along the beam line and Kr has a significantly higher molecular mass than F_2. However, since Ar and F_2 have very nearly the same mass (40 amu versus 38 amu), there is minimal Mach focusing in a F_2/Ar beam, so the absolute flux of F_2 in a 75% F_2 / 25% Ar beam will be 75% of the absolute flux of Ar in a pure Ar beam produced with the same nozzle conditions. To determine the absolute flux of F_2 in the 75% F_2 / 25% Kr cluster beam, we must take time-of-flight spectra of both the F_2/Kr beam and the F_2/Ar beam and fit the spectra to a Maxwell-Boltzmann distribution to determine the relative fluxes of F_2 in each beam. The absolute flux of F_2 in the F_2/Kr beam is then simply the absolute flux of F_2 in the F_2/Ar beam times the ratio of the relative fluxes of F_2 in the two beams as determined from the integrated time of flight spectra.[15,19]

Once the absolute flux of F_2, $I_{in}^{F2,F2}$, and the observed flux from fitting the TOF spectrum to a Maxwell-Boltzmann distribution, $F_{F2,F2}$, are known, we need to determine the ratio of transmission functions for Kr(F_2) and F_2. This determination requires pure effusive beams of noble gases with masses similar to those of the two gases: Ar (40 amu) in place of F_2 (38 amu) and Xe (129 amu) in place of Kr(F_2) (122 amu). This substitution is valid because the transmission functions should not vary significantly over such small—roughly 5%—differences in mass. The observed fluxes for the pure Ar and Xe beams, $F_{Ar,Ar}$ and $F_{Xe,Xe}$, should be calculated from time-of-flight spectra. For effusive beams, the ratio of absolute fluxes is equal to the ratio gases' root-mean-square velocities, and thus to the inverse of the square roots of their masses. The ratio of quadrupole transmission functions, T_{Ar}/T_{Xe} can then be backed out from the equation

$$\frac{I_{in}^{Ar,Ar}}{I_{in}^{Xe,Xe}} = \frac{\sqrt{m_{Xe}}}{\sqrt{m_{Ar}}} = \left(\frac{F_{Ar,Ar}}{F_{Xe,Xe}}\right)\left(\frac{\sigma_{Xe}}{\sigma_{Ar}}\right)\left(\frac{T_{Xe}}{T_{Ar}}\right)$$

where σ_{Ar} and σ_{Xe} are the ionization cross-sections for Ar and Xe and m_{Ar} and m_{Xe} are their atomic masses.[15,16]

With the absolute flux of F_2 in the F_2/Kr beam and the approximate relative transmission functions in hand, we can use the same equation to back out the absolute flux of Kr(F_2) in the cluster beam:

$$\frac{I_{in}^{F_2,F_2/Kr(F_2)}}{I_{in}^{Kr(F_2),F_2/Kr(F_2)}} = \left(\frac{F_{F_2,F_2/Kr(F_2)}}{F_{Kr(F_2),F_2/Kr(F_2)}}\right)\left(\frac{\sigma_{Kr(F_2)}}{\sigma_{F_2}}\right)\left(\frac{T_{Kr(F_2)}}{T_{F_2}}\right)$$

Since the ionization cross section of Kr(F_2) is not known, but the cluster can be approximated as a F_2 molecule and a Kr atom, we approximate the ionization cross section of the cluster as the sum of the cross-sections of its two components.[15]

In addition to the absolute flux measurements needed to determine the Kr(F_2) exposure of the crystal for the thermal desorption spectra, time-of-flight spectra of the scattered products from the reaction of the Kr(F_2) cluster beam with Si are needed. These experiments would be useful in understanding the mechanism by which Kr(F_2) etches Si by determining whether SiF_4

and F atoms are produced. However, a higher nozzle pressure will likely be needed for these experiments to increase the number of $Kr(F_2)$ dimers in the beam, given that the F atom signal in the $Xe(F_2)$ experiments was swamped despite that beam having a higher number of clusters and despite the higher reactivity of $Xe(F_2)$ clusters.[15,16]

Chapter I References

(1) C. Easter and C. B. O'Neal, *Journal of Microelectromechanical Systems* **18**, 1054-1061 (2009).

(2) H. F. Winters and J. W. Coburn, *Appl. Phys. Lett.* **34**, 70-73, (1979).

(3) J. A. Mucha, V. M. Donnelly, D. L. Flamm and L. M. Webb, *J. Phys. Chem.* **85**, 3529-3532, (1981).

(4) D. L. Flamm, V. M. Donnelly and J. A. Mucha, *J. Appl. Phys.* **52**, 3633-3639, (1981).

(5) M. J. Vasile, *J. Appl. Phys.* **54**, 6697-6704, (1983).

(6) D. E. Ibbotson, D. L. Flamm, J. A. Mucha and V. M. Donnelly, *Appl. Phys. Lett.* **44**, 1129-1131, (1984).

(7) Y. L. Li, D. P. Pullman, J. J. Yang, A. A. Tsekouras, D. B. Gosalvez, K. B. Laughlin, Z. Zhang, M. T. Schulberg, D. J. Gladstone, M. McGonigal, and S. T. Ceyer, *Phys. Rev. Lett.* **74**, 2603-2606, (1995).

(8) M. R. Tate, D. Gosalvez-Blanco, D. P. Pullman, A. A. Tsekouras, Y. L. Li, J. J. Yang, K. B. Laughlin, S. C. Eckman, M. F. Bertino, and S. T. Ceyer, *J. Chem. Phys.* **111**, 3679-3695, (1999).

(9) M. R. Tate, D. P. Pullman, Y. L. Li, D. Gosalvez-Blanco, A. A. Tsekouras, and S. T. Ceyer, *J. Chem. Phys.* **112**, 5190-5204, (2000).

(10) J. R. Holt, R. C. Hefty, M. R. Tate, and S. T. Ceyer, *J. Phys. Chem. B* **106**, 8399-8406, (2002).

(11) D. P. Pullman, A. A. Tsekouras, Y. L. Li, J. J. Yang, M. R. Tate, D. B. Gosalvez, K. B. Laughlin, M. T. Schulberg, and S. T. Ceyer, *J. Phys. Chem. B* **105**, 486-496, (2001).

(12) R. C. Hefty, J. R. Holt, M. R. Tate, D. B. Gosalvez, M. F. Bertino, and S. T. Ceyer, *Phys. Rev. Lett.* **92**, 188302, (2004).

(13) R. C. Hefty, J. R. Holt, M. R. Tate, and S. T. Ceyer, *J. Chem. Phys.* **129**, 214701, (2008).

(14) R. C. Hefty, J. R. Holt, M. R. Tate, and S. T. Ceyer, *J. Chem. Phys.* **130**, 164714, (2009).

(15) R. C. Hefty, Ph.D. Thesis, Massachusetts Institute of Technology, (2003).

(16) M. R. Blair, M.S. Thesis, Massachusetts Institute of Technology, (2014).

(17) J. D. Beckerle, A. D. Johnson, Q. Y. Yang, and S. T. Ceyer. *J. Chem. Phys.* **91**, 5756-5777, (1989).

(18) S. T. Ceyer. *Science* **249**, 133-139, (1990).

(19) D. Gosalvez-Blanco, Ph.D. Thesis, Massachusetts Institute of Technology, (1997).

(20) C. J. Wu and E. A. Carter, *Phys. Rev. B* **45**, 9065, (1992).

(21) P. C. Weakliem and E. A. Carter, *J. Chem. Phys.* **98**, 737 (1993).

(22) W. C. Simpson and J. A. Yarmoff, *Surf. Sci.* **359**, 135 (1996).

(23) M. G. Evans and M. C. Polanyi, *Trans. Faraday Soc.* **35**, 178-185, (1939).

Chapter II: A Classical Simulation of Collisions with the Silicon Surface

The main theoretical motivation for studying the reactivity of fluorine-noble gas van der Waals molecules with Si has been the hypothesis that the differences in reactivity between F_2 and XeF_2 are largely attributable to their different masses. $Xe(F_2)$ and $Kr(F_2)$ van der Waals molecules are chemically nearly identical to F_2, but $Xe(F_2)$ is identical in mass to XeF_2 and $Kr(F_2)$ is intermediate in mass between XeF_2 and F_2. Early experiments have shown that $Xe(F_2)$ etches Si in a similar manner to XeF_2, indicating that the mass of the gas molecule is in fact important to the mechanism of Si etching by fluorine compounds.[1,2]

As discussed in Chapter I, further experimental work is needed to better characterize the reactivity of $Xe(F_2)$ and $Kr(F_2)$ with Si surfaces. However, the success of the preliminary experiments indicates the need for further theoretical study of how the mass of the incident fluorine-containing gas molecule might influence its ability to etch silicon. It has been suggested that the difference in reactivity is likely due to the effect of mass on the kinematics of the collision of a gas molecule with a Si surface. An F_2 molecule has a mass of 38 amu, an Si atom has a mass of 28 amu, and an Si-Si surface dimer has a mass of 56 amu. The most abundant isotopes of Xe have masses of 132, 129, and 131 amu, so the mass of XeF_2 molecules will vary from 167-170 amu and be over four times the mass of an F_2 molecule. Such a large mass difference between the impacting gas molecule and the surface atoms necessitates that multiple collisions will occur, as the first collision will not transfer enough momentum to reverse the trajectory of the impacting molecule. Multiple collisions potentially allow for a higher maximum energy transferred to the surface as well as a longer residence time on the surface than a single collision. In some aspects with heavier atom such as Kr and Xe, this mechanism is similar to the "chemistry with a hammer" mechanism that has been observed for the reactions of CH_4 on Ni(111) surfaces.[1,3]

While it is intuitively clear that a more massive incident gas molecule is likely to experience more collisions with the Si lattice before escaping than a significantly less massive gas molecule with the same initial energy, more in-depth calculations are needed to determine the number of collisions and associated energy transfer and residence time for F_2, XeF_2, and van der Waals molecule collisions with the surface. These calculations must take into account both energy transfer between the gas molecule and the surface unit with which it comes into direct contact and energy transfer between that surface unit and the lattice as a whole. As this system cannot easily be modeled analytically, a simulation has been written in the Python programming language to model it numerically.

II.1 The Model

II.1.a Overview

In order to allow the simulation to be run in a reasonable time on desktop computers, the physical situation of a gas molecule colliding with a Si crystal has been reduced to a very simple model. Molecular motions are treated classically and all collisions are assumed to be elastic hard sphere interactions. Furthermore, only one dimension of molecular motion is treated; the impinging gas molecule is only allowed to move along the surface normal and the surface itself is modeled as consisting of two components, each with only one free variable. The "surface unit" that actually collides with the gas molecule is treated as a one-dimensional damped simple harmonic oscillator attached to a lattice treated as a thermal bath defined only by its temperature. The magnitude and sign of the damping is related to the temperature difference between the bath and the oscillator and provides negative feedback to bring the oscillator back into equilibrium with the bath. This model is illustrated in Figure II-1.

The model is intentionally agnostic about the exact nature of the silicon surface unit: by varying its mass and the spring constant of the oscillator, different surface units, such as a single Si atom with a bound F atom or a whole surface dimer with one bound F atom for each of the two Si atoms, can be modeled. However, it assumes that the surface unit has no internal degrees of freedom: its energy is treated as that of a point mass on a one-dimensional spring. The silicon surface unit also defines the coordinate system for the model: the origin is set at the equilibrium position of the surface unit and the +x direction is defined as towards the bulk of the crystal.

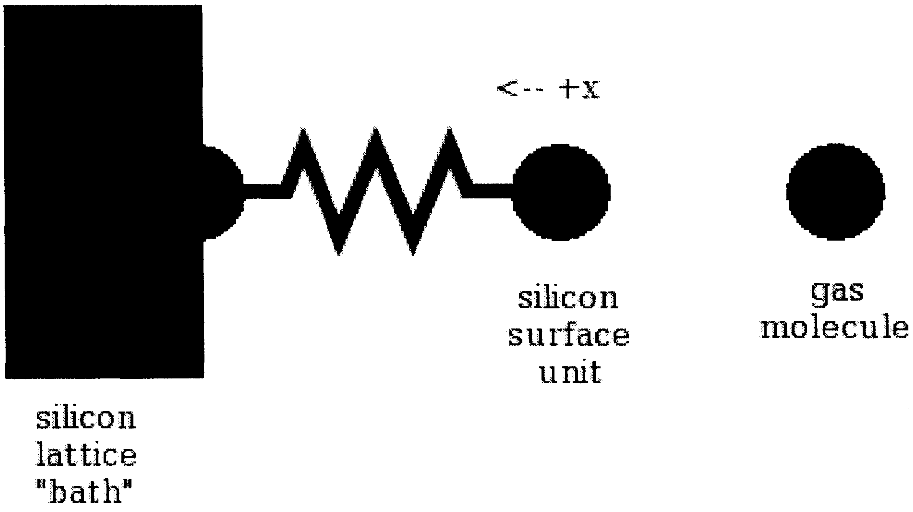

Figure II-1: Model System Used for Simulations

This diagram shows the model system used for the simulations discussed in this chapter. The silicon surface unit is modeled as a hard-sphere mass on a spring connecting it to the lattice. The lattice itself is modeled as a thermal bath, whose only property is a temperature. The spring linking the lattice to the surface unit is treated as a damped simple harmonic oscillator with the magnitude and sign of the damping linked to the temperature difference between the bath and the surface unit oscillations. The incoming gas molecule is modeled as a hard sphere in free space, only interacting with the surface unit instantaneously at the moment of collision. The coordinate system has its origin at the equilibrium point of the silicon surface unit's oscillations and the +X direction is defined as into the crystal.

II.1.b Gas Molecule Translation and Collision Evaluation

Because the gas molecule colliding with the surface is treated as a free object in space, interacting with the surface only instantaneously during collisions, its position as a function of time is just

$$x_1 = x_0 + vt,$$

with x_0 the position at the last collision, v the velocity after the last collision, and t the time since the last collision. Furthermore, the gas molecule's dynamics do not depend on its absolute location, only its distance from the silicon surface unit. This approximation means that we can eliminate the need to estimate the gas molecule's radius by defining its location, x, as the location of its silicon-facing edge rather than the location of its center of mass. Similarly, since the silicon surface unit is treated as a rigid sphere, we can shift our coordinate system so that the location of its outward-facing edge, X, is 0 when the surface unit oscillator is at equilibrium.

When the difference in position between the silicon-facing edge of the gas molecule, x, and the outward-facing edge of the silicon surface unit, X, is zero, a collision occurs. Since the collision is treated as an instantaneous, elastic collision between hard spheres, the values of x and X are the same before and after the collision. However, the velocities of the molecule, v_0, and the surface unit, V_0, change as kinetic energy and momentum are exchanged, resulting in new velocities v_1 and V_1. Calling the mass of the gas molecule m and the mass of the silicon surface unit M, conservation of momentum and energy gives us that:

$$mv_0 + MV_0 = mv_1 + MV_1$$

and

$$\frac{mv_0^2}{2} + \frac{MV_0^2}{2} = \frac{mv_1^2}{2} + \frac{MV_1^2}{2}.$$

We can solve the momentum-conservation expression for v_1,

$$v_1 = v_0 + \frac{M}{m}(V_0 - V_1),$$

giving us an expression for v_1 that can then be plugged into the energy-conservation expression. Cancelling the factors of ½ and dividing all terms by m gives us:

$$v_0^2 + \frac{M}{m}V_0^2 = \frac{M}{m}V_1^2 + \left(v_0 + \frac{M}{m}(V_0 - V_1)\right)^2.$$

Multiplying this out, dividing each term by $^M/_m$, and combining like powers of V_1 results in a quadratic equation in V_1:

$$0=\left[1+\frac{M}{m}\right]V_1^2+\left[-2\left(v_0+\frac{M}{m}V_0\right)\right]V_1+\left[v_0V_0+\left(\frac{M}{m}-1\right)V_0^2\right].$$

Since this expression is quadratic in V_1, we can solve it using the quadratic formula, and expect to get two solutions. One of the solutions is the trivial case of $V_0 = V_1$, which simply indicates that if no collision occurs, the velocity will be unchanged. The other solution gives V_1 if a collision does occur and, because we have solved for V_1 without making any assumptions about the relative values of the masses and initial velocities, we can obtain an equivalent expression for v_1 simply by exchanging the velocities and masses for the two hard spheres. Thus, we find that the velocities after a collision are:

$$V_1=\frac{2mv_0+(M-m)V_0}{M+m}=\frac{2v_0+\left({}^{M}\!/_{m}-1\right)V_0}{{}^{M}\!/_{m}+1}$$

and

$$v_1=\frac{2MV_0+(m-M)v_0}{m+M}=\frac{2\,{}^{M}\!/_{m}V_0+\left(1-{}^{M}\!/_{m}\right)v_0}{1+{}^{M}\!/_{m}}.$$

II.1.c Silicon Surface Unit Damped Harmonic Oscillator

As noted in the previous section, the coordinate system is designed so that the position of the outward-facing surface of the silicon surface unit, X, is 0 when the surface unit oscillator is at equilibrium. The simplest way to model this oscillator would be as a "mass on a spring" harmonic oscillator whose motion could be solved analytically. However, this model would not take into account the dissipation of excess energy from a collisionally excited surface unit into the lattice, nor the potential flow of energy from the lattice into a surface unit that has lost energy in a collision.

To take into account the role of energy exchange between the silicon surface unit and the lattice, the lattice is modeled as a thermal bath coupled to the surface unit harmonic oscillator by a damping term. The surface unit's mass, M, and the Hooke's Law constant of the bond between it and the lattice, K, are both free variables. Between them, they define the angular frequency of the oscillator:

$$\omega = \sqrt{K/M}\,.$$

Meanwhile, the lattice bath has one free variable, its temperature, T. This temperature implies a value for the average energy of a single oscillator in the lattice,

$$E = k_B T,$$

which is also the energy of the surface unit oscillator when it is in thermal equilibrium with the lattice.

The remaining challenge is coupling the oscillator to the lattice, so that energy will flow from a "hot" oscillator into the lattice and from the lattice into a "cold" oscillator. This coupling is done by converting the silicon unit oscillator into a damped harmonic oscillator, obeying the equation of motion

$$0 = \ddot{X} + X\omega^2 + 2c,$$

where c is a positive damping constant where the oscillator is overdamped if $c>1$, underdamped if $c<1$, and critically damped if $c=1$. If we generalize this expression to allow negative values of c, the result is reverse damping that adds energy to the oscillator instead of removing it. Since the lattice is a thermal bath, its temperature is unchanging and its energy content is infinite, so it is only necessary to account for changes in the energy of the oscillator and not the lattice.

Matters are somewhat complicated by the fact that we need the damping term, c, to vary with the difference in energy between the oscillator and the energy it would have if it were in equilibrium with the bath, E. If the energy of the oscillator is greater than its equilibrium energy, it should be damped ($c>0$) to remove energy until it comes back into equilibrium. If its energy is less than its equilibrium energy, it should be reverse damped ($c<0$) to add energy until it comes back into equilibrium. The energy of the oscillator is solely a function of its position and velocity,

$$e(X,\dot{X}) = \frac{KX^2}{2} + \frac{M\dot{X}^2}{2},$$

so the damping should depend on the difference between this and the equilibrium energy,

$$\frac{KX^2}{2} + \frac{M\dot{X}^2}{2} - E.$$

If c was set equal to this value, the strength of the damping would depend on the units used; with energy in SI units of joules; the system would always be so underdamped as to make no observable difference in the energy of the oscillator on time scales many times longer than the timescale of the collision. To correct this, and to allow tuning of the strength of the damping, the energy difference is multiplied by a scale factor of $^{C}/_{E}$, where E is included to cancel units, ensuring critical damping when the system is excited to twice its equilibrium energy if the free scale factor C is set to 1. As a result, the full equation of motion for the silicon surface unit is

$$0 = \ddot{X} + X\omega^2 + 2\frac{C}{E}\left(\frac{M\dot{X}^2}{2} + \frac{KX^2}{2} - E\right).$$

Since this differential equation cannot be solved analytically, it will be necessary to numerically integrate it, which in turn necessitates a computer simulation of the system.

II.2 Parameter Selection

II.2.a Experimental Conditions

The silicon lattice temperature and, the mass of the gas molecule, and the initial gas molecule velocity are the easiest parameters of the model to select, since they simply represent a choice of experimental conditions. These values can be set to replicate experiments that have been performed in order to gain a better understanding of the energy transfer at the surface during those experiments; they can also be set to model experiments that have not been performed but may be worthwhile performing in the future.

Past experiments have primarily been done with a silicon surface temperature of 250 K during the dosing of the crystal, so this value is the natural choice for the silicon lattice temperature. Four gas molecules have been used in experiments: F_2, XeF_2, $Xe(F_2)$, and $Kr(F_2)$. These correspond to masses of 38 amu, 167 amu, 167 amu, and 122 amu respectively. Since our goal is to compare energy transfer in collisions between the surface and gas molecules of different masses but the same energy, the fundamental choice is that of the kinetic energy of the incoming gas molecules, which will determine their velocities.

Table II-1: RMS Velocities of Gas Molecules as a Function of Mass and Energy

Mean Translational Kinetic Energy	**F_2 (38 amu)**	**$Kr(F_2)$ (122 amu)**	**XeF_2 or $Xe(F_2)$ (167 amu)**
0.35 kcal/mol	278 m/s	155 m/s	132 m/s
0.70 kcal/mol	393 m/s	219 m/s	187 m/s
1.46 kcal/mol	567 m/s	316 m/s	271 m/s
3.00 kcal/mol	813 m/s	454 m/s	388 m/s

The velocities given here are root mean square velocities for a beam with the given average translational energy.

Hefty's Xe(F_2) dimer experiments used a 5% F_2 / 95% Xe gas mixture with a nozzle temperature of 223 K to produce a 167 amu beam with an average translational kinetic energy of 1.46 kcal/mol.[1] Tate also did experiments with an 38 amu F_2 beam with an average translational kinetic energy of 0.70 kcal/mol.[4] It is also potentially worth considering beams with average translational kinetic energies of 0.35 kcal/mol (where the velocity of F_2 is nearly the same as that of XeF_2 at 1.46 kcal/mol) and 3.00 kcal/mol. The root mean square velocities for these beam energies are shown in Table II-1. They have been calculated using

$$v_{RMS} = \sqrt{\frac{2E}{m}},$$

where E is the average energy of the supersonic beam and m is the mass of the molecule.

II.2.b Silicon Surface Properties

Selecting the parameters that define the intrinsic properties of the silicon surface—the effective mass of the surface oscillator, M, the spring constant of the surface oscillator, K, and the damping constant for the dissipation of energy into the lattice, C—is somewhat more subjective, since their values depend in part on what exactly the silicon surface unit oscillator corresponds to in the actual surface. Since it is known that XeF_2 etching only begins after the surface is fully fluorinated, we should concern ourselves with the structure of fluorinated dimers, shown in Figure II-2.[5]

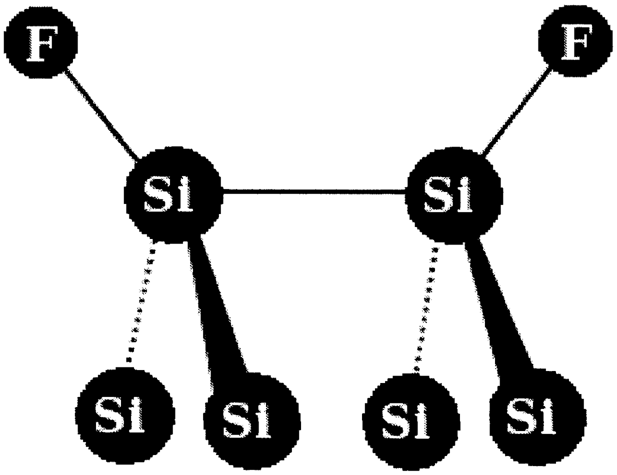

Figure II-2: Fluorinated Dimer Structure

The fluorinated surface consists of Si-Si dimers in which each Si atom is bound to a single F atom and is in turn bound to two Si atoms in the next layer of the crystal.

There are several possible candidates in the structure of the fluorinated dimer for the role of silicon surface unit. It may consist of a single Si atom and its bound F atom, for a mass of 47 amu. However, it could also plausibly consist of the whole F-Si-Si-F dimer, with a mass of 94 amu, or even the dimer and the four Si atoms beneath it, with a total mass of 206 amu. The choice of an effective mass for the silicon surface unit is related to the choice of a spring constant, since the choice of the surface unit indicates what bonds will be vibrationally excited. Based on an EELS study of the surface phonon modes of Si(100)2x1 dimers,[6] we can identify modes that excite the same bonds as would be excited by a collision where a given group of atoms move as a unit.

In the case of a SiF surface unit, the three bonds between one of the dimer silicon atoms and its adjacent silicon atoms should be excited; the mode that this choice most closely approximates has a frequency of 6.16×10^{12} Hz. For an Si_2F_2 surface unit, we would expect the four bonds from the dimer silicon atoms to the second layer to be excited, and for an Si_6F_2 surface unit, we would expect the eight bonds between the four second-layer silicon atoms and the next layer down to be excited. The modes that most closely correspond to these excitations have frequencies of, 1.17×10^{13} Hz and 1.87×10^{12} Hz, respectively. Given the surface unit mass and the vibrational frequency, we can derive the spring constant:

$$\nu = \frac{1}{2\pi}\sqrt{\frac{K}{M}} \Rightarrow$$
$$K = M(2\pi\nu)^2 .$$

The resulting values of M and K for the three potential surface units are shown in Table II-2. Given that the effective masses vary by a factor of four and the angular frequencies by a factor of six—relatively small margins considering the amount of simplification involved—it seems reasonable to select one choice of surface unit to perform simulations. All simulation runs discussed in this chapter will be based on an Si-F surface unit, since it is the smallest and most compact, and thus neglecting its internal degrees of freedom is the most reasonable.

Having selected the Si-F surface unit for our calculations, we still need to decide on a value of C, the damping constant that couples the surface unit to the thermal bath of the lattice. To determine a physically reasonable value for C, it is useful to consider the speed of sound in a Si crystal, which varies between 8.48×10^3 m/s and 9.40×10^3 m/s.[7] Taking an average speed of 9×10^3 m/s and the rough diameter of the surface oscillator to be 5×10^{-10} m, it should take around 4.5×10^{-12} s, about twenty-five times the 1.6×10^{-13} s period of the oscillator, for an excitation to dissipate into the lattice. A choice of C of 0.03 N-s/m empirically achieves roughly this dissipation rate.

Table II-2: Oscillator Properties for Various Silicon Surface Unit Choices

Si Surface Unit	Effective Mass (M)	Spring Constant (K)	Angular Frequency (ω)
Si-F	47 amu	117 N/m	3.87×10^{13} rad/s
F-Si-Si-F	94 amu	843 N/m	7.35×10^{13} rad/s
F-Si(Si$_2$)-Si(Si$_2$)-F	206 amu	47 N/m,	1.17×10^{13} rad/s

II.2.c Position at Initial Collision

Once the initial velocity of the gas molecule and the intrinsic characteristics of the silicon surface unit oscillator have been set, we are still free to specify the phase of the surface unit oscillation when the initial collision occurs. To fully characterize the possible dynamics of the collision of a gas molecule with the silicon surface, we need to sample the full range of possible initial conditions. However, a complication is introduced by the fact that we are defining initial conditions in terms of where in the surface unit's oscillation cycle the initial collision occurs. While every gas molecule incident on the surface will eventually collide with the surface unit, these collisions cannot necessarily occur at all points in the oscillation cycle.

The most obvious case of a physically impossible initial collision is one that occurs when the surface unit is moving towards the crystal at a higher velocity than the gas molecule: it's clearly impossible for the gas molecule to reach the surface unit for an initial collision in this situation. The molecule will reach the surface at a later point in the oscillation, which we should give as the initial condition instead. However, there is actually a larger "excluded zone" in which an initial condition cannot occur, as shown in Figure II-3. Even when the gas molecule is moving towards the crystal faster than the surface unit—in fact, even when the surface unit is moving away from the crystal—it can be impossible for a slow-moving gas molecule to reach the surface unit for an initial collision because it would have had to collide earlier. An extreme case of this situation is a gas molecule that is moving slowly enough that it covers less than twice the amplitude of the surface unit's oscillations during one period of the oscillator: it will never reach the inner (closest to the crystal) point in the oscillation without colliding with the surface unit while both are farther from the crystal. Such a gas molecule's actual initial condition should be specified at the time of that earlier collision. It is important to recognize that the existence of this "excluded zone" in the silicon oscillation in which an initial collision cannot occur is not an artifact of the model, but a fundamental consequence of the dynamics of the system: no matter where the silicon surface unit is when the gas molecule is first one silicon amplitude from the equilibrium point, the gas molecule will always have its first interaction with the surface outside the excluded zone.

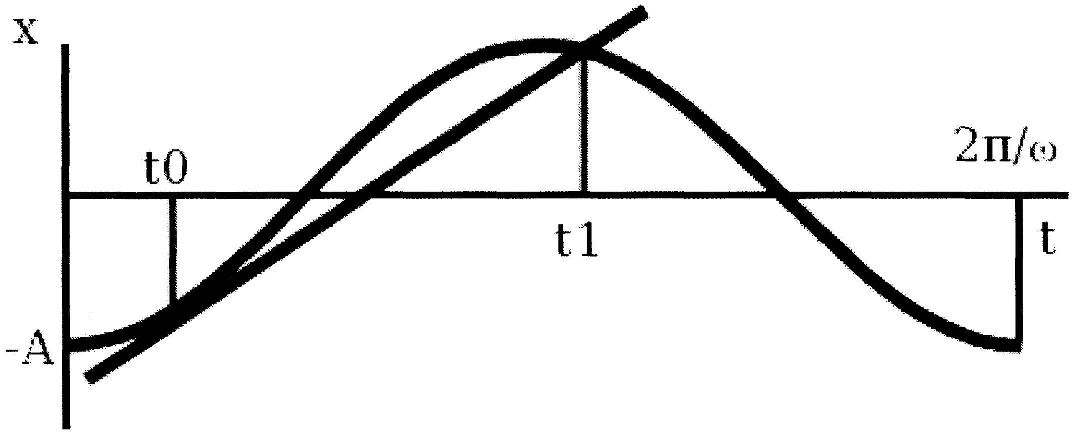

Figure II-3: Limitation on Position at Initial Collision

This plot shows the "excluded zone" between t_0 and t_1 where a gas molecule with velocity vt cannot collide with a silicon surface unit oscillator with amplitude A and frequency ω. Note that this excluded zone includes not only times when the silicon surface unit is moving towards the lattice faster than the gas molecule, but also times where—even if the silicon surface unit is moving away from the crystal—it is impossible for the gas molecule to reach the silicon surface unit without having collided with it at a previous time.

In order to be able to select a sampling of initial collision locations to test, we first need to determine the boundaries of the excluded zone. In doing so, we can consider the silicon surface unit to be an undamped simple harmonic oscillator, since the damping term only comes into effect once the oscillator has been pushed out of thermal equilibrium by the initial collision. While we are free to start our analysis with the oscillator in any position we wish, it is convenient to begin with it at its furthest distance from the crystal (outer turning point) and to define this position as $t = 0$. We will be considering the relative positions of the gas molecule,

$$x_{gas} = vt \text{ and } \dot{x}_{gas} = v$$

and the silicon surface oscillator,

$$X_{silicon} = -A\cos(\omega t) \text{ and } \dot{X}_{silicon} = A\omega\sin(\omega t),$$

where the direction into the crystal is positive, v is the initial velocity of the gas molecule, ω is the angular frequency of the silicon surface oscillator, and A is its amplitude.

At $\omega t = 0$, it is clearly possible for the gas molecule to reach the silicon surface unit for any positive value of v since the $X_{silicon}$ is at its most negative value and the oscillator is instantaneously stationary. As t increases, an initial collision will be possible until the surface unit and gas molecule have the same velocity. This point, t_0, occurs when

$$t_0 = \frac{1}{\omega}\arcsin\left(\frac{v}{A\omega}\right).$$

At a minimum, an initial collision will continue to be impossible until the velocity of the silicon surface unit drops back below that of the gas molecule.

In addition, if we plot the position of the silicon surface unit and the gas molecule, it is clear that any point in the oscillation of the surface unit above its tangent at t_0 will be inaccessible for a gas molecule with velocity v without having already collided with the surface unit. However, any point below this tangent line will be accessible. Thus, the excluded zone consists of the time period between t_0 and the tangent's second crossing of the surface unit's path, t_1. To find t_1, we merely need to find the equation for the tangent line,

$$x_{tangent} = v(t - t_0) - A\cos(\omega t_0),$$

set it equal to the equation for $X_{silicon}$ with t set to t_1,

$$A\cos(\omega t_1) + t_1 = A\cos(\omega t_0) + vt_0,$$

and solve for t to get an expression for t_1. Unfortunately, this expression for t_1 does not appear to be analytically solvable, so we'll have to solve it numerically for each of the sets of parameters we intend to run simulations on. Table II-3

shows the excluded zones for F_2, $Kr(F_2)$, XeF_2, and $Xe(F_2)$ molecules at 0.35 kcal/mol, 0.70 kcal/mol, 1.46 kcal/mol, and 3.00 kcal/mol.

Table II-3: Initial Collision Excluded Zones for Various Gas Molecule Parameters

Gas Molecule Average Translational Energy	Gas Molecule Mass	Excluded Zone Begins (ωt_0)	Excluded Zone Ends (ωt_1)	Excluded Zone Begins (X and Sign of V)	Excluded Zone Ends (X and Sign of V)
0.35 kcal/mol	**38 amu**	**66.1°**	**138.3°**	**$-0.405A$, (+)**	**$0.747A$, (+)**
0.35 kcal/mol	**122 amu**	**30.6°**	**217.1°**	**$-0.861A$, (+)**	**$0.798A$, (–)**
0.35 kcal/mol	**167 amu**	**25.7°**	**229.8°**	**$-0.901A$, (+)**	**$0.645A$, (–)**
0.70 kcal/mol	**38 amu**	N/A	N/A	N/A	N/A
0.70 kcal/mol	**122 amu**	**45.1°**	**180.8°**	**$-0.706A$, (+)**	**$1.000A$, (–)**
0.70 kcal/mol	**167 amu**	**37.9°**	**199.4°**	**$-0.789A$, (+)**	**$0.943A$, (–)**
1.46 kcal/mol	**38 amu**	N/A	N/A	N/A	N/A
1.46 kcal/mol	**122 amu**	N/A	N/A	N/A	N/A
1.46 kcal/mol	**167 amu**	**63.0°**	**144.7°**	**$-0.454A$, (+)**	**$0.816A$, (+)**
3.00 kcal/mol	**38 amu**	N/A	N/A	N/A	N/A
3.00 kcal/mol	**122 amu**	N/A	N/A	N/A	N/A
3.00 kcal/mol	**167 amu**	N/A	N/A	N/A	N/A

The gas molecule average translational kinetic energies given are used to determine the root mean square velocities of the gas molecules, which are then used to determine the excluded zones. In all cases, the spring constant is $K = 117$ N/m, the angular frequency is $\omega = 3.87\times10^{13}$ rad/s, the surface temperature is $T = 250$ K, the oscillator equilibrium energy is $E = 0.497$ kcal/mol and the amplitude is $A = 7.86\times10^{-12}$ m. The angular definition of the excluded zone, ωt, is based on the phase choice that $X = -A\cos(\omega t)$. The boundaries of the excluded zone are also given in terms of the position and sign of the velocity of the surface unit because such is the format that the program described in Section II.3 takes initial condition input.

II.2.d Time Step

Although it is not a physical property of the model, the choice of a collision-checking time step, *dt*, is essential for implementing it. Since the equation of motion for the silicon surface unit cannot be analytically solved, the model can only be implemented as a numerical simulation. As such, time steps need to be set for two purposes in any implementation of the model. A collision-checking time step serves to determine how frequently the simulation checks the relative positions of the gas molecule and silicon surface unit to determine if a collision has occurred. A numerical integration time step sets the time scale for the numerical integration routine. The collision-checking time step must be an integer multiple of the numerical integration time step to allow numerical integration of the change in silicon velocity and position over one collision-checking time step.

The accuracy of the simulation is improved by minimizing both time steps, since numerical integration is more accurate with a shorter time step and a shorter collision-checking time step reduces the error in deciding where a collision occurs. However, shortening the time step will produce a significant increase in the time required to run the simulation, since it will increase the number of calculations and disk operations (to record the state of the system at each time step for plotting) needed. A collision-checking time step, *dt*, of 10^{-16} s (0.1 fs), which allows for roughly 10^3 time steps per surface unit oscillation, has been chosen as a compromise. A numerical integration time step of 10^{-17} s (0.01 fs, one-tenth the collision-checking time step) was chosen to keep the two time steps similar in size rather than improving the accuracy of one at the expense of reducing the accuracy of the other to maintain a reasonable computation time.

II.3 The Simulation Program

II.3.a Overview

To implement the silicon-gas collision model, a numerical simulation was written in the Python 2.7 programming language using the SciPy and NumPy libraries. The code for the simulation can be found in the Appendix. It consists of three basic parts: a section that prompts the user for initial conditions and initializes various variables, a section consisting of definitions of functions needed to detect and evaluate collisions and to change the states of the gas molecule and oscillator between time steps, and a large "simulation loop" which iterates over time, processing the state of the system and writing it to output files at the end of each time step.

For simplicity, the program's function and variable names and internal comments refer to the gas molecule as "the fluorine molecule" and the silicon surface unit as "the silicon atom". Upper-case letters are used for variables relating to the silicon surface unit; lower-case letters are used for variables relating to the gas molecule. Furthermore, while initial conditions are specified at the time of the first collision, the simulation actually starts one thousand time steps earlier, to allow visualization of the trajectories of the fluorine and silicon before the first collision. Although some initial conditions are prompted for in non-SI units and some outputs are given in non-SI units for convenience, all internal calculations are done in SI units to reduce the need for unit-conversion constants and to avoid any ambiguity about the units of the value stored in any given variable.

II.3.b Initial Conditions Set-Up

The first section of the simulation program consists of a collection of statements needed to set up initial conditions of the functions and main simulation loop of the program. These initial conditions come in two basic types: ones that are written directly into the code, and ones that the user is prompted for each time the code is run. The hard-coded initial conditions are largely fundamental constants and unit conversions: `k_B` is Boltzmann's constant, `N_A` is Avogadro's number, `amu` is the value of an atomic mass unit in kilograms, and `kcal` is the value of one joule per molecule in kilocalories per mole.

Three modeling choices are hard-coded into the program. The initial conditions section sets `x_escape`, the distance measured in units of the equilibrium silicon amplitude, that the gas molecule must escape to for the simulation to terminate to -10. (Once the silicon initial conditions are entered by the user, the program converts `x_escape` to meters.) The silicon time step evaluation function, `step_XV`, is hard-coded to numerically integrate the silicon position and velocity over ten mini-time steps between each step of the simulation loop. Finally, the start of the simulation one thousand time steps before the first collision is hard-coded at two separate points in the program. At the end of the initial conditions set-up section, the initial conditions for the gas molecule are moved back one thousand time steps. And in the beginning of the simulation loop, the initial conditions for the silicon surface unit are moved back one thousand time steps.

In addition to initializing hard-coded values, the initial conditions set-up section of the program prompts the user for a number of initial conditions. The silicon surface unit and gas molecule effective masses are prompted for in atomic mass units and converted to kilograms to be stored in the variables `M` and `m`. The silicon surface temperature, `T`, spring constant, `K`, and damping constant, `C`, as well as the initial gas molecule velocity, `v_i`, and collision-checking time step, `dt`, are also prompted for in this way. In addition, the user is prompted for a string, `outputfile`, that will form the basis for the names of the two output files generated by the program, [outputfile].txt and [outputfile].csv. If files with these names already exist, they will be overwritten, so the user must be careful to ensure that unique names are supplied.

Defining the starting position for the silicon surface unit is somewhat more complicated. The values of `M`, `K`, and `T` define the oscillator's angular frequency, `Omega`, equilibrium energy, `E`. and amplitude, `X_max`. However, the user needs to specify where in its oscillation the silicon atom should be at the first collision. The surface unit position is set by inputting the sign of the initial velocity and the initial position as a fraction of the amplitude. The position of the surface unit at the time of the first collision, `X_i`, is then converted to meters and the magnitude of the initial velocity, `V_i`, is calculated from conservation of energy. The initial position of the gas molecule, `x_i`, is the same as that of the surface unit.

II.3.c Collision Detection and Evaluation Functions

Four functions are used to handle collisions between the incoming molecule and the silicon surface unit: one to determine when a collision has occurred, two to adjust the velocities of the incoming molecule and silicon surface unit (the positions are unchanged, since the collision is treated as instantaneous), and one to report the energy change due to the collision. The collision-detection function, `collision(x0,x1,X0,X1)`, takes as its inputs the positions of the gas molecule (lower-case) and silicon surface unit (upper-case) before and after the most recent time step. It then performs two tests. First, it checks to see if `x1` = `X1`; if so, the surface unit and gas molecule are in the same position after the most recent time step, indicating that a collision has occurred. Second, it checks to see if `x0 - X0` and `x1 - X1` have the same sign; if they don't, the surface unit and gas molecule have passed each other between the last two time steps, indicating that a collision has occurred. If either test indicates a collision, the function returns 1; otherwise it returns 0.

The `collision_V(v0,V0,m,M)` and `collision_v(v0,V0,m,M)` functions output the respective velocities of the silicon surface unit and gas molecule after a collision, calculated using the elastic collision equations derived in Section II.1.b . Both functions take the same inputs: the masses and pre-collision velocities of the gas molecule (lower-case) and silicon surface unit (upper-case). A third function, `collision_trans(v0,v1,m)`, takes the mass of the fluorine molecule and its velocities before and after the collision and outputs the energy transferred from the fluorine molecule to the silicon surface unit during the collision.

II.3.d Time Step Evaluation Functions

Each time the main simulation loop iterates, it steps the positions and velocities of the gas molecule and silicon surface unit forward by one step and checks to see if a collision has occurred. Since the gas molecule has a constant velocity except during collisions, the two functions used to advance it by one time step are simple. Both take the length of the time step and the position and velocity of the gas molecule at the start of the time step as inputs. The position function, `step_x(x0,v0,dt)`, simply adds the product of the time step length and velocity to the current position to return the new position. Meanwhile, the velocity function, `step_v(x0,v0,dt)`, just returns the current velocity as the new velocity: the function is primarily included to make the simulation loop more symmetrical.

Time step evaluation for the silicon surface unit is more complicated, since its equation of motion derived in Section II.1.c can't be solved analytically. Instead, it is integrated numerically using the `integrate.odeint` routine from the SciPy library. The second-order differential equation is broken into a system of two first-order differential equations. This system is defined by two functions, `F(y,t_range_M,K,Omega,CE)` and `jacobian(y,t_range_M,K,Omega,C,E)`, as required by the `integrate.odeint` routine. The function `step_XY(X0,V0,dt,t,M,K,Omega,C,E)` is then used to integrate the system in time steps one-tenth the duration of the collision-checking time step `dt`. (The modeling choice to use a factor of ten difference in these time steps is hard-coded into the definition of the variable `t_range` in the first line of the function.) The output of the function is an n-by-2 array whose last row consists of the position and velocity of the silicon surface unit at the end of the time step. These values must be extracted by the simulation loop after it calls the function.

II.3.e Main Simulation Loop

The main component of the program is the simulation loop, which iterates over time in small steps, calling functions to calculate the new positions and velocities of the gas molecule and silicon surface unit and detect and evaluate any collisions that occur. It begins with some initializations that cannot be performed until the functions have been defined. The gas initial position was moved back one thousand time steps during the initial conditions input section of the program, but to move the silicon position back equivalently, the `step_XV` function needs to be used. Since the numerical integration routine it uses can't deal with a negative time step, the velocity of the surface unit is instead reversed and the new initial velocity is taken as the negative of the output velocity. Once this is done, the variables `E_counter`, which is a sum of the energy transfer that occurs in each collision, `coll`, which is 0 if no collision has occurred during the current time step and 1 otherwise, and `coll_counter`, which is a sum of the number of collisions that have occurred up to the current time step are initialized at 0.

Separate variables `t` and `t_counter` are also initialized at this point. Together, they are used to track the time of the current time step. Two variables are needed because we need to know both the total time since the start of the simulation and the time since the last collision. The total time since the start of the simulation at each time step is printed to the output files along with the other system-state information so that the state of the system as a function of time can be plotted. However, since the time step evaluator functions can only be used between collisions, we cannot use this total time to calculate time steps. Since the gas molecule time steps are analytically calculated and have no calculation error, it does not matter whether they are calculated from the last time step or the last collision. However, the numerical integration routine used for silicon time steps will build up error faster if it is used for a series of small time steps instead of one long one with the same total time, so the variable `t` is used to track time since the last collision. For each collision-checking time step, `t` is increased by `dt` and the states of the gas molecule and silicon surface unit are recalculated at the new value of `t`. Each time a collision occurs, the value of `t_counter` is increased by `t` and `t` is then reset to 0.

Next, the two output files (discussed in Section II.3.f) are created and headings are written to them. Once done, the main loop begins. It is structured as a "while true" loop: the loop will continue until it reaches an explicit command to end it. This command will be triggered by an "if" statement at the end of the loop that activates if the gas molecule is ever more than ten times the amplitude of the equilibrium silicon oscillation from the surface. Once triggered, the program closes the output files and terminates.

Each cycle of the loop increases `t` by `dt` and uses the time step functions to recalculate the positions and velocities of the gas molecule and silicon surface unit for the new value of `t`. It then uses the collision-detection function to check whether a collision has occurred. If so, an if statement is triggered to run the collision-evaluation functions, and adjust the values of `t`, `t_counter`, `E_counter`, and `coll_counter` appropriately.

II.3.f Output Files

When the gas molecule escapes to more than ten times the equilibrium amplitude of the silicon surface unit, the simulation terminates and the program reports the net energy transferred from the gas molecule to the surface unit, the net energy transferred from the surface unit to the lattice thermal bath, and the number of collisions that occurred. It also saves two output files with filenames ending in ".txt" and ".csv". The .csv file contains a record of the state of the system at each time step and is intended to be uploaded into a plotting program such as IgorPro; the .txt file is intended as a human-readable summary of this file and only records the state of the system at time steps in which collisions occurred, as well as one time step before and after each collision. The .txt file also ends with the same report—of the net energy transferred from the gas molecule to the silicon surface unit, the net energy transferred from the surface unit to the lattice thermal bath, and the number of collisions that occurred—that the program prints to the screen when it terminates. This information is left out of the .csv file to avoid confusing plotting programs.

Both output files begin with a report of the initial conditions of the simulation: the silicon surface unit mass and gas molecule mass in atomic mass units, the silicon spring constant in newtons per meter, the silicon surface temperature in Kelvin, the silicon energy at thermal equilibrium in kilocalories per mole, and the silicon amplitude at thermal equilibrium in meters. The eighth line of each file consists of tab-separated headings for the system-state data and the tab-separated data begins on the ninth line. The data columns provided are the time in seconds since the start of the simulation, the position of the gas molecule in meters, the velocity of the gas molecule in meters per second, the energy of the gas molecule in kilocalories per mole, the position of the silicon surface unit in meters, the velocity of the silicon surface unit in meters per second, the energy of the silicon surface unit in kilocalories per mole, and a Boolean variable that is 1 if a collision occurred during a given time step and 0 otherwise.

Two potential output conditions deserve special notice. First of all, if the gas molecule and silicon surface unit collide with a very low relative velocity, they may remain in contact for an extended period of time as the changing spring force on the silicon surface unit keeps its velocity aligned with that of the gas molecule which is being accelerated by the surface unit. However, since the simulation checks for a collision at each time step and reports one if the gas molecule and silicon surface unit are in contact during that time step, the program will report that a collision has occurred during each time step that they are in contact. This situation does not impair the energy transfer calculations—in fact it is essential to them, since detecting a collision triggers the calculation of energy transfer due to the gas molecule and silicon surface unit being in contact—but it does mean that surprisingly high "collision counts" will be reported in these situations.

The second special output condition, on the other hand, occurs in some (but not all) circumstances in which the user-provided initial conditions are invalid. As discussed in Section II.2.c , for a given initial gas molecule velocity and silicon surface unit mass and energy, it is not always possible for the initial collision to occur at all points in the silicon atom's oscillation. Specifically, there is no way that the gas molecule can first reach the silicon surface unit to collide with it at points in the surface unit's oscillation where it is moving towards the crystal faster than the gas molecule is moving towards the surface. At other points in the silicon surface unit's oscillation, the gas molecule may be moving towards the crystal faster than the silicon surface unit, but it is impossible for it to reach it without having already collided with the surface unit at an earlier point. If the user attempts to run a simulation with the initial collision occurring at such a point, the initial step backwards one thousand time steps may move the surface unit further from the crystal than the gas molecule. As a result, the initial collision will occur with the gas molecule already "below the surface" and will simply push it farther in that direction. When this occurs, the program will report that the gas molecule "fell through the surface". It is important to keep in mind, however, that not all physically invalid initial condition settings will result in this message. In some cases, moving the system one thousand time steps backward from a physically invalid initial collision may result in a collision at an earlier point than specified, or may result in a collision at the specified point even though in reality the gas molecule could never reach that point without having already collided with the surface unit.

II.4 Results

II.4.a Simulations with 1.46 kcal/mol Gas Molecules

As discussed in Section II.2.a , the first goal of the simulation of the gas-silicon interaction was to model the experimental conditions that have actually been used. To this end, a series of runs were done with a silicon crystal at 250 K and each of F_2 (38 amu), Kr(F_2) (122 amu), and XeF_2 or Xe(F_2) (both 167 amu). Each molecule was tested using initial collisions with the silicon surface unit when it was at its maximum extension towards and away from the crystal and when it was at its maximum velocities towards and away from the crystal, except that there was no test with XeF_2 and the silicon surface unit at maximum velocity towards the crystal, since a collision at this position is impossible, as discussed in Section II.2.c . The results from these runs are summarized in Table II-4 and the changes in surface unit and gas molecule energy and position are plotted in Figure II-4, Figure II-5, and Figure II-6.

As expected, the number of collisions that occurred was greater for the more massive gas molecules. However, there was also a significant variation in the number of collisions depending on the position of the silicon surface unit at the initial collision: in fact, the F_2 molecule had more collisions with the surface unit when the first collision happened at the surface unit's maximum velocity towards the crystal than the XeF_2/Xe(F_2) molecule had when the first collision happened at the surface unit's maximum velocity away from the crystal. In general, more collisions were observed when the first collision happened with the silicon surface unit at its maximum velocity or maximum extension towards the surface.

The number of collisions that occurs, though, does not directly affect the probability of a reaction. The two factors considered in this model that are potentially related to the probability of a collision are the gas molecule's residence time on the surface—since a longer residence time provides more time for a collision to occur—and the transfer of kinetic energy from the gas molecule into the bonds adjacent to the collision site—since this bond excitation may provide needed activation energy to allow the reaction to occur.

There are several ways that one can evaluate the gas molecule's residence time on the surface. However, the hard-sphere model used here is best adapted to evaluating it in terms of the amount of time between the first and last collisions with the surface. While the length of time does correlate positively with the number of collisions, the relationship is less than linear: as the number of collisions increases, the length of time between collisions decreases, so the residence time grows more slowly than the number of collisions. There was significant overlap in the ranges of interaction times with the surface, but the longest $Kr(F_2)$ and $XeF_2/Xe(F_2)$ interactions were 65% longer than the longest F_2 interactions with the surface.

In every simulation, it turned out that the energy of the silicon surface unit was at its maximum immediately after the first collision. Additional collisions sometimes added additional energy to the surface unit, but never more than had been lost to the lattice since the first collision. Furthermore, there was no significant variation between the gas molecules in terms of the maximum excitation achieved. In each case, one location of the initial condition produced a maximum excitation of 1.9 kcal/mol, very close to the total initial energy of the system, 1.96 kcal/mol (0.50 kcal/mol from the surface oscillator at equilibrium and 1.46 kcal/mol from the incoming gas molecule).

While the similar maximum excitations suggest that the difference in reactivity between F_2 and XeF_2 cannot be attributed to higher energy transfer to the Si-Si bonds, it is still possible that the difference in the length of surface excitations is important. In most cases where multiple collisions occurred, the final collision transferred enough energy back to the gas molecule to drop the surface unit's energy to its initial 0.5 kcal/mol or even lower. However, simply measuring the length of the excitation as the length of time between the first and last collision doesn't take into account that the surface unit loses energy to the lattice between collisions, and does not work for single-collision interactions. Without knowledge of the actual amount of excitation needed to push the reaction over the activation barrier—assuming, of course, that mechanical excitation of the bonds is actually needed to activate the reaction—any energy cut-off chosen to identify the boundary of the excitation is only an educated guess. However, 1 kcal/mol is a natural choice of a cut-off, since it is the point where half of the initial energy in the system is in the silicon oscillator, as well as being the point where the silicon oscillator has twice its energy at equilibrium.

Using this 1 kcal/mol cut-off, we find that the longest excitation produced by a F_2 collision is 100 fs when only a single collision between the gas molecule and surface unit occurs. $Kr(F_2)$ consistently produces excitations slightly shorter than this—80 or 90 fs—even when its total surface interaction is longer. The excitations produced by collisions with XeF_2 or $Xe(F_2)$ molecules, however, were noticeably longer, up to 160 fs. It is worth noting, however, that the shortness of the $Kr(F_2)$ and $XeF_2/Xe(F_2)$ excitations may be an artifact of the simplicity of this one-dimensional model. The surface unit oscillator can only lose energy to the lattice when it is actively oscillating. These simulation results show that it is able to continue oscillating between collisions with the surface, but in a three-dimensional model simulating multiple bonds and with finite molecular diameters, it is possible that the heavy gas molecules would restrain some of these bonds from oscillating during their residence time on the surface.

Initial Collision at Outer Turning Point

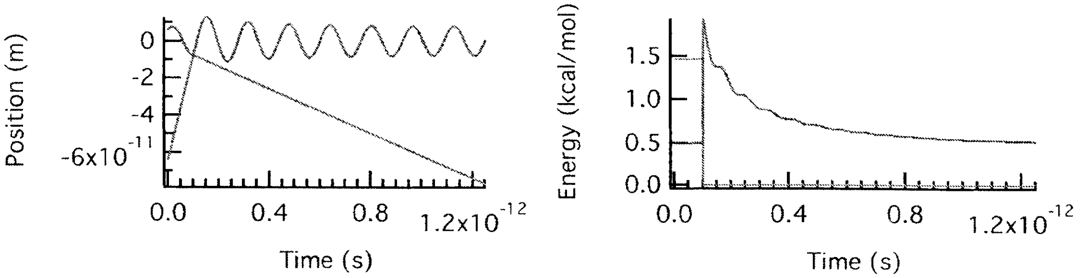

Initial Collision at Equilibrium Position, Moving Towards Crystal

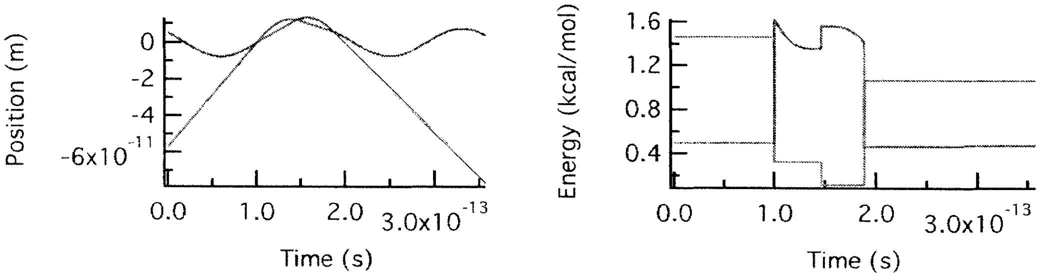

Initial Collision at Inner Turning Point

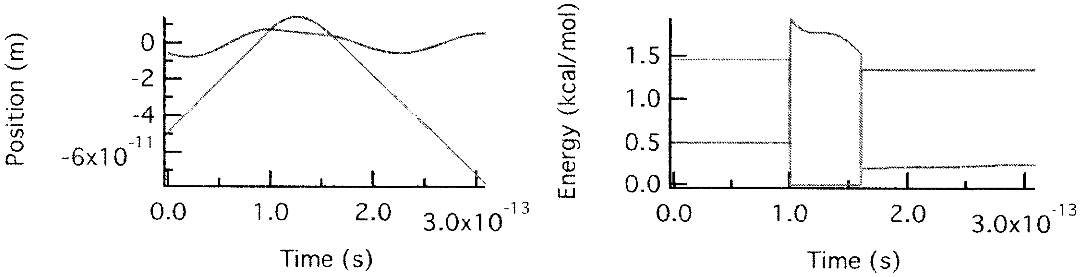

Initial Collision at Equilibrium Position, Moving Away from Crystal

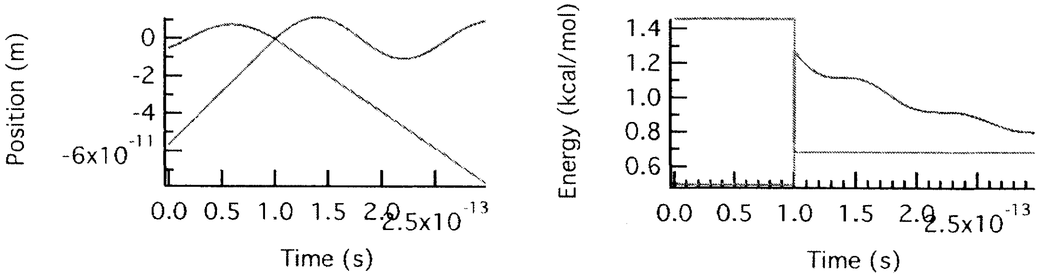

Figure II-4: Si and F_2 Trajectories and Energies at 1.46 kcal/mol

The trajectories and energies of the Si surface unit (blue) and F_2 molecule (red) are plotted for an initial F_2 velocity of 567 m/s. All simulations were run with a model silicon crystal consisting of a surface unit with a mass of 47 amu and a spring constant of 117 N/m coupled to a thermal bath at 250 K by a damping constant of 0.03.

Initial Collision at Outer Turning Point

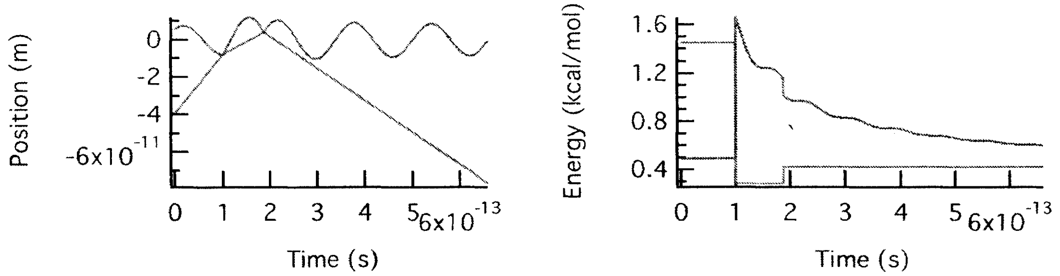

Initial Collision at Equilibrium Position, Moving Towards Crystal

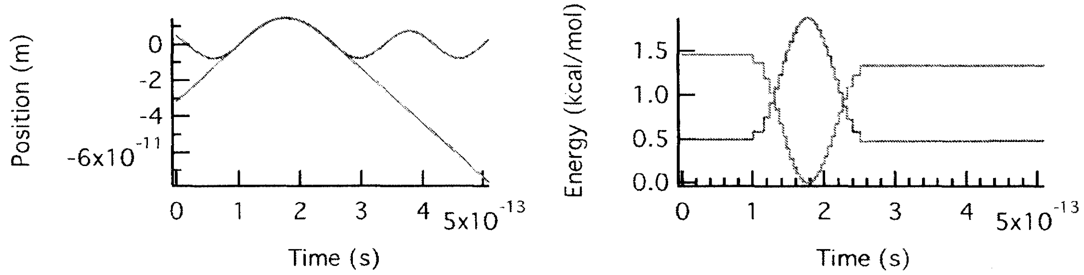

Initial Collision at Inner Turning Point

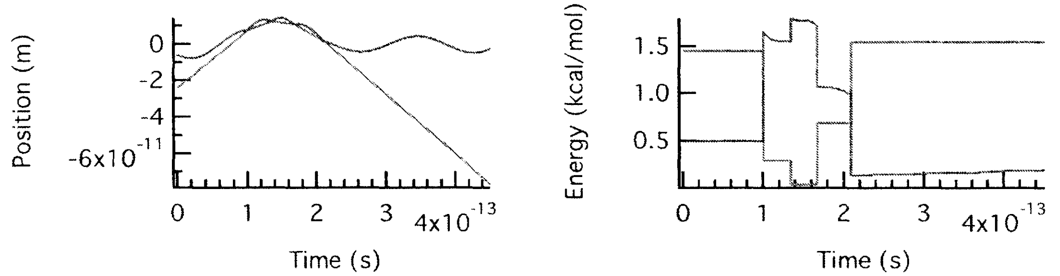

Initial Collision at Equilibrium Position, Moving Away from Crystal

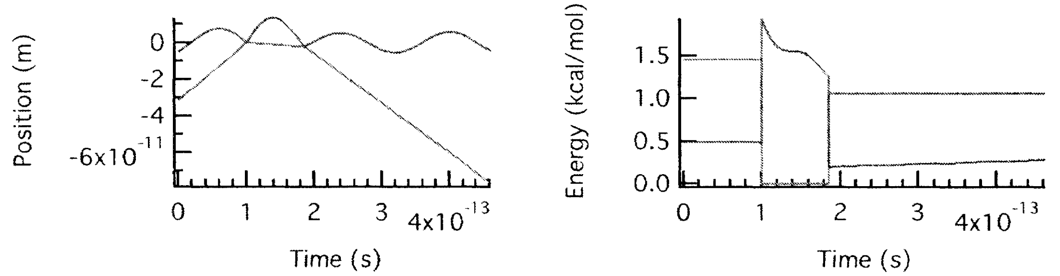

Figure II-5: Si and Kr(F_2) Trajectories and Energies at 1.46 kcal/mol

The trajectories and energies of the Si surface unit (blue) and Kr(F_2) cluster (red) are plotted for an initial Kr(F_2) velocity of 316 m/s. All simulations were run with a model silicon crystal consisting of a surface unit with a mass of 47 amu and a spring constant of 117 N/m coupled to a thermal bath at 250 K by a damping constant of 0.03.

Initial Collision at Outer Turning Point

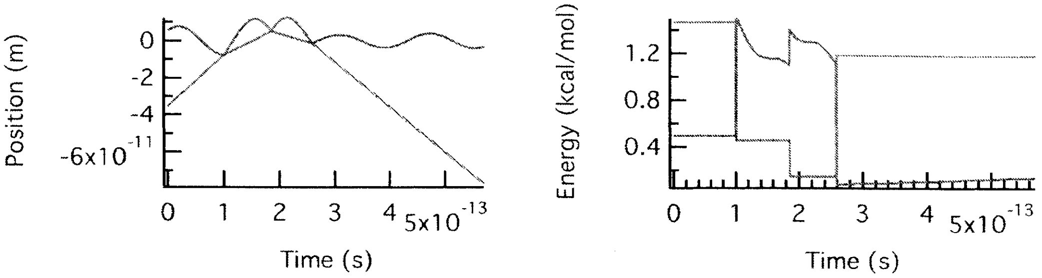

Initial Collision at Inner Turning Point

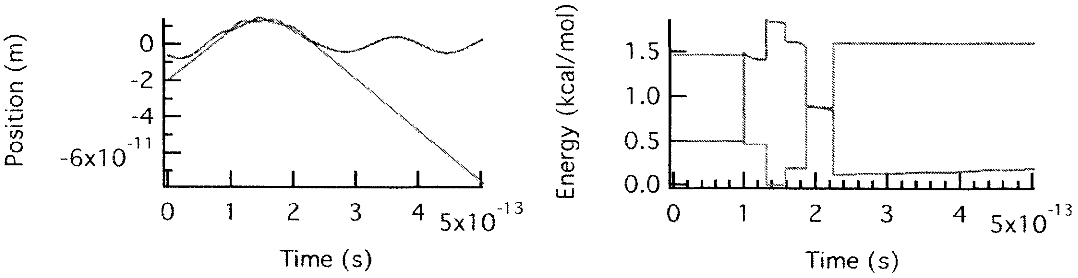

Initial Collision at Equilibrium Position, Moving Away from Crystal

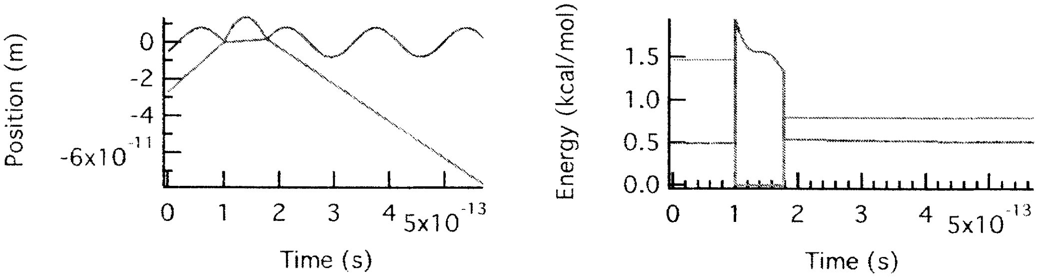

Figure II-6: Si and XeF_2 or $Xe(F_2)$ Trajectories and Energies at 1.46 kcal/mol

The trajectories and energies of the Si surface unit (blue) and XeF_2 molecule or $Xe(F_2)$ cluster (red) are plotted for an initial XeF_2 or $Xe(F_2)$ velocity of 271 m/s. All simulations were run with a model silicon crystal consisting of a surface unit with a mass of 47 amu and a spring constant of 117 N/m coupled to a thermal bath at 250 K by a damping constant of 0.03.

Table II-4: Silicon-Gas Molecule Interactions at 1.46 kcal/mol

Gas Molecule	Initial Silicon ωt	Number Of Collisions	Maximum Surface Excitation	Time Above 1 kcal/mol	Length of Surface Contact
F_2	0°	1	1.9 kcal/mol	100 fs	instantaneous
F_2	90°	3	1.5 kcal/mol	90 fs	90 fs
F_2	180°	2	1.9 kcal/mol	60 fs	60 fs
F_2	270°	1	1.3 kcal/mol	100 fs	instantaneous
$Kr(F_2)$	0°	2	1.6 kcal/mol	90 fs	90 fs
$Kr(F_2)$	90°	27	1.9 kcal/mol	90 fs	150 fs
$Kr(F_2)$	180°	4	1.8 kcal/mol	80 fs	110 fs
$Kr(F_2)$	270°	2	1.9 kcal/mol	90 fs	90 fs
XeF_2 / $Xe(F_2)$	0°	3	1.5 kcal/mol	160 fs	160 fs
XeF_2 / $Xe(F_2)$	90°	N/A	N/A	N/A	N/A
XeF_2 / $Xe(F_2)$	180°	5	1.8 kcal/mol	120 fs	120 fs
XeF_2 / $Xe(F_2)$	270°	2	1.9 kcal/mol	80 fs	80 fs

Values of ωt are defined for $x(t) = -A\cos(\omega t)$, i.e. with $\omega t = 0°$ at the outer turning point, 90° at the equilibrium position moving towards the crystal, 180° at the inner turning point, and 270° at the equilibrium position moving away from the crystal. "Surface contact" is defined as the time from the first to last collision. The 1 kcal/mol threshold was selected because it is the half the total initial energy of the system (gas molecule and surface unit). The 27 collisions for $Kr(F_2)$ at $\omega t = 90°$ are an artifact of the finite time step used: the collisions happen with only one or two time steps between them, and the gas molecule and surface unit are best understood as in constant contact at matched velocities.

II.4.b Simulations with 3.00 kcal/mol Gas Molecules

In addition to the 1.46 kcal/mol simulations, a series of simulations was run with the gas molecule energy roughly doubled, to 3.00 kcal/mol. The results of these simulations are summarized in Table II-5 and the changes in surface unit and gas molecule energy and position are plotted in Figure II-7, Figure II-8, and Figure II-9. Unsurprisingly, much more energetic gas molecules can excite the surface unit to higher maximum energies. However, while the surface residence time is a bit higher for Kr(F_2) and XeF_2/Xe(F_2) than at 1.46 kcal/mol, it is actually lower for F_2 than it was at 1.46 kcal/mol. If we again measure the length of the surface excitation as the time that the surface unit has more than half the energy in the system—this time 1.75 kcal/mol—we find that the excitation times are similar or a bit shorter than at 1.46 kcal/mol. However, in a number of cases—even with multiple collisions—the time above 1.0 kcal/mol is longer than at 1.46 kcal/mol, since the energy of a more-excited oscillator dissipates into the lattice more slowly.

Initial Collision at Outer Turning Point

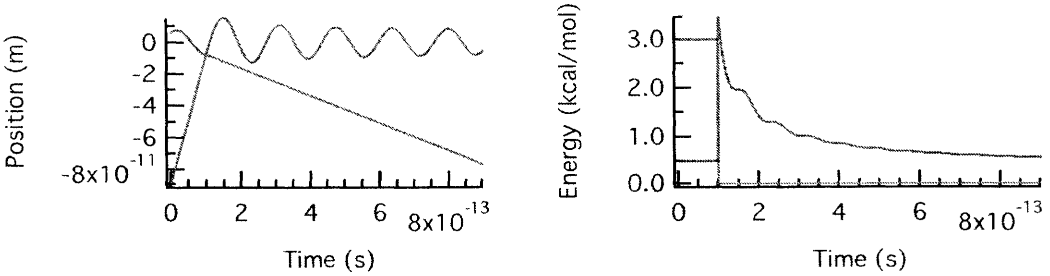

Initial Collision at Equilibrium Position, Moving Towards Crystal

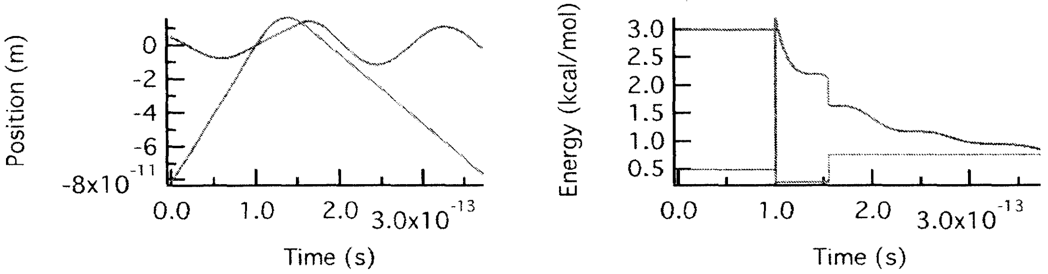

Initial Collision at Inner Turning Point

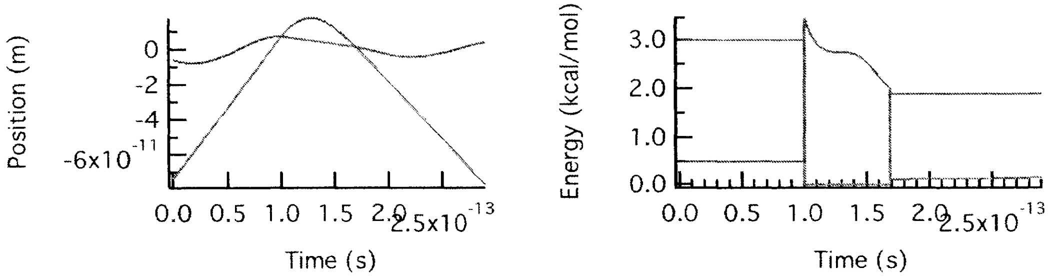

Initial Collision at Equilibrium Position, Moving Away from Crystal

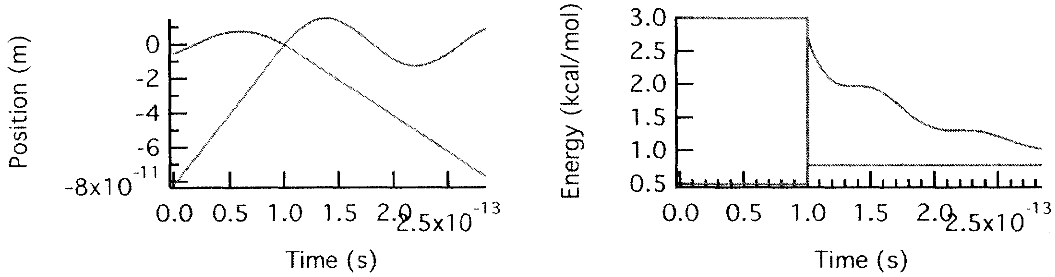

Figure II-7: Si and F_2 Trajectories and Energies at 3.00 kcal/mol

The trajectories and energies of the Si surface unit (blue) and F_2 molecule (red) are plotted for an initial F_2 velocity of 813 m/s. All simulations were run with a model silicon crystal consisting of a surface unit with a mass of 47 amu and a spring constant of 117 N/m coupled to a thermal bath at 250 K by a damping constant of 0.03.

Initial Collision at Outer Turning Point

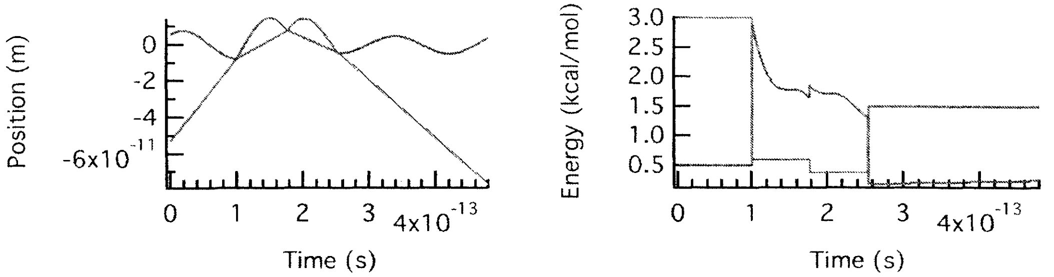

Initial Collision at Equilibrium Position, Moving Towards Crystal

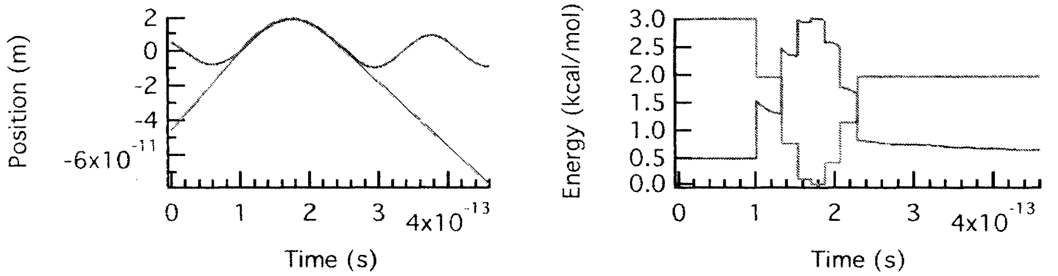

Initial Collision at Inner Turning Point

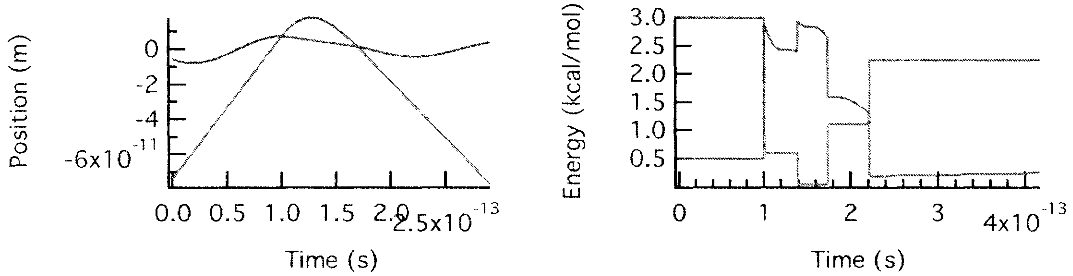

Initial Collision at Equilibrium Position, Moving Away from Crystal

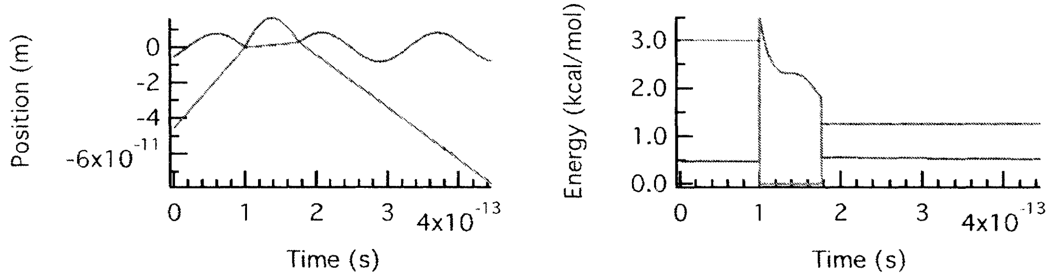

Figure II-8: Si and Kr(F_2) Trajectories and Energies at 3.00 kcal/mol

The trajectories and energies of the Si surface unit (blue) and Kr(F_2) cluster (red) are plotted for an initial Kr(F_2) velocity of 454 m/s. All simulations were run with a model silicon crystal consisting of a surface unit with a mass of 47 amu and a spring constant of 117 N/m coupled to a thermal bath at 250 K by a damping constant of 0.03.

Initial Collision at Outer Turning Point

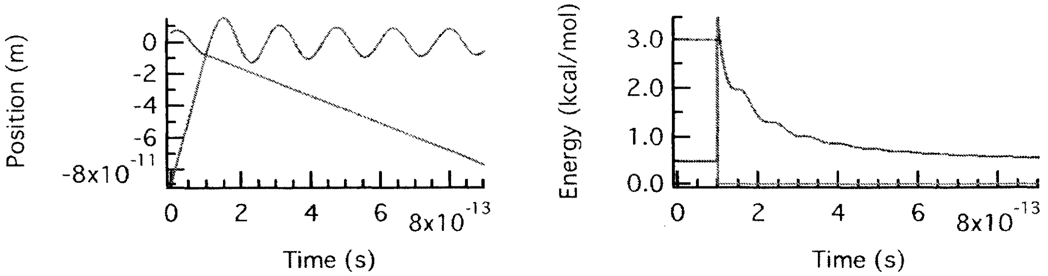

Initial Collision at Equilibrium Position, Moving Towards Crystal

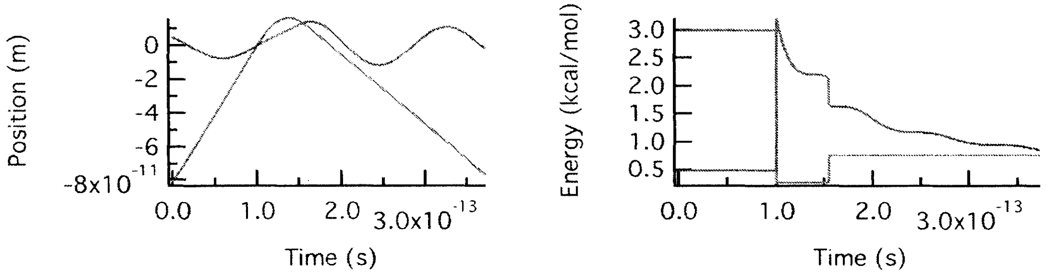

Initial Collision at Inner Turning Point

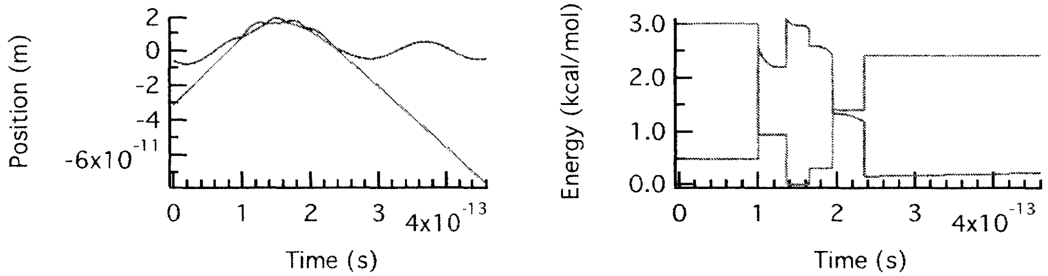

Initial Collision at Equilibrium Position, Moving Away from Crystal

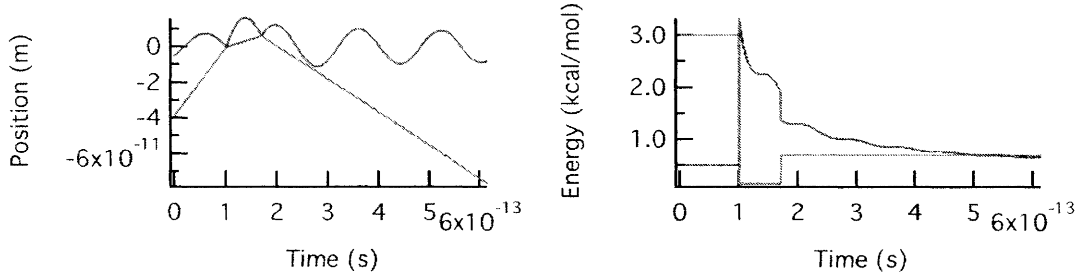

Figure II-9: Si and XeF_2 or $Xe(F_2)$ Trajectories and Energies at 3.00 kcal/mol

The trajectories and energies of the Si surface unit (blue) and XeF_2 molecule or $Xe(F_2)$ cluster (red) are plotted for an initial XeF_2 or $Xe(F_2)$ velocity of 388 m/s. All simulations were run with a model silicon crystal consisting of a surface unit with a mass of 47 amu and a spring constant of 117 N/m coupled to a thermal bath at 250 K by a damping constant of 0.03.

Table II-5: Silicon-Gas Molecule Interactions at 3.00 kcal/mol

Gas Molecule	Initial Silicon ωt	Number Of Collisions	Maximum Surface Excitation	Time Above 1.75 kcal/mol	Length of Surface Contact
F_2	0°	1	3.5 kcal/mol	90 fs	instantaneous
F_2	90°	2	3.2 kcal/mol	50 fs	50 fs
F_2	180°	2	3.5 kcal/mol	70 fs	70 fs
F_2	270°	1	2.7 kcal/mol	70 fs	instantaneous
$Kr(F_2)$	0°	3	2.9 kcal/mol	120 fs	150 fs
$Kr(F_2)$	90°	7	3.0 kcal/mol	100 fs	130 fs
$Kr(F_2)$	180°	4	2.9 kcal/mol	70 fs	120 fs
$Kr(F_2)$	270°	2	3.5 kcal/mol	80 fs	80 fs
XeF_2 / $Xe(F_2)$	0°	3	2.5 kcal/mol	130 fs	130 fs
XeF_2 / $Xe(F_2)$	90°	12	3.2 kcal/mol	110 fs	150 fs
XeF_2 / $Xe(F_2)$	180°	5	3.1 kcal/mol	90 fs	130 fs
XeF_2 / $Xe(F_2)$	270°	2	3.3 kcal/mol	70 fs	70 fs

Values of ωt are defined for $x(t) = -A\cos(\omega t)$, i.e. with $\omega t = 0°$ at the outer turning point, 90° at the equilibrium position moving towards the crystal, 180° at the inner turning point, and 270° at the equilibrium position moving away from the crystal. "Surface contact" is defined as the time from the first to last collision. The 1.75 kcal/mol threshold was selected because it is the half the total initial energy of the system (gas molecule and surface unit).

II.4.c Simulations with 0.70 and 0.35 kcal/mol Gas Molecules

Simulations were also run at lower gas molecule energies: 0.70 kcal/mol and 0.35 kcal/mol, the latter of which has the interesting property that the velocity of F_2 at 0.35 kcal/mol is very nearly the same as that of XeF_2 or $Xe(F_2)$ at 1.46 kcal/mol. The results of these simulations are summarized in Table II-6 for 0.70 kcal/mol and Table II-7 for 0.35 kcal/mol. The plots are shown in Figure II-10, Figure II-11, and Figure II-12 for 0.35 kcal/mol and Figure II-13, Figure II-14, and Figure II-15 for 0.35 kcal/mol.

Reducing the energy of the incoming gas molecule both makes the excluded zones described in Section II.2.c larger and generally reduces the number of collisions that occur. It also, of course, reduces the maximum surface excitation, although each molecule is still capable of exciting the surface to the point where it contains nearly all of the energy initially in the system. However, the residence time—at least when defined in terms of the time between first and last collisions—is not significantly increased. At 0.35 kcal/mol, the maximum residence time for F_2 molecules is still half the minimum residence time for XeF_2 or $Xe(F_2)$ molecules at 1.46 kcal/mol, even though the incident velocities of F_2 and XeF_2 or $Xe(F_2)$ are equivalent.

Initial Collision at Outer Turning Point

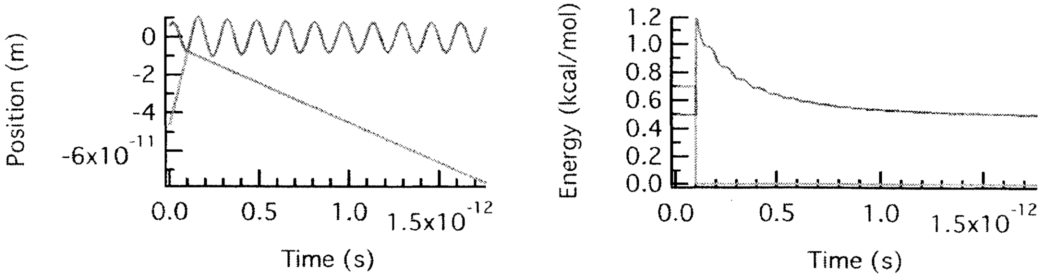

Initial Collision at Equilibrium Position, Moving Towards Crystal

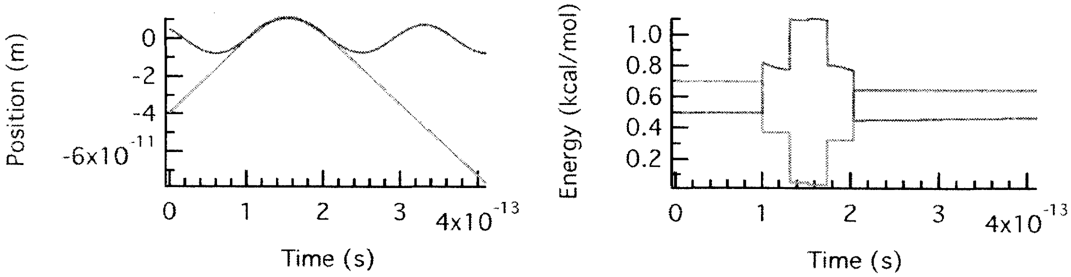

Initial Collision at Inner Turning Point

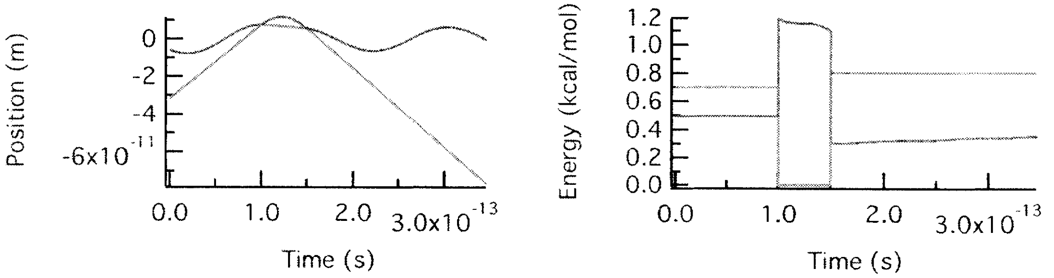

Initial Collision at Equilibrium Position, Moving Away from Crystal

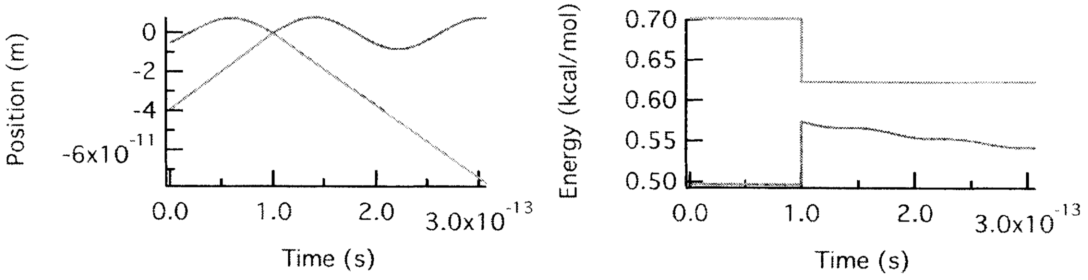

Figure II-10: Si and F_2 Trajectories and Energies at 0.70 kcal/mol

The trajectories and energies of the Si surface unit (blue) and F_2 molecule (red) are plotted for an initial F_2 velocity of 393 m/s. All simulations were run with a model silicon crystal consisting of a surface unit with a mass of 47 amu and a spring constant of 117 N/m coupled to a thermal bath at 250 K by a damping constant of 0.03.

Initial Collision at Outer Turning Point

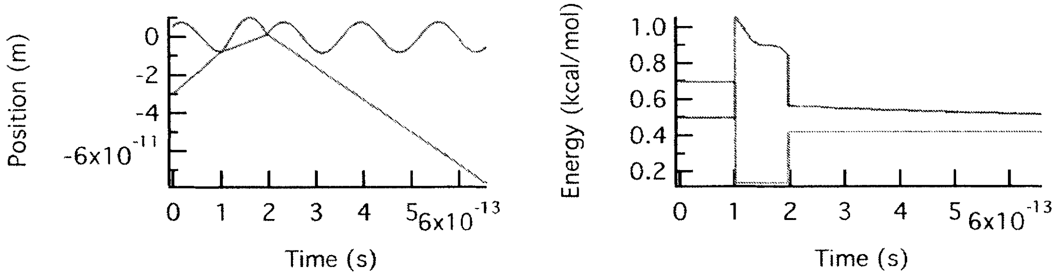

Initial Collision at Equilibrium Position, Moving Away from Crystal

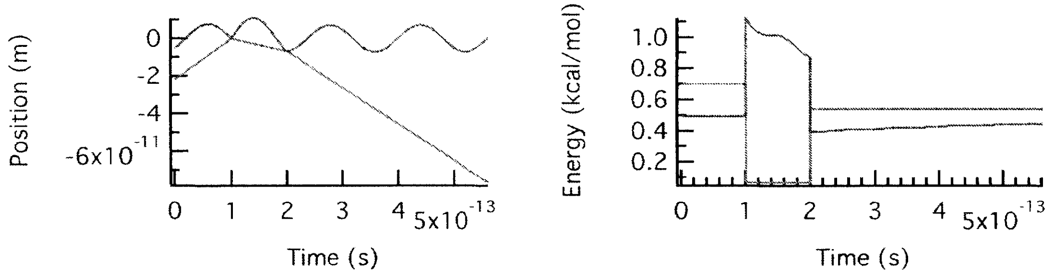

Figure II-11: Si and Kr(F_2) Trajectories and Energies at 0.70 kcal/mol

The trajectories and energies of the Si surface unit (blue) and Kr(F_2) cluster (red) are plotted for an initial Kr(F_2) velocity of 219 m/s. All simulations were run with a model silicon crystal consisting of a surface unit with a mass of 47 amu and a spring constant of 117 N/m coupled to a thermal bath at 250 K by a damping constant of 0.03.

Initial Collision at Outer Turning Point

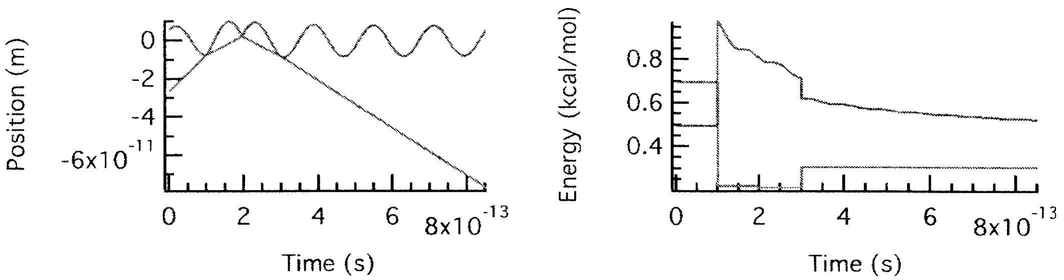

Initial Collision at Equilibrium Position, Moving Away from Crystal

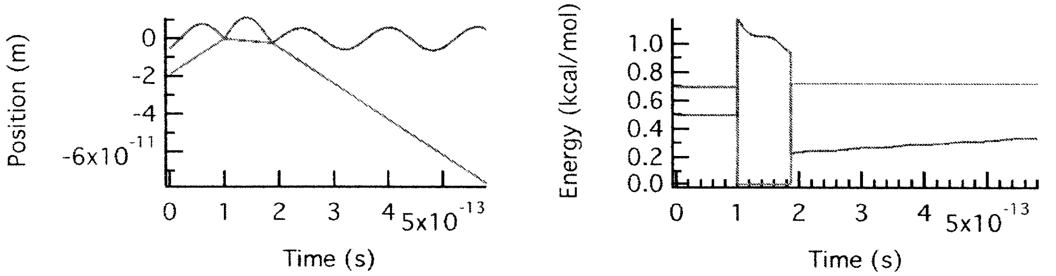

Figure II-12: Si and XeF_2 or $Xe(F_2)$ Trajectories and Energies at 0.70 kcal/mol

The trajectories and energies of the Si surface unit (blue) and XeF_2 molecule or $Xe(F_2)$ cluster (red) are plotted for an initial XeF_2 or $Xe(F_2)$ velocity of 187 m/s. All simulations were run with a model silicon crystal consisting of a surface unit with a mass of 47 amu and a spring constant of 117 N/m coupled to a thermal bath at 250 K by a damping constant of 0.03.

Table II-6: Silicon-Gas Molecule Interactions at 0.70 kcal/mol

Gas Molecule	Initial Silicon ωt	Number Of Collisions	Maximum Surface Excitation	Time Above 0.6 kcal/mol	Length of Surface Contact
F_2	0°	1	1.2 kcal/mol	40 fs	instantaneous
F_2	90°	5	1.1 kcal/mol	100 fs	100 fs
F_2	180°	2	1.2 kcal/mol	50 fs	50 fs
F_2	270°	1	0.6 kcal/mol	0 fs	instantaneous
$Kr(F_2)$	0°	2	1.1 kcal/mol	100 fs	100 fs
$Kr(F_2)$	90°	N/A	N/A	N/A	N/A
$Kr(F_2)$	180°	N/A	N/A	N/A	N/A
$Kr(F_2)$	270°	2	1.1 kcal/mol	100 fs	100 fs
XeF_2 / $Xe(F_2)$	0°	3	1.0 kcal/mol	100 fs	100 fs
XeF_2 / $Xe(F_2)$	90°	N/A	N/A	N/A	N/A
XeF_2 / $Xe(F_2)$	180°	N/A	N/A	N/A	N/A
XeF_2 / $Xe(F_2)$	270°	2	1.2 kcal/mol	90 fs	90 fs

Values of ωt are defined for $x(t) = -A\cos(\omega t)$, i.e. with $\omega t = 0°$ at the outer turning point, 90° at the equilibrium position moving towards the crystal, 180° at the inner turning point, and 270° at the equilibrium position moving away from the crystal. "Surface contact" is defined as the time from the first to last collision. The 0.6 kcal/mol threshold was selected because it is the half the total initial energy of the system (gas molecule and surface unit).

Initial Collision at Outer Turning Point

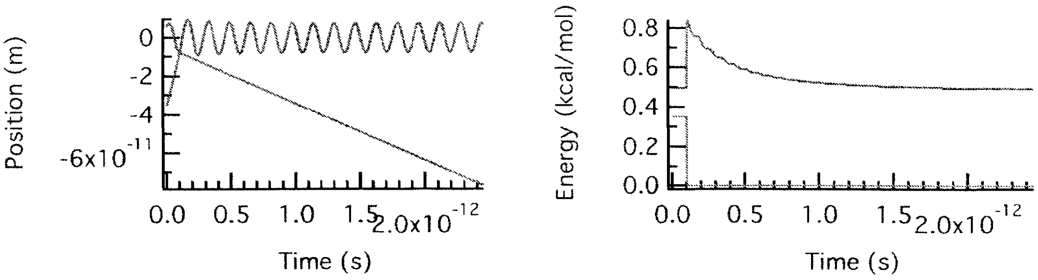

Initial Collision at Inner Turning Point

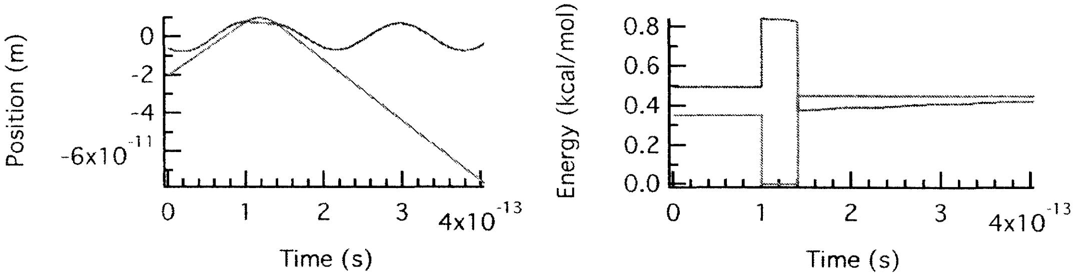

Initial Collision at Equilibrium Position, Moving Away from Crystal

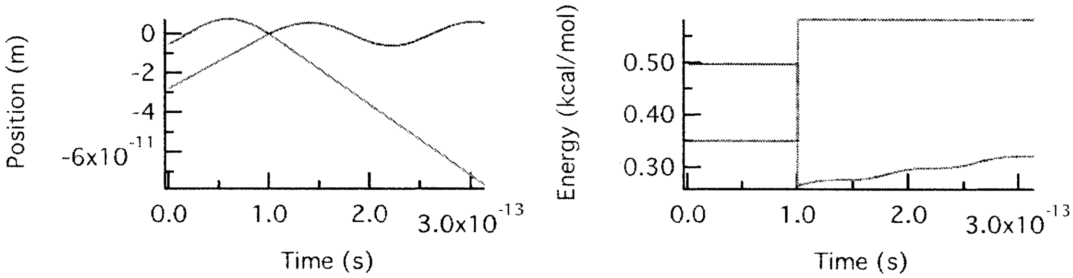

Figure II-13: Si and F_2 Trajectories and Energies at 0.35 kcal/mol

The trajectories and energies of the Si surface unit (blue) and F_2 molecule (red) are plotted for an initial F_2 velocity of 287 m/s. All simulations were run with a model silicon crystal consisting of a surface unit with a mass of 47 amu and a spring constant of 117 N/m coupled to a thermal bath at 250 K by a damping constant of 0.03.

Initial Collision at Outer Turning Point

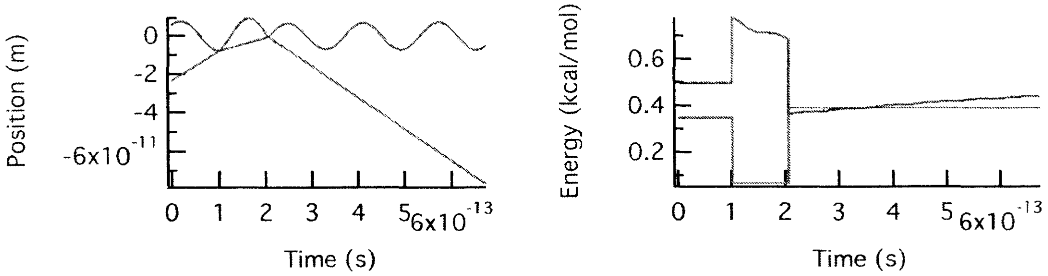

Initial Collision at Equilibrium Position, Moving Away from Crystal

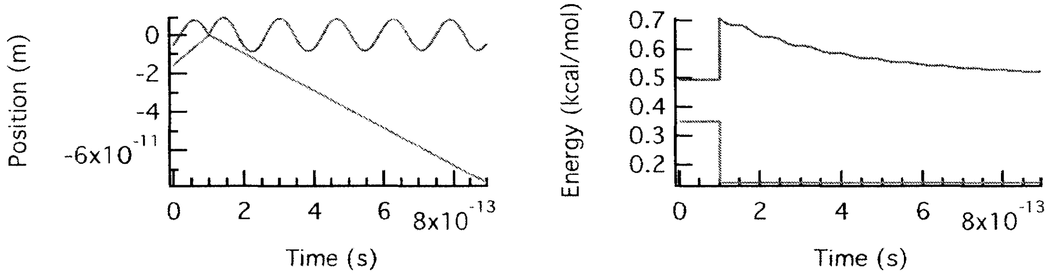

Figure II-14: Si and Kr(F_2) Trajectories and Energies at 0.35 kcal/mol

The trajectories and energies of the Si surface unit (blue) and Kr(F_2) cluster (red) are plotted for an initial Kr(F_2) velocity of 155 m/s. All simulations were run with a model silicon crystal consisting of a surface unit with a mass of 47 amu and a spring constant of 117 N/m coupled to a thermal bath at 250 K by a damping constant of 0.03.

Initial Collision at Outer Turning Point

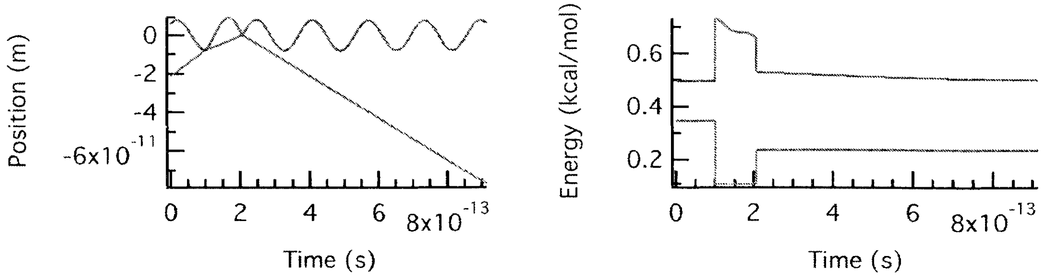

Initial Collision at Equilibrium Position, Moving Away from Crystal

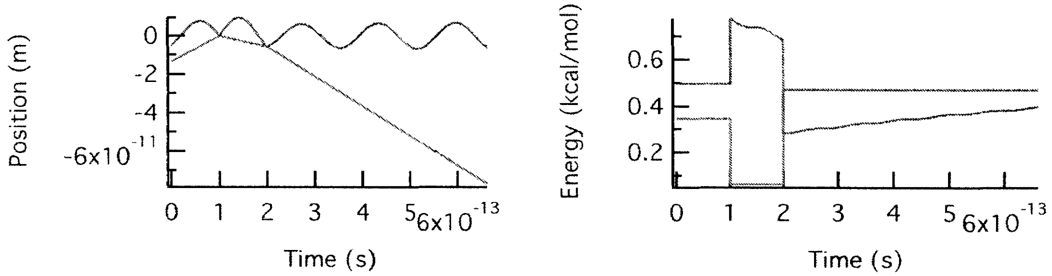

Figure II-15: Si and XeF_2 or $Xe(F_2)$ Trajectories and Energies at 0.35 kcal/mol

The trajectories and energies of the Si surface unit (blue) and XeF_2 molecule or $Xe(F_2)$ cluster (red) are plotted for an initial XeF_2 or $Xe(F_2)$ velocity of 132 m/s. All simulations were run with a model silicon crystal consisting of a surface unit with a mass of 47 amu and a spring constant of 117 N/m coupled to a thermal bath at 250 K by a damping constant of 0.03.

Table II-7: Silicon-Gas Molecule Interactions at 0.35 kcal/mol

Gas Molecule	Initial Silicon ωt	Number Of Collisions	Maximum Surface Excitation	Time Above 0.5 kcal/mol	Length of Surface Contact
F_2	0°	1	0.8 kcal/mol	100 fs	instantaneous
F_2	90°	N/A	N/A	N/A	N/A
F_2	180°	2	0.8 kcal/mol	40 fs	40 fs
F_2	270°	1	0.5 kcal/mol	0 fs	instantaneous
$Kr(F_2)$	0°	2	0.8 kcal/mol	110 fs	110 fs
$Kr(F_2)$	90°	N/A	N/A	N/A	N/A
$Kr(F_2)$	180°	N/A	N/A	N/A	N/A
$Kr(F_2)$	270°	1	0.7 kcal/mol	700 fs	instantaneous
XeF_2 / $Xe(F_2)$	0°	2	0.7 kcal/mol	100 fs	100 fs
XeF_2 / $Xe(F_2)$	90°	N/A	N/A	N/A	N/A
XeF_2 / $Xe(F_2)$	180°	N/A	N/A	N/A	N/A
XeF_2 / $Xe(F_2)$	270°	2	0.8 kcal/mol	100 fs	100 fs

Values of ωt are defined for $x(t) = -A\cos(\omega t)$, i.e. with $\omega t = 0°$ at the outer turning point, 90° at the equilibrium position moving towards the crystal, 180° at the inner turning point, and 270° at the equilibrium position moving away from the crystal. "Surface contact" is defined as the time from the first to last collision. The 0.5 kcal/mol threshold was selected because it is the initial energy of the silicon surface unit, and greater than half the total energy of the system (gas molecule and surface unit).

II.5 Conclusions

II.5.a Significance of the Results

The simulation results at all energies tell a fairly consistent story: the mass of the incoming gas molecule does not affect greatly the total energy it can transfer to the surface. However, it does have an effect on the duration of the surface vibrational excitation and of the proximity of the incident gas particle on or near the surface. There is a general correlation between more massive gas molecules and longer periods between the first and last collision, as well as between more massive gas molecules and longer periods in which the local Si-Si bonds contain the majority of the energy in the system, creating a "hot spot" where the Si-Si bonds are extended and compressed in non-equilibrium configurations. The longer existence of this hot spot is also enhanced by the fact that, at a given energy, the more massive gas molecules will also be moving more slowly, meaning that there is a longer period in which they are near, though not in contact with, the surface. It is likely that the combination of longer residence times and longer excitation of the surface give a greater opportunity for the reaction of fluorine with the more extended and compressed Si-Si bonds in the area of this hot spot.

II.5.b Potential Improvements to the Model

The model presented in this chapter is a relatively gross simplification: the surface is reduced to a single simple harmonic oscillator, and this harmonic oscillator is treated classically. While treating it classically does make the calculations simpler, it is questionable whether it is a particularly reasonable approximation. The reasonableness of the classical approximation can be quantified by comparing the thermal equilibrium energy of the oscillator with the ground level energy of a quantum oscillator with the same frequency. We modeled the silicon surface unit as an oscillator with angular frequency $\omega = 3.87\times10^{13}$ Hz and a thermal equilibrium energy of

$E = k_B \times 250$ K $= 3.45\times10^{-21}$ J. The energy levels of a quantum simple harmonic oscillator, for $n = 0, 1, 2, \ldots$ are

$$E_n = \hbar\omega\left(n + \tfrac{1}{2}\right),$$

so the ground-state energy of a quantum harmonic oscillator with the same frequency would be $E_0 = 2.04\times10^{-21}$ J. Given that this value is roughly half the thermal equilibrium energy of the oscillator in the classical model, the validity of modeling the system classically is fairly questionable. Treating the system as a quantum harmonic oscillator might be beneficial.

In addition, modeling the surface as a single simple harmonic oscillator is rather simplistic, especially since there is no one element of the actual surface to which it clearly corresponds. As shown in Figure II-2, the surface dimers consist of a pair of Si atoms bonded to each other and each bonded to a F atom projecting up from the crystal and to two Si atoms one layer down. In the simulations in this chapter, we assumed a surface unit consisting of one Si and one F atom, but we ignored the internal energy associated with vibrations of the Si-F bond and treated the remainder of the dimer as simply part of a thermal bath consisting of the whole lattice. Similarly, we treated the incoming gas molecules as point masses and ignored their potential rotational and internal vibrational modes. A more detailed three-dimensional model that treated each atom and bond separately and in particular, of finite size, would account for reality more accurately.

Chapter II References

(1) R. C. Hefty, Ph.D. Thesis, Massachusetts Institute of Technology, (2003).

(2) M. R. Blair, M.S. Thesis, Massachusetts Institute of Technology, (2014).

(3) S. T. Ceyer, *Science* **249**, 133-139, (1990).

(4) M. R. Tate, Ph.D. Thesis, Massachusetts Institute of Technology, (1999).

(5) J. R. Holt, Ph.D. Thesis, Massachusetts Institute of Technology, (2002).

(6) N. Takagi, S. Shimonaka, T. Aruga, and M. Nishijima, *Phys. Rev. B* **60**, 10919-10925, (1991).

(7) H.-Y. Hao and H. J. Maris, *Phys. Rev. Lett.* **84**, 5556-5559, (2000).

Chapter III: The Oxidation of Silicon by Molecular Oxygen

The formation of oxide layers on silicon surfaces is another industrially important reaction of silicon with small gas molecules. Oxides are used as protecting groups during etch procedures and as insulators, for example as dielectrics in on-chip capacitors. The formation of oxides on silicon surfaces is also important to the manufacture of silicon photovoltaic cells, an important clean energy technology due to their scalability, portability, and adaptability to different sites. There is current interest in the manufacture of metal-insulator-semiconductor (MIS) cells, in which a thin SiO_2 layer serves as an interface between layers of Si and a metal oxide. The thickness of the SiO_2 layer can be tuned to control the open-circuit voltage of the cell. The layer should be as thin as possible but still thick enough to serve as an effective insulator.[1,2] Another technique of interest is the manufacture of cells consisting of multiple layers of Si and SiO_2, with each layer tuned to absorb a different wavelength of light. Here, it is also important to be able to control the SiO_2 layer thickness precisely to maximize the efficiency of the cell.[3] Our group's study of the interaction of Si(100) surfaces with oxygen, fluorine, and fluorine compounds is relevant to an improved understanding of these and related processes.

In principle, dissociative adsorption of O_2 on a Si surface should not occur because it is a spin forbidden reaction. Molecular oxygen is paramagnetic, with a triplet ground state. The Si-Si dimer bonds that are cleaved in the oxidation reaction have a singlet electronic ground state as do the Si-O or Si=O products. Hence, a triplet-to-singlet transition of the oxygen, with a cost of 0.98 eV (22.6 kcal/mol), is required. The probability of the necessary transition from triplet to singlet O_2 is very low when the O_2 interacts with a covalent, nonmagnetic surface, which suggests that the probability of dissociative adsorption of O_2 on Si should be very low.[4,5] The few researchers who have accounted for the triplet-to-singlet conversion in theoretical studies have considered very constrained reaction geometries[4], or else only considered chemisorption of molecular O_2 rather than dissociative chemisorption[5].

The molecular beam scattering apparatus used for the studies of silicon etching by fluorine compounds discussed in Chapter I is well suited to study the dissociative adsorption of O_2 on an Si surface. The use of supersonic molecular beams and a rotatable crystal makes it possible to probe the kinetic energy and directional dependence of the reaction. Several potential mechanisms that would allow the reaction to proceed despite the triplet ground state of O_2 could be effectively tested.

One relatively likely possibility is that triplet O_2 dissociates on Si(100) surfaces via atom abstraction, as opposed to classic dissociation that requires a triplet-to-singlet transition in which two singlet Si-O bonds are formed simultaneously. If a dangling bond on the Si surface abstracts an oxygen atom from triplet O_2, as it does in atom abstraction, a free ^3P oxygen atom is produced and no triplet-to-singlet transition is necessary. As with the observations of atom abstraction from F_2 and XeF_2 discussed in Chapter I, the scattering apparatus's differentially pumped mass spectrometer with angular and time-of-flight sensitivity makes it possible to distinguish the unreacted partners of abstracted atoms from unreacted molecules that have cracked in the mass spectrometer ionizer.

Another interesting possibility is raised by the fact that gas-phase O_2 molecules can form van der Waals dimers, $(O_2)_2$, with a bond energy of 0.4 kcal/mol. Because O_2 has an open-shell electronic structure, the spin orientation of the two molecules in the dimer, as well as the geometry of the dimer, dictate the potential energy surface. The potential energy surface for two triplet, ground-state O_2 molecules correlates to three possible electronic states in the dimer's ground state geometry of two parallel O_2 molecules in an "H" configuration, separated by a bond length of 3.56 Å. The lowest energy electronic state is a singlet with a dimer bond energy of 17 meV (0.39 kcal/mol).[6,7,8] This geometry means that a four-centered reaction of a dimer in its ground state with the Si surface would be spin-allowed. Additionally, theoretical studies have suggested that collisions of $(O_2)_2$ dimers or larger clusters with a surface could convert translational energy into an excitation to the first O_2 singlet state via a process called non-adiabatic ladder-climbing.[9,10] The dimers needed to test both of these possibilities should be easily produced by properly tuning the nozzle pressure and temperature used to produce a supersonic beam.

III.1 Overview of O_2 Reactivity with Silicon

III.1.a Triplet O_2 Oxidizes Si(100) Surfaces

The ground state of the Si(100) surface consists of a 2x1 reconstruction with surface atoms paired up in surface dimers in which each Si atom has two σ bonds into the bulk and one to its partner in the dimer, along with a single electron forming a "dangling bond" pointed away from the surface. There is also evidence of a π-bonding interaction between the dangling bonds.[11] The dangling bond electrons in the two atoms of a dimer have opposite spins, making the overall electronic ground state a singlet. Since O_2 has a triplet ground state, ${}^3\Sigma_g^-$ and its first excited state, ${}^1\Delta_g$, is 22.6 kcal/mol higher, the reaction of molecular O_2 with a Si(100) surface is spin-forbidden and should have a very low reaction probability.[4,5]

Past experimental studies have investigated the reactivity of O_2 with Si(100) surfaces over a wide variety of temperature and energy regimes. Electron energy loss spectroscopy work has revealed the presence of physisorbed O_2 on Si(100) at 20 K, but found that it had fully desorbed by 35 K, indicating that a physisorbed intermediate is only plausible at very low temperatures. The same study found evidence of transient peroxy bridging oxygen—O_2 molecules chemisorbed across a surface dimer—and stable monatomic bridging oxygen—O atoms chemisorbed across a surface dimer—present on the surface at 20 K.[12] A molecular beam study using the King and Wells[13] beam reflectivity method has suggested an intermediate-mediated mechanism for the chemisorption of O_2 on Si(100) at cryogenic surface temperatures and low impact energies. Based on the surface-temperature and beam-energy dependence of the rate of chemisorption at low temperatures, a ~28 meV (~0.6 kcal/mol) barrier to the chemisorption of physisorbed O_2 was estimated.[14]

The same study found evidence of direct chemisorption at higher impact energies and surface temperatures. For surfaces above 600 K, increasing surface temperature and beam energy both increased sticking probability for beams with translational energies between 7 kcal/mol and 29 kcal/mol with a maximum sticking probability of nearly 80% for a 29 kcal/mol beam on a 1200 K surface.[15] An X-ray photoelectron spectroscopy study at higher temperatures found that, at surface temperatures from 500 K to 800 K, increasing the surface temperature resulted in an increased sticking probability for molecular beams with translational energies of 2, 5, and 14 kcal/mol with maximum sticking probabilities of 1-2%. However, the temperature dependence was much less pronounced for the 14 kcal/mol beam.[16] Another study conducted on a 1200 K surface with a pulsed molecular beam and using thermal desorption mass spectroscopy to measure sticking probabilities found that the sticking probability varied linearly with temperature from ~3% with a ~0.2 kcal/mol beam to ~40% with a ~20 kcal/mol beam. Only a weak surface temperature dependence was observed: the sticking probability was about 1.5 times higher at 1200 K than at 800 K.[15]

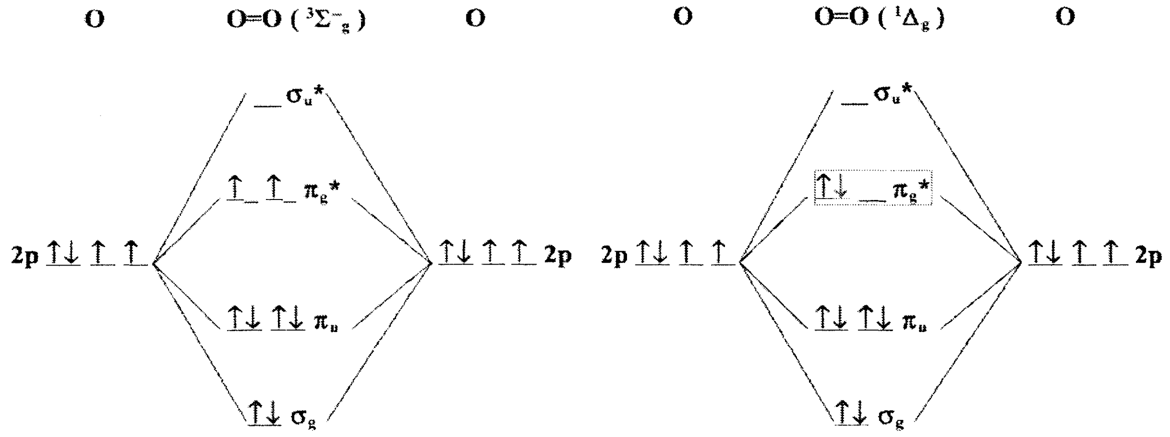

Figure III-1: Triplet and Singlet O_2

Molecular orbital diagrams of the ground state (left) and first excited state (right) of O_2.

III.1.b Previous Studies of the Mechanism

The studies of the reaction probability of O_2 on Si(100) surfaces discussed in the previous section make it clear that at least two different mechanisms are responsible for the chemisorption of O_2, but leave open the question of how these mechanisms result in the spin-forbidden triplet-singlet transition necessary for the reaction. Unfortunately, past theoretical work on the matter has been limited and has not resulted in a good solution to the problem, requiring constrained reaction geometries that are only possible if the O_2 molecule is trapped on the surface for an extended period.[4,17,18] In particular, this physical description involving constrained geometries is hard to square with the observation of impact-energy dependence on reactivity at high temperatures and energies and the direct reaction mechanism these observations suggest.

Fortunately, there have also been some recent coupled experimental-computational investigations into the mechanism by which O_2 reacts with the Si(100) surface. These studies, using infrared spectroscopy[19], reflectance isotropy[20], and scanning tunneling microscopy[21,22] data, show that dissociation occurs primarily at pristine Si-Si dimer sites, not defect sites. The IR and STM studies also indicate that the initial reaction product may be a metastable silanone (Si=O) species on the dimer Si atoms and that O atoms are very prone to remain on the surface rather than incorporating themselves deeper into the lattice. The STM studies also show evidence that at coverages greater than a quarter-monolayer, concerted two-molecule reactions begin to dominate. We shall see how this mechanism may be relevant to a means of circumventing the spin issue.

III.2 Atom Abstraction

III.2.a A Potential Mechanism, If Thermodynamics Allows It

The dissociative chemisorption of O_2 on silicon surfaces is spin forbidden because it involves a spin-forbidden transition between the triplet O-O bond in free O_2 and the singlet Si-O bonds in the oxidized silicon surface. This transition can be avoided, however, if the reaction occurs via an atom abstraction mechanism in which only one singlet Si-O bond is formed and the other O atom released by the dissociation of the O_2 molecule is released into the gas phase in a triplet ^3P electronic state. Although this mechanism has a lower maximum sticking probability---one O atom per O_2 molecule impacting the surface, rather than two O atoms per O_2 molecule impacting the surface, it can otherwise produce an oxidized surface indistinguishable from that which would be produced by classical dissociative chemisorption.

What is not clear is whether or not atom abstraction is thermodynamically allowed. Breaking an O_2 bond requires 119 kcal/mol; for atom abstraction to be allowed, the formation of a single Si=O bond must release at least this much energy. Classical dissociative chemisorption, on the other hand, involves the formation of two Si=O bonds for every O_2 bond broken, so it requires only half as much energy be released per Si=O bond formed. Unfortunately, the Si=O bond energy is not well known: calculations have varied from 105 kcal/mol to 207 kcal/mol, making it unclear whether an atom abstraction mechanism is thermodynamically possible.[5,6,21,23,24]

Abstraction of O atoms by a Si surface has never been observed, and no experiments intended to detect it have been carried out. Since the surfaces produced by atom abstraction and classic dissociative chemisorption are likely to be indistinguishable, identifying an atom abstraction mechanism requires observation of the free O atoms scattered from the surface when their partners are abstracted. These atoms can be detected by a mass spectrometer when the reaction is conducted with a molecular beam of O_2 in ultra-high vacuum. However, care is needed to distinguish the scattered O atoms from O atoms produced by ionizer cracking of unreacted O_2 molecules scattered from the surface. The first step in studying this system will be to investigate the possibility of atom abstraction using the techniques previously developed in the lab to investigate F atom abstraction by Si surfaces.[25,26,27]

Once an oxygen atom is abstracted from O_2, the excess exothermicity from Si=O bond formation will be partitioned between the free unreacted O atom and the lattice. Depending on the strength of the Si=O bond, as much as 90 kcal/mol may be released, and a substantial fraction of this exothermicity is likely channeled into the lattice, heating it vibrationally and electronically. This excitation could potentially excite a Si surface dimer to its first excited state, a triplet, at a cost of around 9 kcal/mol.[28] If such an excitation occurs, the free ^3P oxygen atom released in the original abstraction might then react with the excited dimer bond.

III.2.b Demonstrating Atom Abstraction

To demonstrate that atom abstraction has a role in the dissociative chemisorption of O_2 on Si surfaces, the scattered unreacted O atoms produced by the abstraction must be observed. This task is difficult because the reaction probability is likely significantly less than unity, resulting in a significant population of scattered O_2 molecules, some of which will crack into O atoms in the mass spectrometer ionizer, likely swamping the unreacted O atom signal. The easiest way to distinguish between these two populations of O atoms is by their kinetic energies. Ionizer cracking of O_2 should not affect the kinetic energy of the O atoms it produces and, in any case, the neutral flight time is the main contributor to observed flight times in our system. Thus, O atoms produced by ionizer cracking of O_2 molecules will have an identical time-of-flight spectrum as the background of scattered O_2 molecules. Unreacted O atoms from atom abstraction, on the other hand, can be expected to have a different velocity profile than scattered O_2 molecules.

Much of the scattered O_2 signal is likely to be produced by elastic scattering, producing a peak at the specular angle with the same velocity profile as the initial O_2 beam. Inelastic scattering may contribute to the scattered signal as well, producing a broadened velocity profile and angular distribution. Thermal accommodation of O_2 atoms with the surface is also possible (if unlikely, since physisorbed O_2 is unstable on silicon above 35 K[12]) and would result in an isotropic angular distribution with a maximum intensity along the surface normal. Atom abstraction is not an elastic process, and the free O atoms produced by it will be translationally heated by the exothermicity of the abstraction reaction, with a shorter flight time than elastically scattered O_2 molecules.

In any case, unreacted O atoms produced by atom abstraction will be identifiable in time-of-flight data as a second population with a different velocity distribution than those produced by O_2 cracking in the ionizer. To separate out the background of cracking-produced O atoms, the cracking ratio can be measured be comparing the O and O_2 signals in a direct beam of O_2 with the same ionizer settings. By taking time-of-flight spectra of both O and O_2 during atom abstraction measurements and using this cracking ratio, the expected time-of-flight spectrum if all O atoms were due to cracking can be calculated and subtracted from the observed O spectrum.

III.2.c Understanding the Atom Abstraction Mechanism

In addition to having different time-of-flight spectra, background O atoms from ionizer cracking and O atoms produced by atom abstraction at the surface should also be distinguishable by their angular distributions. If unreactive O_2 atoms scatter elastically, they—and the O atoms they produce by cracking in the ionizer—should scatter at the specular angle. The angular distribution of O atoms produced by atom abstraction, on the other hand, depends on the details of the abstraction mechanism. If the transition state for atom abstraction is not geometrically constrained by approach geometry, an isotropic angular distribution of unreacted partner O atoms is expected. However, if the transition state is "tight" and is constrained by the approach geometry—for example, if the O_2 molecules align with the dangling bonds before abstraction—an anisotropic angular distribution of unreacted partner O atoms would be expected.

The kinetic energy of the scattered partners of abstracted O atoms can also allow us to deduce something about the abstraction mechanism. If the surplus energy of the O atoms is a significant fraction of the reaction exothermicity, a late activation barrier is likely. However, if the surplus energy is only a few percent of the reaction exothermicity, as with F_2 atom abstraction by Si, that would be a sign of an early activation barrier reaction of the type first described by Evans and Polanyi.[26,29]

III.3 Four-Center Reactions with $(O_2)_2$ Dimers

III.3.a $(O_2)_2$ Dimers: Singlets in the Ground State

The existence of $(O_2)_2$ van der Waals dimers provides another possible route for bypassing the spin-forbidden nature of classical dissociative chemisorption. These dimers can be formed in supersonic molecular beams or, potentially, from O_2 molecules physisorbed on a surface. However, although they are held together by a van der Waals dispersion interaction, because of the open-shell electronic structure of O_2, the overall potential energy surface of the dimer depends on the spin orientations of the individual molecules. The ground state for a dimer consisting of two triplet oxygen molecules is an "H"-shaped arrangement with the two molecules' axes parallel to each other and separated by a bond length of 3.56 Å. The bond energy for this ground-state dimer is 0.39 kcal/mol and its overall electronic state is a singlet. Above the ground state is a triplet state, 0.04 kcal/mol higher, and a quintet state, an additional 0.03 kcal/mol above the triplet.[6,7,8]

The distribution of dimers among these three states has been experimentally measured several times. A recent Stern-Gerlach expansion beam study showed that all of the dimers in a beam cooled to the singlet ground state,[30] while an earlier experiment under similar conditions had shown a mixture of all three states, but in both cases, there was a significant population of singlets.[31] The presence of these singlet $(O_2)_2$ dimers indicates that a four-center reaction with the surface could occur without a triplet-singlet transition. This possibility has been suggested by theoretical work: a recent study that uses DFT calculations to interpret STM results suggests that at coverages higher than a quarter monolayer, Si oxidation involves two O_2 molecules reacting in concert.[22]

Since the dimers can be formed in molecular beams, such a reaction could occur even at high surface temperatures. However, the most obvious situation for such a four-centered reaction is a dimer that has already physisorbed on the surface, or formed from two molecules already physisorbed on the surface. This suggestion is consistent with experimental observations that, at low impact energies and surface temperatures, a trapping-mediated precursor mechanism dominates the oxidation of Si by O_2 molecular beams, while at higher temperatures a direct mechanism dominates.[14]

III.3.b Producing $(O_2)_2$ Dimers

The formation of van der Waals dimers in supersonic beams can be controlled by manipulating the nozzle temperature and stagnation pressure, and thus the time over which the supersonic expansion occurs. Decreasing nozzle temperature and increasing stagnation pressure both contribute to increased dimer formation: higher pressure because it increases the number of potentially dimer-forming collisions in the beam, lower temperature because it reduces the average relative velocities in these collisions, increasing the sticking probability. However, the final kinetic energy of the beam is directly related to both nozzle temperature and stagnation pressure. This fact means that it is possible to vary the cluster content of the beam independently of its kinetic energy, for example by raising stagnation pressure and lowering nozzle temperature to keep beam energy constant while increasing the percentage of dimers in the final beam. However, varying the stagnation pressure will make it hard to maintain the tight energy distribution of a supersonic beam.[32]

The nozzle set-up previously used for the $Xe(F_2)$ and $Kr(F_2)$ cluster experiments described in Chapter I[33,34] has the capability to produce O_2 beams both with and without $(O_2)_2$ dimers. Previous studies of noble gas clusters[35,36,37] and N_2 and O_2 clusters[38] provide a starting point for determining optimal conditions for dimer production. However, experimentation will be needed to determine optimal nozzle conditions to maximize the production of $(O_2)_2$ dimers while minimizing the production of higher-order clusters. It will also be necessary to determine nozzle conditions for minimizing dimer production to provide a pure O_2 beam for comparison to dimer beams.

III.3.c Distinguishing Four-Center Dimer Reactions

While it is uncertain how high a dimer concentration can be achieved, it is likely to be a relatively small fraction of the total O_2 molecules in the molecular beam. For example, the optimal conditions for producing $Kr(F_2)$ beams produced beams with only 0.21% of the fluorine flux coming from dimers.[34] Although the vast majority of molecules in dimer-containing beams will be triplet O_2 molecules, the rapid reaction of singlet O_2, produced by photoexcitation of porous Si, with silicon[39] suggests that the reactivity of singlet $(O_2)_2$ will be several orders of magnitude greater than that of triplet O_2, making its contribution easily identifiable.

Another difficulty is the matter of how four-center dimer reactions can be observed. Unlike atom abstraction, a four-centered dimer reaction would produce no unreacted O atom partners to be scattered from the surface and detected by mass spectrometry. Instead, dimer reactivity will have to be measured indirectly by using thermal desorption spectroscopy to determine the amount of O atoms chemisorbed on the silicon surface after exposure to dimer-containing and dimer-free beams. If most of the reactivity, at least at low surface temperatures and impact energies, is due to $(O_2)_2$ dimers, a sizable reactivity difference should be observed. Furthermore, this reactivity difference should decrease at higher surface temperatures or incident energies, since both would lower the probability of dimers staying on the surface long enough to allow four-centered reactions to be geometrically likely.

III.4 Non-Adiabatic Ladder Climbing with $(O_2)_2$ Dimers

III.4.a Theoretical Work on $(O_2)_2$ Dimer Ladder Climbing

Just as the open-shell electronic structure of O_2 means that the relative spin orientation of the molecules affects the overall potential energy of the $(O_2)_2$ dimer, it also means that changes to the geometry of the $(O_2)_2$ dimer upon collision with the surface can affect the spin states of the constituent O_2 molecules. This fact introduces the possibility of "chemistry-with-a-hammer"-type collisional activation.[40] Specifically, there is a possibility of non-adiabatic ladder climbing, in which spin-orbit coupling in the dimer and compression of the dimer bond create a degeneracy between an electronic state that dissociates into two triplet O_2 molecules and an electronic state that dissociates into one triplet and one singlet O_2 molecule.

The three lowest electronic states of an $(O_2)_2$ dimer correspond to a dimer formed from a pair of triplet O_2 monomers and so will dissociate to two triplet monomers. However, there are higher electronic states that correspond to a dimer formed from a singlet monomer and a triplet monomer, as seen in Figure III-2. An $(O_2)_2$ dimer in one of these electronic states will dissociate to a triplet O_2 molecule and a singlet O_2 molecule. Since changes to the dimer geometry can effect its overall electronic state, it is possible for deformation due to a collision with the surface to cause a dimer originally formed from two triplet O_2 molecules to transition to one of these triplet-and-singlet states. If the dimer then dissociates, it will produce a singlet O_2 molecule that can easily react with the surface.

In the most stable geometric configuration of the dimer—with the two molecular axes parallel to each other and perpendicular to the dimer bond in an "H" shape—the lowest set of triplet-and-singlet states are 22 kcal/mol above the ground electronic state of the dimer. However, when the dimer bond is compressed, as in a collision with a surface, from its usual length of 3.6 Å to about 2.0 Å, one of the ground electronic states that correlates to two triplet monomers becomes degenerate with a state 22 kcal/mol higher that correlates to one singlet and one triplet O_2, as shown in Figure III-4.

The $^5A_1$ state corresponding to two triplet O_2 molecules that becomes degenerate with states corresponding to a singlet and a triplet O_2 molecule is only 0.07 kcal/mol above the ground state and has been observed to be present in molecular beams of $(O_2)_2$ dimers.[31] Furthermore, the spin-orbit coupling for the transition is quite favorable: potentially as high as 58% when one of the molecules in the dimer is vibrationally excited. A transition with favorable spin-orbit couplings also exists for twisting of the dimer from an "H" to a "T" configuration. Hence, the collision of a ground-state $(O_2)_2$ with a Si surface could result in the production of singlet O_2 at the surface.[9,10]

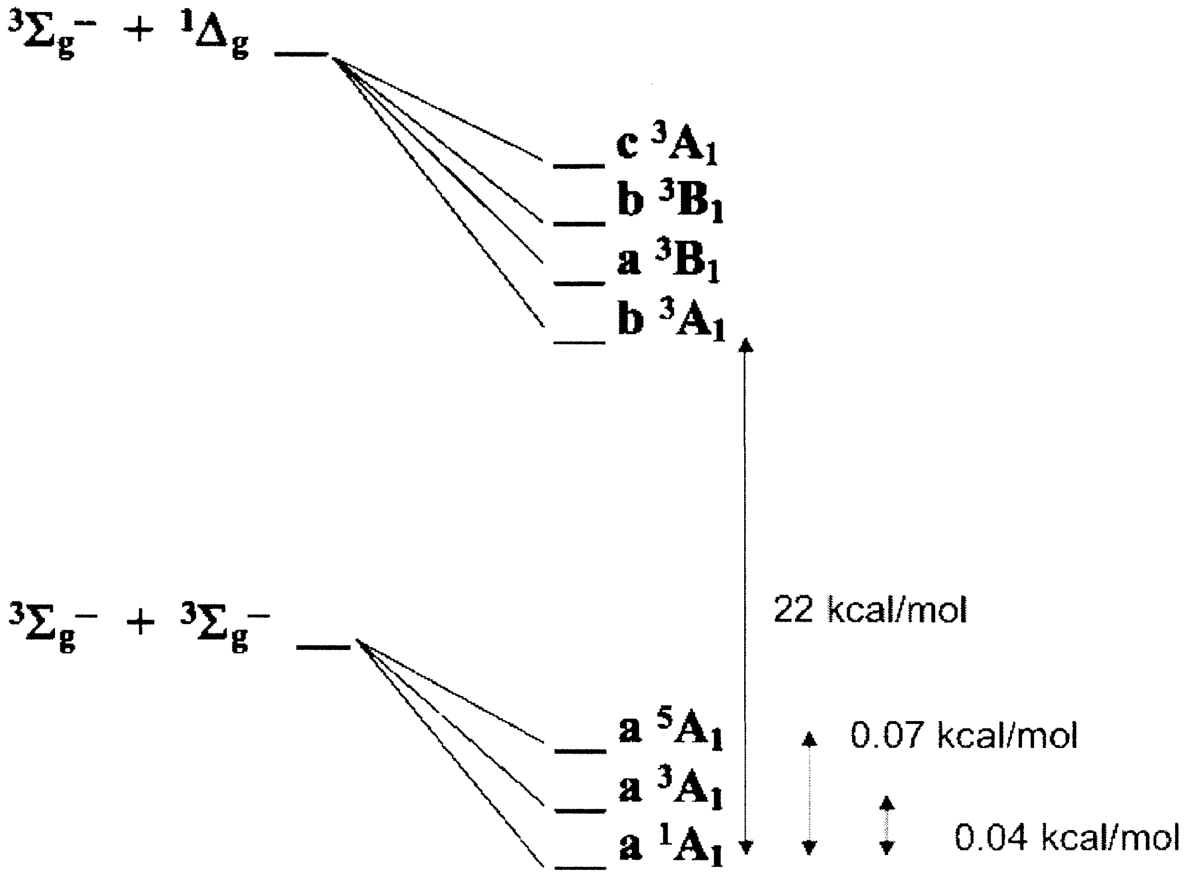

Figure III-2: Dissociation of $(O_2)_2$ Dimers into Triplet and Singlet O_2

The lowest electronic energy states of $(O_2)_2$ dimers in their "H" configuration can be divided into three closely-spaced states that correlate to two triplet O_2 molecules and four closely-spaced states that dissociate into a triplet and a singlet O_2 molecule with a difference of 22 kcal/mol between the two sets of states.

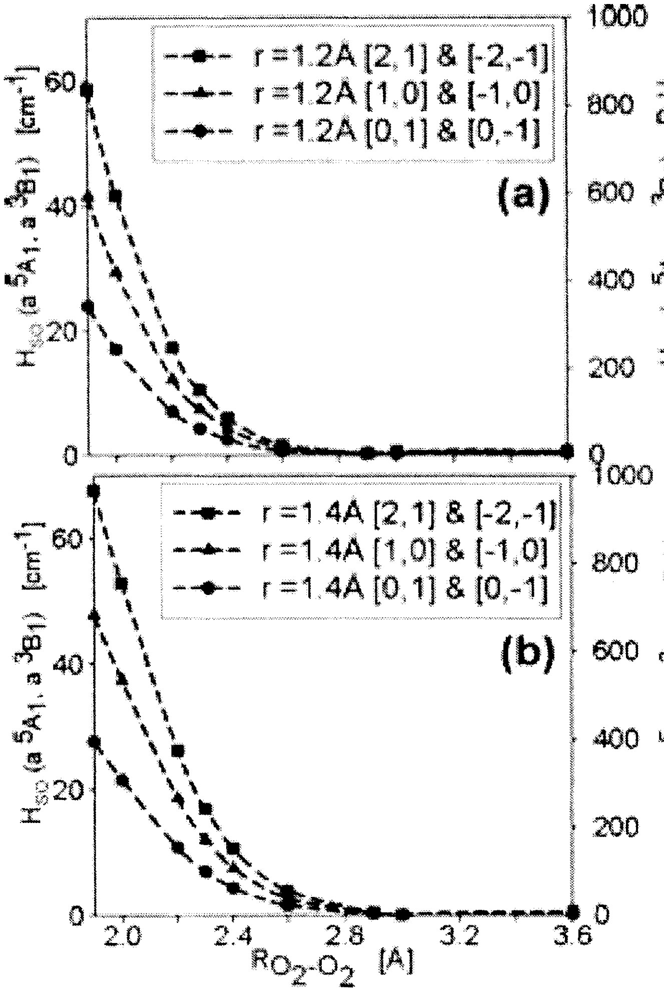

Figure III-3: Spin-Orbit Coupling for $(O_2)_2$ Dimer Electronic State Conversion

Spin-orbit coupling between the a$^5A_1$ and a$^3B_1$ states for $(O_2)_2$ in the "H" configuration, as a function of the intermolecular distance, $R_{O2\text{-}O2}$. (a) Both molecules at $r_{O\text{-}O}$ = 1.2 Å and (b) one of the molecules stretched to $r_{O\text{-}O}$ = 1.4 Å. The a$^5A_1$ state dissociates to two triplet monomers and the a$^3B_1$ state dissociates to a singlet and a triplet. This plot is Figure 8 from Nguyen et. al. 2011.[10]

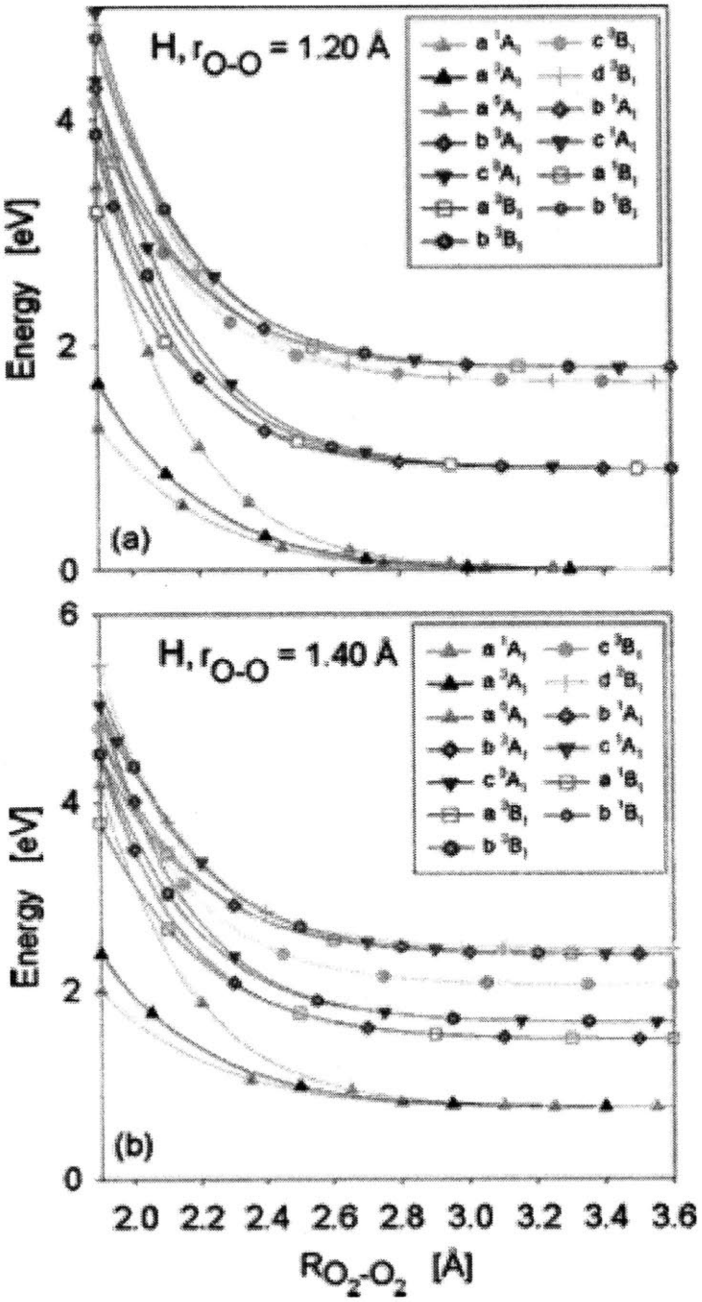

Figure III-4: $(O_2)_2$ Dimer Electronic States and Dimer Bond Compression

Potential energy surfaces along the intermolecular coordinate for $(O_2)_2$ in the H configuration. All four states shown in dark blue correspond to a triplet and a singlet monomer, while the orange, black, and green states correspond to two triplet monomers. (a) Both molecules at r_{O-O} = 1.2 Å and (b) one of the molecules stretched to r_{O-O} = 1.4 Å. The energy reference corresponds to two separated ground-state molecules. This plot is Figure 5 from Nguyen et. al, 2011.[10]

III.4.b Silicon Oxidation by Large $(O_2)_n$ Clusters

While $(O_2)_2$ dimers are the simplest form of van der Waals cluster of O_2 molecules and, as such, are the simplest to model, much larger clusters can be formed in supersonic beams, sometimes containing thousands of molecules. Large clusters colliding with a surface can potentially transfer a significant fraction of their total kinetic energy into compression of the bonds between molecules at the front of the cluster, resulting in a high probability that non-adiabatic ladder climbing will occur and singlet O_2 will be produced. It has been calculated that up to a quarter of the molecules in a large cluster may be non-adiabatically excited to a singlet state by this mechanism, allowing a large cluster of triplet O_2 to behave as a source of singlet O_2 upon collision with the surface.[9,10] However, very little of the cluster's kinetic energy is transferred to bond vibration within the O_2 molecules, so the energy cannot be channeled directly into dissociation of O_2 and the production of reactive O radicals.[41]

Experiments conducted with molecular beams of van der Waals clusters of six hundred to four thousand O_2 molecules provide some experimental evidence for this mechanism. STM studies of the Si surface oxidation from the collision of these clusters show two different modes of oxidation occurring with a very sharp dividing line between the regions where they occur, with sticking probabilities much higher than would be expected for monomer O_2 oxidation.[42,43]

III.4.c Finding an "On Switch" for Non-Adiabatic Ladder Climbing

While molecular beam cluster studies have the advantages of allowing for more complicated activation pathways and producing large-scale oxidation surface features that can be examined by STM, a major downside of working with clusters is that it is difficult to determine what exactly is happening on the scale of an individual dimer bond. Studying the collision of dimers rather than large clusters should allow collisional activation to be observed without the complication of energy transfer from a large number of molecules.

Without intra-cluster energy transfer to the molecules at the silicon surface, conversion of triplet O_2 to singlet O_2 will require that an individual dimer collide with the surface with sufficient energy to compress or distort the dimer bond to the degeneracy point. At a minimum, a translational energy of 22 kcal/mol—the difference between the dimer states corresponding to two triplets and to a triplet and a singlet—is needed. However, the barrier may be as high as 60 kcal/mol due to the activation energy needed to compress the dimer bond. When a sufficient translational energy is reached, the dissociative chemisorption reaction should "turn on" and an increase in oxidation as measured by thermal desorption spectrometry should be observed. As beam energy increases above this level, the reactivity should increase gradually as less favored collision geometries become able to channel enough energy to produce a transition.

III.4.d Observing Unreacted Partners from Dimer Reactions

In addition to looking for an "on switch" to adiabatic ladder-climbing, studying the reaction of $(O_2)_2$ dimers with the Si surface should allow for the observation of unreacted partner molecules. For collisionally activated adiabatic ladder-climbing by $(O_2)_2$ dimers to lead to spin-allowed dissociative chemisorption on the Si surface, two steps need to occur. First, the collision of a dimer with the surface needs to compress or distort the dimer bond sufficiently to lead to a transition from an electronic state corresponding to two triplet O_2 molecules to one 22 kcal/mol higher corresponding to a triplet and a singlet O_2 molecule. Then, the dimer would need to break up into its constituent molecules, freeing the singlet O_2 molecule to react with the surface and the triplet O_2 molecule to scatter away.

Like the unreacted O atoms produced by atom abstraction, these unreactive triplet O_2 molecules should be detectable by mass spectrometry. The unreactive triplet partners should be distinguishable from scattered O_2 monomers and scattered O_2 molecules from $(O_2)_2$ dimers that broke up without converting one partner to a singlet state by their much lower velocities, since the majority of their kinetic energy will have been expended exciting their partner molecules to singlet electronic states.

III.4.e Ar(O_2) Dimers as a Control for Mass Effects

As discussed in Chapter I, it has previously been observed that the increased reactivity of Xe(F_2) and Kr(F_2) van der Waals dimers versus F_2 monomers on Si(100) is due to more efficient vibrational excitation of the lattice due to multiple collisions by heavier molecules, rather than due to any difference in the F_2 molecules' electronic structures.[33,34] To determine whether a similar effect is present in the reactivity differences between O_2 monomers and $(O_2)_2$ dimers, it is prudent to run a control comparing the reactivity of O_2 monomers to that of a van der Waals dimer similar in mass to the $(O_2)_2$ dimers but with the same electronic structure as the monomer.

Ar(O_2) dimers serve this purpose well, as their mass (72 amu) is just over twice that of O_2 monomers (32 amu) but, since Ar is a closed-shell noble gas, the O_2 molecule in the dimer has the same triplet electronic state as a free O_2 monomer. Molecular beams of Ar(O_2) dimers can be produced in the supersonic beam from gas mixtures of Ar and O_2 in a similar fashion to the Kr(F_2) and Xe(F_2) dimers produced for the study discussed in Chapter I.

If increased reactivity with Si is observed for Ar(O_2) versus O_2 at similar beam energies, the most likely explanation is more efficient collisional lattice excitation being channeled into electronic excitation of the Si lattice and making reaction of triplet O_2 with the Si lattice more facile. On the other hand, differences in the reactivity of Ar(O_2) and $(O_2)_2$ are likely to be due to differences in reactivity of triplet and singlet oxygen, whether due to four-centered reactions (which should be more favored at low translational energies) or non-adiabatic ladder climbing (which should be more favored at high translational energies).

Chapter III References

(1) D. Hocine, M.S. Belkaïd, and K. Lagha, *Revue des Energies Renouvelables* **1**, 379-384, (2008).

(2) S.-C. Chiao, J.-L. Zhou, and H. A. Macleod, *Applied Optics* **32**, 5557-5560, (1993).

(3) H. Colder, P. Marie, and F. Gourbilleau, *Thin Solid Films* **516**, 6930-6933, (2008).

(4) X. L. Fan, Y. F. Zhang, W. M. Lau and Z. F. Liu, *Phys. Rev. Lett.* **94**, 016101, (2005).

(5) K. Kato and T. Uda, *Phys. Rev. B* **62**, 15978-15988, (2000).

(6) B. Bussery and P. E. S. Wormer, *J. Chem. Phys.* **99**, 1230-1239, (1993).

(7) V. Aquilanti, D. Ascenzi, M. Bartolomei, D. Cappelletti, S. Cavalli, M. de Castro Vítores and F. Pirani, *Phys. Rev. Lett.* **82**, 69-72, (1999).

(8) V. Aquilanti, D. Ascenzi, M. Bartolomei, D. Cappelletti, S. Cavalli, M. de Castro Vítores and F. Pirani, *J. Am. Chem. Soc.* **121**, 10794-10802, (1999).

(9) H. Vach, T.-N. V. Nguyen, Q. K. Timerghazin and G. H. Peslherbe, *Phys. Rev. Lett.* **97**, 143402, (2006).

(10) T.-N. V. Nguyen, Q. K. Timerghazin, H. Vach, G. H. Peslherbe, *J. Chem. Phys.* **134**, 064305, (2011).

(11) M. P. D'Evelyn, Y. L. Yang, and L. F. Sutcu, *J. Chem. Phys.* **96**, 852-855, (1992).

(12) C. Silvestre and M. Shayegan, *Solid State Comm.* **77**, 735-738, (1991).

(13) D. A. King and M. G. Wells, *Surf. Sci.* **29**, 454, (1972).

(14) B. A. Ferguson, C. T. Reeves and C. B. Mullins, *J. Chem. Phys.* **110**, 11574-11584, (1999).

(15) M. L. Yu and B. N. Eldridge, *Phys. Rev. Lett.* **58**, 1691-1694, (1987).

(16) M. P. D'Evelyn, M. M. Nelson and T. Engel, *Surf. Sci.* **186**, 75-114, (1987).

(17) K. Kato, T. Uda and K. Terakura, *Phys. Rev. Lett.* **80**, 2000-2003, (1998).

(18) T. Hoshino, M. Tsuda, S. Oikawa and I. Ohdomari, *Phys. Rev. B* **50**, 14999-15008, (1994).

(19) Y. J. Chabal, K. Raghavachari, X. Zhang, and E. Garfunkel, *Phys. Rev. B* **66**, 161315, (2002).

(20) A. Incze, R. Del Sole and G. Onida, *Phys. Rev. B* **71**, 035350, (2005).

(21) A. Hemeryck, A. J. Mayne, N. Richard, A. Estève, Y. J. Chabal, M. D. Rouhani, G. Dujardin and G. Comtet, *J. Chem. Phys.* **126**, 114707, (2007).

(22) A. Hemeryck, A. Estève, N. Richard, M. D. Rouhani and Y. J. Chabal, *Phys. Rev. B* **79**, 035317, (2009).

(23) F. Fuchs, W. G. Schmidt and F. Bechstedt, *J. Phys. Chem. B* **109**, 17649-17653, (2005).

(24) T. Oshiro, C. K. Lutrus, D. E. Hagan and S. H. Suck Salk, *Solid State Comm.* **100**, 439-444, (1996).

(25) Y. L. Li, D. P. Pullman, J. J. Yang, A. A. Tsekouras, D. B. Gosalvez, K. B. Laughlin, Z. Zhang, M. T. Schulberg, D. J. Gladstone, M. McGonigal, and S. T. Ceyer, *Phys. Rev. Lett.* **74**, 2603-2606, (1995).

(26) M. R. Tate, D. Gosalvez-Blanco, D. P. Pullman, A. A. Tsekouras, Y. L. Li, J. J. Yang, K. B. Laughlin, S. C. Eckman, M. F. Bertino, and S. T. Ceyer, *J. Chem. Phys.* **111**, 3679-3695, (1999).

(27) M. R. Tate, D. P. Pullman, Y. L. Li, D. Gosalvez-Blanco, A. A. Tsekouras, and S. T. Ceyer, *J. Chem. Phys.* **112**, 5190-5204, (2000).

(28) J. S. Hess and D. J. Doren, *J. Phys. Chem. B* **106**, 8206-8210, (2002).

(29) M. G. Evans and M. C. Polanyi, *Trans. Faraday Soc.* **35**, 178-185, (1939).

(30) A. Malakhovskii, E. Sominska, and A. Gedanken, *J. Chem. Soc. Faraday Trans.* **92**, 1319-1322, (1996).

(31) A. van Deursen and J. Reuss, *Int. J. Mass. Spectrom. Ion Phys.* **23**, 109-122, (1977).

(32) M. Kappes and S. Leutwyler, *Atomic and Molecular Beam Methods, Volume 1*, 380-415, (1988).

(33) R. C. Hefty, Ph.D. Thesis, Massachusetts Institute of Technology, (2003).

(34) M. R. Blair, M.S. Thesis, Massachusetts Institute of Technology, (2014).

(35) T. A. Milne and F. T. Greene, *J. Chem. Phys.* **47**, 4095-4101, (1967).

(36) A. van Deursen, A. van Lumig, and J. Reuss, *International Journal of Mass Spectrometery and Ion Physics* **18**, 129-135, (1975).

(37) A. van Deursen and J. Reuss, *International Journal of Mass Spectrometry and Ion Physics* **24**, 199-206, (1977).

(38) A. van Deursen and J. Reuss, *International Journal of Mass Spectrometry and Ion Physics* **23**, 109-122, (1977).

(39) D. Kovalev, E. Gross, J. Diener, V. Yu Timoshenko and M. Fujii, *Appl. Phys. Lett.* **85**, 3590-3592, (2004).

(40) S. T. Ceyer. *Science* **249**, 133-139, (1990).

(41) T.-N. V. Nguyen, D. M. Koch, H. Vach, and G. H. Peslherbe, *J. Chem. Phys.* **119**, 7451-7460, (2003).

(42) D. V. Daineka, F. Pradère and M. Châtelet, *Surf. Sci.* **519**, 64-72, (2002).

(43) D. V. Daineka, F. Pradère, M. Châtelet, and E. Fort, *J. Appl. Phys.* **92**, 1132-1136, (2002).

Chapter IV: Scattering Machine Operations Manual

The past experiments discussed in Chapter I were performed, and the future experiments proposed in Chapter I and Chapter III are intended to be performed, using a molecular beam surface-scattering apparatus (the "Scattering Machine") that was built in the late 1980's by Professor Ceyer and three of her grad students: David Gladstone, Marianne McGonigal, and Michelle Schulberg.[1,2,3] Dual supersonic molecular beams are produced in two triply differentially pumped sources. The primary source nozzle can be temperature-controlled between 200 K and 375 K and both beams are directed into an ultra-high vacuum (UHV) chamber with a base pressure of 5×10^{-11} Torr, where they intersect at the surface of a rotatable Si(100)2×1 single crystal that can be temperature controlled between 130 K and 1300 K. A rotatable, triply differentially pumped line-of-sight mass spectrometer equipped with a chopper wheel for time-of-flight capability is used to analyze products scattered or desorbed from the surface. Even at experimental pressures two orders of magnitude above the base pressure, the mean free path of small diatomic molecules (N_2, O_2, F_2) in the chamber is well over a kilometer, ensuring that products reach the detector before experiencing additional collisions.

The Scattering Machine has accumulated modifications over the years as other grad students have repaired it and changed various functionalities,[4,5,6,7,8,9] but no unified documentation has been maintained for either maintenance or operation of the machine over this time. The following chapter is an attempt to rectify that omission.

IV.1 Overview of Basic Operations

IV.1.a Using the Pumps and Ion Gauges

IV.1.a.1 Main Chamber and Second Stage Pumping

The main chamber and second stage chamber are pumped by oil diffusion pumps with liquid nitrogen baffle traps and backed by rotary vane mechanical pumps. The liquid nitrogen for the traps is supplied from 240 L tanks provided by the MIT Cryogenic Lab; a thermistor sensor in each trap triggers automatic fills as needed and when both pumps are running, they consume about 120 L of ℓN_2 per day. The diffusion pumps are controlled through an interlock box that monitors foreline pressure, cooling water flow, diffusion pump temperature, ℓN_2 level, and—for the main chamber only—whether current is flowing through one of the three legs of the three-phase diffusion pump heater. Each pump is topped with a pneumatic gate valve that automatically closes when the interlock box turns off the pump to prevent diffusion pump oil from contaminating the chamber. In addition, the main chamber diffusion pump also has a pneumatic foreline valve that closes in the case of a fault.

IV.1.a.2 Source and First Stage Pumping

The source A, source B, first A, and first B chambers on the molecular beam source are, like the main chamber and second stage, pumped by oil diffusion pumps backed by rotary vane mechanical pumps. However, these four chambers do not have gate valves or ℓN_2 traps, as it is not necessary to maintain UHV or near-UHV in these chambers. Their diffusion pumps are controlled through an interlock box that monitors cooling water flow and foreline pressure. The interlock box also has temperature interlocks, but as the diffusion pumps for these chambers do not currently have temperature sensors, the temperature interlocks are not monitored at present.

Since most of the gas that escapes from the nozzle in the formation of a molecular beam does not make it through the skimmer between the source and first stage chambers, running a supersonic beam with a high nozzle pressure can cause a significant increase in foreline pressure that taxes the pumping speed of the mechanical pumps. A roots blower pump is installed in the source A foreline and there is provision for one in the source B foreline to increase the pressure at the mechanical pump intake and so increase its pumping speed. Since the roots blower pump is not interlocked, but will be damaged if it is run at too high foreline pressure, it is best to keep this pump turned off unless one is actually running a beam. However, since it reduces the gas conductivity of the source A foreline, it is often necessary to pulse it on while pumping out that foreline to temporarily increase conductivity.

IV.1.a.3 Lid Pumping

The rotatable lid of the main chamber contains the detector box, itself an independent, differentially pumped ultra-high vacuum chamber. The detector box consists of two nearly-independent chambers (the first and second stages) connected solely by a beam hole. Each of these chambers is pumped by a turbomolecular pump, and a third turbomolecular pump is located on top of the liquid nitrogen-cooled cryostat that contains the mass spectrometer ionizer, essentially a third pumping stage. These three turbomolecular pumps are backed by a turbomolecular backing pump, which itself is backed by a mechanical vane pump. The three primary turbomolecular pumps on the lid require cooling water to run and, along with the backing turbomolecular pump, are controlled by an interlock box that monitors foreline pressure and the pressure at the intake of the backing turbomolecular pump. In the case of a fault, the interlock box will close the pneumatic gate valves between the detector box and pumps to avoid venting the detector box, stop and vent the turbomolecular pumps, and close the foreline valve on the backing turbo, thereby maintaining the foreline under vacuum and preventing the stalling of the mechanical backing pump..

In addition to the differential pumping chambers of the detector box, the lid also has a separate chamber holding the motor for the chopper wheel. This chamber is completely isolated from the detector box, but connected to the main chamber via a Viton seal on its maintenance door and via the axle of the chopper wheel. The chopper chamber can also be roughed out and vented through an all-metal right-angle valve connecting it to the main chamber. The primary pump on the chopper chamber is an ion pump attached directly on top of it with a mechanical gate valve to allow the ion pump to remain under vacuum when the chopper chamber is vented.

IV.1.a.4 Seals and Manifold Pumping

The gas manifold that supplies gas for sputtering the crystal and producing molecular beams is pumped by a turbomolecular pump backed by a rotary vane pump. This pump is not interlocked, but it is configured with vent and gate valves that will isolate and vent it if power to the pump controller is lost. One unusual feature of this pump is that it needs to be "run in". When you start the pump controller, it will offer you two running-in programs. If the pump has been turned off for an extended period—more than a few days—you should run it in using Program 2, which will take about 2-1/2 hours. (Program 1 is used only after the pump's bearings have been replaced.) Unlike the majority of pumps on the machine, where we only measure the pressure of the foreline between the backing and high vacuum pumps, the manifold has two gauges. The foreline pressure is monitored by a thermocouple gauge with a readout on the electronics rack with the other foreline pressures. The pressure at the intake of the turbomolecular pump is monitored by a Pirani gauge with a readout on the same cart as the pump and its controller.

The rotatable lid and crystal manipulator, as well as the large door flanges and the window flange directly in line with the primary beam, have differentially pumped Viton or Teflon seals to allow the main chamber to maintain UHV. The rotatable seals and flange seals share a common first stage, pumped by a rotary vane mechanical pump and monitored by a foreline thermocouple gauge with its reader (uniquely among the pressure gauges on the Scattering Machine) located on the analytic instruments electronics rack. There are two separate second pumping stages, one for the lid and manipulator seals and one for the door and window seals. Each of these is pumped by an ion pump. The lid and manipulator also have a third stage of seals, which is not currently pumped. Although there is a small ion pump attached to it, this pump does not work and so the bypass valve between the second and third stages is kept open at all times to prevent a virtual leak in the third stage.

IV.1.a.5 Ion Gauges

The main chamber pressure is monitored via a nude UHV ion gauge controlled by a computerized controller that maintains a record of the pressure over time and allows one to plot this record at arbitrary scales. It also outputs the pressure signal via an analog signal through a BNC cable to the data acquisition computer, allowing pressure data to be recorded more permanently when necessary. The controller also has an automatic timed degas function, which will degas the filament and return to normal operation without further user involvement once the degas function is selected. When the controller loses power, however, it reverts to factory settings and must be set for "nude UHV gauge" before it will give accurate readings.

An older ion gauge controller is used for the nude UHV ion gauge that monitors the pressure in the second stage. This controller's degas switch is not timed; it requires human intervention to turn off the degas feature when the pressure has stabilized, usually after about half an hour. Nude ion gauges are also installed in first A and first B through feedthroughs on the sides of these chambers and a glass bulb ion gauge is present on the source A chamber with provision for one to be attached on the source B chamber as well. However, these gauges are not currently attached to ion gauge controllers; to monitor them it is necessary to turn off one of the controllers and connect it to these gauges instead.

IV.1.b Using the Crystal and Crystal Manipulator

IV.1.b.1 Setting the Vertical Crystal Position

The crystal manipulator flange is mounted to a small up-down translation stage attached to the main in-out translation stage controlled by the chain drive. This vertical translation stage, shown in Figure IV-1, has a range of one inch and its midpoint, 0.50 in from the bottom, should be in the plane of the molecular beams and detector. The position is read from the bottom of the moving block to the bottom of the translation range. There are two black marks on the stationary part, the higher of which corresponds to the 0.50 in position.

The up-down motion of the crystal is controlled by a rotating threaded rod; you can turn it by hand via the large nut at the bottom of the stationary part of the translation stage, though it is sometimes necessary to use a wrench, particularly when raising the crystal.

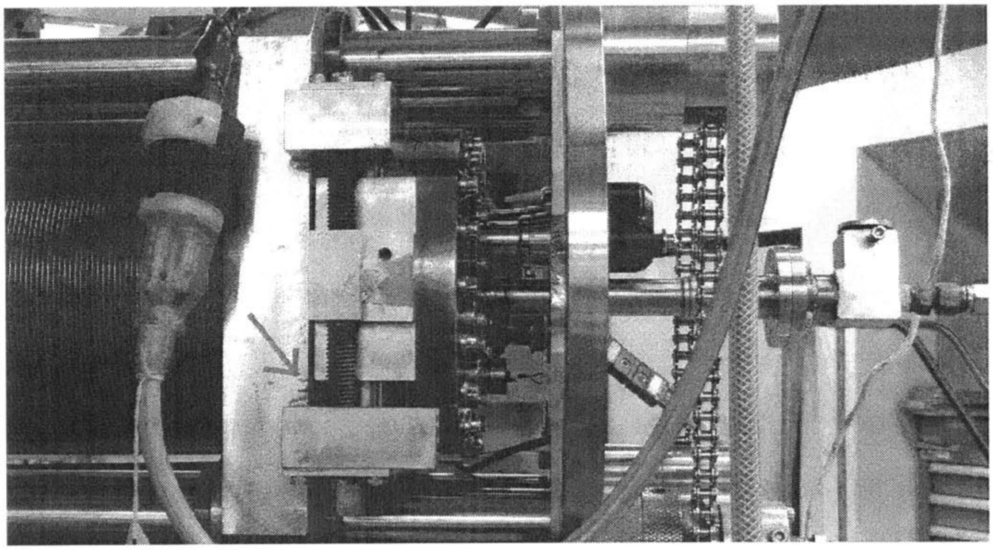

Figure IV-1: Setting the Vertical Crystal Position

The red arrow indicates the mark for the 0.50 inch vertical position on the vertical translation stage.

IV.1.b.2 Setting the Horizontal Crystal Position

The chain drive at the end of the crystal manipulator is used to set the horizontal position of the crystal. When the crystal is not actively being translated, the lock-wheel at the top of the chain drive should be engaged to keep the manipulator from sliding into the machine under the influence of atmospheric pressure. The position of the crystal can be read off a long metal ruler that properly should be fixed in place along the manipulator with aluminum tape. Recently, though, we've had trouble keeping it secured, so it sits under the manipulator and is held in place by hand as needed. Put it against the Auger side of the manipulator arm, flush with the lower (not-vertically-translating) part of the block that supports the manipulator flange, and read the position on the left end of said block, as shown in Figure IV-2. Several important positions are marked on the ruler:

- Vent, at 27.70 inches, is the position the manipulator should be in for venting and for baking out; it is the farthest safe extension of the manipulator.
- Sputter, at 26.55 inches, is aligned in front of the ion gun for sputtering the crystal.
- Auger, at 20.40 inches, is aligned in front of the Auger and is used for taking Auger spectra.
- Scattering, at 11.70 inches, is at the point where the two molecular beams cross, and the center of the rotation of the detector. It is used for all molecular beam experiments.

IV.1.b.3 Setting the Crystal Angle

The linear motion feed-through, shown in Figure IV-3, that we use to set the crystal angle is a bit counter-intuitive to read. As seen in the following diagram, the linear motion feed-through has a rod extending from it; the rod is fully extended when the crystal is facing the Auger (180°) spectrometer and fully retracted when the crystal is normal to the primary beam

(0°). The feed-through gives read-outs in terms of the position of the rod, which then has to be converted into the crystal angle.

There are twenty-six tick marks incised on the rod, so that when the rod is fully extended, twenty-five tick marks are exposed and we read the position as 0 ticks. As you turn the dial to retract the rod (and rotate the crystal), tick marks disappear into the body of the dial and we can count the position by how many have disappeared. The dial of the feed-through is marked in fractional tick marks with the pointer at 11-o'clock when one is looking down the manipulator arm. Each tick mark represents 7.05° and the crystal is at 180° (Auger angle) at 0 ticks. The crystal angle decreases as the tick reading increases, so the crystal is normal to the primary beam (0°) at 25.53 ticks.

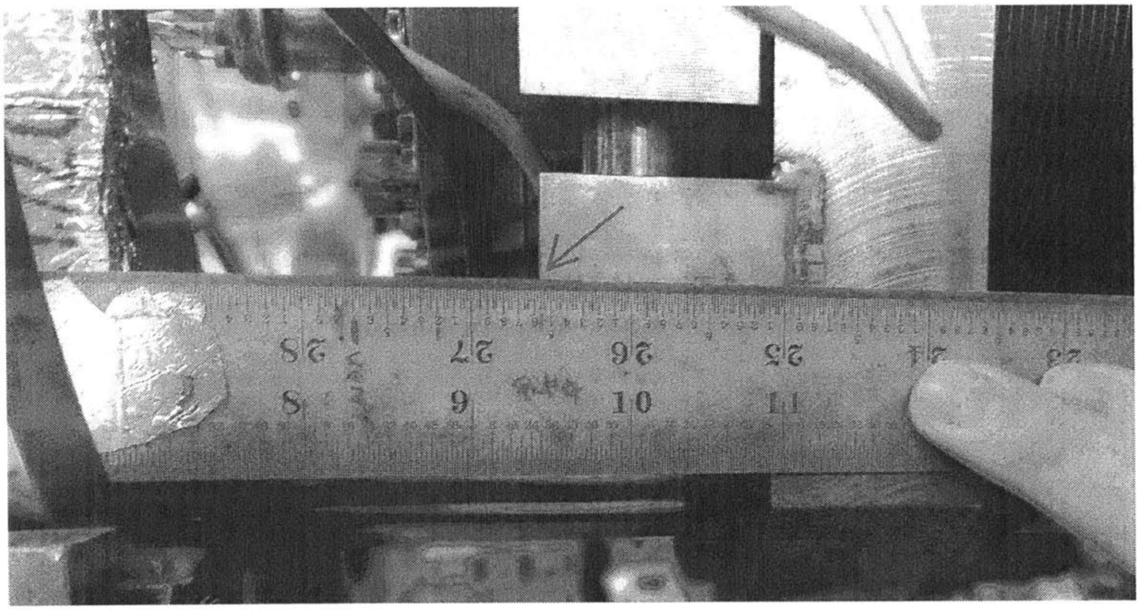

Figure IV-2: Setting the Horizontal Crystal Position

In this photo, the crystal is set in the sputter position and the red arrow points to where the position is read.

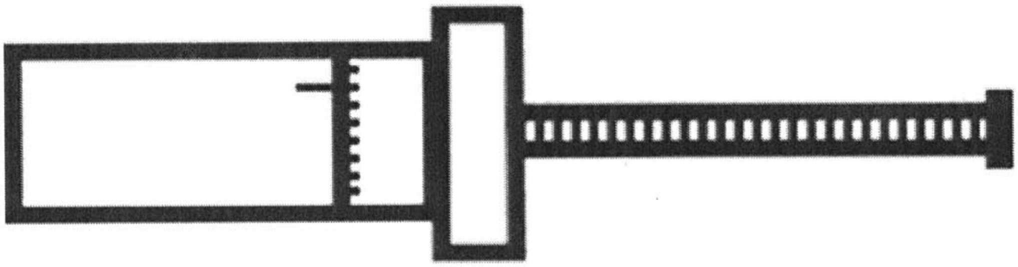

Figure IV-3: Linear Motion Feed-Through for Setting the Crystal Angle

A diagram of the linear motion feed through. The rod to the right has 25 tick marks visible and the 26th is at the edge of the dial, so the reading is 0 tick marks (as none are fully covered). The dial on the left reads fractional tick marks.

IV.1.b.4 Rotating the Manipulator About its Long Axis

For experimental purposes, we mainly care about rotating the crystal around the vertical axis, to face the detector box or molecular beams, or be at other angles while normal to the beam plane. This rotation (which also changes the angle of incidence of the beam to the crystal) is done with the linear-motion feedthrough discussed in the previous section. However, the entire crystal manipulator assembly is attached to the main chamber via a set of differentially pumped St. Gobain seals, just as the lid is. A large chain drive allows you to rotate the manipulator assembly itself along its main axis, changing the azimuthal angle of the beam to the crystal. If the crystal is not in the center of rotation of the manipulator, this rotation will move the crystal above or below the beam plane. This rotation has not been used for experimental purposes up to this time, but you may need to shift the manipulator assembly a very small amount in one direction or another when attaching the manipulator to the manipulator removal jig, or when reinstalling the manipulator, to get everything to align and fit together.

IV.1.b.5 Crystal Thermocouple Readout

The crystal temperature is monitored by the thermocouple read-out box directly below the manipulator. It gives the reading of the type-C (tungsten-5% rhenium versus tungsten-26% rhenium) thermocouple in millivolts; the chart in Figure IV-4 gives the conversion to temperature.

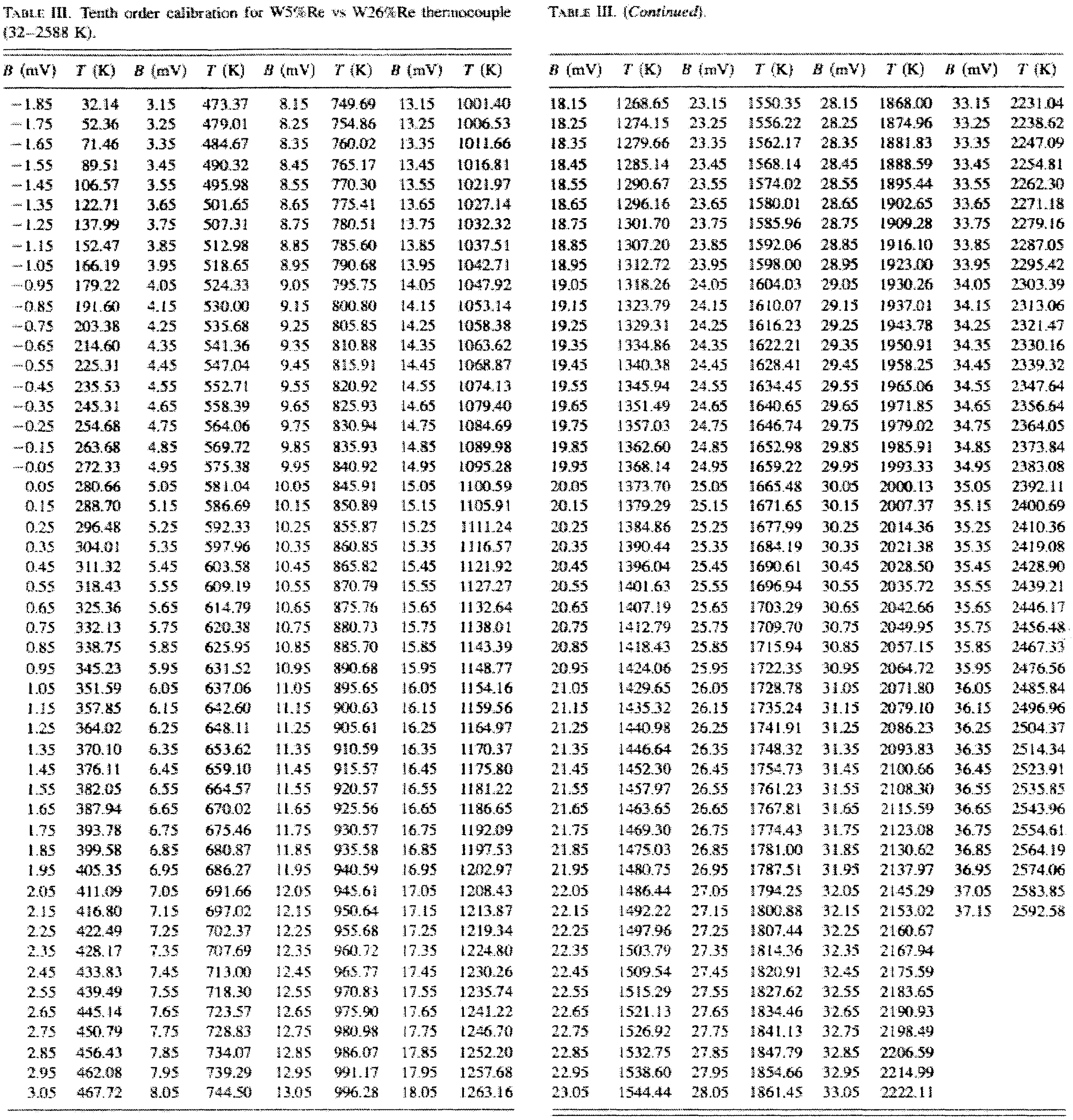

TABLE III. Tenth order calibration for W5%Re vs W26%Re thermocouple (32–2588 K).

B (mV)	T (K)	B (mV)	T (K)	B (mV)	T (K)	B (mV)	T (K)
−1.85	32.14	3.15	473.37	8.15	749.69	13.15	1001.40
−1.75	52.36	3.25	479.01	8.25	754.86	13.25	1006.53
−1.65	71.46	3.35	484.67	8.35	760.02	13.35	1011.66
−1.55	89.51	3.45	490.32	8.45	765.17	13.45	1016.81
−1.45	106.57	3.55	495.98	8.55	770.30	13.55	1021.97
−1.35	122.71	3.65	501.65	8.65	775.41	13.65	1027.14
−1.25	137.99	3.75	507.31	8.75	780.51	13.75	1032.32
−1.15	152.47	3.85	512.98	8.85	785.60	13.85	1037.51
−1.05	166.19	3.95	518.65	8.95	790.68	13.95	1042.71
−0.95	179.22	4.05	524.33	9.05	795.75	14.05	1047.92
−0.85	191.60	4.15	530.00	9.15	800.80	14.15	1053.14
−0.75	203.38	4.25	535.68	9.25	805.85	14.25	1058.38
−0.65	214.60	4.35	541.36	9.35	810.88	14.35	1063.62
−0.55	225.31	4.45	547.04	9.45	815.91	14.45	1068.87
−0.45	235.53	4.55	552.71	9.55	820.92	14.55	1074.13
−0.35	245.31	4.65	558.39	9.65	825.93	14.65	1079.40
−0.25	254.68	4.75	564.06	9.75	830.94	14.75	1084.69
−0.15	263.68	4.85	569.72	9.85	835.93	14.85	1089.98
−0.05	272.33	4.95	575.38	9.95	840.92	14.95	1095.28
0.05	280.66	5.05	581.04	10.05	845.91	15.05	1100.59
0.15	288.70	5.15	586.69	10.15	850.89	15.15	1105.91
0.25	296.48	5.25	592.33	10.25	855.87	15.25	1111.24
0.35	304.01	5.35	597.96	10.35	860.85	15.35	1116.57
0.45	311.32	5.45	603.58	10.45	865.82	15.45	1121.92
0.55	318.43	5.55	609.19	10.55	870.79	15.55	1127.27
0.65	325.36	5.65	614.79	10.65	875.76	15.65	1132.64
0.75	332.13	5.75	620.38	10.75	880.73	15.75	1138.01
0.85	338.75	5.85	625.95	10.85	885.70	15.85	1143.39
0.95	345.23	5.95	631.52	10.95	890.68	15.95	1148.77
1.05	351.59	6.05	637.06	11.05	895.65	16.05	1154.16
1.15	357.85	6.15	642.60	11.15	900.63	16.15	1159.56
1.25	364.02	6.25	648.11	11.25	905.61	16.25	1164.97
1.35	370.10	6.35	653.62	11.35	910.59	16.35	1170.37
1.45	376.11	6.45	659.10	11.45	915.57	16.45	1175.80
1.55	382.05	6.55	664.57	11.55	920.57	16.55	1181.22
1.65	387.94	6.65	670.02	11.65	925.56	16.65	1186.65
1.75	393.78	6.75	675.46	11.75	930.57	16.75	1192.09
1.85	399.58	6.85	680.87	11.85	935.58	16.85	1197.53
1.95	405.35	6.95	686.27	11.95	940.59	16.95	1202.97
2.05	411.09	7.05	691.66	12.05	945.61	17.05	1208.43
2.15	416.80	7.15	697.02	12.15	950.64	17.15	1213.87
2.25	422.49	7.25	702.37	12.25	955.68	17.25	1219.34
2.35	428.17	7.35	707.69	12.35	960.72	17.35	1224.80
2.45	433.83	7.45	713.00	12.45	965.77	17.45	1230.26
2.55	439.49	7.55	718.30	12.55	970.83	17.55	1235.74
2.65	445.14	7.65	723.57	12.65	975.90	17.65	1241.22
2.75	450.79	7.75	728.83	12.75	980.98	17.75	1246.70
2.85	456.43	7.85	734.07	12.85	986.07	17.85	1252.20
2.95	462.08	7.95	739.29	12.95	991.17	17.95	1257.68
3.05	467.72	8.05	744.50	13.05	996.28	18.05	1263.16

TABLE III. (*Continued*).

B (mV)	T (K)	B (mV)	T (K)	B (mV)	T (K)	B (mV)	T (K)
18.15	1268.65	23.15	1550.35	28.15	1868.00	33.15	2231.04
18.25	1274.15	23.25	1556.22	28.25	1874.96	33.25	2238.62
18.35	1279.66	23.35	1562.17	28.35	1881.83	33.35	2247.09
18.45	1285.14	23.45	1568.14	28.45	1888.59	33.45	2254.81
18.55	1290.67	23.55	1574.02	28.55	1895.44	33.55	2262.30
18.65	1296.16	23.65	1580.01	28.65	1902.65	33.65	2271.18
18.75	1301.70	23.75	1585.96	28.75	1909.28	33.75	2279.16
18.85	1307.20	23.85	1592.06	28.85	1916.10	33.85	2287.05
18.95	1312.72	23.95	1598.00	28.95	1923.00	33.95	2295.42
19.05	1318.26	24.05	1604.03	29.05	1930.26	34.05	2303.39
19.15	1323.79	24.15	1610.07	29.15	1937.01	34.15	2313.06
19.25	1329.31	24.25	1616.23	29.25	1943.78	34.25	2321.47
19.35	1334.86	24.35	1622.21	29.35	1950.91	34.35	2330.16
19.45	1340.38	24.45	1628.41	29.45	1958.25	34.45	2339.32
19.55	1345.94	24.55	1634.45	29.55	1965.06	34.55	2347.64
19.65	1351.49	24.65	1640.65	29.65	1971.85	34.65	2356.64
19.75	1357.03	24.75	1646.74	29.75	1979.02	34.75	2364.05
19.85	1362.60	24.85	1652.98	29.85	1985.91	34.85	2373.84
19.95	1368.14	24.95	1659.22	29.95	1993.33	34.95	2383.08
20.05	1373.70	25.05	1665.48	30.05	2000.13	35.05	2392.11
20.15	1379.29	25.15	1671.65	30.15	2007.37	35.15	2400.69
20.25	1384.86	25.25	1677.99	30.25	2014.36	35.25	2410.36
20.35	1390.44	25.35	1684.19	30.35	2021.38	35.35	2419.08
20.45	1396.04	25.45	1690.61	30.45	2028.50	35.45	2428.90
20.55	1401.63	25.55	1696.94	30.55	2035.72	35.55	2439.21
20.65	1407.19	25.65	1703.29	30.65	2042.66	35.65	2446.17
20.75	1412.79	25.75	1709.70	30.75	2049.95	35.75	2456.48
20.85	1418.43	25.85	1715.94	30.85	2057.15	35.85	2467.33
20.95	1424.06	25.95	1722.35	30.95	2064.72	35.95	2476.56
21.05	1429.65	26.05	1728.78	31.05	2071.80	36.05	2485.84
21.15	1435.32	26.15	1735.24	31.15	2079.10	36.15	2496.96
21.25	1440.98	26.25	1741.91	31.25	2086.23	36.25	2504.37
21.35	1446.64	26.35	1748.32	31.35	2093.83	36.35	2514.34
21.45	1452.30	26.45	1754.73	31.45	2100.66	36.45	2523.91
21.55	1457.97	26.55	1761.23	31.55	2108.30	36.55	2535.85
21.65	1463.65	26.65	1767.81	31.65	2115.59	36.65	2543.96
21.75	1469.30	26.75	1774.43	31.75	2123.08	36.75	2554.61
21.85	1475.03	26.85	1781.00	31.85	2130.62	36.85	2564.19
21.95	1480.75	26.95	1787.51	31.95	2137.97	36.95	2574.06
22.05	1486.44	27.05	1794.25	32.05	2145.29	37.05	2583.85
22.15	1492.22	27.15	1800.88	32.15	2153.02	37.15	2592.58
22.25	1497.96	27.25	1807.44	32.25	2160.67		
22.35	1503.79	27.35	1814.36	32.35	2167.94		
22.45	1509.54	27.45	1820.91	32.45	2175.59		
22.55	1515.29	27.55	1827.62	32.55	2183.65		
22.65	1521.13	27.65	1834.46	32.65	2190.93		
22.75	1526.92	27.75	1841.13	32.75	2198.49		
22.85	1532.75	27.85	1847.79	32.85	2206.59		
22.95	1538.60	27.95	1854.66	32.95	2214.99		
23.05	1544.44	28.05	1861.45	33.05	2222.11		

Figure IV-4: Crystal Thermocouple Volt-to-Temperature Conversion

This chart is taken from Smentkowski & Yates, 1996.[10]

IV.1.b.6 Crystal Cooling Procedure

We cool the crystal with a flow of liquid nitrogen from the same ℓN_2 tank that is used to fill the diffusion pump ℓN_2 traps. To set up crystal cooling, attach the branched ℓN_2 line to the nitrogen cooling tube on the end of the crystal manipulator, being sure to align it properly and tighten it firmly, but not to over-tighten it. Open the valve to the branched ℓN_2 line, adjusting it until you get a flow that results in a few visible droplets of ℓN_2 escaping from the vent on the nitrogen cooling tube, but no droplets falling to the floor from the tube. If the crystal is in a position where the vent line is spraying the manipulator gear train, you should set up a piece of aluminum foil to block the spray.

After about a half an hour, the crystal should reach its minimum temperature, roughly -1.40 V on the type-C thermocouple, or 115 K. It will return to this temperature significantly more quickly after being heated, since the main thermal mass of the manipulator arm and the copper block to which the crystal support is attached remains cold when the crystal is resistively heated.

When finished with crystal cooling for the day, close the valve and allow half an hour for the ℓN_2 tube fittings to warm enough to no longer be frosted. Then remove the ℓN_2 branch line and replace it with the lab nitrogen gas line; blow nitrogen through the tube overnight, or at least until the crystal is no longer below freezing. This action is critical because it prevents water from condensing inside the crystal cooling line, and then being refrozen upon application of the next ℓN_2 cycle. Because water expands when it freezes, the expansion may cause stress on the cooling lines, and hence cracks and leaks in the cooling lines.

IV.1.b.7 Crystal Sputtering Procedure

- Move the crystal to the sputter position: in the center (0.5" from the bottom) of the vertical translation stage and at the sputter mark (26.55") on the long metal ruler used to indicate horizontal translation. If you intend to anneal the crystal after sputtering, it is best to cool the crystal beforehand, as it will take at least twenty minutes for its temperature to stabilize at 130 K (-1.34 V on the type-C thermocouple).
- Set up the manifold for argon sputtering, with a manifold pressure of ~20 psi. Make sure that the sputtering leak valve remains closed, however.
- Ensure that both heater clips are clipped to a grounding braid while you sputter.
- Turn on the sputter gun controller and raise filament current to 1.3 A as read on the attached multimeter (which should be on the 20 V DC scale—don't ask). Be careful not to touch the focus knob. (If you do by accident, the correct setting is 1.50. Also, the beam voltage should be set at 1500 V.)
- While the filament sits at that setting, open the sputter leak valve, raising main chamber pressure to $5 \bullet 10^{-5}$ Torr.
- Do not leave the room while the leak valve is open, because the main chamber pressure will skyrocket if the gate valve closes. (In the past, sputtering has tended to cause random gate valve closes, though recent improvements to interlock grounding have mostly fixed this problem. In particular, a metal plate was clamped to the top of the open metal box containing the relays between the nitrogen fill controllers and the main chamber and second stage interlock box and connected by grounding braid to the machine ground. The main chamber diffusion pump current monitoring box was also grounded more thoroughly.) If the gate

valve does close, reopen it immediately and make sure to sputter for at least five minutes past the point when you reopened it.

- Immediately raise the filament current to 2.27 A and switch the sputter control to manual. Start time on the sputter.
- When the sputter is complete, close the leak valve, turn off the sputter gun filament, and finally pump out the manifold. (It's okay to leave gas in the manifold if you're planning on sputtering again in the next hour or two.) The main chamber pressure should recover within a few minutes of the leak valve being closed.

IV.1.b.8 Crystal Annealing Procedure

- Cool the crystal to at least 130 K (-1.34 V on the type-C thermocouple). This cooling will take some time, perhaps twenty minutes. You can turn on the crystal heating power supply at this point. (It is not fundamentally necessary that the crystal cryostat be cooled before a flash. However, if it is not cooled, it will be necessary to determine a lower peak current to avoid overheating and potentially melting the crystal.)
- Move the heater clips on the manipulator to their ungrounded positions, making sure that they aren't shorted together.
- Switch the input setting on the heating power supply to PID and start the FLASH program on the computer. (If you start FLASH program before switching input mode to PID, though, bad things will happen and you may need to reboot the computer.)
- Check that the FLASH program's settings are:
    - peak current = 3.6 A
    - pause current = 8.0 A
    - pause time = 60 sec

  - ramp up = 0.02 A/sec
  - ramp down = 0.02 A/sec
  - hold time = [time you want to anneal for in seconds]
- Run the flash. Watch to make sure that it reaches the correct temperature and current and stops there.

IV.1.c Using the Nozzles and Molecular Beams

IV.1.c.1 Nozzle Heating

To heat the nozzle, use a variac and the nozzle heating control box on the manifold baratron controller stand. The nozzle heating plug can be plugged into the variac, which itself should be plugged into the nozzle heating control box on the baratron readout stand. With the nozzle (not the nozzle cryostat) thermocouple also connected to the box, it acts as a temperature-control PID, keeping the nozzle at a preset temperature. To set the temperature, hit the "menu" button on the thermocouple readout, then use the up and left arrow buttons to cycle through values for each digit until you've reached the ones you want. You shouldn't set this temperature above 60°C; during initial heat-up, though, the nozzle temperature will overshoot by around 10°C. Set the variac to no higher than 15 V to keep it from overshooting by even more.

Be very careful to make sure you have the right thermocouple attached to the temperature-monitoring PID: there are two plugs coming out of the back of source A. One is for a thermocouple on the tip of the nozzle, the other for one attached to the base of the cooling cryostat. Both are type K (nickel-chromium versus nickel-alumel) thermocouples. The heating wire is wrapped around the tip of the nozzle, but the cryostat is some distance away and connected by a long copper braid, meaning that the cryostat thermocouple generally (during heating or cooling) will measure a much lower temperature than the actual temperature. This awareness is especially important during heating, because if you heat the nozzle much above 70°C, you risk damaging the heating wires wrapped around it and softening the nozzle holder, which is made of polyether ketone (PEK) that has a glass transition temperature of 143°C.

IV.1.c.2 Nozzle Cooling

To cool the nozzle to minimum temperature, you want to set the temperature on the PID as low as possible so that it won't keep trying to turn on the heating variac (which shouldn't be on/attached, anyway) to warm the nozzle back up. The liquid helium refrigerator doesn't interact with the PID: the refrigerator just tries to get the nozzle as cool as it can. If you want to set to a specific temperature, you can attach the PID to the nozzle thermocouple (not the nozzle cryostat thermocouple) and have the heating variac heat the nozzle to counteract the cooling. Note that while you can leave the compressor on for extended periods, you only want the cold head on when you're actually cooling. The switch to turn it on (on the body of the compressor) is a bit dodgy. You want to turn off the DP interlocks while turning it on or off, because it generates a lot of electrical noise, and you need to be sure it actually locks on. You should be able to hear a regular pulsing pumping sound when it is on. I recommend looking at the manual for it before operating it. It also gives directions for recharging the helium and doing helium purges using a special fixture in the form of a long copper tube with two special fittings on one end. Be sure to use the ultra-pure (99.999% pure) helium for this, not the low-purity helium we use for leak-checking. In general, we've found that one can get a lower minimum temperature the first day we use the cooling after having baked out the nozzle overnight. This phenomenon is attributed to oil condensation on the nozzle when it is at cryogenic temperatures.

IV.1.c.3 Cleaning a Clogged Nozzle

See Section IV.4.a.3 .

IV.1.c.4 Opening the Beam Valve

The source chambers are separated from the main chamber via a beam valve in the second stage that can be opened via a linear motion feedthrough that comes out of the side of the main chamber wall at an angle. Turning the feed-through clockwise—spin in—closes the valve and turning it counter-clockwise—spin out—opens it. There are actually two separate beam holes, one for each beam line, and since the feed-through is closer to the source B side, it's possible to open only the source A beam hole, which is preferable if you're only using the primary beam. You can determine if the beam valve has opened properly by looking for pressure changes in the second stage and main chamber ion gauges. Be careful not to over-tighten it (or over-open it), as the sliding beam valve is an angled chain of aluminum links that can be broken fairly easily if you put too much strain on them.

IV.1.c.5 Using the Beam Flags

Within the second stage, there are two solenoid-powered beam flags that can block either or both of the molecular beams. Both are default closed. They can be opened via a control box located on the upper left of the left analytic instruments electronics rack. The box has two switches and a red LED that is illuminated when the flags are open. The upper switch selects between manual control (up) and computer control (down), and the lower switch selects between open (up) and closed (down) for the flags.

However, both flags don't actually have to be opened and closed simultaneously. There is a second control box attached to the side of the source chamber itself, near the beam valve feed-through that determines which flag or flags will open. It has three-way switches for each flag: if a flag's switch is in the down position, it will remain closed constantly; if it is in the up position, it will open or close in accordance with the signal from the control box on the electronics rack. Behavior with the switches in the up position is undefined. The beam flag set-up is also described in Section IV.4.a.1 .

As a note of warning, the beam flag mechanisms can be a bit flimsy, and if the flag is closed with a high-pressure beam hitting it, it may jam closed. If it jams, turning off the beam by pumping out the nozzle and cycling the solenoid open and closed will usually fix the problem. If it doesn't, you may need to vent and pull back the source to adjust the flag by hand. Also, whenever you have the source pulled back, your last test before reinstalling it should be to make sure that the beam flags still work.

IV.1.d Using the Detector Box

IV.1.d.1 Opening the Beam Valve

Although the detector box is its own stand-alone differentially-pumped ultra-high vacuum chamber, there are two valves that connect it to the main chamber. One is an all-metal right-angle valve attached to a lid bellows that, when opened, connects the first differential pumping stage of the detector box to the main chamber for roughing and venting purposes. The other is the beam valve that opens to allow a molecular beam into the detector box mass spec.

The beam valve consists of a slider that moves up and down in front of the beam hole in the detector box as controlled by a linear motion feed-through in the center of the lid. Turning it spin-down (clockwise) closes the valve and turning it spin-up (counterclockwise) opens it. There are two "open" settings for the beam valve. In the first, a 0.012 in diameter hole in the beam valve plate is centered over the beam hole. In the second, the beam valve plate is entirely above the detector box beam hole. The purpose of the 0.012" diameter hole is to allow a reduction in sensitivity to avoid swamping the detector box when observing, for example, a beam being run directly into the detector without scattering. The full detector box beam hole is used for scattering experiments to maximize sensitivity. Unfortunately, there is no marking on the feed-through to identify when you're centered on the small hole. The best way to center the small hole on the beam hole in the detector chamber wall is to have the mass spectrometer sit on a mass that you know is present in the chamber in quantity (such as a beam you're running) and watching the counts while opening the valve. There should be peak count for each of the two beam holes: position the valve to maximize whichever of them you are looking for.

This valve is much more durable than the source beam valve, but it has also broken once in my time in the lab. The feed-through itself is a bit old and may be in danger of failing: in June

2014 we had to remove and disassemble it to fix a snapped retaining pin. After that pin was replaced, we were able to reinstall it. However, a replacement feed-through has been purchased so that we have a spare if necessary.

IV.1.d.2 Rotating the Lid

The lid can be rotated by using a wrench—there is one dedicated to this purpose—to turn the large nut on the lid chain drive. There is an angle scale marked in degrees on the lid with a position marker and vernier on the side of the chamber opposite the crystal manipulator. The vernier has four long ticks in each direction, with two small ticks between each pair of long ticks. Although not documented elsewhere, it appears that the long ticks indicate offsets of 15 minutes and the small ticks indicate offsets of 5 minutes. The scale is also slightly offset: true straight-through reads as 270.05° rather than 270°.[9] When rotating the lid, it is important to pay attention to make sure that nothing catches. The person rotating it should keep a close eye on the chain drive to make sure that no wires catch in the chain. They should also watch to make sure that the detector box foreline bellows and the copper pneumatic line of the detector box gate valves don't catch as the lid rotates. The best view is from the far side of the machine, so if a second person is available, it is useful to station them on a ladder near the crystal manipulator and source to watch the far side of the lid for snags.

IV.1.d.3 Using the Cryostat

Besides the three turbo pumps for the detector box's three differential pumping regions, the ionizer region is also pumped by a liquid nitrogen cryostat cooling a large copper block that surrounds the ionizer region. A large blue vacuum flask called the "chicken feeder" attaches to the fill arm on the rear of the cryostat via an annular disk with a nozzle and valve that control the escaping boiled-off nitrogen gas. The chicken feeder is filled through an opening at its top.

When it is not actively being filled, however, a rubber stopper with a length of hose about a foot long extending from it should be used to cover this vent opening. The function of the stopper and hose is to keep humid outside air from entering the chicken feeder and producing ice deposits.

The cryostat must be completely emptied and warmed to above freezing before a detector box vent (to avoid condensation inside the detector box) or bake-out. However, when the machine is operating properly and under vacuum, we keep the cryostat filled and cooled continuously to save time and reduce stress from repeated thermal cycling.

It is possible to run the detector box mass spectrometer with the cryostat warm, and this is in fact done to leak-check the detector box after a vent, since cooling the cryostat right before needing to bake out or vent again would be wasteful. However, one should not run it for too long in this condition, as the filament will eventually heat up the cryostat region and your spectrum quality will degrade. Also, while running the mass spec in this mode is fine for leak-checking, scattering data cannot be collected in this mode, because the entrance to the ionizer is not in the scattering plane due to thermal contraction of the ℓN_2 filled cryostat.

When the cryostat is filled, the venting valve on the annular disk is used to control the rate at which nitrogen boils off. There is a long hose with a mechanical gas flow meter that can be attached to the nozzle to calibrate the rate. During the day, to keep the cryostat at its operating temperature of -184°C, we usually run the flow at roughly 30 psig. Overnight, to keep the cryostat from drying out for the eighteen or so hours that it may be left unattended, we run a flow of roughly 10-15 psig.

One common problem that can interfere with the cryostat is ice clogging the intake at the bottom of the chicken feeder. This problem can partly be avoided by scrupulously removing ice deposits that form in the fill hole at the top of the chicken feeder without letting them fall into it. If there is an ice clog, opening the valve all the way will not produce as much flow as expected and the cryostat thermocouple temperature will rise rapidly despite a good supply of liquid nitrogen. If this problem occurs, use a long, thin rod to poke at the hole in the center of the bottom of the chicken feeder to try and dislodge the clog. If that doesn't work, a last-ditch option is to warm the cryostat to room temperature to melt the clog and run dry nitrogen through it so that the water will evaporate.

IV.2 Using the Analytic Instruments

IV.2.a Using the Mass Spectrometers

IV.2.a.1 Overview

Both mass spectrometers on the Big Machine use roughly the same set of electronics on the racks by the data acquisition computer. The main difference is that, for the detector box mass spec, we use a separate power supply for the extractor, because the ionizer power supply doesn't generate a high enough extractor voltage. Because we use the same equipment, though, when switching between mass spectrometers, you need to switch:

- the RF cables (two cables) to the high-Q head for the spectrometer you're using
- the tuning of the RF power supply to be on a peak for that spectrometer
- the cables on the back of the ionizer power supply and the channeltron power supply to go to the right instrument
- the preamplifiers to be attached to the right instrument
- the signal line at the data acquisition computer's breakout boxes (We use different signal lines for each instrument.).

IV.2.a.2 Main Chamber Residual Gas Analyzer

The cable connections for the main chamber RGA are fairly obvious. To attach the BNC cables for the channeltron HV and the signal line, the protective jacket that slides off the back of the RGA must be removed. We never remove the two RF lines that go to the high-Q head, even for bake-outs. In general, we use high-Q head 11 for the RGA. The extractor voltage for the main chamber RGA is provided by the ionizer power supply, along with the other lens voltages.

IV.2.a.3 Detector Box Mass Spectrometer

The detector box channeltron flange on the lid has three connections. One is the former deflector plate connection, now a ground connection. The other two are a male MHV connection for the channeltron high voltage and a male BNC connection for the channeltron signal. With the deflector plate connection at 12 o'clock, the HV connection is at 8 o'clock and the signal connection is at 4 o'clock.

Unlike the main chamber RGA, we do remove the RF cables from the lid during bake-outs. We also remove the stand that the high-Q head rests on and the threaded rod that supports it. In general, we use high-Q head 14 for the detector box mass spectrometer. Historically, we used high-Q head 15 with added capacitors for high mass clusters.[6]

Since the ionizer power supply doesn't produce a high enough extractor voltage for our purposes, we use a separate power supply for the detector box extractor voltage.

The power cable for the mass spec preamp is connected with a Philmore T607C "3-pin mike connector". If you look at the solder connections with the indentation and screw hole at the top, the black wire goes to the upper left terminal, the right wire to the upper right terminal, and the bottom terminal is blank.

IV.2.a.4 Mass Spec Ionizer and Lens Settings

The mass spectrometer ionizer consists of a three-plate einzel lens with an additional extractor plate. For all masses, we use $L_1 = L_3 = 0$ V on the einzel lens, and –250 V on the extractor lens. We use $L_2 = -60$ V and an ion energy of 25 eV for He scattering, $L_2 = -200$ V and an ion energy of 35 eV for spectra in the 0 to 50 amu mass range, and $L_2 = -300$ and an ion energy of 45 eV for heavy-mass spectra. The channeltron HV can be used in the range from –2200 V up to –3000 V, but has recently been used as -2400 V.

IV.2.a.5 Tuning the Mass Spectrometer

The procedure for tuning either mass spectrometer is as follows. The mass spectrometer should be fully connected, although the signal line needn't be, before you begin. The ionizer, extractor, and channeltron HV don't need to be turned on.

- Put the quadrupole controller in standby and set the mode dial to "Align". Then, turn the controller on.
- If you're using High-Q Head 11, set "Frequency Range" (on the lower box) to "2"; if you're using High-Q Head 14, set it to "3".
- Turn the "Level" knob until the plate current meter (on the lower box) reads 100 mA.
- Turn the "Set" knob through its full range to find the value that maximizes the "Mass" meter reading.
- Flip the "DC/RF Balance" switch to "DC" and turn the "DC Balance" knob until the "DC/RF Balance" meter reads zero.
- Flip the "DC/RF Balance" switch to "RF" and turn the "RF Balance" knob (on the high-Q head) until the "DC/RF Balance" meter reads zero.
- Repeat the previous two steps until both RF and DC balances are balanced.
- Turn the "Level" knob all the way back down to zero.
- Put the quadrupole controller in standby and set the mode dial to "External Command," if the mass is to be set by the computer. The quadrupole is now tuned and can be turned on.

IV.2.b Taking Time-of-Flight Spectra

IV.2.b.1 Basic Set-Up

Besides components installed on the electronics rack, using the time-of-flight requires two small boxes—the "photodiode amplifier box" (PAB) and the "photodiode signal conditioner" (PSC)—on the lid. Figure IV-5 shows the wiring of these boxes. The PAB connects to the LED/photodiode feed-through on the center of the lid via a BNC and to the chopper motor power cable via a power cable. The PSC connects to the chopper power line hanging from the ceiling and to the multi-channel scalar via a BNC with a yellow wire and to an oscilloscope used to monitor the photodiode signal via a BNC with a green wire.

There are two switches on the PAB. The switch by the power line is the power on-off; towards the circuit board is on and away from it is off. The other switch, by the BNC connection, should be flipped towards the BNC at all times. The switch on the PSC between the two BNC connections next to the power cable that comes out of this box should be switched towards whichever connection you're using (the BNC connections are interchangeable). This BNC connection, along with the power cable, should be connected to the PAB on the opposite side of the PAB as the power cable from the PAB to the lid.

Details for setting up the electronics on the electronics rack can be found in Michelle Schulberg's PhD thesis. Note that the switch settings on the chopper motor power supply are "down down down up" for 392 Hz and "down down up up" for 280 Hz. In addition to setting up the electronics, it is *very important* to make sure that the chopper cooling water is turned on before starting up the chopper; failing to do so will cause it to overheat. Unlike the other cooling lines, the water is kept turned off unless it is actually in use, since it runs inside the chopper chamber and a leak would be disastrous.

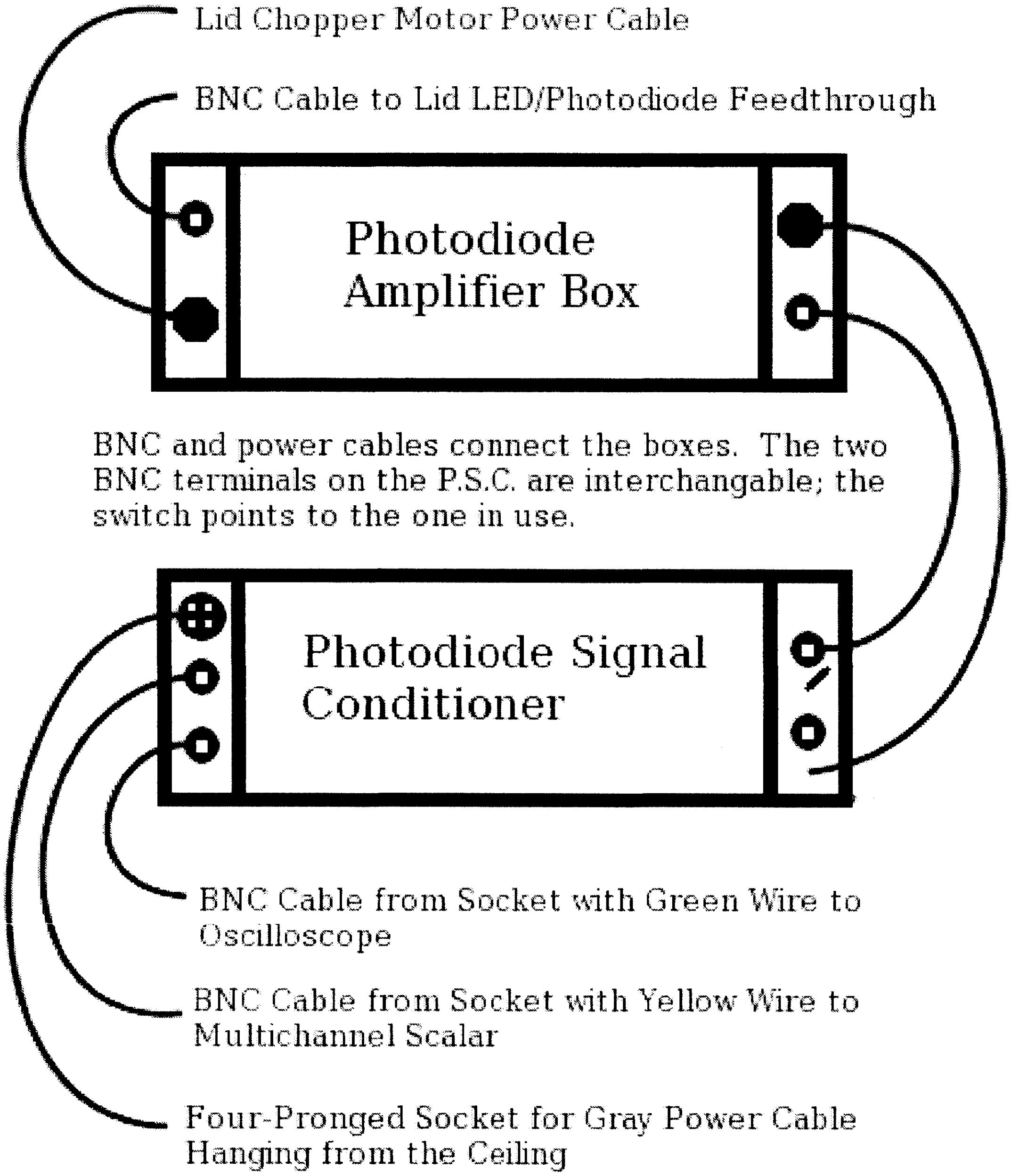

Figure IV-5: Diagram of the Chopper Electronics Set-Up

Note that there are two switches on the end of the Photodiode Amplifier Box that connects to the lid. The one closer to the BNC plug should be flipped towards the BNC plug (and the circuit board). The one closer to the power plug is the LED power; towards the circuit board is on and towards the edge of the box is off.

IV.2.b.2 Time-of-Flight Analysis

Currently, we use the IgorPro script "TOF_fit v 7_25_08_mrb#9CAFC_1.ipf" to analyze the time-of-flight data. This script contains several macros, not all of which are used. The procedure is:

- Use Macro 9, "Load single TOF file", to load a data file.
- Use Macro 1, "Initialize TOF fitting", where "number of components" is the number of Boltzmann distributions you expect at the mass, ionizer length is 0.0254 m, neutral flight path length is 0.293 m and quadrupole length is 0.02327 m.
- Use Macro 3, "Guess". If you get an error message, try again.
- Use Macro 4, "Fit data". If you get an error message you need to start again from Macro 1.
- Use Macro 6, "Append comments", to add comments to the plot before printing.

The full source code for the IgorPro script can be found in the Appendix B of Michael Blair's MS thesis.[9]

IV.2.c Taking Helium Diffraction Data

The scattering-angle sensitivity of the detector box mass spectrometer allows it to be used to observe the diffraction of helium atoms off of the crystal as a measure of crystal surface order. The "MassSet4" program that monitors the mass spectrometer signal on a given mass has features specifically for helium diffraction experiments. It can plot and save the signal on a given mass as a function of time, and controls a beeper box that produces a audible beep and flash of light once per second to signal the experimenter to rotate the lid by half a degree, producing a spectrum where two seconds corresponds to one degree of detector angle.

To achieve an appropriate helium wavelength while maintaining a supersonic expansion, a mixture of 75% He anti-seeded with 25% Ar is used. A stagnation pressure of 300 Torr with our 0.002 inch diameter nozzle produces He atoms with a de Broglie wavelength of 0.93 Å, a velocity of 1000 m/s, and a translational energy of 0.49 kcal/mol. The helium beam is usually produced with the source B nozzle to keep source A free to introduce reactants to the surface.[7]

Besides the specular feature, first-order and half-order peaks should be identifiable due to the 2x1 reconstruction of an annealed Si(100) surface. The 2x1 surface unit cell has dimensions of 3.84 Å parallel to the dimer rows and 7.68 Å perpendicular to the dimer rows. Given the diffraction constraint $sin(\theta_f) - sin(\theta_i) = ka/\lambda$ where k is the crystallographic index, λ is the helium wavelength, and a is the lattice spacing (3.84 Å), if the incoming beam is incident 20° from the surface normal, the half-order peak will be at 28° from the surface normal and the first-order peak will be at 36° from the surface normal. If the beam is incident at 40° from the surface normal, the half-order peak will be at 50° from the surface normal and the first-order peak will be at 62° from the surface normal.[6,8]

IV.2.d Using the Auger Spectrometer

IV.2.d.1 Crystal Set-Up for the Auger Spectrometer

In general, the crystal should be sputtered clean and annealed and allowed to return to its minimum temperature—about 115 K—before Auger spectra are collected. However, it is possible to take spectra with a warm crystal, useful for the purpose of testing the spectrometer itself. When doing so, it is important to keep in mind that the horizontal position of the crystal will be slightly off due to the thermal expansion of metal in the manipulator arm. When the crystal manipulator is warm, the crystal will be somewhere between 0 and 0.15 inches further into the machine than it would be at the same horizontal position setting with a cold manipulator.

When the crystal is clean and at temperature, it can be set in Auger position. Its vertical position should be 0.5 inches above the bottom of its vertical range (i.e. at the midpoint), its angular position should be 180°, and its horizontal position should be one tick mark before the line marked "Auger" (i.e. should be at 20.40 inches). If there is any uncertainty about the exact position, measurements of current to the crystal can be taken to determine the optimal crystal position. The crystal must be grounded; there are two ways of achieving this. The first is to connect the Auger target coaxial cable to the crystal BNC connection on the crystal heating block on the manipulator. The second is to connect the alligator clips on the crystal heating block to a grounding braid attached to the main chamber. Either grounding method should work, but it is important not to use both, as doing so can create a ground loop.

The Auger aperture needs to be very close—0.25 inches according to Gladstone's thesis[1] or 0.261 inches according to a drawing from the manufacturer—to the crystal surface to collect a spectrum. When the Auger is in this position, it is in danger of colliding with the crystal manipulator (if it is moved inward, towards the scattering position) and the detector box chopper wheel. To avoid this danger, the Auger should only be moved into position just before taking a spectrum and should be pulled back as soon as data collection is complete. Furthermore, the lid should not be rotated away from 180° and the manipulator should not be moved while the Auger is in position.

To move the Auger into position, a socket wrench should be used to rotate the drive rod on the Auger manipulator until the tip of the micrometer on the manipulator makes contact. (Before beginning, check that the tip is fully extended, as it does not always fully extend on its own.) Then slowly move the Auger manipulator in to the desired micrometer reading. In November 2013, measurements were taken with the lab surveying scope aligned to the center of the crystal manipulator flange center of the detector box beam hole with the detector box at 180° to calibrate the distance between the Auger aperture and the crystal surface. A Auger-crystal distance of 0.250 inches was found to correspond to a reading of 50 mil on the dial micrometer used to position the Auger. Since the micrometer is removed for bake-outs, caliper measurements were also made between the outer edges of the two machined plates on the Auger manipulator—4.344 inches—and the inner edges of the same plates—2.505 inches. (See Figure IV-6.)

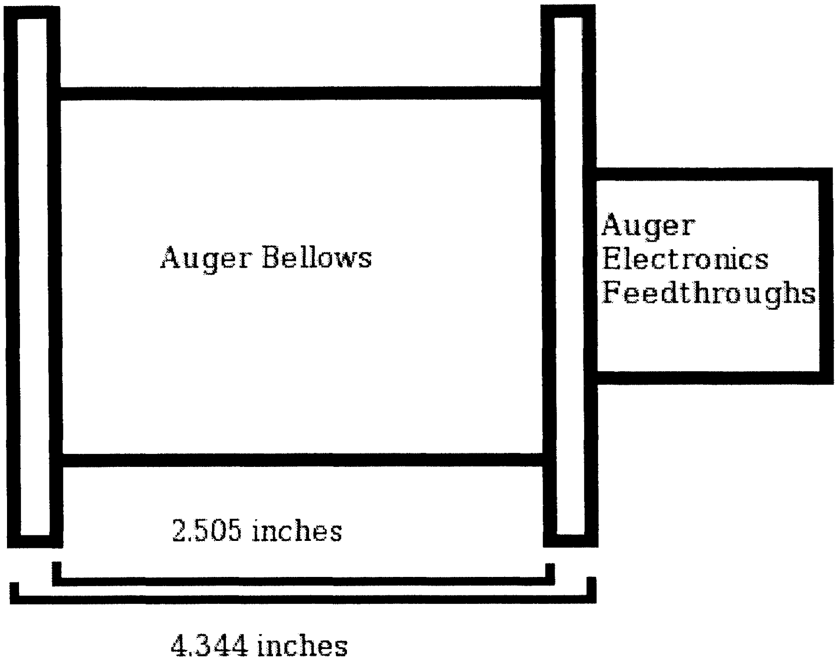

Figure IV-6: Auger-Crystal Distance Measurements

IV.2.d.2 Auger Electronics Set-Up and Sweeping Electron Energy

The Auger spectrometer is controlled by three boxes on the left of the two analytic instrument electronics racks: the Auger electron gun power supply, the Auger control box, and the lock-in amplifier used to process the signal. In addition, to collect data, the high-voltage power supply marked "Auger" at the top of the right electronics rack has to be turned on to power the channeltron. The Auger filament is generally kept running at 2.5 A whenever the main chamber has been baked out, but the other two boxes are only turned on when needed to collect Auger spectra. When turning them on, the filament current needs to be raised to 2.7 A and the filament emission needs to be raised to roughly 0.2 mA to maximize the emission shown on the read-out. For experiments, we usually use the calibrated 2000 eV electron energy setting. However, since the detector can only sweep to 1000 eV, lower settings are needed to find the elastic peak for troubleshooting: an electron energy of 700 eV is typically used for this. The lens settings can be optimized to maximize current to the crystal and signal and then left in that state even when the boxes are turned off. In general, optimal settings for both lenses is close to "5" (their scales go from 0 to 10 in arbitrary units).

Unlike the mass spectrometers and crystal heating power supply, the Auger spectrometer is not fully computer controlled. Although a LabView program on the secondary data acquisition computer is used to plot spectra, electron energy sweeps are controlled directly via the controls on the Auger control box. To perform a sweep, set the upper and lower bounds of the sweep, noting that "upper" and "lower" refer to the absolute value of the electron energy, so the "upper" bound should be more negative than the "lower" bound. Pressing the green start button will start the sweep and pressing the red stop button will end it and return the electron energy to the lower bound. The sweep rate can be varied, providing a trade-off between sensitivity and time to complete a sweep: we usually sweep at 5 eV/s.

IV.2.d.3 Recording Auger Spectra

To record Auger spectra, we use a LabView program that runs on the secondary (right) data acquisition computer. The program is "Auger_4_works.vi" in the "Programs" folder on the desktop; double-clicking on it will automatically open it in LabView. However, it is important to note that being open in LabView is not the same thing as the program actually being running. Once it is open, it can be started by clicking the white arrow button near the left of the LabView toolbar at the top of the screen. The program must be started before configuration data can be entered. However, starting the program does not mean that the program has started recording data. Likewise, pressing the stop-sign button on the LabView toolbar will abort the program immediately without allowing it to save its recorded data.

Once the program is running, the next step is to enter configuration settings. While doing so, be sure to note the difference between "sample rate" and "block size". The former is the rate at which the program observes the Auger signal. The latter is the number of such observations that it averages into a single data point. For the standard settings of a 1000 Hz sample rate and a block size of 100 counts, the program observes the signal one thousand times a second but only records ten data points a second, each of which is the average of one hundred consecutive observations.

The other configuration settings should be relatively intuitive. "Signal channel" should match the port on the computer's coaxial breakout box that is connected to the output port on the front of the lock-in amplifier. "Electron energy channel" should match the port on the computer's coaxial breakout box that is connected to the electron energy output on the rear of the Auger control box. "Output file path" should be the path to the file in which recorded data should be saved.

Just before starting the electron energy sweep on the Auger control box, click the "start run" button twice—a green light on the button should come on—to begin collecting data. If the data from the run is to be saved, the "save data" button must be pressed after the run has begun (a green light on the button should come on). When the run is complete, pressing the "stop run" button—*not* the stop sign button on the LabView toolbar—will stop the run and, if the green light on the "save data" button is on, save the data into the file given in the "output file path" field.

The program needs to be closed and re-opened, and configuration settings re-entered to reset it for a new run. The closing and reopening of the program is necessary to reset the program's real-time plot and may be necessary to clear the internal data cache used to collect data to be saved.

IV.2.d.4 Measuring Current to the Crystal

One method for improving the Auger signal is to adjust the lens settings and crystal position to maximize the electron current that reaches the crystal. To do this, a picoammeter is used to measure current between the crystal heating terminals on the manipulator and the body of the machine, which is grounded. Since the current to be measured is very small, it is important to remove the screw connectors that link the crystal heating terminals to the crystal heating block on the manipulator. Measurements of current to the crystal have varied significantly, but a value between 10^{-5} A and 10^{-6} A is typical.

IV.3 Venting, Pumping Down, and Baking Out the Machine

IV.3.a Venting, Opening, and Pumping Down the Main Chamber

IV.3.a.1 Venting the Main Chamber

Venting the main chamber is a rather involved procedure. While it is easy to fill the chamber with air in an uncontrolled way, one has to be rather more careful to do so without contaminating the chamber or damaging pumps and bellows or causing unwanted condensation on cold components. To minimize the amount of water vapor introduced into the chamber, we also generally vent with dry nitrogen gas rather than air.

- Before you begin to vent, it is important to ensure the following preparations:
    - All the ℓN_2 in the ionizer cryostat needs to boil off and the cryostat needs to warm to room temperature. If the cryostat is full, boiling off all the nitrogen will generally require waiting overnight with the cryostat nitrogen boil-off valve set to fully open. The process can be accelerated by using the house vacuum line to suck out the ℓN_2. It may also help to use the cryostat heater, powering it with 30 W from a constant-voltage power supply or variac.
    - Unscrew the Auger target / crystal heating connection block from the manipulator, and remove the screw-connector from the wires on the crystal heater feed-through. (The wires from the connection block are soldered in.)
    - Extend the manipulator bellows fully, putting the lower left corner of the slider to the “vent” position. Make sure to have a piece of cardboard under the bellows to support it while vented. (It is safe to vent with the manipulator in any position so long as the bellows is supported. However, the need to keep the bellows supported makes it hard to change the manipulator position while vented, so it is usually best to extend it fully to

  maximize working space inside the chamber in case internal repairs turn out to be needed.)

  - Make sure that all five filaments in the main chamber are turned off: both mass spectrometer ionizers, the sputter gun, the Auger, and the ion gauge. (Only the Auger filament and the ion gauge are normally turned on, but you should still check the others.) Also be sure that channeltron electron multipliers and the mass spectrometer RF are turned off.
  - Make sure that the second stage beam valve is closed.

- If you are not going to vent the detector box, isolate it by closing the detector box beam valve and checking that the detector box roughing valve connection to the main chamber is closed. If you are going to vent the detector box, open the detector box roughing valve to the main chamber and close the detector box gate valves ("primary gate valve" on the detector box interlock box).
- Isolate the seals and chopper chamber ion pumps and the first seals mechanical pump:
- Close the valves for the second lid seals and second door seals ion pumps (on floor under main chamber). You will need a small torque wrench or socket wrench for door seals. Also close the valve to the third seals ion pump (red box on top of main chamber) if it is open. However, this pump has not generally been used in the recent past, so it likely is not open.
- Close the hand-crank gate valve to the chopper chamber ion pump. Open the chopper chamber roughing valve using the same socket wrench as the door seals.
- Close the green valve on the bellows leading to the first seals mechanical pump.
- Close the main chamber gate valve. If you are only venting for one day, leave the diffusion pump and ℓN_2 on. If you plan on venting overnight, turn off the liquid nitrogen at this point.

However, you should still leave the main chamber diffusion pump on for an hour while the trap thaws, allowing it to remove the contaminants that have condensed on the trap as it thaws. Be sure to leave the foreline valve open, at least until the pump cools.

- Fill a hand dewar with liquid nitrogen. Also, get one of the styrofoam dewars and fill it with hot water.
- A copper coil about six inches tall and three inches in diameter with tygon tubing coming off each end is used to boil the nitrogen: put it in the styrofoam bucket such that each of the connections to the rubber tubing are above water level. Place one of the ends of the tubing in the hand dewar and attach the other to the venting tube. It may also be possible to use the gas exhaust on the LN tanks, but this method has not been used previously.[11]
- Open the two valves between the venting / sorption pump / high pressure gauge assembly, along with the all-metal right angle valve directly attached to the main chamber, ensuring that the sorption pumps and Venturi valve are left closed off. Make sure that the sorption pumps are not still baking out, especially if you plan on pumping down today.
- Making sure that the venting line and high pressure gauge are open to the main chamber, open the small green valve to open the venting line to the rubber tube. Use this valve to control the rate at which liquid nitrogen spurts into the coil to make sure that you don't get any liquid past the coil, since ℓN_2 must not be allowed to enter the main chamber due to the overpressure risk as it boils. Too much ℓN_2 is coming in if the copper tube freezes all the way to the green-handled valve. On the other hand, a pressure increase of 100 Torr should only take about 5 minutes; longer than that and you're not allowing enough ℓN_2 in.
- Remember to turn off the main chamber diffusion pump an hour or so after turning off its ℓN_2 supply.

IV.3.a.2 Opening the Main Chamber

For most repairs within the chamber it is necessary to open one or both of the large door flanges on the chamber. The following is the procedure for doing so.

- After venting the main chamber, it is best to disconnect the seals bellows at the mini-conflat flanges that are not connected directly to the door. This practice prevents possible wear of and hence damage to the threads on the tapped mini-conflat flanges on the door flange, which would be difficult to repair.
- Cover the mini-conflat openings with foil.
- Remove the bolts on the door using an allen wrench. If you open both doors, note that the bolts on the two doors require different sized allen wrenches. Be sure to keep the two sets straight.
- Open the door flange. There is a large square-cross-section bar kept under the manipulator that can be bolted to holes in the door to act as a handle if needed.
- When you take an extended break from work in the chamber, it's best to use a single bolt to keep the door closed so dust doesn't get in.

IV.3.a.3 Closing the Main Chamber

When closing the chamber, you should reverse the steps in the previous section. However, there are three additional things you should do first:

- Clean out the inside of the chamber thoroughly with acetone, being sure to wipe any surfaces you've touched or gotten near until an acetone-soaked Kimwipe rubbed on them comes back clean. Also check for any grit or small debris. It's particularly important to check for debris in the gate valve depression, since any grit or debris could damage or destroy the gate valve o-ring when the valve opens.

- Make sure that the two seals o-rings are properly in position. (If you're confused, they go into the two depressions that don't have connections to the seals lines.) They should fit fairly tightly.
    - If one breaks or gets lost, there are Teflon St. Gobain seals in the Lista cabinets that can be used temporarily to allow you to pump down, but you should put a Viton o-ring back in as soon as possible.
    - If you do need to replace the o-ring, note that we buy them whole; we don't make them out of cord and o-ring glue. The thickness is 5/16"; check the machine drawings for the diameter. In September 2011, a replacement was ordered from Marco Rubber in Seabrook, NH.
- Before closing, make one last check that you haven't left anything in the chamber.

IV.3.a.4 Pumping Down the Main Chamber

Pumping down the main chamber is intrinsically a bit safer than venting is, since a failure will generally return the system to its initial, vented state. However, one still needs to be rather careful to pump down successfully. A procedure for doing so follows:

- If the sorption pumps have not been baked out since the last time they were used (they should have been baked out immediately after use), they need to be plugged in and baked out for several hours, preferably overnight, and then allowed to cool to room temperature for a couple hours. Remember to put the pressure release plugs back in them when you unplug them.
- If the detector box and lid have also been vented, check that the bypass valve between the detector box and main chamber is open to allow the detector box to be roughed through the chamber.

- Make sure that the round green valve to the copper venting tube is closed, but that the valves connecting the main chamber to the venting / sorption pump / high pressure gauge assembly are open.
- Open the green-handled valve to open the first seals to their mechanical pump and wait for the foreline pressure to return to normal. Then open the green-handled valve to open the bypass from the second lid seals to the first seals. (This valve is near the manipulator.)
- Attach a full nitrogen gas tank (NI-300 from Airgas) to the Venturi pump (connection is on the side closer to the main chamber). You'll have to remove the attachment on the end of the nitrogen gas line first.
- Set the regulator on the nitrogen tank to 80 psi and open the valve to the Venturi pump. While the Venturi pump is running, monitor the pressure drop in the main chamber: it should fall to about 100 torr, though it is possible to pump down successfully as long as the Venturi pump gets the pressure down to at least 150 torr.
- While the Venturi pump is running, attach the styrofoam ℓN_2 baths to the sorption pumps and fill them with ℓN_2 from hand dewars until the nitrogen in them stops boiling and they are completely full. Once they are full, top off both hand dewars.
- When the nitrogen gas tank runs low enough that the regulator pressure falls below 80 psi, close the valve to the Venturi pump. (This should take fifteen to twenty minutes.) The valve to the Venturi pump must be closed quickly, since once the nitrogen pressure through the pump falls too low, air will start returning to the main chamber.
- Attach a portable thermocouple gauge reader into the thermocouple gauge on the venting / sorption pump / high pressure gauge assembly. Turn it on when the high pressure (a

mechanical dial) gauge reads 0 Torr. (It may be worth turning it on around the time the nitrogen gas tank is running out, though, since the high-pressure gauge is not very reliable.)

- Once the Venturi pump valve is closed, open the valve to one of the cooled sorption pumps. The pressure should rapidly drop and a lot of ℓN_2 should boil off. Keep the ℓN_2 bath completely full. When the rate of boiling in the bath finally slows to the rate of boiling in the other bath, the sorption pump is full. (At this point, the pressure should read around 0 Torr.) Close the valve to it and then open the valve to the other sorption pump, repeating this procedure with it.
- If the detector box was vented with the lid turbomolecular pumps on, the turbo pump gate valves can be opened with foreline and backing pressure interlocks bypassed, when the pressure falls to 35 mTorr. However, if the pressure in the turbomolecular pumps does not fall fairly rapidly, they should be shut off.
- By the time the second sorption pump's bath stops boiling, the thermocouple gauge should read 0 mTorr. However, at any time after it reads 100 mTorr, you can open the gate valve and close the sorption pump and the right-angle valves between the main chamber and the venting / sorption pump / high pressure gauge assembly. Close the bakeable right-angle valve with a torque wrench at a minimally higher torque than the most recent value in the lab notebook and record the torque you used. (All-metal valves require slightly more torque to close them each time, as the gasket gets increasingly dented.)
- Once the gate valve is open, you can turn on the ion gauge. It is important to avoid turning it on too early: even if you don't burn out the filament, turning it on early does incremental damage to a chip inside the ion gauge controller, which will eventually fail resulting in nonsensical (usually an order of magnitude too low) pressure readings.

- Close the green-handled valve to isolate the second lid seals from the first seals.
- Turn on the lid second seals ion pump to "start" mode, open the valve at its entrance, and allow it to sit for ten minutes or more until it is at a safe operating pressure. Then turn the pump control to "protect" mode.
- Slowly open the valve at the entrance to the door second seals ion pump. Watch the main chamber pressure as this pump is opened, as it may have a much higher pressure inside than the main chamber. (It probably won't.) The reason we don't rough out the second seals with the first seals mechanical pump is because they have high conductivity to the main chamber, and doing so ends up roughing the main chamber with the first seals mechanical pump.
- Open the main chamber gate valve and, after five minutes, turn on the main chamber ion gauge. Set the main chamber pressure interlock back to "protect" mode if you bypassed it when you opened the gate valve. The pressure should drop into the 10^{-7} Torr range within half an hour.
- Remember to plug in the sorption pumps to bake out overnight, and to unplug them in the morning so that they can cool down for the next time you use them. Put the pressure release plugs back in when you unplug them.

IV.3.b Venting and Pumping Down the Lid

IV.3.b.1 Venting and Pumping Down the Detector Box

There is some ambiguity in referring to venting "the lid", as this phrase can refer to two different things: the detector box itself, which consists of three connected chambers below the lid gate valves, and the lid turbomolecular pumps, which are above the lid gate valves. When venting or pumping down either of these, they should be isolated from each other by closing the lid gate valves via the switch on the lid turbo interlock box. (The gate valves are pneumatic and fail-closed, so if there's a power or pneumatics loss, they should automatically close.)

The detector box is best vented or pumped down by connecting it to the main chamber via the beam valve and detector-to-main chamber roughing valve while the main chamber itself is being vented or pumped down. In a pinch, if the main chamber is already vented, you could probably safely vent the detector box by opening the roughing valve, though you'd be venting with air rather than dry nitrogen, so you should talk to Professor Ceyer before doing this. The detector chamber can also be vented through the turbo pumps vent valve. The vent valve intake can be hooked up to dry nitrogen with the regulator delivery pressure set to 1 atm. It is unlikely that you can pump down the detector box by opening the valve while the main chamber is being pumped by the main chamber DP, because the DP can readily choke with a rapid influx of atmospheric pressure and the atmospheric pressure air will condense in the liquid nitrogen trap above the DP. The detector box could be roughed down through the turbomolecular pumps, by first roughing out the backing turbo pump and then roughing out the three other turbo pumps (see next section).

IV.3.b.2 Venting and Pumping Down the Lid Turbomolecular Pumps

As for the lid turbomolecular pumps, once the lid gate valves are closed, there is no connection between them and the main chamber, so they have to be vented or pumped down separately. The procedure for venting them and pumping them down is given in detail on page 359 of Matthew Tate's thesis, as part of his description of the construction of the lid turbo interlock box. The text of that page follows:

> ***III.A. Resetting the system after a failure***
>
> *After a failure, the system must be reset before normal operation can resume. The primary gate valves ought to be actively closed via a switch on the front panel of the interlock system. Otherwise the gate valves will open when the system is reset and the pressure monitors are bypassed, venting the main chamber. Of course, the cause of the fault must be fixed. When the system is ready for operation, the interlock can be reset in the following manner. First, the interlock must be temporarily bypassed via the individual switches for each monitored input. This is necessary because the initial state of the turbomolecular pumping system is not satisfactory upon startup. The interlock is bypassed to prevent the detection of a failure and the shutdown of the system. Second, the vent valves must be closed; this is done by pushing the two close vent valve buttons on the front panel of the interlock system. Third, the foreline valve needs to be open so that the three primary turbomolecular pumps can be exhausted. Finally, the power to the turbomolecular pumps must be reset; this is done by pushing the two reset buttons on the front panel of the interlock system. When the pumping system reaches a satisfactory state, the interlock should no longer be bypassed.*

III.B. Intentionally venting the system

There are times when the turbomolecular pumps are actively shutdown. This is accomplished via the interlock system by holding down the appropriate vent button for more than 10 seconds. This creates an artificial fault in the system, which leads to the proper shutdown and venting. The 10 second activation conveniently utilizes the logic of the grace period and prevents accidental venting from reckless switch flipping and button pushing.[6]

IV.3.c Venting and Pulling Back the Source

IV.3.c.1 Venting the Source

Because the source A, source B, first A, first B, and second stage chambers of the molecular beam source are interconnected through the beam holes and there are no beam hole valves, it's necessary to vent the whole source to open any of them to atmosphere. Furthermore, it is often necessary to detach the beam source from the main chamber and to pull it back along the track it rests on in order to access the inside of the second stage chamber, as well as access doors into first A, first B, source A, and source B.

Before the source can be vented, it needs to be isolated from the main chamber by closing the beam valve from the second stage and, if the gas manifolds are not also to be vented, they should be isolated as much as possible. The filaments on the second stage ion gauge and any other ion gauges on the source need to be turned off as well, of course. Once these steps are complete, you can begin venting:

- The gate valve on the second stage diffusion pump should be closed and the pump and its nitrogen trap can be turned off.
- Turn off the source A, source B, first A, and first B diffusion pumps and set up a fan to cool them, although the fan is not necessary. The bottom of the pumps should be allowed to cool until they can be touched before you proceed to the next steps. You may want to carry out the procedure up to this step in the evening so that the diffusion pumps can cool over night and be ready for you to finish the vent when you come in the next morning. Close the foreline valve once the bottom of the pumps are cool to touch.
- Once the diffusion pumps have cooled for several hours, vent the source A, source B, first A, and first B forelines one at a time, preferably starting with source A. This operation is ideally

a two-person task, with one person turning off the mechanical pump and the other person pulling the vent pin as soon as the mechanical pump is off. It is important to turn the mechanical pump off first so that it doesn't pull on atmosphere, but one wants to pull the vent pin as quickly as possible once the pump is off to avoid back-streaming of oil into the foreline.

- To vent the source, open the source A foreline valve; it will take around fifteen minutes for the entire source to vent through source A. It is preferable to only vent through one foreline to avoid creating complicated air currents inside the source.
- Once the vent is completed, it is wise to re-insert the vent pins, both to keep it from getting lost and to make sure that it is in place when the foreline is next pumped down.

IV.3.c.2 Disconnecting and Pulling Back the Source Chambers

Before you pull back the source, the source chambers need to be vented, as does the manifold foreline. Make sure this vent is properly done before continuing. Then, disconnect the various connections between the source and the main chamber and between the source and the wall:

- The water cooling lines for the first A, first B, source A, and source B diffusion pumps need to be removed. First, turn off the water-in valve to each pump, then, after ten seconds, turn off the water-out valves. You can then remove each of the eight water lines from the diffusion pumps by undoing the quick-disconnects located behind the source. Make sure to have a rather large bucket beneath each quick-disconnect as you undo it because quite a lot of water may drain out. It is wise to detach the lines one pump at a time, as disconnecting the second of the two lines from a pump may cause water to drain either out of it or out of the first, already disconnected, line.

- The lines between the manifold and the large He and Ar cylinders need to be disconnected. You will also have to partially remove the heating tapes wrapped around them. Be sure to not accidentally vent the manifold while doing this. You don't need to remove the small Kr or Xe tank attached to the manifold, but if you leave it in place, remember to move it as you are pulling back the source chambers cart.
- The Ar sputter line needs to be disconnected (just under the connection between the source and second stage). Once again, remove the heating tape as necessary and don't accidentally vent the manifold.
- The manifold turbomolecular pump cart needs to be disconnected and pulled back. Prior to this operation:
    - The manifold foreline needs to be vented.
    - The manifold foreline needs to be removed and disconnected from the manifold turbomolecular pump cart.
    - The compressed air copper line to the turbomolecular pump cart needs to be disconnected at the valve where it joins the other lines attached to the main chamber—make sure to close the valve first.
    - The line connecting the turbomolecular pump cart to the manifold needs to be disconnected. Make sure to remove the heating tape connection and to not accidentally vent the manifold.
- After disconnecting the relevant electrical lines, pull back the stand with the nozzle heating controller and nozzle pressure readout on it.
- Remove the forelines for source A, source B, and first A. Disconnect the first B foreline behind the machine, but do not actually remove it.

- Disconnect the beam flag control line, along with any additional power or data lines that appear likely to be caught on things.
- Unplug the diffusion pumps.

If everything has been disconnected, you are now ready to undo the bolts that connect the source to the second stage. Make sure to undo the ones at the center bottom first, since they are very hard to reach. Some of the bolts will require a socket wrench to undo; others are impossible to get with a socket wrench and require a regular wrench. Once done, use the long pry bar in the gap between the source chambers cart and the main chamber's frame to break the seal. *Do not use the pry bar at the sealing surface between the source chamber and the main chamber!* You can now pull back the cart. This operation should really be done by two people so that someone can be on each side to watch and make sure that nothing gets caught.

IV.3.c.3 Reconnecting the Source

Before reconnecting the source, you should wash the seal to the second stage and the exposed area that will become part of the wall of the second stage with acetone. Make sure not to get acetone on the Viton rubber o-ring. Then make sure that the o-ring is properly seated and push the source back into place. Once it is as close as you can get it, screw in the bolts holding the source to the second stage, leaving the ones in the bottom middle for last. It may take several attempts to be sure that they are all tight. Once the source is back in place, you should connect everything you had to disconnect to pull it back before pumping it down.

IV.3.c.4 Pumping Down the Source

- The first step to pumping down the source is to pump out the forelines. To do this, make sure the foreline valves are closed and that the vent pins are in place. Then turn on the mechanical pumps, listening to make sure that they don't sound like they're sucking air. If they appear to be doing so, you have a leak. If the source A foreline pressure does not seem to be falling, you can use the portable thermocouple gauge reader to read the pressure at the gauge between the source A Roots blower and the source A mechanical pump. If this pressure is noticeably lower than the foreline pressure, you can turn on the Roots blower for ten seconds or so to improve conductivity through it. Once the foreline pressures are satisfactorily low, you can begin to pump down the source, through either the source A or source B mechanical pumps, or both simultaneously. Definitely use a source mechanical pump, as opposed to the first stage mechanical pumps, because their throughputs are larger and thus these pumps are harder to choke with the large amount of air you'll be putting through them.

- To pump down, open the source A or B foreline valve just a crack, making sure not to make the foreline pressure rise above about 10^{-1} Torr. If the pressure jumps up and doesn't immediately start to fall, you may need to close the valve entirely until the pressure falls to keep the pump from choking.
- Once the source is pumped down, you can open all the foreline valves. At this point, it is safe to turn on the diffusion pumps (check to make sure that the water cooling is on if you pulled back the source). You should wait an hour or two to make sure that they are in fact heating up properly. After the second stage diffusion pump has been on for about an hour and a half, you can fill its nitrogen trap and then open the gate valve.
- Since we don't bake out the molecular beam source, venting it does not generally necessitate a bake-out. However, venting the source involves cutting pumping to the gas manifold. While we try to isolate it as well as is possible, it is still generally necessary to bake them out again after a vent and before use, especially if fluorine-containing compounds will be used.

IV.3.d Venting and Bypassing the Manifold

IV.3.d.1 Venting the Manifold

The first step to venting the manifold is to vent the manifold foreline while isolating the manifold itself from the foreline. Once done, you can continue to vent the manifold itself if necessary.

- Close the valve connecting the manifold turbo to the manifold.
- Turn off the manifold turbomolecular pump, wait for it to spin down, and then turn off the turbo controller.
- Close the valve connecting the manifold turbo to the foreline (pneumatic, close by unplugging) and the valve connecting the manifold to the foreline (used for roughing, should be closed).
- With the manifold turbo now isolated and off, you can open its vent valve (pneumatic, open by unplugging).
- Once these are closed, you can turn off the manifold mechanical pump and then pull the vent pin (if possible, using two people so the vent pin can be pulled as soon as the pump is off) to vent the foreline.
- Once you have vented the foreline, you can continue to vent the manifold, if necessary. To do this, make sure that the manifold is isolated from the source and open the valve connecting the manifold to the foreline to vent the manifold as well.
- Once the foreline and manifold are vented, you should be certain to reinsert the vent pin, both to keep it from getting lost and to make sure it is in place when you next pump down the foreline.

IV.3.d.2 Pumping Down the Manifold

Pumping down the manifold is roughly the reverse of venting it. However, there are some minor differences. The procedure is as follows:

- Close all four relevant valves:
  - The manifold-foreline roughing valve should be closed.
  - The manifold-manifold turbo valve should be closed.
  - The pneumatic manifold turbo-foreline valve should be closed (unplugged).
  - The pneumatic manifold vent valve should be closed (plugged in).
- Making sure the vent pin is in place, turn on the manifold mechanical pump to pump down the manifold foreline.
  - Once the pressure is acceptable (generally less than 100 mTorr; less than 50 mTorr is preferred), you can open the roughing valve to rough out the manifold, opening the connection to the manifold slowly to avoid choking the mechanical pump.
  - Once the foreline pressure has dropped into the 10^{-3} range, you can open the manifold turbomolecular pump's foreline valve and turn on the pump.
  - Once the turbo is up to full speed, open the manifold to the turbomolecular pump.
  - Close the manifold-foreline roughing valve.
- Once the manifold has been pumped down, it should be baked out overnight, particularly if fluorine-containing compounds are to be used.

IV.3.d.3 Bypassing the Manifold Turbomolecular Pump

If the manifold turbomolecular pump's bearings seize, or the pump becomes otherwise inoperative, it is possible to bypass it by pumping the manifold through the second stage. There is a bypass line installed between the upper part of manifold A and the second stage, with valves to close it on either side. We usually keep the second stage side valve closed and the manifold side valve open so that this line is always pumped by the manifold. You can also (very carefully) rough out the manifold this way if the manifold mechanical pump is not working. Since pumping through the second stage doesn't maintain as low a manifold pressure as using the turbomolecular pump, you should do a manifold bake-out each night while you pump down the manifold this way.

IV.3.e Baking Out the Machine

IV.3.e.1 Setting Up a Main Chamber Bake-Out

The main chamber and lid need to be fully baked out after a vent before the machine will be able to reach ultra-high vacuum. Furthermore, additional (sometimes main chamber only—but *never* attempt to bake out the lid without the main chamber) bake-outs may be needed after extended gate valve closures or other contamination of the chamber. While we do not separately bake out the molecular beam source, the gas manifold that supplies gas to it does need to be baked out after any vent, and should be baked out again as a precaution before using fluorine compounds in it.

Before you start setting up heating tapes for a bake out, you should prep the chamber:

- Remove any loose material or tools lying on top of the chamber. Also remove any tape or other non-metal materials attached to the chamber.
- Turn off mass spec filaments, the Auger filament, and the sputter gun filament. (See venting instructions for details.) The ion gauge filament can be left on, and in fact needs to be left on to allow you to monitor the pressure and determine when the bake-out is complete.
- Disconnect and remove the preamps, signal lines, high voltage lines, and high-Q head for the main chamber RGA and detector box mass spec. Also remove the high-Q head cables for the detector box mass spec (but not the main chamber RGA). Remove all lines attached to the Auger and to the mass spectrometers, other than the pairs of cables to the high-Q head for the main chamber RGA (These never come off.).
- Remove the Auger micrometer by disconnecting its mounting block from the Auger flange. Do not remove the micrometer from the block; doing so will mess up its alignment.

- Remove the thermocouple and heating control block / Auger target from the manipulator. Also remove the ℓN_2 cooling line for the crystal if it's attached.
- If there is ℓN_2 in the detector chamber cryostat, it needs to be warmed back to room temperature before you can bake out. This can be achieved by opening the nitrogen flow to full overnight without refilling the cryostat. The process can be accelerated by heating the cryostat with 30 W from a power supply.

To bake out the main chamber, we use the four quartz lamps that are installed inside the chamber, and controlled by a power supply in the leftmost of the electronics racks by the source. We also use a number of heating tapes to heat the lid and protruding flanges that would otherwise not heat properly:

- Two heating tapes are needed to wrap the main chamber RGA flange (not the electronics on the back), the Auger bellows and the flanges at each end of it (you don't need to actually wrap the bellows, and the heating tape should not touch the bellows directly due to the risk of damage from sparking), and the two windows adjacent to these. The whole area should then be covered in aluminum foil.
- The manipulator bellows should be carefully wrapped in sheets of new aluminum foil (to protect it from sparks from faulty heating tapes) and then wrapped with two heating tapes. An additional, two-foot, heating tape is needed for the outer flange of the bellows. The manipulator heating box then needs to be fit over the manipulator. The power strip for the manipulator tapes and heating box should be plugged into the heating tape controller (see below) rather than a variac.
- Heating tapes should already be installed around the seals for the lid and manipulator.

- Heating tapes should already be installed and covered in aluminum foil around the leak valve used for sputtering, the protruding window flange between the two doors, and the main chamber gate valve.
- The windows that don't protrude need to be covered with aluminum foil, although no heating tapes are required.
- There should already be heating tapes installed and covered with foil on the connections to the turbo pumps.
- A heating tape is needed for the arm that connects the chicken feeder to the detector box cryostat. The arm also needs to be covered in foil.

When installing heating tapes, you should check that their resistance is between 45 Ω and 75 Ω. Several heating tapes can then be connected on power strips, so long as the resistance of each power strip remains above 11 Ω or so. The power strip with the lowest resistance (generally the manipulator heater box) should be connected to the heating tape controller on the leftmost electronics rack by the source and supplied with 6 A. We use the heating-tape controller for this power strip because it is current-controlled, and so presents a lower fire risk with low-resistance loads. All other power strips should be connected to variacs supplying 60 V. Check the resistances of all power strips and the voltages of all variacs before turning anything on, even if you think you know that they were working recently. Also make sure that all power strips have infinite resistance to ground.

IV.3.e.2 Baking Out the Main Chamber

Before turning on a bake-out, it is useful to decrease ventilation air flow through the lab to reduce air cooling of the machine. To do this, set the "Fan Control Unit 3" switch to "off" and the "Bake out Damper" switch to "closed." These switches are on the wall between the two closets across from the machine. When the bake out is over, you can reopen the "Bake out Damper" and turn "Fan Control Unit 3" back on. You may wish to turn it to high to help the machine cool faster.

Once everything is set up and checked, you can turn on the quartz lamps in the main chamber (set to 65 V) and the heating tapes that are on the body of the machine (including those on the outside of the lid and manipulator seals). However, the heating tapes on the lid and manipulator (powered with the heating tape controller at 6 A), as well as the lid quartz lamps (set to 30 V), should not be turned on until five hours after the quartz lamps and machine body heating tapes have turned on. This procedure is necessary to make sure that the outsides of the lid and manipulator seals expand before the insides do; if this is not done correctly, the bearings will be crushed.

When you turn on the main chamber lamps, you should rotate the lid so that detector box is directly above one of the lamps on the floor of the main chamber. Rotation is done by sight, since the lamps are illuminated and very visible at this point.

About half an hour after turning on each stage of the bake-out, you should check to see that the heating tapes are in fact warming up. Also, immediately after turning on the quartz lamps in the main chamber, you should do a visual check to insure that they've all turned on correctly. It is also useful to track the temperature of the bake out based on the crystal temperature and cryostat temperature thermocouples. They should ideally reach maximum temperatures have 1.73 V (crystal) and 110°C (detector box cryostat); it is unsafe to allow the temperatures to get higher than this when heating with lamps and heating tapes alone, as you risk melting the chopper photodiode.

However, higher temperatures in the detector box can be achieved by using the heating wire built into the bottom of the ionizer cryostat. You can use a power supply or variac to supply up to 60 W (but no more than 30 W overnight or when you're not around) to the cryostat heater to raise cryostat temperature (which is measured at the heater, on the bottom of the cryostat) to 140°C. Since the cryostat heater and cryostat thermocouple are adjacent and a significant distance from the photodiode, it is safe to use the cryostat heater to raise the cryostat temperature above the melting point of the photodiode. On the other hand, the internal lamps shine directly on the photodiode but not the cryostat thermocouple, so when baking out with lamps and heating tapes only, the cryostat temperature should be lower than the 125°C melting point of the photodiode.)

Finally, to determine when the bake-out is complete, you should monitor the main chamber pressure. It should initially rise (possibly as high as 10^{-7} Torr) as heating drives absorbed water and gases off the chamber walls. Once it begins to drop again, the walls have finished outgassing. You can turn off the bake-out when the pressure falls to roughly 5×10^{-9} Torr, or when it has been stable for about twelve hours.

The process for turning off the bake-out is the reverse of that for turning it on. Shut off the lid lamps and the heating tapes on the lid and manipulator and allow them to cool for five to six hours before turning off the lamps and heating tapes on the main chamber. This procedure is essential to ensure that the lid and manipulator cool (and contract) before the main chamber does so that the lid and manipulator bearings are not crushed.

IV.3.e.3 Baking Out the Manifold

Before baking out the manifold, open all the valves on the manifold that don't lead to atmosphere, and be sure that the valve to the turbomolecular pump is open. Then make sure that all parts of the manifold are covered in heating tapes (they should be, as these are usually not removed). Furthermore, make sure that the lines to the turbomolecular pump cart, the various gas cylinders, and the sputter line have heating tapes on them, and that these are properly connected. Then make sure that all heating tapes are connected to the four power strips built into the source cart. (Not including the power strip that only connects to heating tapes on Manifold B, which should only be used if you are baking out Manifold B.) As with a main chamber bake out, make sure that the resistances of the power strips are above 11 Ω and connect them to variacs supplying 60 V (check that they actually are). The lowest-resistance power strip should be connected to the heating tape controller on the electronics rack and supplied with 6 A. Make sure to check that all of the heating tapes are actually warming up once you have started the bake out. The manifold should ideally be baked out overnight. Once the bake out is complete, turn off the variacs and heating tape controller and let it cool for one to two hours. Make sure that it is cool to the touch before attempting to use it.

IV.4 Repairs Inside the Machine

IV.4.a Source and Nozzle Repairs

IV.4.a.1 Beam Flags

Inside the common second stage are beam flags for the two molecular beams. Their control wires run through first stage B and out an eight-wire electrical feed-through on the side of first stage B. The top three wires on this feed-through are connected: upper-left to common ground (white wire), top to flag B positive voltage (red wire), and upper-right to flag A positive voltage (black wire). The wires from the feed-through run to a beam-selector control box that should be taped to the side of the source, which in turn is connected via a long coaxial cable to the main beam flag control box (see Figure IV-7) on the Auger / mass spec / electron gun electronics rack. There are two switches on the selector box. When switch A is down and B is in the middle position, the main control box operates flag A. When switch B is down and A is in the middle position, the main control box operates flag B. When both switches are down, the main control box operates both flags, and when both are in the middle position, it operates neither.

The beam flag mechanisms can be a bit flimsy, and if the flag is closed with a high-pressure beam hitting it, it may jam closed. If it jams, turning off the beam by pumping out the nozzle and cycling the solenoid open and closed will usually fix the problem. If it doesn't, you may need to vent and pull back the source to adjust the flag by hand. Also, whenever you have the source pulled back, your last test before reinstalling it should be to make sure that the beam flags still work.

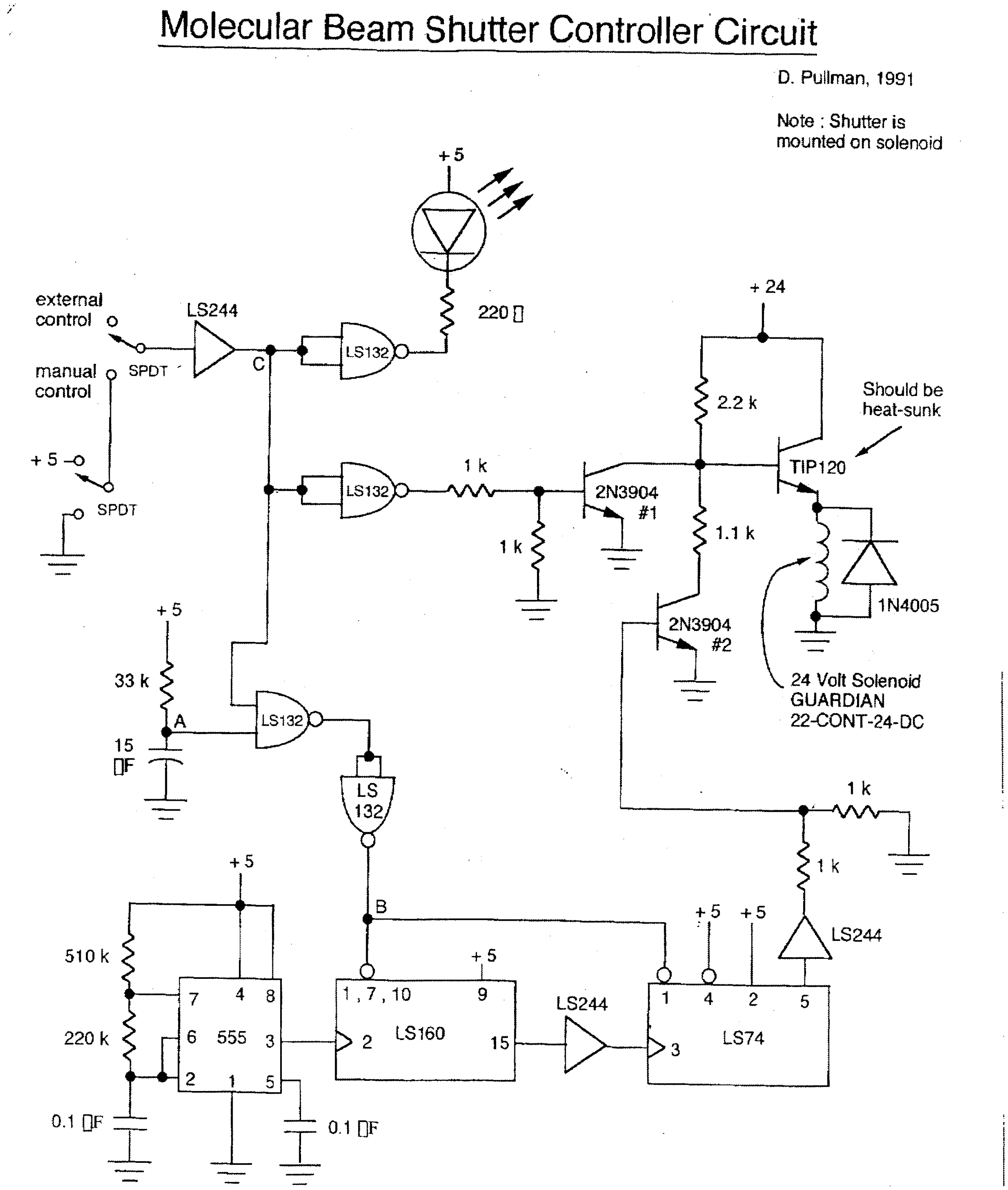

Figure IV-7: Circuit Diagram for Beam Shutter Control Box

This diagram describes the circuit inside the beam shutter control box mounted on the electronics rack above the mass spectrometer ionizer control box. However, the solenoid is inside the second stage chamber, connected via a BNC cable and switching box mounted on the source.

IV.4.a.2 Beam Valve

It is important not to over-tighten the beam valve when opening or closing it. Doing so can cause metal fatigue to snap the hinged train of metal parts that open and close the beam in response to the linear feed-through that controls the valve. This train is somewhat complicated because the motion has to traverse an angle: the linear motion feed-through is not parallel to or in the same plane as the wall of the second stage that contains the beam slits. If the train breaks, you can have the machine shop make replacement parts out of aluminum. We use aluminum rather than stainless steel to prevent galling as the valve slides along the stainless steel wall of the second stage and the stainless steel guides. However, the use of aluminum means that the train is relatively weak and can be broken easily.

IV.4.a.3 Clearing Nozzle Clogs

At times, the nozzle can partly or completely clog with grease and oil from the inside of the source. Baking the nozzle to 50°C overnight is a preventative measure, but is not always sufficient. The usual symptom of a clog is high (several hundred Torr) nozzle pressure not producing the expected increase in second stage pressure or source foreline pressure. If you're lucky, this problem can be corrected without venting the source by heating the nozzle and blasting it out with high pressures of argon. The nozzle can be heated with 15 V to as high as 70°C to loosen the clog and a sudden pulse of 100 psi argon can be supplied to blow it out. (Keep in mind that the nozzle holder is made of polyether ketone (PEK), which has a glass temperature of 143°C; you do not want the nozzle temperature to approach this temperature.) Several such pulses may be needed, separated by allowing the nozzle to slowly depressurize through the clogged beam hole.

If heating and blowing out the nozzle aren't sufficient, it may be necessary to vent and pull back the source. The skimmer can be removed by rotating it with tweezers, allowing one to look straight into the nozzle. Blow 115 psi argon through the nozzle while rinsing with squirt bottles of acetone and isopropanol and with a Pasteur pipette of toluene. (Toluene tends to damage the squirt bottles, but it's better for dissolving non-polar oil and grease.) When the nozzle is fully clear, its pressure should drop from 100 psi to 50 psi within 15 s when gas to the nozzle is cut off. A squirt bottle that has been used for toluene should probably be thrown out when you're done with it; it will soon crack and may result in a spill.

IV.4.b Pulling the Manipulator and Crystal

IV.4.b.1 Minor Tests and Repairs Without Venting

In general, if something is wrong with the crystal or the crystal manipulator, you're going to have to vent the main chamber and pull out the manipulator. However, there are a few things you can test without venting, and at least one quick—though temporary—fix that you can do without venting.

- Both the thermocouple and the crystal heating should have infinite resistance to ground.
- Room-temperature resistance across the thermocouple should be around 40 Ω.
- Room-temperature resistance across the crystal heating wires should be around 450 Ω.
- Room-temperature resistance between the thermocouple and the crystal heating wires should be around 400 Ω.

If any of these resistances are badly wrong—indicating a short circuit or a broken connection, you're probably going to have to vent. However, especially in the case of a short circuit, you may be able to effect a temporary fix by moving the manipulator in and out between the sputter and Auger positions a few times. This motion sometimes readjusts wires and fixes things. If this works, you may be able to get away with repeating this fix each time the resistance goes bad for a month or two, but you should fix it the next time you vent.

IV.4.b.2 Pulling Out the Manipulator

If you're unable to fix a crystal problem without direct access to the crystal, you'll need to vent the main chamber. Once the main chamber is vented, you can pull out the manipulator by following this procedure:

- Remove the thermocouple and heating control block / Auger target from the manipulator. Also remove the ℓN_2 cooling line for the crystal if it's attached.

- Remove the handle on the wheel that moves the manipulator in and out. Then remove the attached chain. (There should be one weak link that you can undo, allowing you to remove the chain.)
- Loosen all eighteen of the bolts that hold the manipulator flange to the end of the bellows slightly (half a turn). Remove the four at the bottom of the flange, as well as the pairs closest to the three tapped holes in the flange. Do not remove all of them, though, or the manipulator will fall out, likely damaging both it and the bellows severely.
- Roll the manipulator jig into place on the manipulator frame and screw the three removable partially-threaded posts into the three tapped holes on the manipulator flange. Tighten them with a $^3/_4$-inch wrench.
- Slide the jig in so that the three holes on it line up with the ends of the three posts. Then use the large nuts to attach the posts securely to the jig, and tighten these with a $^3/_4$-inch wrench as well.
- Once the manipulator flange is securely attached to the jig, remove the remaining bolts holding it to the end of the bellows.
- Pull gently back until the manipulator is entirely out of the bellows. Then cover the opening to the chamber with aluminum foil. If the manipulator is to be kept out of the vacuum chamber for an extended period, it may be wise to also cover it.

To reinstall the manipulator, reverse the above procedure after replacing the copper gasket on the manipulator flange. For more details on this procedure, see pages 127-131 of Gladstone's thesis.

IV.4.b.3 Reconnecting the Thermocouple to the Crystal

The type-C thermocouple contact consists of the two thermocouple wires spot-welded together as an X-junction. This X-junction is spot welded to a small 5 mm by 5 mm tab of 75 μm thick tantalum, which is held to the back of the crystal by a screw capped by a piece of alumina, with the tab between the X-junction and the crystal. If the tantalum sheet has simply slid out but the spot welds remain intact, you might be able to get away with simply reattaching it. More likely, you will have to redo the spot welding.

First, you should make the X-junction by spot welding the two wires together with about 80 V. Cleaning the tips of the wires with acetone will help with this, as will wetting the junction with a *drop* of acetone while you spot weld. It may be worthwhile to make two spot welds at the point of the X, but be careful as a second weld may destroy the first. Also, note that if you fail repeatedly, you are probably best off trimming the ends of the wires and trying again. Once you have succeeded in making an X-junction, cut out a fresh tantalum tab and wash it with acetone. Then, spot weld the center of the X-junction to a corner of the tab with about 110 V. If you fail at this more than once, you will probably want to replace the tab, as after a few attempts to spot weld to a given tab it becomes virtually impossible to weld to it successfully. Once the X-junction is successfully welded to the tab, the tips of the X-junction should be trimmed to ensure that they do not come directly into contact with the crystal. You can then tighten the screw to hold the tantalum piece in place, making sure that the ceramic screw tip is directly on the cross-point of the X-junction to ensure good thermal contact. Be very careful about tightening the screw for the thermocouple. It needs to be tight enough that with multiple fast back-and-forth rotations of the crystal, the resistance thermocouple-to-crystal doesn't vary more than about 20

Ω. However, over-tightening it can crack the crystal. Once the thermocouple is tight enough, the screw can be locked by tightening the nut on the screw.

One additional cause of spot-welding difficulties to watch out for is dirty tips on the copper wires used as spot-welding clamps. Minor cases of this can be corrected by repeated sparking with the tips in direct contact. If this is insufficient, you may need to sandpaper off the tips until clean copper is exposed.

IV.4.b.4 Replacing Thermocouple Wire

If the thermocouple connection to the crystal appears intact but the thermocouple still has infinite resistance, the next thing to check is whether the thermocouple wire is broken inside the manipulator arm. If it is, you will need to pull the wire out and replace it. It is a type-C thermocouple, so the positive terminal wire is tungsten with 5% rhenium and the negative terminal wire is tungsten with 26% rhenium. You can determine which wire broke by comparing the resistance of the broken wire with the resistances of equal lengths of each type of wire. Both wires should have a diameter of 0.005". Most recently, we have obtained replacement wire from ConceptAlloys.com.

The ends of the thermocouple wires are attached to the metal tabs on the type-C thermocouple feed-through. The wire is wrapped around a hole in the tab, then the end of it is spot-welded to the length of the tab. The tab is then spot-welded to the feed-through with the wire in between them. Be sure not to mix up which tab and feed-through wire goes to which thermocouple wire. And be sure to put a gasket on before attaching the wires to the feed-through!

If you have to replace or change thermocouple wire anywhere in the system, be careful to not mix up the two types. An incorrect or nonsensical reading can be produced if you switch the positive and negative wires for any of the segments of the thermocouple (the wires inside the manipulator, the wires connecting the manipulator to the thermocouple reader, or the contacts on the thermocouple reader itself). Replacement wires should be several feet longer than the wires they're replacing to provide replacement wire as the thermocouple connections are remade as a result of use. The wire should be insulated with the thinnest fiberglass insulation practical—a single piece if at all possible to avoid shorts within the arm—and strung through the arm with the aid of a thin metal rod. Be sure to use acetone to wash off any residue from tape used to attach the wire to the rod.

IV.4.b.5 Changing the Crystal

Once the manipulator is out, you can remove and replace the crystal. The 1998 "Scattering Chamber Manual" gives a procedure for changing the crystal, but that predates Bob Hefty's redesign of the crystal mount sometime between 1998 and 2003. The following is a rough procedure for changing the crystal. See pages 336-350 of Bob Hefty's thesis for a detailed description with diagrams if you need to repair the mount or cut new crystals.

First, loosen the screw (you must first loosen the locking nut) holding the thermocouple tantalum tab to the back of the crystal and carefully pull the tab and thermocouple wires away from the crystal. You can then remove the assembly holding in the thermocouple bolt by undoing two nuts. At this point, you can remove the four nuts that hold in the screws connecting the tantalum crystal clamps to the crystal mount, but be very careful not to lose the washers and sapphire spacers. (There should be one washer and one spacer next to the nut, and two spacers between the mount and the clamps.) To do this, you will need to counter-torque the screws themselves, but make sure the nuts, not the screws are rotating. This procedure should allow you to loosen and slide out the crystal. You can then slide in a replacement and reassemble the screw-spacers-washer-nut arrangement, tightening the nuts so that the crystal is held tightly and square with the mount. The new crystal surface must be perfectly flush with the tabs: make sure that all angles are right angles. Then, reattach the thermocouple bolt assembly and place the tantalum tab of the thermocouple behind the crystal and tighten the bolt while the tab is kept as straight as possible to prevent the thermocouple wires from twisting and touching the crystal or crystal holder. Check the resistances of the following connections using the feed-through posts, and make sure that they do not vary by more than 20% when the crystal is rotated back-and-forth three times:

- thermocouple-crystal ~ 400 Ω
- crystal-ground = ∞
- thermocouple-ground = ∞
- across the crystal ~ 450 Ω

The crystal should be rotated while the resistances are checked to ensure that there is good contact. These resistances are essential for a successful crystal replacement. Clean the face of the crystal with lens paper using the following procedure. Cleanly fold one piece of lens paper into a small packet slightly wider than the width of the crystal. Hold the lens paper with a hemostat (locking forceps) with the last crease of the paper facing outwards, trim to the width of the crystal using scissors, and wet with a solvent such as methanol or ethanol. Swipe each piece of lens paper over the face of the crystal only once. Fold, trim, and wet a new piece of lens paper if more cleaning is necessary.

IV.4.b.6 Repairing the Crystal Mount

The copper heater wires should be brazed to the copper lugs that screw into the manipulator arm with pure Ag-Au solder. The mount itself is made of tantalum because it doesn't mix with silicon even at high temperatures. The copper heating wires are brazed to the tantalum mount with 82:18 Au:Ni brazing wire.

IV.4.b.7 Replacement Sapphires for the Crystal

Replacement sapphire washers for the crystal can be purchased from Swiss Jewel Co. in Philadelphia, PA. (They refer to them as "ring jewels".) The larger clear sapphires are R177.8 and the smaller red sapphires are R175.0. Both are roughly $6/each for an order of 25.

IV.4.c Removing and Repairing the Auger Spectrometer

IV.4.c.1 Auger Resistances

The easiest check to do if the Auger is misbehaving is to check the resistances of the various connectors to ground and to each other.

- V1 and V2 are the two main lenses; they should have infinite resistance to ground and to everything else.
- F1 and F2 are the two filament terminals. They should have only a couple of ohms of resistance between them, but infinite resistance to everything else.
- C, +, and - are the channeltron connections. They should have infinite resistance to ground and everything else.
- VM is the energy-filter lens. It should have a 5 MΩ resistance to ground and infinite resistance to everything else.

IV.4.c.2 Taking Out the Auger

The Auger is sufficiently long and heavy that taking it out safely requires two people: one inside the machine to steady the end while the other removes the final bolts and pulls it out. While it is physically possible for one person to remove or install it without help, doing so puts undue stress on the bearings on the Auger horizontal translator and will break them if done repeatedly.

- First, vent the main chamber and open the door that is closer to the Auger.
- Disconnect the cables attached to the back of the Auger and undo all but four of the bolts holding it in place.
- Have a second person climb into the machine and steady the end of the Auger with their hands. Once they are in place, you can undo the remaining bolts and pull it out.
- Set it on the Auger stand, which is a three-legged metal stand with a U-shaped cut-out.

IV.4.c.3 Disassembling the Auger

Disassembling the Auger spectrometer is fairly self-explanatory. It consists of a series of nested shields to be removed in order. A diagram can be found in Figure IV-8.

- The outermost two shields are held in by four screws each and can be easily lifted off once they are unscrewed.
- The next shield consists of a metal shield with a ceramic cap. The cap should pull off fairly easily. The shield can also be removed once the screw holding a copper grounding wire to it is undone.
- Next comes a shield with metal mesh over various apertures. This shield has three screws holding it in place. Once they are removed, it can be pulled off and it may require some force

to pull it off. Examine the mesh: in the likely case that some of it is damaged you'll need to reattach or replace it by spot-welding the mesh at 100 V.

- Beneath this shield is a mu-metal shield, which you may need to use some force to pull off.
- Once all shields are removed, you can undo the three long screws holding together the filament-and-lenses assembly. This assembly consists of three pieces of metal shaped like stovepipe hats separated by two ceramic ring spacers. The middle metal piece is the V2 lens and the bottom one is the V1 lens, as well as containing the filament.
- When removing the V1 lens, take care to disconnect the filament barrel connectors from the filament posts, not from the copper wires that go to the flange.

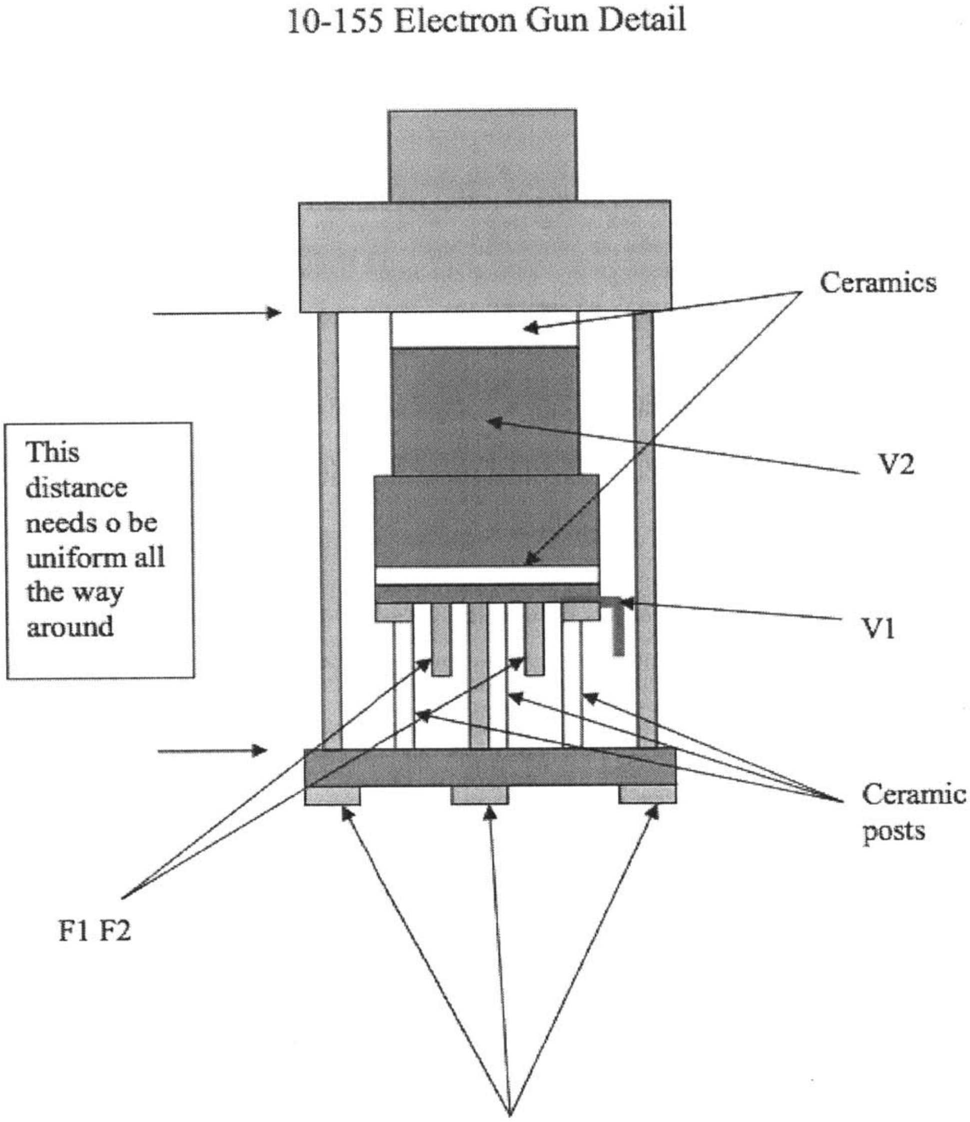

This distance needs o be uniform all the way around

These screws hold the gun assembly together. It is stacked on the ceramics. Tighten it up, but not too much. All 3 screws should have the same distance with-in .001".

Figure IV-8: Diagram of the Phi 10-155 Auger Electron Gun

This diagram was taken from an RBD Instruments "Tech Tips" entry, copyright 2006.[12]

IV.4.c.4 Replacing the Auger Filament

If the filament is broken, or if the ceramic on which it is mounted has become so metalized that it shorts to V1, you need to remove the filament by unscrewing the three screws connecting the top and bottom halves of the V1 lens. You can then remove the ceramic filament mounting and replace it with a new one. You then need to check the alignment: unfortunately this is a guess-and-check procedure.

To check the filament alignment, put the V1 lens in the alignment jig, tightening all three screws to hold it in place firmly. There are then three alignment tests you can do.

- Using the lab's stereomicroscope with its overhead lamp on, you can see the tip of the filament as a white dash in the small hole in the center of the V1 lens. This dash should be in the center of the hole. (You may need to look with one eye at a time and try to average to figure out if it is.)
- Using the stereomicroscope, you can also turn off the overhead lamp and use a flashlight to illuminate the lens from below. The filament will now look like a dark line, and should be centered.
- You can hold the jig up to a ceiling light and peer through the hole with one eye. If you tilt the jig, you should be able to see the filament as a dark line and, if you tilt it more, the two holes in the mounting ceramic as bright spots of light. The filament should be about equidistant from each of these holes.

If the filament does not seem centered, loosen the screws on the bottom of the V1 lens (not the screws holding the lens in the jig), and shift the ceramic in the direction you think it needs to move. Then, re-check the alignment. Repeat until satisfied that it is aligned.

IV.4.c.5 Reassembling the Auger

Reassembling the Auger is essentially just a reversal of the steps required to disassemble it. During reassembly, it is very important to make sure that parts snap together properly, and that you align the barrel connectors on the filament so that they aren't touching or nearly-touching. (This alignment may take several attempts.)

The inner cylinder has a wire mesh covering several windows on it. This mesh sometimes tears or breaks, and having it intact and taut over the windows is important to getting good signal. This mesh is tungsten, although beryllium-copper can also be used (that's what the Auger originally shipped with). Replacement mesh can be purchased from Alfa Aesar: we've used a "40 mesh tungsten gauze" for this purpose, which is made of wire 0.001 inches in diameter with holes 0.0165 inches in diameter, the same dimensions as the original mesh.

Replacement mesh should be spot-welded to a number of locations around the edge of the windows to produce a taut covering. Once the spot-welding is complete, trim off any loose fringe beyond the spot-welds. A difficulty that can occur during this procedure is that the cross-wires of the gauze are not secured to each other, so once you cut out a piece of gauze, it is very fragile and individual wires may slip out of position. To remedy this, it is useful to go around the edge of the piece you've cut, spot-welding crossed wires together to make secure joints before you begin spot-welding the piece of gauze to the cylinder.

IV.4.c.6 Reinstalling the Auger

Reinstalling the Auger is essentially a reverse of the process of removing it, and is also a two-person job. Degauss it and clean it with acetone, then put a fresh copper gasket on the Auger flange. Then have one person climb inside the machine to receive and steady the Auger as the other person passes it in and bolts it to the flange. Once four bolts have been securely tightened, the person inside can let go of the Auger. Before they come out, though, they should make sure that the outer magnetic shield is still aligned on-axis: handling it can cause it to become tilted. Before installing and tightening the remaining bolts, all resistances should be checked.

IV.4.c.7 Purchasing Replacement Filaments

We've been buying replacement filaments from RBD Instruments in Bend, Oregon. This replacement is much cheaper if you send them the ceramic from a broken filament: they charge $285.00 and the part number is C75010RE. They supposedly will also, for roughly $100, clean a metalized filament ceramic.

IV.4.d Aligning the Auger Spectrometer

IV.4.d.1 Measurement of Auger Support Rods Droop

The manuals that came with the Auger spectrometer, plus other information from the RBD Instruments website, are quite useful for performing repairs on the Auger. However, one thing that they don't discuss is the translation stage and extender rods that are used to support the Auger. These also don't have an equivalent on the Little Machine: their Auger, although the same model as ours, is bolted directly to the wall of their Machine.

Unlike the crystal manipulator translation stage, the Auger translation stage doesn't have a chain drive. Instead, one of the four support rods is a threaded rod, while two of the other three are on bearings and the fourth is a greased bronze piece to provide additional stability. Three steel rods screw into the Auger flange and extend into the main chamber some distance, where they support the Auger itself.

Checking the alignment of the support rods is relatively easy, since they are attached to the Auger flange and so can be removed from the machine and taken to the MIT Central Machine Shop to be measured precisely. This check is done by using perpendicular blocks to hold the Auger flange perpendicular to a flat measurement table and then measuring the distance between the table and the plate at the base of the Auger can with the Auger flange in different angular orientations. This distance should be 1.310" at all orientations if the support rods are not drooping, as the plate diameter is 3.350" and the flange diameter is 5.969".

In summer 2013, this procedure was performed and the difference in Auger height depending on the orientation was found to be over 0.2". New rods were machined and a lathe was used to remachine the surface of the flange to make sure all rods would be flush with the same plane.

IV.4.d.2 Alignment Check with Surveying Scope

In November 2013, the Auger spectrometer's alignment was checked using a modification of the surveying scope method that is used to align the detector cryostat with the molecular beam. The crystal manipulator was removed and alignment threads were placed in the cross-hairs etched into the resulting opening. The lid was rotated so that the detector box entrance slit was normal to the manipulator axis and the detector box entrance slit was used as a second alignment point to align the surveying scope along the manipulator axis.

Once the scope was aligned along the manipulator axis, it was possible to measure vertical position of the Auger aperture relative to the crystal as well as the distance between the Auger aperture and the crystal. However, this method does not allow measurement of the correct position of the crystal horizontal translator to center the crystal in front of the Auger, since the scope is aligned with that axis. Two measurements of vertical position were done: one found the Auger aperture to be 0.030 in higher than the midpoint of the crystal vertical translator—indicating that the correct position of the crystal vertical translator is 0.53 in—and the other found the aperture to be 0.010 in lower than the midpoint of the crystal vertical translator—indicating that the correct position of the crystal vertical translator is 0.49 in. The two different vertical positions measured reflect the difficulty in determining the edge of the Auger aperture.

There is some ambiguity in what the correct Auger-crystal distance is—Gladstone's thesis gives it as "not more than 0.250 in[1]—while a drawing in one of the manuals provided by Phi with the instrument itself suggests that 0.26 in is the optimal distance. According to the measurements with the scope, 0.26 in corresponds to a reading of 39 mil on the Auger manipulator's dial micrometer, while 0.250 in corresponds to a dial micrometer reading of 50 mil. The 0.250 in crystal-auger distance corresponds to 4.344 in between the outer edges of the two plates that support the auger bellows, or 2.505 in between the inner edges of those plates.

IV.4.d.3 Alignment Check with Laser

A second measurement of the Auger spectrometer's alignment was done in September 2014 using a laser and stand normally used to align the Little Machine crystal. The goal was to determine whether the crystal, when in Auger position, is correctly centered on the center of the Auger manipulator and normal to the axis of the Auger. In order to do this, the crystal was first set in the previously recorded Auger position:

- angle: 180° = 0.00 tick marks
- vertical: 0.50" above bottom
- horizontal: 20.35" (at the "Auger" mark)

The Auger was removed from the Auger manipulator, leaving an open flange through which the crystal was visible. The Little Machine alignment laser was then aligned with the crystal so that the beam reflected directly back to the laser source, indicating that the laser beam was normal to the crystal. A blank was placed on the Auger flange and the laser dot was observed to be 0.33 in from the center of the flange, almost directly below (but slightly to the left of) the center. If the position of the Auger flange is not significantly changed by the weight of the Auger, this means that the center of the Auger should be 0.165" above the center of the crystal. As the crystal itself is 0.415" from left to right and 0.460" from top to bottom,[8], this would mean that the Auger beam is centered near the top of the crystal at the recorded Auger settings.

To attempt to correct for this height difference, the crystal was moved to a new vertical position. The horizontal position was also slightly changed to be consistent with estimates of the crystal position from measurements of electron current to the crystal:

- angle: 180° = 0.00 tick marks
- vertical: 0.64" above bottom
- horizontal: 20.40"

When the laser was aligned normal to the crystal in this position and the flange was replaced, the laser dot was found to be within 0.05 in of the center of the flange, though still slightly too low. This distance is a little more than 10% of the height of the crystal (the crystal is a rectangle 0.460 in tall and 0.415 in wide). Furthermore, it is certainly within the experimental error of the procedure, as it is unlikely that we successfully centered the laser beam on the center of the crystal with an error of less than 0.05 in.

A second laser test was done by first aligning the beam normal to the center of the Auger flange (bolted onto a used gasket) and then attempting to align the crystal to be centered on and normal to the beam. Unfortunately, it proved impossible to use the reflection of the beam on the Auger flange to ensure the laser was normal because the reflection was too diffuse, so a mirror taken from a cosmetics compact was pressed firmly to the flange to provide a reflection. Once the laser beam was aligned normal to this mirror, the flange was removed and the crystal was adjusted so that the reflection of the beam off of the crystal would return to the laser aperture, indicating that the beam was normal to the surface of the crystal. We were unable to get the crystal perfectly normal to the beam because we did not rotate the manipulator around its axis via the manipulator differential seals, and the reflection was 1.3 in lower than the laser beam source. However, we were otherwise able to align the reflection with the following crystal settings:

- angle: 178.7° = 0.18 tick marks
- vertical: 0.47 in above bottom
- horizontal: 20.94 in

With a 92.5 in separation between the laser source and the crystal, the 1.3 in vertical offset comes out to a difference of only 0.8°. Neither this nor the 1.27° difference in observed angular crystal positions between the two laser methods (180° by aligning the laser beam normal to the crystal surface and through the center of the auger flange versus 178.7° by aligning the beam normal to the center of the auger flange first and then rotating the crystal normal to it) is particularly significant for Auger sensitivity, given that the Auger aperture is located less than 0.3 in from the crystal during experiments. The differences in vertical and horizontal position, though, shed some doubt on the accuracy of these methods. The two most likely causes of error are the difficulty in being sure the laser is centered on the crystal (which exists for both methods) and the difficulty in being sure that the mirror used to align the beam normal to the Auger flange is indeed parallel to the flange (which is an issue only for the second laser method). However, it is worth noting that, for the rather long baselines used here—the laser-crystal distance was 92.5 in and the laser-flange distance, while not recorded, was roughly 30 in—mean that small angular errors would produce into large translational errors. Overall, I believe that the first set of laser measurements is more reliable, given the uncertainty of how close to parallel with the flange the mirror's surface actually was in the second set of measurements. However, the fact that this measurement finds the center of the auger flange to be at 0.64 in on the crystal vertical translation stage is concerning, as this is 0.12 in above the 0.50 in midpoint of the crystal translation stage. As such, it is probably wiser to rely on surveying scope and electron current measurements.

IV.4.d.4 Crystal Flatness Measured via Laser Reflection

One serendipitous consequence of measuring the alignment of the Auger spectrometer with a laser was that it provided a means to quantify the flatness of the crystal. In order to align the laser normal to the surface of the crystal, paper was attached to the aperture of the laser to allow the reflected beam to be observed. Unexpectedly, the reflected beam was not circular, but was projected on the paper as an oval with its long axis parallel to the floor and 3.07 in long and its short axis 0.74 in long. With this information, the incident laser beam diameter—0.12 in—and the distance between the crystal and the paper on which the beam was projected—92.5 in—it was possible to estimate the flatness of the crystal. As shown in Figure IV-9, the surface normals on the left and right side of the crystal differ by 6.4° and the crystal is bowed out by 0.006 in.

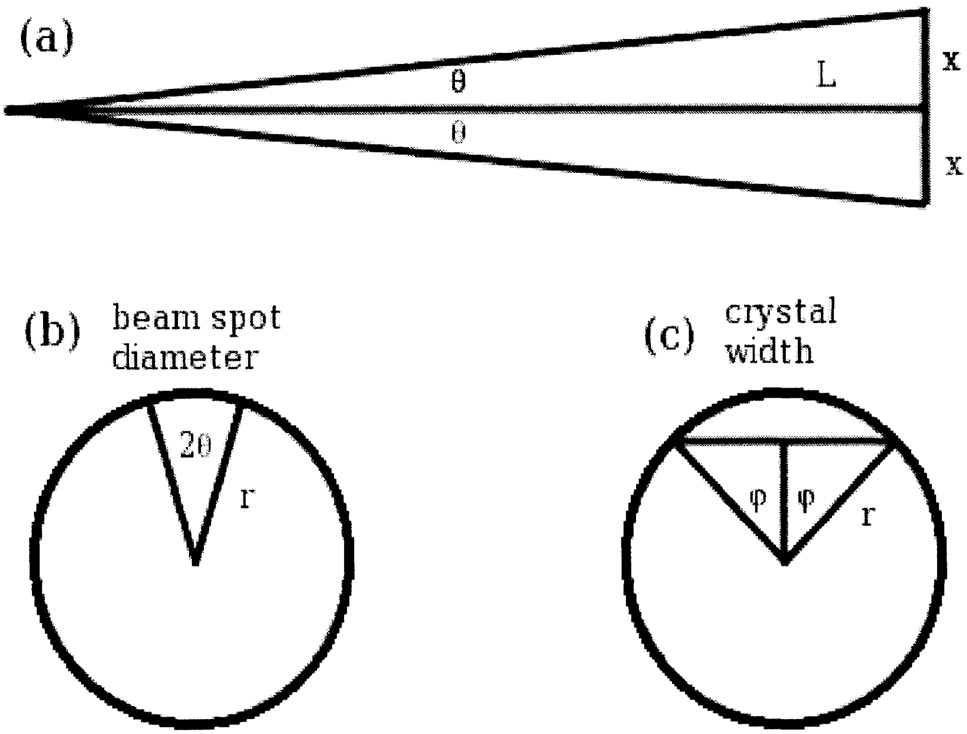

Figure IV-9: Calculation of Crystal Deformation

(a) The angular difference in surface normals across the laser beam spot on the crystal is 2θ where θ = *arctan*(x/L), x = 1.535 in (half the 3.07 in horizontal beam spread), and L = 92.5 in (the distance between the crystal and the screen the reflected beam was projected on). This gives θ = 0.95° and 2θ = 1.9° = 0.033 rad

(b) If we assume that the crystal curvature is circular, we find that the radius of the curvature must be the beam spot diameter—0.1235 in—divided by its angular size, 0.033 rad, giving a radius of r = 3.74 in.

(c) Since the full width of the crystal is 0.415 in, the surface normals on the left and right edges of the crystal differ by 0.415 in / 3.74 in = 0.111 rad = 6.4°. We can determine how much the center of the crystal is bowed out from the edges by subtracting r *cos*(ϕ) from r, where ϕ = 3.2°, half the difference in the normals. This gives us r – (r *cos*(ϕ)) = 0.006 in.

IV.5 Detector Box Repairs

IV.5.a Removing the Detector Box Quadrupole and Channeltron

IV.5.a.1 Accessing the Quadrupole and Channeltron

The detector box quadrupole and channeltron are housed in a series of cylindrical chambers bolted to the rear of the detector box. They can best be reached by rotating the lid so that the rear of the detector box is facing the pump-room side door of the main chamber and opening that door. The channeltron itself only needs to be separated from the quadrupole if you need to replace the channeltron, most easily done when the quadrupole is itself bolted to the detector box to provide counter-torque on the bolts. The entire quadrupole-and-channeltron assembly can be removed as a single piece to access the rear entrance of the detector box, for example for cryostat alignment or to disconnect or remove the ionizer plate (as is necessary before removing the cryostat).

IV.5.a.2 Removing Only the Channeltron

The channeltron is mounted on the first (furthest towards the back) 4-$^{5}/_{8}$ inch flange on the detector box. There are three electrical connections on the flange. On the left is the channeltron signal out. On the right, the lower connection is the channeltron ground and deflector plate and the upper connection—which is larger than the other two—is the channeltron high voltage. (Since we are detecting positive ions, the front of the channeltron is held at a negative voltage and the rear is held at ground.)

To remove the channeltron, first disconnect the electrical connections from this flange and label the wires. Then remove this flange and take off the channeltron by removing the 4-40 bolts that connect it to the flange. The channeltron should be installed so that the channeltron horn arcs upward and the channeltron deflector plate faces downward.

IV.5.a.3 Removing the Quadrupole

The quadrupole can be removed with or without removing the channeltron first. There is no reason to remove the channeltron unless you specifically need to repair or replace it. The quadrupole assembly needs to be removed, however, to reach the ionizer and to disconnect the ionizer wires before the ionizer can be removed or the whole quadrupole can be pulled out. To remove the quadrupole:

- First, remove the electrical wires from the rear of the channeltron—being sure to label them—as well as the two RF supply lines that are connected to the top of the quadrupole cylinder.
- Although it is not strictly necessary, it is wise to disconnect and remove the heating lamp and ceramic-insulated heating wires in the vicinity of the area you will be working. Removing and (especially) reinstalling the quadrupole is one of the most physically demanding repair jobs on the machine, and the chances of breaking the lamp or ceramics with a slipped wrench or elbow are high if you do not do so. It is also useful to cover the area under the quadrupole with aluminum foil to catch dropped screws and keep them from falling into the gate valve or pressure-release valve, both of which are located in this area.
- Before you can put the jig for removing the quadrupole in place, you'll need to remove the bottom six of the ring of gold-plated screws holding the quadrupole to the detector box.
- The jig consists of a lab jack with two square wooden blocks fixed to opposite ends of it to create a U-shaped bed to support the quadrupole. Find this, cover it in aluminum foil, and place it inside the chamber in position to support the quadrupole.
- Gradually loosen the remaining gold-plated screws holding the quadrupole to the detector box until you have removed most of them. At this point, you will want a second person on

hand as you remove the last few screws, steady the quadrupole on the stand, and use an Allen key or screwdriver to disconnect the barrel connector on the ground wire that runs from the inside of the quadrupole to the detector box. Since the quadrupole sits on a lip, it is essential that you pull it straight out before allowing it to rest on the stand. An alternate technique that may be useful is to have the second person crawl into the machine through the other door to undo the barrel connector while you support the quadrupole.

- Once the quadrupole is fully disconnected, you can lift it out of the chamber and, with the help of a second person, carry it to a flat surface that has been prepared with aluminum foil.

Reinstalling the quadrupole is largely a reversal of these steps, but it is rather physically more onerous for three reasons: the need to steady the quadrupole on the stand while attaching the ground wire and putting in the initial bolts, the need to lift the quadrupole so as to put it in straight over the lip without dislodging the special wire gasket, and the extreme force needed to crush the gasket.

The wire gasket used for the quadrupole is homemade from Al welding wire. The Central Machine Shop makes them, using an old quadrupole flange as a model. This gasket needs to be squeezed extremely flat to assure a good seal: you will need to use feeler gauges to make sure that the quadrupole is going in straight as you tighten the bolts: you are done when a 0.001 inch feeler gauge can't fit between the quadrupole and the wall of the detector box on any side.

IV.5.b Ionizer Removal and Repair

Since the detector box ionizer is accessed through the quadrupole flange on the back of the detector box, the quadrupole must be removed (See Section IV.5.a.3 .) before you can remove the ionizer. Once the flange is removed, you can—very carefully, as the copper feed-throughs they're attached to are very fragile—remove the push-on connectors for the filament current and lens voltage cables, making sure to label the cables. (A wiring diagram is shown in Figure IV-10.) With the cables detached, you can put bolts into four empty holes in the plate to use as handles and then—very carefully, as these screws are incredibly short and very easy to drop—use a screwdriver to remove the four screws holding the plate in. With these screws removed, you can pull the plate out of the lip it fits into and carefully guide it out of the cryostat, being careful not to damage the lenses or the wires leading to them.

If it proves necessary to disassemble the ionizer stack or replace the filament, relevant diagrams can be found in pages 126-140 of Marianne McGonigal's thesis where the original design of the ionizer is discussed. One short-circuit and filament burnout modality that can occur isn't mentioned there, and is important to watch out for, though. The lower of the two plates that the filaments are attached to has a shield that extends along much of the filament length from it. If the filaments aren't sufficiently taut, it's possible for one of them to short to the upper part of the shield. This configuration will temporarily result in an unusually low filament resistance and a high emission. After a few hours, though, the filament will burn out due to the excessive current going through one of the filaments, and almost all of the emission being generated in a smaller region than usual.

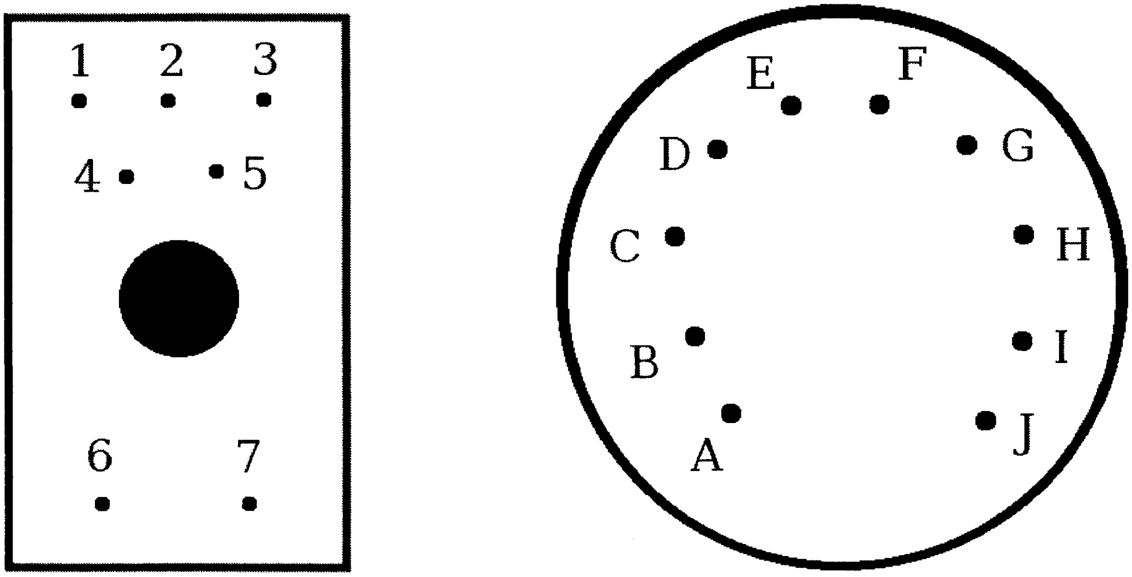

Figure IV-10: Detector Box Ionizer Plate and Ionizer Feed-Through Wiring Diagrams

The diagram to the left shows the rear of the ionizer plate, as viewed with the plate installed in the cryostat. The connections are: (1) Lens 3—bottom lens, (2) Lens 1—top lens, (3) Grid, (4) Lens 2—middle lens, (5) Extractor, (6) Bottom Filament Plate, and (7) Top Filament Plate. The diagram to the right shows the ionizer feed-through on the lid, as viewed from above. The connections are (A&B) Filament, (C) Blank, (D) Extractor, (E) Lens 1, (F) Lens 3, (G) Lens 2, (H) Grid, (I&J) Filament. Terminals A&B and I&J are shorted together to provide increased current capacity through the feed-through.

IV.5.c Removing the Cryostat

This procedure is complicated and unusual and if you make any errors, you can do a lot of damage that will be hard to undo, so you should definitely look at the blueprints and talk through the procedure with Professor Ceyer before you start.

- Turn off cooling water to the turbopumps. Then you can disconnect the water, foreline, compressed air, and power connections to the third stage turbomolecular pump.
- Next, you need to remove the helium lines from the helium cryostat on the lid. These are connected with the same special self-sealing connections used on the nozzle cryostat, and you need the same special wrenches to remove them, being careful to apply stationary counter-torque appropriately. (Make sure you know which part should rotate and which part shouldn't, or you are likely to create a leak.)
- Next, you will need to remove the ℓN_2 "chicken feeder". Do this by undoing the four bolts that connect it and the ring with the nitrogen outlet to the vertical part of the arm, rather than the large number of star-head bolts that connect the vertical and horizontal parts of the arm. (The latter requires three people to reinstall, and even then is difficult, because of aligning the internal bellows in the arm.)
- Now you can undo the twenty-four bolts that connect the helium cryostat to the adaptor flange on the top of the turbomolecular pump. Once these are undone, lift off the cryostat--it is lighter than it looks, and one person can lift it, but it is helpful to have a second person on hand to help you get it down from the lid once you are holding it.
- Unbolt the third stage turbo below the gate valve and lift it off (with gate valve attached to it) with the crane. It may be easiest to suspend it by the flange at the top, but in any case you must be careful to lift it straight so the studs don't catch.

- The next step is to remove the quadrupole from the machine, as discussed in section IV.5.a. Once complete, you can remove the connections from the ionizer and remove it, as discussed in section IV.5.b
- Now, before you can take the ionizer cryostat out, you have to remove the second stage turbo with the gate valve attached to it. Do this with the crane after disconnecting forelines, water, compressed air, and power. The second stage turbo gate valve is mostly bolted to the lid by screws, but there are two studs that you'll have to remove while the turbo and gate valve are suspended from the crane before you can put them down.
- Once the second-stage turbo has been removed, you can disconnect the thermocouple and heater connections that run through the second stage turbo flange.
- Now it is finally possible to remove the ionizer cryostat with the crane. There is a wooden board with a properly-sized hole cut out from it that can be used as a cryostat stand. It should be C-clamped to the forklift at the proper elevation, and then the cryostat should be lowered into it.
- If you need to seal the detector box for leak-checking purposes, you can use a standard flange for the second stage turbo connection. However, a custom stainless steel flange with an O-ring exists for the lid cryostat connection and a custom plexiglass flange with a taped-on O-ring exists for the open flange on the detector box inside the machine where the quadrupole goes.

IV.5.d Re-Aligning the Cryostat

IV.5.d.1 Aligning the Surveying Scope

Any work done on the ionizer cryostat or associated flanges requires that the ionizer be realigned along the beam line. For this purpose, we have a surveyor's scope in the lab, which we align along the source A beam path. Once the surveying scope is aligned with the thread crosshairs, it is wise to make chalk marks on the floor around its feet so it can be repositioned if it is knocked out of place. Furthermore, vibration in the vicinity of the scope should be minimized. To this end, liquid nitrogen cylinders should not be brought into the lab through the big machine lab door. Instead, bring them in through the new machine lab door and store them there until needed. The procedure for aligning the scope is as follows:

- There are two pairs of etched marks on the outside of the main chamber that define the source A beam path into the main chamber. One pair is etched into the surface where the second stage mates with the source chambers; the other is etched on the differentially pumped flange with a window to the left of the left door. Thus, the first two steps in alignment are pulling back the source chambers and removing the window from the flange (leaving the flange in place, but removing the leftmost and rightmost bolts because they cover the horizontal crosshairs).
- Align thin thread in the crosshair notches and tape it firmly in place, creating a pair of thread crosshairs that should cross directly at the center of the beam line. Make sure that the thread is in fact properly aligned down the centers of the notches.
- Open the beam valve between the main chamber and the second stage all the way so that the rear crosshairs will be visible through the removed window. Now, set up lighting for each pair of crosshairs. For the rear ones, there is a standard-sized light bulb attached to a small

plexiglass plate that should be placed inside the second stage on top of a block of wood and approximately in line with the rear crosshairs and the slit.

- Next, align the scope so that its central crosshair (there are additional ones on each side of the central one) is aligned with both thread crosshairs when the scope is focused on them. This involves both horizontal and vertical translations and rotations and making sure that the scope is in fact level according to its built-in spirit levels. It may also be useful or necessary to adjust the feet of the scope. It is not, however, useful to use a laser for initial alignment, since there is no reason to expect the wall of the machine--or the base of the scope--to be perpendicular to the beam line.
- Once the thread crosshairs are aligned, it is important to make sure that the scope's crosshairs aren't rotated with respect to them. This alignment can be checked by translating the scope and making sure the scope's crosshair lines stay aligned with the thread ones. However, note that the scope's vertical translation is a bit broken and it will only move straight while going down: when it is moved up there is horizontal movement as well. Furthermore, the centerline of the thread crosshairs should pass through the center of the beam slit. If it does not appear to do so, the most likely culprit is shadows from the lighting, and you should try to adjust the light sources until the issue goes away.

IV.5.d.2 Measuring the Entrance and Exit Slit Positions

With the scope aligned, one must next measure the positions of the old (pre-realignment) entrance slit plate and ionizer plate relative to the thread crosshairs to determine locations for new entrance and exit slits that will be centered on the cross hairs. When Tate originally developed this procedure for the then-new cryostat, there were no old plates, so he drilled 1/32 inch diameter holes in the estimated locations of the slits and measured their locations.[6] The process was most recently performed as described by Blair[9] after the cryostat flange on the lid was replaced due to the March 2011 leak.

To measure the positions of the entrance and exit slits, the lid must be rotated into the straight-through position (270.05°) with one (but not both) of the slits installed in the cryostat. The vertical and horizontal distance between the thread cross-hairs and the slits can then be measured with the surveying scope. As an additional complication, the vertical length of the cryostat decreases due to thermal contraction when it is filled with liquid nitrogen. Since the cryostat is always kept cold when experiments are run, the vertical position of the slits needs to be aligned so that they will be in the scattering plane with the cryostat cold.

The cryostat cannot be cooled to liquid nitrogen temperatures in atmosphere due to the risk of condensation, so it is necessary to pump out the detector box to perform the cold measurements. There is a special plexiglass blank with a taped-on o-ring for the quadrupole flange at the rear of the detector box that can be used to seal the detector box while leaving a clear line-of-sight for alignment purposes. It must be installed in a specific orientation: "left", "right", "top", and "bottom" are written on its edges to indicate this orientation.

To pump down the detector box with the main chamber vented and the lid turbomolecular pump assembly disassembled to allow for easy removal of the cryostat, the cryopump roughing cart intended for use on the new machine is attached via bellows to an adapter plate on the top of the cryostat. One of the cryopumps on this cart has a leaky stopper and is unusable, but the other two provide sufficient pumping to pump the detector box down to 10 mTorr and maintain this pressure for at least twenty hours. Once the detector box pressure reaches 10 mTorr, the cryostat can be filled as usual to reach its usual operating temperature of -183°C and measurements can be taken. Once measurements are completed the detector box should not be vented until the cryostat temperature has warmed above 0°. This whole process will take about twelve hours, and the cryopumps will need to be topped off with liquid nitrogen every half hour or so for that period. As such, it is best to have two people available for this job to allow alternating shifts.

The indexes of refraction of air and vacuum are essentially the same, but that of plexiglass is not, so the plexiglass window introduces a slight shift in the measured positions of the entrance and exit slits. To account for this, take three sets of measurements: one at room temperature with no window, one at room temperature with the window installed, and one with a cold cryostat with the window installed.. The vertical shift due to the cold cryostat can be calculated from the two measurements taken with the window installed and this shift can then be applied to the measurements taken with no window to determine the true vertical position of the slits with a cold cryostat.

IV.5.e Chopper Wheel Repairs

Replacing or repairing components of the chopper set-up requires, at a minimum, removing the chopper cap and wheel from the front of the axel inside the main chamber. To do this, use a flat-head screwdriver to remove the screw that holds the chopper assembly together. Next, remove the cap of the aluminum mount. Then, remove the chopper wheel from the aluminum mount.

More involved repairs will require removing the door to the chopper chamber from the main chamber, which is sealed with a Viton o-ring and held on via screws. Once this is open, it is possible to unscrew the three screws holding the motor into the wall of the chamber—they are on the outside of the chamber, hidden behind the chopper wheel until you remove it—and to remove the motor assembly. To replace the bearings, remove the aluminum mount from the chopper motor shaft and take the motor shaft out of the motor. Remove the two bearings on the motor shaft and put on new bearings. Reinsert the shaft into the motor and replace the aluminum mount, chopper, cap, and screw.

The chopper wheel / shaft system has to be balanced before use. We've had this done by a company called Lindskog. The motors are manufactured by a company called Globe, with the following specs:

- Part Number: 75A1646
- Hysteresis synchronous motor, 115 V, 400 Hz, 2.25 length, Ultra High Vacuum Capable
- Barden Bartemp bearings (model # SR4SSTB5) Please ensure that bearings are snug in housing.
- Stainless steel replacing all brass parts inside motor.
- High temperature ML wire (bakeable to 400 deg C) for windings.
- Teflon insulated external wires.
- This motor is very similar to the 75A1003-2 motors. However, all the parts requested for the new motor are needed for ultra high vacuum capability.

The cost for a new motor and shaft—they won't make them separately—is about $3500 with a three to four month lead time at present. Globe can be contacted at sales@globemotors.com, but their local representative is Forbes Engineering Sales in Danvers, Massachusetts, info@forbesengineering.com.

IV.6 Pump Repairs

IV.6.a Turbomolecular Pump Repairs

IV.6.a.1 Changing the Oil on the Lid Turbomolecular Pumps

The oil needs to be changed on the main lid turbopumps (not the lid backing turbomolecular pump, which has magnetic bearings) about once a year or when it starts to turn noticeably dark. It should be replaced with Pfeiffer TL 011 turbomolecular pump oil, 20 mL for each of the three main turbopumps on the lid. Before changing the pump oil, you will need to vent the lid turbomolecular pumps. While the job is easier to do if the turbopumps have been removed, there is no reason to do this if you're only doing an oil change: the oil can easily be changed with the pumps still installed.

A 10 cm needle attached to a syringe that can hold at least 10 mL is needed to change the pump oil. There should be several in a large, heavy cardboard box in the drawers with the turbomolecular pump supplies, or else in one of the thinnest drawers in the far back of the lab. If for some reason you can't find any in the lab, you will have to buy one from the VWR stockroom with Sylvia there in person: only faculty members are authorized to buy syringes and needles. Since the oil is relatively viscous, it is best to buy the widest gauge needles available: you aren't actually using them to pierce anything, they just need to be able to fit through the oil-change apertures.

A special tool is needed to open the turbopumps to change the oil. We actually have two versions of this tool. One is made of aluminum and consists of a 30 cm handle with a ~3 cm diameter, ~8 cm long cylinder mounted perpendicular to the handle. The cylinder can be loosened with a set screw to allow you to place it at the end or the center of the handle. At the end of the cylinder, a 2-mm thick semi-circle the diameter of the cylinder juts out. It is exactly fitted to the indentations in the oil-change flanges on each side of the turbopumps and is needed to unscrew the flanges. The other tool is a steel disk about 5 cm in diameter that is also fitted to the indentations in the oil-change flanges. *Please do not use these tools to retighten the flanges: do that with a large flat-head screwdriver. Tightening the flanges with these tools will generally result in over-tightening and be nearly impossible to undo even if you remove the turbopumps from the lid to do it.*

Once you have located the necessary tools, you will need to open the flanges on the sides of the turbopumps, syringe out the old oil, and replace it with new oil by syringe.

- First, using the special tool described above, unscrew the opaque inner part of one of the oil-change flanges on one of the turbopumps. Since your biggest difficulty will be keeping the tool from slipping out, you are probably best off placing the cylinder at the center of the handle. In any case, you will most likely want to brace the cylinder with your knee while trying to rotate the handle.
- Once you get the flange loose, unscrew and remove it, being very careful not to lose the spring seated in the copper cylinder that the flange holds in and the o-ring that makes the flange's seal.
- You now need to syringe out the oil in the pump. If you find that this requires an inordinate amount of effort, you may need a wider gauge of needle.

- Once the old oil has been removed, syringe in 10 mL of oil. You may first want to rinse the syringe and needle by taking up a small amount of oil and expelling it as waste.
- Replace the copper cylinder, making sure to properly seat the spring, and then screw the opaque inner flange back in. *Tighten it with a flathead screwdriver, not the flange-loosening tool.*
- Repeat the procedure on the other side of the turbo pump, and then on each side of the other three pumps.

IV.6.a.2 Lid Turbomolecular Pump Controllers

The controllers for the second and third stage lid turbopumps have an internal interlock that triggers in the event of a sudden power loss, turning off the pumps. To reset this, you need to hold down the "pumping unit" and "standby" buttons on the controller simultaneously.

IV.6.a.3 Lid Turbomolecular Pump Repairs

I don't really have much to say about the matter of repairing the lid turbomolecular pumps. There's a limited amount we can do to them, since we don't have the equipment needed to balance the rotors. It is very important not to disassemble the pump region, as if the rotors/fan blades come out, it is impossible to reassemble them and the whole pump will need to be sent in for a rebuild. However, the oil casing regions can be removed to access the motors. Gang Liu, the Chemistry Department electronics technician has experience with doing this, and should be contacted (as should Sylvia!) before you try any sort of repair on the turbopumps.

IV.6.a.4 Manifold Turbomolecular Pump

The small Alcatel ATH 201 H turbomolecular pump on the gas manifold has magnetic bearings, so it doesn't need its oil changed. It does occasionally need to have its bearings replaced when the fail: this failure is likely to be accelerated if you regularly run too much gas through it at once (forcing it to slow down) while pumping out the manifold, and can happen catastrophically if a very large amount of gas is allowed into it. If the bearings fail, you need to send the pump in to Alcatel to have them replaced. One unusual feature of this pump is that it needs to be "run in". When you start the pump controller, it will offer you two running-in programs. Program 1 is only used immediately after a bearing replacement and takes about twenty hours. Program 2 is used when the pump has been turned off for an extended period and takes about 2-1/2 hours.

IV.6.b Mechanical Pump Repairs

IV.6.b.1 Overview

All of the high vacuum pumps in lab, except of course the ion pumps, are backed by Alcatel mechanical pumps of various models, meaning that we have a lot of mechanical pumps. We try to maintain them ourselves with as little outside help as possible. Hence, we rebuild them to clean them and to replace broken components and old seals. It is worth noting that although the metal parts from two pumps of the same model should be interchangeable, in general they are not. If you intermix the metal parts from two same-model pumps, you will often get two pumps that don't fit together or jam, so it is best to keep the parts of a given pump together. The art of pump repair is really the subject for a manual of its own, and is beyond the scope of this one. However, there are some basic points worth covering here.

A number of different types of mechanical pumps are used in the lab, as follows:

- Alcatel 2020CP corrosion-proof pump is used on the gas manifold.
- Alcatel 2033 pumps are used on the main chamber, second stage, and first B.
- Alcatel 2033CP corrosion-proof pump is used on first A.
- Alcatel 2063 pumps are currently not used on the Scattering Machine.
- Alcatel 2063CP corrosion-proof pumps are used on source A and source B.
- Alcatel 2010SD pumps are used on the outer seals and to back the lid turbomolecular pumps.

IV.6.b.2 Oil Changes

Most of the mechanical pumps on the Big Machine are standard pumps interchangeable with the pumps used on the Little Machine. These pumps: the two Alcatel 2010 SDs on the first stage seals and the detector box and the three Alcatel 2033s on the main chamber, second stage, and first B, use the same pump oil as the Little Machine pumps: LDS-19, purchased from LDS Vacuum in Florida.

However, due to the fact that they see higher fluorine fluxes, we use corrosion-resistant pumps on source A and source B′(Alcatel 2063CPs), first A (an Alcatel 2033CP), and the gas manifold (an Alcatel 2020CP, previously an Alcatel 2012CP). These pumps are distinguishable by the black (rather than orange) paint on their oil casings, and they should not be replaced with non-CP pumps as long as the Machine is still using fluorine. The CP pumps use a corrosion-resistant pump oil called MT Technical White, purchased from a company called Specialty Fluids in California. This oil is not a fluorinated oil, it's just higher purity mineral oil, so the problems with mixing regular mineral oil and fluorinated oils doesn't apply. (Actually, it is not entirely clear to me how much benefit we get from using this special oil, and whether it's worth the cost difference.)

The oil-change procedure is fairly intuitive. Close the foreline for the pump you're changing the oil on after having turned off whatever it's backing (with a cool-down period if needed). Then turn off the mechanical pump and vent the foreline with the vent pin on the machine side of the wall. Remove the QF flange connections to the pump's inlet and outlet, and let the pump cool to near room temperature, possibly with the aid of a box fan. Tilt the pump forward with a wooden block---you may need a second person to help you do this, particularly with the 2063s---and open the oil inlet and oil outlet to drain the oil into a tub for disposal. Once the pump is fully drained, you can close the oil outlet and refill it.

Pump oil should be checked and changed if needed every three months. Also, if the oil in the sight glass starts to look yellow, the pump needs an oil change. The CP pumps in particular tend to go through oil faster than you'd expect, and if you delay an oil change too long it will turn into a horrible black gum that's almost impossible to clean out, so you should probably err on the side of checking and changing the oil more frequently.

IV.6.b.3 Using Flushing Oil

Cleaning a pump that has become gummed up with badly contaminated oil requires a complete rebuild. However, if the oil in a pump has not gotten bad enough to require this, but is in worse shape than after an ordinary oil change, it can be worthwhile to clean out the pump with flushing oil. This flush may also be done as a final step after rebuilding and hand-cleaning a badly gummed-up pump to get rid of any last residue of the contaminated oil.

To use flushing oil (we use TKO-FF from Kurt Lesker), first drain the old oil in the pump. Then fill the pump with flushing oil—we use the same flushing oil for both CP and non-CP pumps—and blank off the pump intake while opening the gas ballast to allow air into the pump to create bubbles that will help with cleaning. Run the pump for half an hour before draining the flushing oil, closing the gas ballast, and adding fresh operating oil. If possible, have the pump's exhaust connected to an exhaust line: otherwise, large quantities of vaporized oil will be released in the pump room and no one should be in the room while the pump is running.

IV.6.b.4 Maintaining the Foreline Traps

Since the Big Machine uses corrosive gases, such as F_2 and XeF_2, their foreline traps need to be able to neutralize these gases before they reach the mechanical pumps (where they damage seals and foul the oil) and escape into the atmosphere, as well as the usual function as foreline traps to keep mechanical pump oil from back-streaming into high vacuum components. To this end, we use a 50/50 mixture of soda lime and molecular sieves in the traps. Since the soda lime dust is caustic, the traps should only be opened, emptied, and filled in the fume hood, and of course the used sieves and soda lime are hazardous waste.

The molecular sieves and soda lime should be baked out overnight at over 100°C before use to drive water off. Be sure to use a glass beaker for this; plastic ones will melt.

It is wise to check the traps whenever you change the oil in a pump; you certainly should do so if the pump turns out to need a rebuild. The main problem the traps seem to suffer from is the buildup of back-streamed oil on the sieves and soda lime. This buildup reduces the effectiveness of the sieves and soda lime and can clog the mesh that holds them in place. If oil build up and clogging of the traps are observed, the best solution is usually washing and scrubbing the traps with water and soap and then rinsing with acetone.

IV.6.b.5 Motor Removal and Repairs

The easiest disassembly step---it doesn't even require draining the oil---for the Alcatel 2033, 2033CP, 2063, and 2063CP pumps is to undo the four bolts holding in the motor and slide it off. This maneuver should be done by two people, one supporting the motor and one undoing the bolts, but it can be done by one in a pinch. Note that the motors on Alcatel 2012CP and Alcatel 2020CP pumps are not attached in the same way: a single set of long bolts holds both the oil casing and the motor for those pumps, so you can't remove one without the other, and you need to be sure to drain the oil before taking the motor off. As for the Alcatel 2010 SD pumps, these are fancier, more modern pumps and are unfortunately designed so you can't easily disassemble them.

One of the easiest things to replace on a mechanical pump is the rubber coupler—called the "spider"—between the motor coupling and the pump fan coupling. It should be replaced if it seems worn down or if it lacks elasticity. If a pump is making a loud clanging sound while running, the spider should be replaced immediately, because the metal couplings are starting to wear against each other and will eventually destroy each other. If this does happen, you can replace both of them yourself, though the motor-side coupling requires a special technique that I believe only Chris Leon currently knows.

IV.6.b.6 Pump Rebuilding

Sometimes, due to a leak or due to really badly gummed-up innards that need to be cleaned by hand, you need to disassemble and rebuild a pump. We have manuals for the 2020, 2033, and 2063 pumps and generally keep rebuild kits for them in stock. (If you use the last one, be sure to replace it.) There are both minor rebuild kits, which just have replacements for single-use seals---often enough to fix a small leak---and major rebuild kits, with replacements for all but the major pieces of the pump, which you need for seriously chewed-up or gummed-up pump parts, since only the metal parts and the vanes can be cleaned with acetone safely. It's also important to keep track of whether a rebuild kit is for CP or non-CP pumps, as the non-metal components are non-interchangeable.

When the pump parts get horribly gross with grime, one way to clean them is with a toothbrush and Crest "Baking Soda & Peroxide Whitening" toothpaste. If you do this, though, you need to clean the toothpaste off immediately and acetone off the parts, because they will rust if left wet with an aqueous solution.

IV.6.b.7 Alcatel 2012CP+ and 2020CP

The manifold mechanical pump used to be an Alcatel 2012CP+, but is currently an Alcatel 2020CP. The Alcatel 2012CP+ has three distinct bushings. We have most recently ordered replacements from Capitol Vacuum Supplies.

- Central Housing bushing P/N 052637 (Capitol Vacuum P/N A0507) (about 0.37 in long)
- End Plate bushing, Alcatel P/N 052649 (Capitol Vacuum P/N A0508) (about 0.54 in long)
- Intermediate Plate bushing P/N 052651 (Capitol Vacuum P/N A0509) (about 0.75 in long)

These are carbon bushings that must be pressed into the plate, than reamed to size. The final inner diameter should be 15.000 ± 0.018 mm. It should also be noted that the MIT Central Machine shop and I think that Capitol Vacuum may have transposed where A0507 and A0508 go in the pump and that A0507 is actually the end plate bushing and A0508 is the central housing bushing, as they seem to fit into these positions better..

I don't recall whether the Alcatel 2012CP+ bushings are interchangeable with the 2020CP bushings, but they likely are. However, in any case, we've had bad luck with replacing these bushings ourselves, as the alignment is critical and the machine shop usually gets it just off enough for the bushings to shatter and then the pieces to grind away at other surfaces in the pump. I recommend sending the pumps to Eastern Scientific for rebushing if needed.

Unlike the 2033 and 2063 pumps, the fan in Alcatel 2012CP+ and 2020CP pumps is not removed by levering it out with bolts screwed in tapped holes in it. Instead, there is a set screw holding it in place that can only be accessed by removing the plastic base plate of the pump and rotating the fan until the set screw is visible through the bottom of the pump. Then you need a long enough Allen wrench to reach the screw.

IV.6.b.8 Alcatel 2033

The main chamber, second stage, and first B use Alcatel 2033 mechanical pumps. These have four brass bushings, large ones on the central housing and the end plate and a pair of short ones on the intermediate plate between the two stators. They have most recently been ordered from Capitol Vacuum Supply. These bushings need to be reamed to size after installation. The final inner diameter should be 20.000 mm.

- short bushings, Alcatel P/N 082905 (Capitol Vacuum P/N A0503), measured OD 0.911", measured ID 0.748", measured length 0.355"
- long bushings, Alcatel P/N 082906 (Capitol Vacuum P/N A0504), measured OD 0.911", measured ID 0.748", measured length 0.592"

IV.6.b.9 Alcatel 2033CP

The corrosion-resistant 2033CP and 2063CP pumps use carbon bushings instead of brass bushings: large ones on the central housing and the end plate and a pair of short ones on the intermediate plate between the two stators. They have most recently been ordered from Capitol Vacuum Supply and need to be reamed in the same way as non-corrosion-resistant bushings. However, past issues with carbon bushings cracking on reaming or use suggests it may be better not to try to rebush these pumps ourselves.

- short bushings, Alcatel P/N unknown (Capitol Vacuum P/N A0505), measured OD 0.911", measured ID 0.748", measured length 0.355"
- long bushings, Alcatel P/N unknown (Capitol Vacuum P/N A0506), measured OD 0.911", measured ID 0.748", measured length 0.592"

IV.6.c Diffusion Pump Water Line Repairs

IV.6.c.1 Turning Off Cooling Water

Although the water for cooling the diffusion pumps runs through a series of filters before going to the Big Machine's water manifold, the water cooling lines for the diffusion pumps still do manage to clog up after some time, which results in decreased flow and the pump interlocks shutting off the pumps. When this occurs, it becomes necessary to clean out the water flow meters and water lines. Before any of the following three procedures can be carried out, you need to turn off and cool the diffusion pump and turn off the water:

- First, turn off the pump in question. If it's already being interlocked off, turn it off with the switch anyway: you do not want a diffusion pump running without coolant. (If the pump in question is the second stage or main chamber diffusion pump, close the gate valve and turn off the LN$_2$ as appropriate.)
- Wait ninety minutes or so with a fan blowing over the pump. You're waiting until the pump feels room temperature or only slightly warm to the touch, even at the very bottom where the heaters are.
- Once the pump is cool, you'll want to turn off the water flow to that pump, using the valves on the Big Machine water line manifolds located under the side of the machine along the side facing the wall. Depending on the pump, these can be reached either by reaching down from the platform or from underneath the machine. You need to turn off the supply first, then wait ten seconds and turn off the return.
- Once repairs are done, you should turn the return on, then wait ten seconds and turn on the supply. If the water line now works and nothing is leaking, you can then turn on the

diffusion pump immediately. (Don't open gate valves or turn on the liquid nitrogen until the pump is up to temperature, of course.)

Also, it is useful to make a note of how the inputs and outputs for the water lines go. On the water manifold, the upper pipe is for water return; the lower pipe is for water supply. This can easily be determined by temperature: the return should be much warmer to the touch. On the diffusion pumps, the supply connects to the top of the pump where it connects to the chamber and the return connects to the end of the foreline after having just passed the base of the pump. This positioning of the water input and output is important because the top of the pump needs to be cooled as much as possible to condense oil and keep it from making its way into the chamber.

IV.6.c.2 Water Meter Cleaning

When a particular water sensor starts to trip regularly, the first course of action is to try to clean out the sensor itself. Often, gunk collecting inside it will slow the flow of water to below the rate that the sensor expects. The gunk can clog the water line as well, but since cleaning out the water meter is easier, it's a good first step.

Before disassembling a water meter, make sure you've turned off the DP in question and, once it has reached room temperature, the water line in question. Then, unscrew the six screws holding the face plate in, making sure that you keep track of the orientation of the plate and don't lose the o-ring. Although the plate looks like it fits correctly if you rotate it by a half-turn, it turns out that it doesn't make a good seal and will leak water in this position, so making sure you reinstall it in the same orientation you removed it is important.

You'll want to scrape off any gunk that's accumulated on the faceplate itself and on the magnetic wheel inside the sensor, as well as on the inside of the sensor chamber. Note that the faceplate and o-ring will dissolve in acetone, so you should only use water or—if really necessary—isopropanol to clean them. You can also use a length of wire to clean out gunk that has accumulated in the entrance and exit spigots of the water meter.

At this point, you should generally reassemble the meter and test it. If problems persist, you'll want to proceed to cleaning out the water lines. However, in some really bad cases, you may find that the water meter is such a mess that you need to completely disassemble it and use a sonicator (ultrasonic cleaner) and soapy water to get it clean. If you need to do so, you should remove the pipe fittings on the top and bottom of the meter and clean them as well, and remove the brass sensor chamber from the black plastic electronics casing behind it. (It does come completely off, though there are a number of screws to undo.)

IV.6.c.3 Water Line Cleaning

Unsurprisingly, cleaning out the water lines also requires turning off the diffusion pump in question and water flow to that pump. Once you've done so, you can loosen the hose clamps holding the water lines to the supply and return spigot nozzles and pry the hoses off the spigot nozzles. You may need to use a razor blade to slit the end of the hose to do this if it's wedged on too hard; if you do so, be sure to cut off the split portion of hose immediately, so that you don't try reconnecting it and make a leaky connection. Make sure to have a bucket—I recommend a Styrofoam ℓN_2 bucket—on hand to catch the water that will come out of the hose as soon as it's removed. (Note that the main chamber and second stage water lines are copper tubes; to clean these remove the relevant Swagelok connectors and treat them similarly.)

Once the hoses are removed, you'll need a second person's help. (Do not try to do this on your own; it may seem possible but will end with you soaked in filthy water.) One person should use a nitrogen gas cylinder with the spray nozzle attached to the regulator hose to blow air through one end of the hose at 80 psi to 100 psi while the other person should hold the other end of the hose in the bucket. The usual procedure is to first blow air through the hose backwards (from return to supply) until water stops coming through, and then blow air through in the opposite direction.

After you've blown air through the hose, you can reattach everything. However, if you want to be thorough, an additional step is to attach the return end of the hose to the supply spigot nozzle and run water through the water line backwards into a bucket. This procedure often dislodges gunk that won't be dislodged by forward water flow or by blown air. Once you've done this, detach the return end of the hose and repeat the air-blowing procedure.

A particularly advanced and difficult technique is to remove the hoses from the copper tubing on the diffusion pump ends and to run a bit of vinegar through the water lines on the pumps themselves to try to dissolve accumulation on the insides of these lines. However, this is very rarely needed—it's been done once in the five years I have been in the lab—and it's not clear to me that it makes much difference.

IV.6.c.4 Water Meter Calibration

If you've cleaned out the water lines and it's clear that water is flowing fast enough, but tripping persists, the problem may be with the meter electronics. Before replacing the meter, the first thing you may want to check is whether the meter is set to be overly sensitive. The main risk is that you don't want to set the sensitivity too low, since it does need to trip if the water flow is insufficient for cooling. The needed flow rate is different depending on the pump size:

- 400 mm pump (source A) — 0.40 gal/min (80 L/hr)
- 10" pump (source B) — 0.40 gal/min (80 L/hr)
- 250 mm pump (main chamber) — 0.25 gal/min (50 L/hr)
- 6" pump (first A, first B, and second stage) — 0.25 gal/min (50 L/hr)

To change the sensitivity setting on the water meter, you need to use a screwdriver to turn a recessed potentiometer in the back of the meter. Since the potentiometers don't display their settings, you'll want to check the manual or spec sheet for the meter you're adjusting to figure out where in the potentiometer's range the desired flow rate should be. If it becomes necessary to purchase a new meter, select one with the desired flow rate at 50%-60% of the range of flow rates it can measure.

IV.6.d Diffusion Pump ℓN_2 Trap Repairs

IV.6.d.1 Thawing the Traps

The main chamber and second stage diffusion pumps are topped by ℓN_2 traps. These are intended to trap diffusion pump oil to keep it from getting into the chambers. Thermistor sensors in the traps trigger automatic trap fills when the ℓN_2 level gets too low and, if the ℓN_2 level fails to be raised (for example, if the tank has run out), triggers the relevant diffusion pump's interlock to turn off the diffusion pump and close the gate valve.

One common cause of high main chamber pressure, and especially of a large pressure rise soon before the trap fills, is a build-up of water or Ar frozen onto the trap. These tend to come off the trap and contaminate the main chamber every time the ℓN_2 level in the trap gets low. This nuisance can be corrected by thawing the trap:

- Begin when a trap fill is expected soon, but before there has been a large pressure rise.
- Close the main chamber gate valve, leaving the diffusion pump on.
- Turn off the ℓN_2 fill sensor for the main chamber trap, so that the ℓN_2 level can fall below the sensor setting without triggering a fill.
- Wait until the trap is nearly empty, but do not allow it to empty completely. You can monitor its temperature by watching the ice build-up on the trap inlet--you want to wait until much of it—but not all of it—has melted. This procedure will likely take around an hour.
- Turn the fill sensor back on, triggering a fill.
- Once the trap is filled, open the gate valve.

If this procedure is ineffective or you want to do a more thorough job, you can thaw the trap completely. The procedure for a complete thaw is similar to the above procedure, but with two changes. First, while waiting for the trap to thaw, you can use the house vacuum line to remove the ℓN_2 faster. Once the trap has completely thawed, you need to be sure that there is no water in it before you fill again: otherwise freezing water may produce cracks in the trap. To do this, you should wait at least half an hour after all of the ice on the inlet has melted and blow dry N_2 through the trap for five minutes to ensure that it is dry.

IV.6.d.2 Replacing the ℓN_2 Fill Line

There is a flexible metal hose connecting the ℓN_2 tank fitting to the copper tubes on the base of the main chamber that take ℓN_2 to the traps. This hose is manufactured by Swagelok, and is part number SS-FL8TA8-36. As of February 2011, it cost ~\$160.

IV.6.d.3 Replacing the ℓN_2 Level Sensor

The ℓN_2 traps are filled automatically by two control boxes that monitor the ℓN_2 level in the traps and open solenoids to allow more ℓN_2 in when the traps are close to empty. The most common failure mode for these control boxes is a failure of the thermistor used to sense the ℓN_2 level. When the sensor fails, the control box will believe the trap is full even if the sensor is at room temperature or higher. (The same effect happens if the sensor line is completely removed: the box's internal logic interprets any resistance above 8 kΩ, including an open loop, as "cold", and any resistance lower than 8 kΩ as "warm".)

In the past, special ℓN_2-rated thermistors were used for the sensor. However, it's recently been found that more standard thermistors, rated down to only -80°C work as well. This replacement is fortunate, since it seems to no longer be possible to obtain replacements for the original ℓN_2-rated thermistors. In addition, these thermistors are much cheaper (about \$10 each) and can be found in stock at Newark.

The original thermistors had a resistance of 136 Ω at 300 K and 2.6 MΩ at 77 K. This implies a thermistor constant of B = 939 K, and a fill-triggering temperature of 130 K, where B is the thermistor constant, $((T \cdot T_{300K})/(T_{300K} - T)) \cdot ln(R/R_{300K})$.

The first attempt at a replacement thermistor was Newark catalog number 52F3328, an NTC thermistor with a room temperature resistance of 5 kΩ, an unknown thermistor constant B, and a claimed minimum operating temperature of -80°C. This thermistor worked somewhat, but had too high of a switch-over temperature, allowing the trap to get too low and resulting in a less-clean chamber. More recently we purchased EPCOS B57237S109M (Newark catalog number 30C7938) NTC thermistors, which have a room temperature resistance of 1 Ω and a thermistor constant of B = 2700 K. These thermistors should have a resistance of 8 kΩ—and so trigger a fill—at 150 K, and have worked quite well for several years without replacement. The thermistor can just be soldered to the end of the sensor line, with heat-shrink used to cover the leads.

IV.6.d.4 Replacing the ℓN_2 Controller Lamps

The ℓN_2 controllers have status lamps that use very unusual light bulbs. The bulbs in question are called "telephone slide" connectors. We use Multicorp 120PSB lamps from Newark. If you're ordering new ones, be sure to get the same length of bulb as the one you're replacing: we have a number of too-long bulbs someone ordered that don't fit anywhere.

IV.6.d.5 ℓN_2 Delivery Tubes

The ℓN_2 delivery tubes for the Big Machine were historically just the standard 3/8" OD copper tubing that we use in lab for a variety of purposes. However, several years ago, Chris Leon replaced the copper ℓN_2 delivery tubing on the Little Machine with 3/8 in OD stainless steel tubing with a 0.035 wall and reported that he was able to nearly halve his nitrogen consumption. The presumed reason for the decreased nitrogen usage is that, since stainless steel is a much worse thermal conductor than copper, the tubing is a much less effective pathway for heat to get into the trap and boil off nitrogen. In December 2014, I decided to replace the tubing on the Big Machine as well. I used 3/8 in OD stainless steel tubing with a 0.035 wall. It is not yet evident how much of a savings in ℓN_2 consumption has been produced. It's probably not possible to use a thinner-walled tube, though: I originally tried with the next thickness down, 0.010 in wall, and found that the tubing crumpled when I attempted to bend it with a tubing bender.

IV.6.e Diffusion Pump Oil Changes and Cleaning

Unlike mechanical pumps and turbomolecular pumps, diffusion pumps do not need regular, frequent oil changes. However, if the oil becomes contaminated or burnt (such as due to a cooling or backing pump failure), it may be necessary to change the oil or even to disassemble the pump for a full cleaning. If this becomes necessary, the pump manual should be consulted for details. The main chamber pump uses polyphenyl ether oil, source A uses DC 704 oil, and source B uses DC 705 oil.

If a full disassembly and cleaning becomes necessary, it may be useful to consult with the little machine group, since they have recently had to disassemble and clean several of their diffusion pumps. Once the pump is disassembled, it can be cleaned by scouring with steel wool and grill cleaning fluid to remove carbon buildup.

IV.6.f Ion Pump Repairs

IV.6.f.1 Baking Out Ion Pumps

If the ion pump pressures are consistently too high and the pumps are struggling, you can bake them out by wrapping them with several heating tapes and running the tapes (whose total resistance should be above 11 Ω) with a 60 V variac while the pump is on and has its entrance valve open. The whole pump should be covered in aluminum foil to trap heat during this process.

IV.6.f.2 Dealing with Shorts

When an ion pump won't start at all, one possible cause is the presence of internal shorts. Metal whiskers can grow on the grids, shorting them to ground. It is often possible to remove these while the pump is under vacuum by striking the sides sharply with a rubber mallet. If this doesn't work, you'll need to vent and open the pump to clean it out.

IV.6.f.3 Cleaning Ion Pumps

If the above solutions don't seem to help, a more involved option is to vent the ion pump and clean it out.

- Make sure that the pump is disconnected from its power line before you consider disassembling it.
- Make sure you're not wearing a watch or magnetic jewelry or carrying cards with magnetic strips on them, as the body of the ion pump contains powerful permanent magnets. You'll also want to be careful not to pinch yourself between the tools you're using and the magnets.
- Remove the top flange of the pump. You will now see an open area with metal strips connecting the two grids to the power line feed through. You'll need to unbolt the connections of these strips, and unbolt the grids from the pump body, to pull them out of their

chambers on the sides of the pump. While doing this, be careful of the fact that the screws and nuts—and the tools you're using—will be strongly drawn to the magnets.

- Once the grids are removed, both the grids and the interior of the pump should be cleaned by alternately blowing dry nitrogen gas and cleaning with Kimwipes and acetone. You should continue until there are no visible metal whiskers, and until the Kimwipes come back looking clean.
- Reassemble everything and reseal the pump using a new copper gasket.

IV.7 Other Repairs and Maintenance

IV.7.a Main Water Manifold

IV.7.a.1 Changing the Water Supply

The diffusion pumps, lid turbopumps, and chopper motor are water-cooled. There is a large water manifold along the wall of 2-115 next to the fume hood. This manifold filters water from the building water mains and sends it off to the Machines. A schematic of this manifold can be found on page 169 of Michael Blair's MS thesis.[9] This section discusses maintenance at this manifold; for maintenance of the Scattering Machine's water lines, see the sections on the relevant water-cooled components.

There are three water supply lines that run to the water manifold: Building 6 process (non-potable) water, Building 2 process (non-potable) water, and Building 6 potable water. Both Machines are, in theory, supposed to be running on process water, and there are direct connections from the Building 2 process water to the Big Machine manifold and from the Building 6 process water to the Little Machine manifold. A third water supply line, of Building 6 potable water, runs just below both manifolds. There are valves that can be closed to separate the Machines' manifolds from their usual process water lines. On the manifold sides of these valves are hose connection valves allowing the manifold to be connected to the other manifold or to one of the two hose connection valves on the Building 6 potable water line. Hence, assuming sufficient water pressure, both Machines can be run off any one of the three lines. Alternatively, one Machine can run off its default line while the other runs off Building 6 potable water, or both Machines can run off their default lines.

At present, both Machines are being run off Building 6 potable water because of high temperature and low pressure (the pre-filter pressure should be above 60 psi) on the process lines. Changing the water supply for one or both Machines is simply a matter of opening and closing valves and possibly changing the relevant hose connections. You may be able to do this without an interruption to the water supply. However, it is important to never have either manifold open to both a potable and a process line at the same time, because doing so may contaminate the drinking water with non-potable process water.

IV.7.a.2 Changing Water Filters

Whatever its source, the cooling water runs through three filters in series before going to the Machines. There are two rows of filters, each with three filters. The upper row goes to the Big Machine, and can be bypassed by opening a valve to a bypass line. There are also valves just before and after the filters, allowing them to be isolated from the water line for changing. (The lower row goes to the Little Machine, and is essentially equivalent in functioning.) The filter manufacturer recommends changing the filters at least once every six months; Sylvia thinks they ought to be changed every three months to be safe. The three filters should be of decreasing pore size: 50 microns, 25 microns, and 5 microns. Currently, we're using filters made by 3M and marketed as Aqua-Pure models AP814, AP811, and AP810, respectively. The procedure for changing the filters is as follows:

- Isolate the Scattering Machine filter manifold by closing the valves both before and after it. If you are running any pumps that need cooling, you'll want to open the bypass valve before doing this.
- Use the filter wrench to loosen the blue filter holder--which is screwed into the white filter-holder lid built into the manifold--to hand tightness. The filter wrench is a circular loop with four teeth on a stick; it looks rather like a child's bubble-blower. We have two: one made of

black plastic and a longer-armed one made of steel. Either may be used to loosen the filters, but only the plastic one should be used to tighten them to avoid over-tightening.

- While holding a bucket under the filter holder, finish unscrewing it, being prepared for the fact that it is full of water and quite heavy.
- Pour the water in the filter-holder down a sink drain and remove the old filter. Then, with paper towels, wipe clean the filter holder and filter-holder lid as necessary.
- Repeat with the second and third filter holders before reinstalling any of them, since the ones in the front block access to the ones in the rear.
- Starting at the rear with the 5 micron filter, put a new filter in each filter-holder and screw it back into place, tightening with the filter wrench and being sure not to over-tighten.
- Reopen the valves isolating the filter manifold. Once water has begun to flow, depress the red button on the top of each filter-holder lid until water begins to run out of it. This procedure allows the air trapped in the filter holders to escape.
- If you opened the bypass valve, be sure to close it to stop the flow of unfiltered water to the Machine.

IV.7.b Leak-Checking

IV.7.b.1 Procedure for Using Alcatel Leak-Checker

The lab has a semi-portable Alcatel leak checker for testing individual components. It consists of a mechanical pump and a turbomolecular pump that produce a good enough vacuum to allow a built-in mass spectrometer set to 4 AMU to run. Since the English directions are rather incomprehensible, I'm including the procedure for using it here, along with some tips for leak-checking. This procedure is mostly empirically determined, but it seems to work. Note that the main knob on the front of the leak-checker is broken off, so you need an adjustable wrench to turn it. It is "pointing" in the direction of the flattened side.

- Attach the item to be tested to the inlet, and make sure that the main knob is pointing to "0".
- Press the green button on the right side to turn on the mechanical pump. Then turn the main knob to "1" to rough out the system with the mechanical pump.
- Once the pressure gauge in the upper-left corner of the main box has fallen to a minimum reading, turn the main knob to "2". This action isolates the inlet and turns on the turbo pump to pump down the mass spec chamber. Initially a yellow light on the right side of the main box should turn on, indicating that the turbo is speeding up.
- Once the yellow light switches to green, the turbomolecular pump is at speed. At this point, you can try to turn on the filament by flipping the switch just below the three green status lights on the filament box. Watch the ion gauge on the right side of the filament box while doing this. The needle should jump to the red and then quickly fall back before starting to rise again due to out-gassing. It is okay for the needle to be slightly in the red, but you don't want it to get all the way to 10^{-3} Torr (the far right edge of the gauge). You may need to turn

it off to let the mass spec pump down a little several times to get to a point where you can leave it on.

- Once the ion gauge is consistently in the green, you can very slowly start to open valve “3”, opening the inlet to the turbomolecular pump. Do this very slowly, as the pressure is likely to rise quickly, and don't worry if you're unable to get the valve all the way open.
- When valve “3” is as open as you think you'll be able to get it, turn off the filament and then close the valve. Then turn the main knob to “4”, creating a direct connection between the inlet and the mass spec. (The inlet is still closed as long as valve “3” is closed, though.) You should be able to turn on the filament immediately now.
- Once the filament is on, slowly open valve “3” again. Once it is all the way open, you are ready to begin leak-checking, assuming the helium signal (the gauge on the left of the filament box) is stable.

IV.7.b.2 Leak-Checking Using the Mass Spectrometers

The main chamber and detector box can both be leak-checked using their mass spectrometers. A preliminary check can be done simply by taking a background mass spectrum and comparing the peaks at mass 28 (N_2 and CO) and mass 32 (O_2), as well as the peaks at mass 12 (C) and mass 14 (N). In non-leaky chamber, mass 12 should dominate mass 14 and mass 28 should be at least twenty times mass 32. However, if there is a leak, the mass 14 signal is likely to exceed that of mass 12 and the ratio of mass 28 to mass 32 will approach the four-to-one ratio of nitrogen to oxygen in air.

If you do have a leak, you’ll need to use the “MASSSET4” program to monitor the number of counts at mass 4 while you supply helium to potential leak sites. In order to do so, you'll want to use the background mass spectrum to calculate the expected setting for mass 4: the relation between the actual masses and reported masses should be linear.

IV.7.b.3 Tips for Leak-Checking

It is surprising how well o-ring seals work at stopping helium. You can often get away with leak-checking something near an o-ring without serious interference from the o-ring. But if you do see signal through the o-ring, putting masking tape over the joint generally fixes the problem.

Be aware that the Scattering Machine is quite capable of having impressive virtual leaks in the seals when you first pump down, especially if the seals ion pumps aren't working well or need to be baked out. A leak through the seals may be the explanation for an apparent leak that you can't find anywhere. Also, if the detector box is vented, leakage through the beam valve can look like an air leak.

IV.7.c Dealing with RF Noise

IV.7.c.1 Distinguishing RF and Dark Current Noise

One common problem with mass spectrometer data collection, especially on the detector box mass spec, is RF noise getting picked up by the signal cables. The quadrupole RF power is the presumed source of this noise, but it's made worse by problems with poorly insulated and shielded signal cables.

There are several possible sources of noise that one might observe in the mass spectrometer signal. One is dark current: spurious counts produced by the detector channeltron itself, due to cosmic ray hits or other random excitations. Another is the RF noise from the quadrupole, which can be reduced by better grounding and shielding of cables.

One way to distinguish between the two types of noise is by using a oscilloscope to look at the shape of the noise: dark current noise should theoretically have the same pulse shape as a real count, and only occur when the channeltron high voltage is turned on, while RF noise should not. Another solution is to look at the time distribution of the noise. To do this, collect count rate as a function of time, and make a histogram of the amount of time spent at each count rate. Dark current noise should have a Poisson distribution on this histogram, while random RF noise should not.

IV.7.c.2 Elimination of RF Noise

RF noise can usually be reduced or eliminated by doing a better job of shielding the signal cables, and especially by making sure that the built-in shielding on the signal cables is in good shape. Quality of the shielding seems to matter more than length of cable or other factors. It's worth checking the internal shielding on coaxial cables: it's important that the shielding be well-connected to the outer part of the BNC connector so that the shielding is grounded and kept further from the inner conductor. (Since the issue here is RF noise, we have to be concerned about surface effects.)

A related issue is the presence of ground loops. While it is important that shielding be grounded, you need to be careful to ensure that there is only a single path to ground: the circuit diagram for all grounded components should look like a star, without any closed loops. A single path to ground is important, because temporary voltage differences (sometimes induced by RF signal in the first place) can set up currents in the ground if it forms a closed loop, contributing to RF noise. Establishing a single path to ground and eliminating ground loops can be a particular issue when grounding the pulse-counting electronics for the detector box mass spectrometer.

IV.7.d Shiraki Etch Procedure for New Crystals

Once new crystals have been cut and ground as described in Hefty's thesis,[8] they need to undergo a surface etch as described by Ishizaka and Shiraki.[13] Performing this procedure requires having taken the EHS Office's hydrofluoric acid web training course and having calcium gluconate gel on hand. (We should always have it on hand because we have hydrofluoric acid and fluorine gas present in the lab.)

Step 1: Degreasing

- Rinse in overflowing deionized water for 10 min.
- Sonicate in methanol for 5 min twice.
- Boil in trichloroethylene bath for 15 min.
- Sonicate in methanol for 5 min twice.
- Rinse in overflowing deionized water for 10 min.

Step 2: Nitric Acid Boiling

- Boil in a 70% nitric acid bath for 10 min to etch Si surface and form an oxide layer.
- Dip in 2.5% HF solution for 10-15 sec to remove the oxide layer.
- Rinse in overflowing deionized water.
- If the surface does not dry uniformly, repeat Step 2. The paper suggests that Step 2 will need to be performed three to four times but, in January 2013, we found performing it twice to be sufficient.

Step 3: Ammonium Hydroxide Boiling

- Boil in a 1:1:3 solution of ammonium hydroxide: hydrogen peroxide: water for 10 min to form an oxide layer. Bring the ammonium hydroxide and water to temperature, then add the hydrogen peroxide just before the crystals. The addition of peroxide should result in significant bubbling: if it doesn't, you need fresher peroxide.

- Dip in 2.5% HF solution for 10-15 sec to remove the oxide layer.
- Rinse in overflowing deionized water.

Step 4: Hydrochloric Acid Boiling

- Boil in a 3:1:1 solution of hydrochloric acid: hydrogen peroxide: water for 10 min to form an oxide layer. As before, bring the hydrochloric acid and water to temperature, then add the hydrogen peroxide just before the crystals. As in Step 3, the addition of peroxide should result in significant bubbling.
- Rinse in overflowing deionized water for 10 min.
- Make sure that the surface becomes uniformly wet.

This procedure takes a day to go through once, so it's definitely worthwhile to perform it in large batches, after an initial test run of a couple crystals. You'll need to use the large pair of Teflon tweezers for both the nitric acid and hydrofluoric acid, since the smaller white plastic tweezers that we have several pairs of---while easier to use---aren't hydrofluoric or nitric acid safe.

For waste disposal, the EHS Office has clarified that if hydrofluoric acid is completely neutralized with sodium bicarbonate, the resulting solution is safe to be rinsed down drains. However, we should use pH paper to confirm that the solution is neutral before doing so. (Similarly, the base and acid baths can be disposed of down the drain once fully neutralized.)

IV.7.e Crystal Heating Power Supply

The Big Machine's silicon crystal is heated by resistive heating of the crystal while it is being cooled by a constant stream of ℓN_2 run through the manipulator to anneal the surface and for thermal desorption spectrometry (TDS) experiments. This heating is carried out from a base temperature of 100 K (achieved by ℓN_2 with no current) to 1200 K. It must be done relatively smoothly when annealing to avoid cracking the crystal via thermal shock, and it must be done very smoothly in TDS experiments to achieve a linear-in-time temperature ramp. Producing a linear temperature ramp is complicated by the fact that silicon is a semiconductor. At 100 K, the crystal's resistance is around 300 Ω. It increases linearly with temperature up to around 500 K, where the resistance is around 1300 Ω. At around 500 K, the thermal energy of the valence electrons is high enough to push them over the band gap into the conduction band, and the crystal very rapidly becomes a conductor, with a resistance of 50 Ω by 600 K and of less than 10 Ω above 700 K. (See Figure IV-11.)

Despite this variable resistance, we need to smoothly increase the power supplied to the crystal, $P = IV = V^2/R = IR^2$, to produce a smooth and linear temperature ramp. A linear temperature ramp requires a power supply that can function in two regimes: a high-resistance regime where high voltages are needed to provide small currents, and a low-resistance regime where much higher currents are provided by much smaller voltages. Furthermore, the power supply needs to be able to transition between these two modes smoothly and rapidly during heating. (See Figure IV-12.)

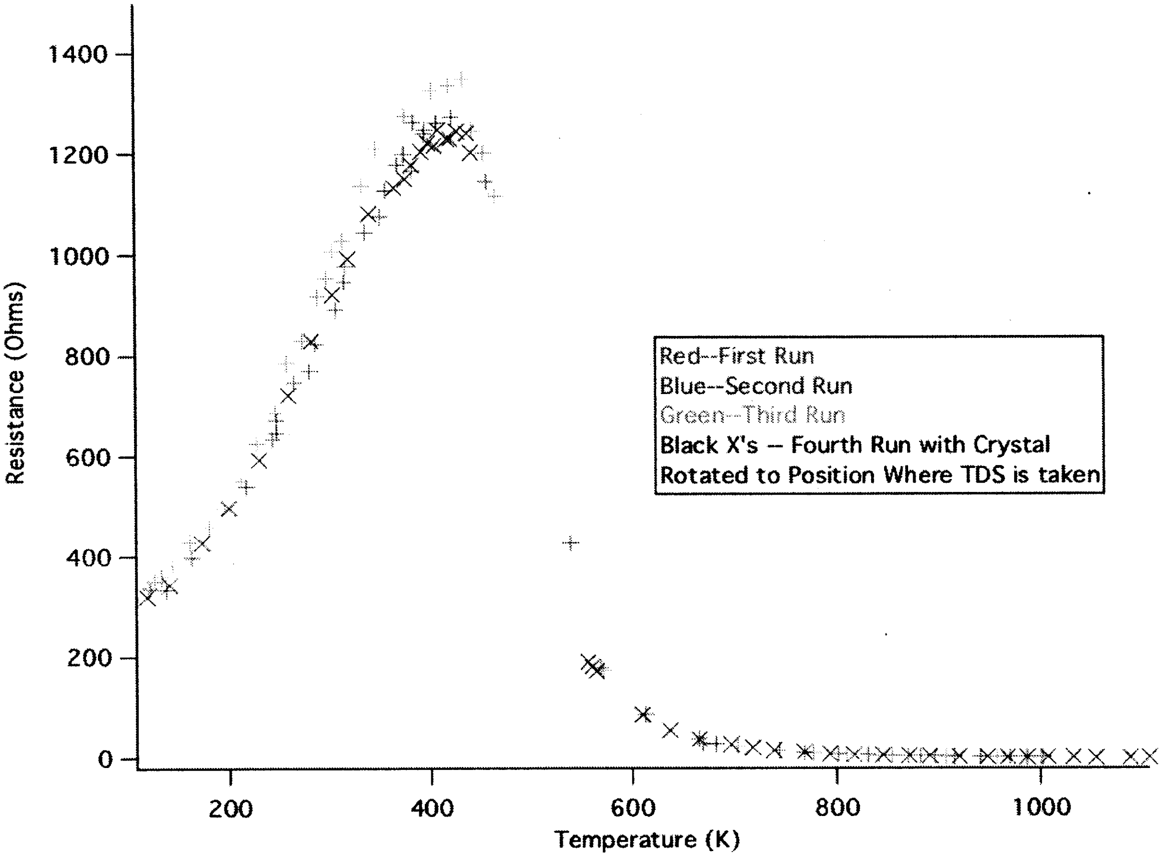

Figure IV-11: Crystal Resistance as a Function of Temperature

The resistance of the crystal as a function of temperature was measured by heating the crystal with an ammeter in the circuit and a voltmeter across the crystal and observing the voltage and current as the crystal temperature was held steady at increasing values. The crystal has been replaced since these measurements were taken, but similar behavior should hold true for all crystals as long as they are properly tightened into their tantalum clamps.

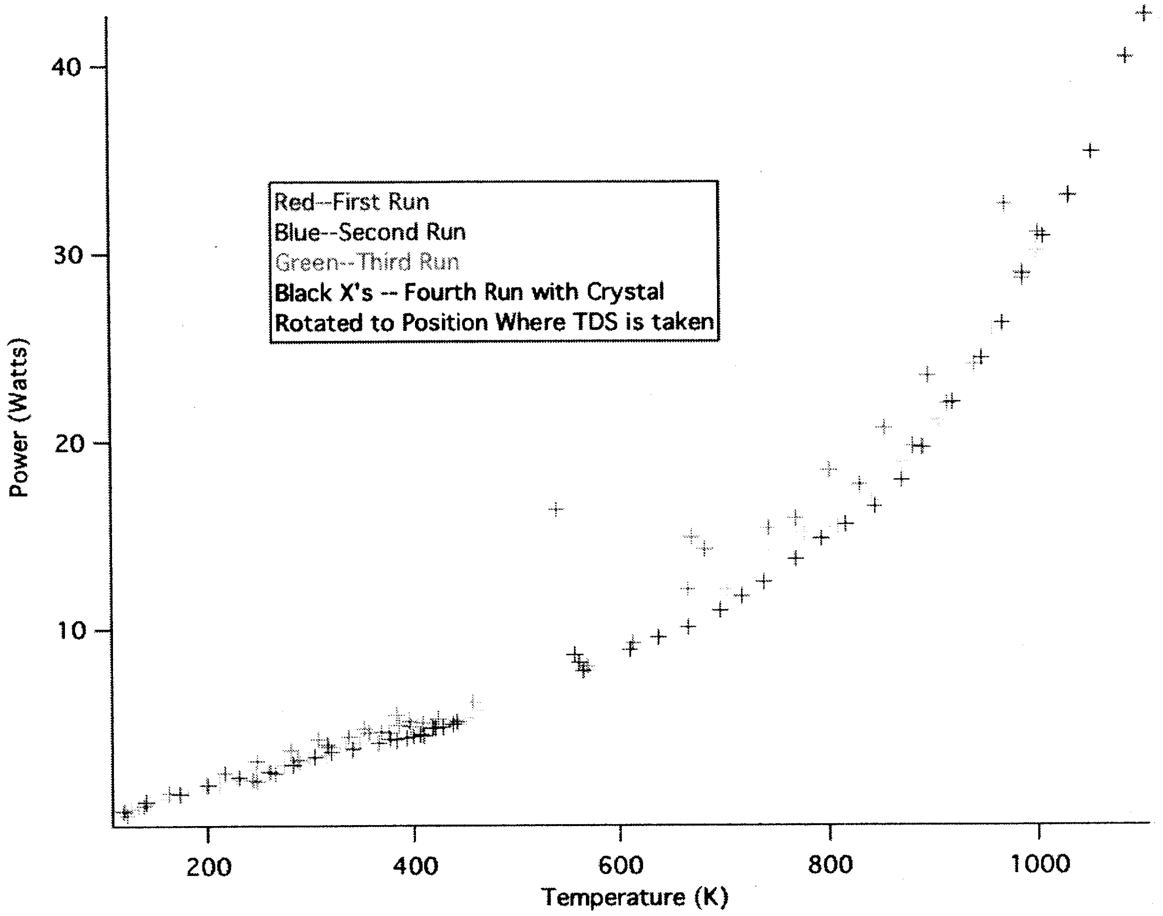

Figure IV-12: Power Needed to Heat Crystal as a Function of Temperature

The power needed to hold the crystal temperature steady as a function of temperature was measured by heating the crystal with an ammeter in the circuit and a voltmeter across the crystal and observing the voltage and current as the crystal temperature was held steady at increasing values.

The crystal heating power supply designed by Jae-Gook Lee and described in Mike Blair's thesis[9] failed in 2011. Repeated efforts to repair it over the course of about a year were unsuccessful and, in 2012, we received a long-term loan of a homebuilt power supply from David Pullman at San Diego State University. Like the Lee design, this power supply is based on Gladstone's original design. However, it uses insulated-gate bipolar transistors in place of the older 2N3055 NPN power transistors used in Gladstone's design.[1]

We have retained the PID controller that was used with Lee's power supply and continue to use it to control the temperature ramp for thermal desorption spectra. However, the separate PID controller that Gladstone provided is needed as well because, as well as PID circuits—which are not used—it contains an interlock to cut off the high voltage supply if the crystal temperature rises too high. (The circuit diagram for Gladstone's PID controller is shown in Figure IV-13; only the circuit labeled "High Voltage On-Off Control Circuit" is currently in use.) This interlock prevents the high voltage supply from remaining engaged when the crystal is in its high temperature, low-resistance regime, where supplying a high voltage would produce excessive current and melt the crystal.

PID Feedback Circuit for Controlling Crystal Temperature

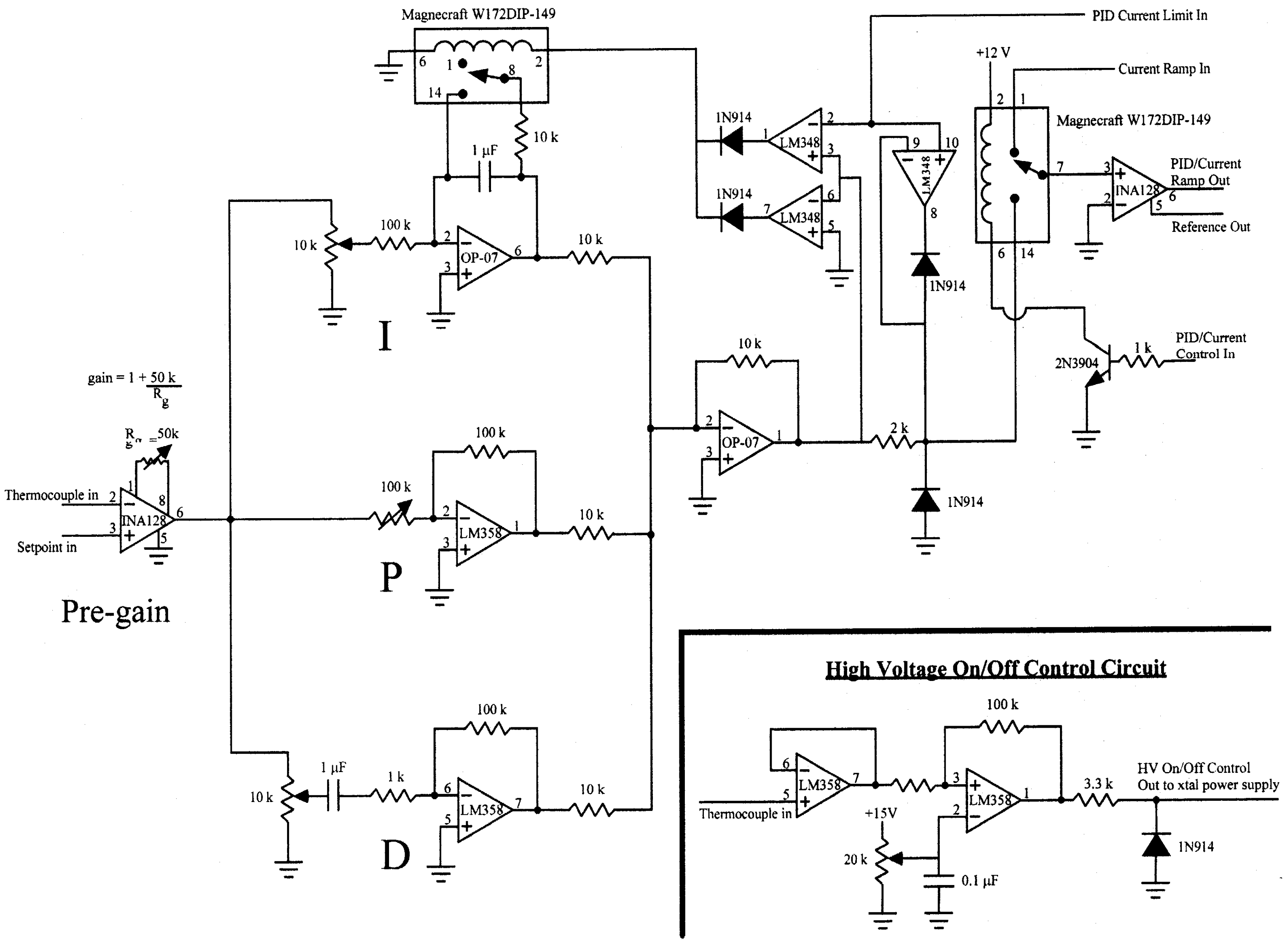

Figure IV-13: Pullman's Crystal Heating Power Supply (Part 1)

HV/LV power supply for heating silicon crystals

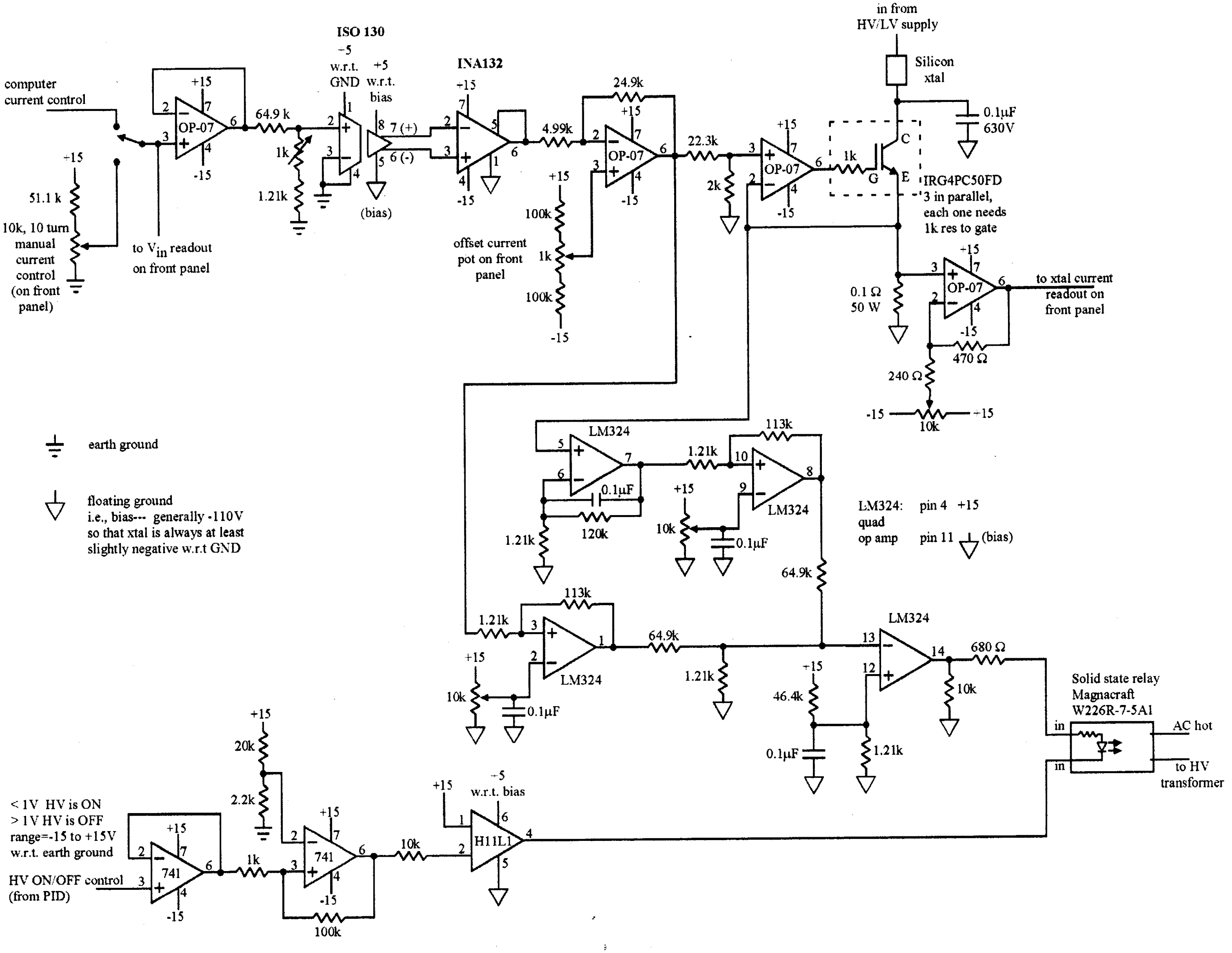

Figure IV-14: Pullman's Crystal Heating Power Supply (Part 2)

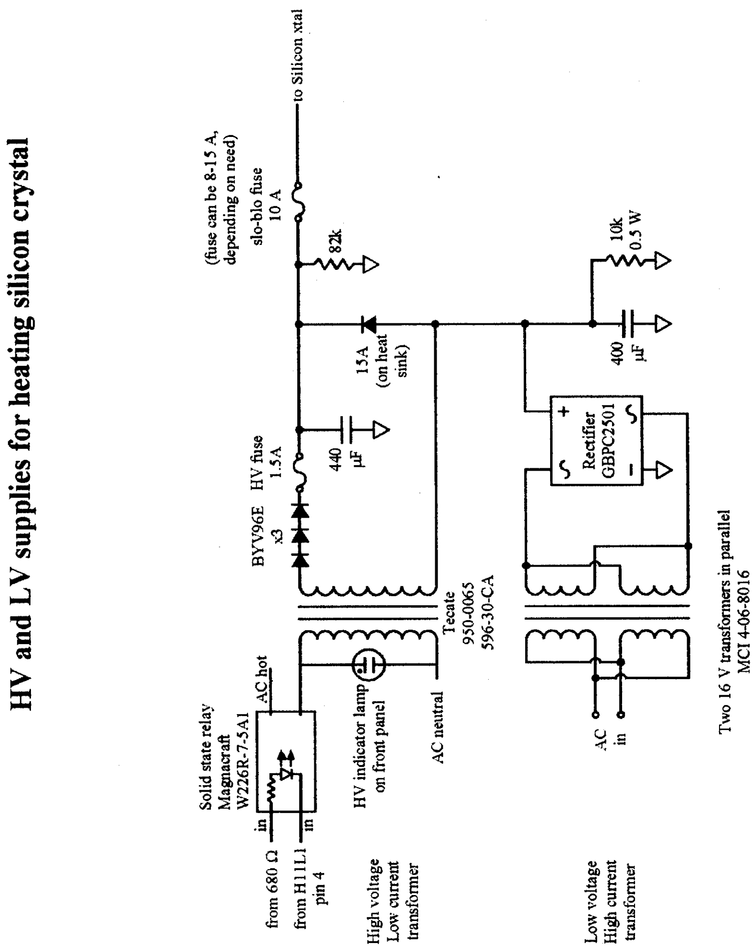

Figure IV-15: Pullman's Crystal Heating Power Supply (Part 3)

The circuit diagrams in this and the previous two figures were provided by David Pullman at San Diego State University. Parts 2 and 3 show circuits contained in the main power supply box while Part 1 shows circuits contained in the PID control box. The PID control box is currently only used for the high voltage on/off control circuit; we bypass Pullman's PID circuit and use the old PID that was designed for our crystal set-up.

IV.8 References to Machine Design and Operation in Theses

The main documentation for the design and operation of the Scattering Machine consists of the theses of former grad students. Additional information can be found in old lab notebooks, but they are generally not indexed and older notebooks may be of questionable utility in understanding the current state of the Machine. The following is a list of the Machine-related topics covered in past theses. Some of this material is obsolete, as it refers to components that have since been removed, replaced, or redesigned. Further more, with the exception of Mike Blair's thesis, all of the theses discussed predate the rebuilding of the Big Machine by Jae-Gook Lee and Mike Blair.

IV.8.a David Joseph Gladstone (June 1989)[1]

- main chamber and source pumping (pages 61-76)
    - pump configuration and roughing pumps for the main chamber (pages 61-62)
    - power supply for the main chamber bake out lamps (pages 62-65)
    - the original set-up of the lid turbopumps, which has changed significantly (pages 65-71)
    - the pump configuration for the source (pages 71-76)
- manifold, nozzles, and beam path (pages 76-84)
    - original design for the manifold (pages 76-80)
    - design for beam flag controller: this may have changed, since we now have two beam flags (pages 80-83)
    - nozzle heating power supply (pages 83-84)
- design of Auger bellows and linear-motion feed through: the bellows at least has been replaced, but the design may not have changed (pages 84-86)
- manipulator (pages 95-131)
    - design and construction of the manipulator translation stage (pages 95-99)
    - design and construction of the manipulator (pages 101-109)
    - discussion of sample alignment (pages 110-114)
    - discussion of crystal mounting (pages 114-120)
    - discussion of original crystal heating system (pages 120-126)
    - discussion of crystal cooling design (page 127)
    - procedure for manipulator removal, installation, and repair (pages 127-131)

IV.8.b Marianne McGonigal (September 1989)[2]

- molecular beam source (pages 31-88)
  - source A beam characteristics, skimmer / nozzle design, and source pumping load calculations (pages 31-40)
  - ionizer differential pumping design and pumping load / detection limit calculations (pages 40-51)
  - discussion of alignment of source A beam and detector (pages 51-59)
  - design and construction of source A & B and first A & B, with description of cart (pages 59-78)
  - design and construction of second stage and beam valve (pages 78-88)
- main chamber (pages 84-140)
  - design and construction of main chamber and lid seals (pages 84-107)
  - design and construction of detector box (pages 107-113)
  - design and construction of chopper and chopper chamber (pages 113-120)
  - design and construction of detector pumping stages (pages 120-126)
  - detector mass spectrometer and cryostat (pages 126-140)
- operating procedures (pages 143-176)
  - discussion of practices needed to reach UHV and pumping down the main chamber, as well as main chamber interlock box (pages 143-149)
  - time-of-flight system: operations and electronics (pages 149-155)
  - time-of-flight system: data processing (pages 155-171)
  - use of tuning-fork chopper--I'm not sure this is even still installed (pages 171-176)

IV.8.c Michelle Tobi Schulberg (June 1990)[3]

- design and construction of nozzles and skimmers; the nozzle heating and cooling set-up has since changed (pages 41-57)
- time-of-flight system: theory (pages 58-64)
- time-of-flight system: design and construction (pages 64-71)
- time-of-flight system: algorithm and calibration (pages 71-80)
- DAC settings and programs (pages 84-119)

IV.8.d Julius Jong Yang (September 1993)[4]

- old procedures for making gas mixtures (pages 27-31)
- procedure for aligning nozzles (pages 31-33)
- statement that main chamber volume is 886±10 L (pages 33-34)
- procedures for venting and pumping down the main chamber (pages 33-37)
- modification of manipulator to remove one rotational degree of freedom (pages 37-38)
- time-of-flight system: calibration (pages 39-50)
- beam flux calibration (pages 51-59)
- helium diffraction measurements (pages 60-71)
- scattering experiment calibration (pages 72-77)
- thermal desorption measurements and calibration (pages 77-88)

IV.8.e David Gosalvez-Blanco (September 1997)[5]

- description of silicon crystal thermocouple mounting (pages 27-29)
- replacement of the detector first stage ion pump with a turbomolecular pump (pages 29-30)
- change to detector box beam valve, introducing a smaller pinhole opening for straight-through beam experiments (pages 30-32)
- discussion of He diffraction, with diagrams (pages 53-60)
- description and use of an old configuration of the manifold mixing cylinders (pages 157-162)

IV.8.f Matthew Richard Tate (June 1999)[6]

- redesign and rebuild of the ionizer cryostat and detector box (pages 318-344)
  - procedure for repairing a leak (pages 321-324)
  - changes to the ionizer mounting plate (pages 324-328)
  - procedure for aligning the cryostat detector (pages 329-333)
  - the ionizer cryostat heater and use of house vacuum to improve cryostat cooling (pages 333-338)
  - detector box cryopump (pages 338-339)
  - use of a capacitor to increase the high mass limit of the detector box quadrupole from m/e=200 to m/e = 400 (pages 340-343)
- design of the current lid turbomolecular pump interlock box (pages 346-360)
  - description of the electronic logic, with circuit diagrams (pages 347-358)
  - discussion of normal operation (page 359)
- nozzle B translation and alignment (pages 362-364)

IV.8.g Judson Robert Holt (May 2002)[7]

- procedures for handling XeF_2 (pages 68-70)
- redesign of the gas handling manifold (pages 71-72)
- helium diffraction beam (78-80)
- description of pulse-counting electronics (pages 236-239, 243-244)
- updating of computer interface to Gateway2000 with Windows 98, PDP-11 data acquisition cards retained (pages 239-242, 245-246)

IV.8.h Robert Charles Hefty (November 2003)[8]

- redesign of source A nozzle heating and installation of helium cryostat (pages 247-252)
- design and installation of nickel nozzle (pages 253-258)
- helium diffraction (pages 278-279)
- time-of-flight error propagation calculations (pages 309-319)
- methods for calculating absolute beam flux (page 321-334)
- redesign of the skimmer mount ring (pages 336-337)
- redesign of the Si crystal and crystal mount to use precut crystals from the MIT Microsystems Technology Lab (pages 338-350)

IV.8.i Michael Ryan Blair (February 2014)[9]

- changes to mass spectrometer pulse counting electronics (pages 19-20)
- discussion of a new, but now replaced, crystal heating power supply (pages 20-24)
- time-of-flight spectroscopy and wheel manufacturing (pages 25-27)
- time of flight spectroscopy neutral flight length calculations (pages 28-42)
- replacement of metal nozzle holder with polyether ether ketone (pages 43-44, 47-49)
- cleaning nozzle and helium cold head (45-46)
- replacement of lid flange for ionizer cryostat (pages 50-57)
- measurement of straight-through angle as 207.05° (page 57)
- new detector box beam valve with large and small beam holes (pages 58-60)
- new electrical power wiring(pages 158-167)
- new cooling water filter manifold (pages 168-170)

Chapter IV References

(1) D. J. Gladstone, Ph.D. Thesis, Massachusetts Institute of Technology, (1989).

(2) M. McGonigal, Ph.D. Thesis, Massachusetts Institute of Technology, (1989).

(3) M. T. Schulberg, Ph.D. Thesis, Massachusetts Institute of Technology, (1990).

(4) J. J. Yang, Ph.D. Thesis, Massachusetts Institute of Technology, (1993).

(5) D. Gosalvez-Blanco, Ph.D. Thesis, Massachusetts Institute of Technology, (1997).

(6) M. R. Tate, Ph.D. Thesis, Massachusetts Institute of Technology, (1999).

(7) J. R. Holt, Ph.D. Thesis, Massachusetts Institute of Technology, (2002).

(8) R. C. Hefty, Ph.D. Thesis, Massachusetts Institute of Technology, (2003).

(9) M. R. Blair, M.S. Thesis, Massachusetts Institute of Technology, (2014).

(10) V. S. Smentkowski and J. T. Yates, *J. Vac. Sci. Tech. A* **14**, 262, (1996).

(11) It is *not* safe to vent the main chamber with a dewar of liquid nitrogen without a coil to warm the nitrogen first; doing so creates a risk of overpressure. The main chamber's volume is about 886 L, so it holds n = PV/RT = 36 mol of gas at 298 K and 1 atm. Liquid N_2 has a mass of 28 g/mol and a density of 0.81 g/mL, so this corresponds to about 1.2 L.

(12) RBD Instruments, *RBD Tech Spot*, "10-155 Filament Replacement Procedure", 2013, Accessed at http://www.rbdinstruments.com/blog/10-155-filament-replacement-procedure/ on 14 May (2014).

(13) A. Ishizaka and Y. Shiraki, *J. Electrochem. Soc.* **133**, 666-671, (1986).

Appendix A: Simulation Code

```
# *******************************
# IMPORT LIBRARIES AND FUNCTIONS
#
# First, we should import libraries and functions that we're going to need.  We
# need odeint to evaluate the motion of the silicon.
#
#

import scipy
import numpy
from scipy.integrate import odeint
from scipy import *
from numpy import *

#
#
# *******************************


# ***************************
# INPUT INITIAL CONDITIONS
#
# This program is written to use all variables in SI units to avoid stupid
# unit issues.  However, for convenience, the user is sometimes prompted for
# inputs in other units and they are immediately converted
#
# The coordinate system is one-dimensional, with its zero at the equilibrium
# position of the silicon atom.  The direction of the silicon surface is
# positive:
#
# -x <---      F_2     Si/\/\/\surface      ---> +x
#
# Also, majuscule variables correspond to the silicon atom; minuscule variables
# correspond to the fluorine molecule.
#
#

# The following inputs are fundamental physical and mathematical constants,
# and should not need to be varied unless the universe is changed.

k_B = 1.380649e-23 # the value of Boltzman's constant in J/K
amu = 1.660538e-27 # the value of an amu in kg
N_A = 6.022141e23 # the value of Avogadro's number
# kcal = 2.5197e21  # conversion factor from J/molecule to kcal/mol
kcal = 1.439e20

# The following inputs are modeling choices, but are not anticipated to need
# to be varied.

x_escape = -10.0 # Location of fluorine at which is is assumed to have escaped
                 # the surface with no risk of further collisions.  It is set to
                 # ten times the amplitude of the silicon at thermal equilibrium.
```

```
# The following inputs should be entered each time the program runs, since they
# are likely to be varied between simulations.

M = (float(raw_input('Silicon effective mass in amu: '))*amu) # converted to kg
m = (float(raw_input('Fluorine effective mass in amu: '))*amu) # converted to kg
K = float(raw_input('Silicon spring constant in N/m: '))

Omega = (K/M)**(0.5) # natural frequency of silicon oscillations

T = float(raw_input("Silicon surface temperature in K: "))

E = k_B*T # thermal energy of silicon at surface temperature

X_max = (2.0*E/K)**(.5) # amplitude of silicon at thermal equilibrium

print "The equilibrium amplitude of the silicon in m is: %e" %(X_max)
print "The position of the initial collision should be specified as a fraction"
print "of the silicon amplitude, where the +x direction is towards the surface."
X_i = x_i = ( float(raw_input("Position of initial collision: "))*X_max ) # converted to m

x_escape = x_escape*X_max # converted to m, using now-known silicon amplitude
                          # should still be negative

print "Input '1' or '-1' to indicate the sign of the initial velocity of the"
print "silicon, with the +x direction towards the surface."
V_i_sign = float(raw_input("Sign: ")) # sign of initial velocity;
                                      # needed to avoid ambiguity

V_i = V_i_sign * (((2.0/M)*abs(E-(K*.5)*X_i*X_i))**(.5))
       # initial velocity of silicon, from temperature and initial position

print "The initial velocity of the silicon atom in m/s is: " + str(V_i)

v_i = float(raw_input("Fluorine initial velocity in m/s: "))

dt = float(raw_input("Collision-checking time step in s: "))
      # This is the time step between collision-checking.  The time step of the
      # integrator will be one-tenth of this.

print "Select a viscous damping constant to approximate the rate at which"
print "silicon energy above than thermal energy is dissipated into the lattice."
print "(1 --> critically damped; >1 --> overdamped; <1 --> underdamped)"
C = float(raw_input("Dissipation constant; 1 = crit damped: "))

C = C/E
     # Scale C to make up for the fact that the ODE multiplies it by the difference between
     # thermal and actual energy, which in MKS units will be very small.
     #
     # multiply by 2*Omega to get multiplier in the ODE

outputfile = raw_input("Name of output file.  ([name].txt and [name].csv will be
                  overwritten.): ")
```

```
# At this point the system is in the position of the first collision, without processing that
# collision.  Now we can move fluorine back by 1000# time steps.

x_i = x_i - 1000*dt*v_i  # Moves the fluorine starting position back by 1000 times the
                         # distance the fluorine moves in one timestep at its initial
                         # velocity.


#
#
# ************************




# ******************************
# FUNCTION: COLLISION DETECTION
#
# This function takes the positions of the fluorine and the silicon
# at two points in time, and determines if they have switched order--in other
# words, if a collision should have occurred.  If a collision has occurred, it
# returns 1, otherwise it returns 0.
#
# The inputs are: x0,x1,X0,X1
#
# x0 = initial fluorine position
# x1 = final fluorine position
# X0 = initial silicon position
# X1 = final silicon position
#
#

def collision(x0,x1,X0,X1):

    a0 = x0 - X0 # a0 is signed silicon-fluorine vector at the last collision.
    a1 = x1 - X1 # a1 is signed silicon-fluorine vector at present.

    # a0 represents the situation at the last collision; even if it is 0,
    # we don't want to count that collision twice, so don't check.
    #
    # If a1 is 0, however, the atoms are at the same point again, and so there
    # is another collision.

    if a1 == 0 :
        return 1
    # If a1 is not 0, we check if the two vectors have the same
    # sign.  If they do, there has been no collision.  But, if they don't, there
    # has been a collision.
    elif ( abs(a0) + abs(a1) ) == abs( a0 + a1 ) :
        return 0
    else :
        return 1

#
#
# ****************************
```

```
# ******************************
# FUNCTION: COLLISION EVALUATION
#
# This set of functions outputs the velocities of the fluorine and silicon
# after a collision.  There are three functions: one to output the fluorine
# velocity, one to output the silicon velocity, and one to output the energy
# transfer during the collision.  Position is assumed not to change during
# a collision, since collisions are treated as instantaneous events.
#
# collision_V returns V1, the silicon velocity after the collision.
# collision_v returns v1, fluorine velocity after the collision.
# collision_trans returns trans, the energy transferred to the silicon by the
#     fluorine.
#
# The first two use the same inputs: v0,V0,m,M.
#
# v0 = initial fluorine velocity
# V0 = initial silicon velocity
# m = mass of fluorine
# M = mass of silicon
#
# These formulae are based on calculations by Jae-Gook Lee.
#
# The third uses v0,v1,m as inputs.
#
# v0 = initial fluorine velocity
# v1 = final fluorine velocity
# m = mass of fluorine
#

def collision_V(v0,V0,m,M):

    Mm = M/m
    V1_top = ( 2*v0 )+( (Mm-1)*V0 )
    V1_bottom = ( 1 + Mm )
    V1 = V1_top/V1_bottom
    return V1


def collision_v(v0,V0,m,M):

    Mm = M/m
    v1_top = ( (1-Mm)*v0 )+( 2*Mm*V0 )
    v1_bottom = ( 1 + Mm )
    v1 = v1_top/v1_bottom
    return v1


def collision_trans(v0,v1,m):

    trans = (.5)*m*v0*v0 - (.5)*m*v1*v1
    return trans

#
#
# ******************************
```

```
# ******************************************
# FUNCTION: TIMESTEP EVALUATION FOR FLUORINE
#
# This set of two functions evaluates the change in state of the fluorine
# after one timestamp occurs.  It does not check for collisions.
#
# There are two functions:
#
# step_x returns x1, the new fluorine position after a time step.
# step_v returns v1, the new fluorine velocity after a time step.
#
# step_x and step_v take three inputs: x0,v0,dt
#
# x0 = initial position of fluorine
# v0 = initial velocity of fluorine
# dt = length of a time step
#
# Since the fluorine doesn't experience any forces other than during
# collisions, the functions are trivial.
#
#

def step_x(x0,v0,dt):

    x1 = x0 + (v0*dt)
    return x1


def step_v(x0,v0,dt):

    v1 = v0
    return v1

#
#
# ******************************************

# *****************************************
# FUNCTION: TIMESTEP EVALUATION FOR SILICON
#
# Evaluating the motion of the silicon is rather more annoying, since it has
# to account for the fact that it is a mass-on-a-spring harmonic oscillator
# and, furthermore, is constantly dissipating energy to the lattice.  This
# dissipation is modeled as a viscous damping term proportional to the
# difference between the energy of the mass-on-spring system and the energy
# it would have were it in thermal equilibrium with the surface.
#
# 0 = X'' + X(w^2) + 2CwX'( (M/2)X'^2 + (K/2)X^2 - E )
#
# To make the math tractable, this can be converted to a system of two first-
# order ODEs.  Redefine our variables as:
#
# y[0] = X
# y[1] = X'
#
# and define F(y) = { y[0]' , y[1]' }
#
```

```
def F(y,t_range,M,K,Omega,C,E):

    return [ y[1] , -1*(Omega**2)*y[0] - C*Omega*( M*(y[1]**3) +

            K*y[1]*(y[0]**2) - 2*E*y[1] ) ]

#
# Next, we need the Jacobian of F, defied as:
#
# { { dF[0]/dy[0] , dF[0]/dy[1] } ,
#   { dF[1]/dy[0] , dF[1]/dy[1] } }
#

def jacobian(y,t_range,M,K,Omega,C,E):

    return [ [ 0 , 1 ] ,
             [ -2*C*Omega*K*y[0]*y[1] - (Omega**2),
               -1*C*Omega*( 3*M*(y[1]**2) + K*(y[0]**2) - 2*E ) ] ]

#
# We can feed these, along with initial conditions, into the
# scipy.integrate.odeint routine to timestep X and V.  The output, XV_array,
# is an array of the form:
#
# [ [ X@t0 , V@t0 ] ,
#   [ X@t1 , V@t1 ] ,
#   ...
#   [ X@tfinal , V@tfinal ] ]
#
# The simulation loop will need to extract X@tfinal and V@tfinal as X1 and V1.
#
# The step_XV function that calls odeint also sets up a timebase for the
# integration.  It assumes that we want the timebase steps to be one-tenth the
# size of the steps used in collision-checking.
#

def step_XV(X0,V0,dt,t,M,K,Omega,C,E):

    t_range = linspace(0,t,10*t/dt)        # Note that 10 is a magic number!
    XV_array = odeint(F,[X0,V0],t_range,Dfun=jacobian,args=(M,K,Omega,C,E))
    return XV_array

#
#
# ****************************************
```

```
# ***************
# SIMULATION LOOP
#
# With the various functions out of the way, this is the actual body of the
# program.  It consists of several nested loops to evaluate the behavior of
# the silicon and fluorine until the fluorine gets far enough away from the
# surface that collisions are no longer possible.
#
#

# While we've already moved the fluorine initial position back by 1000 time
# steps, we need to do so for silicon as well.  To do this, we use the
# step_XV function.  As an added complication, this function won't work if
# given a negative amount of time to evolve the silicon by.  Instead, we'll
# reverse the sign of the velocity we give it, which will be effectively
# the same as running time backwards.  We'll have to turn the velocity back
# before starting the actual simulation, though.

V_i_neg = V_i * -1
t_neg = 1000*dt
XV1 = step_XV(X_i,V_i_neg,dt,t_neg,M,K,Omega,C,E)

X_i = XV1[-1,0]
V_i = -1*XV1[-1,1]

# Now it's time to actually run the simulation loop.
# We begin by defining the needed variables:
#
#   E_counter, which will sum the energy transferred to  silicon from fluorine
#   in each collision.
#
#   t_counter, which will keep track of the time of the last collision.
#
#   t, which will keep track of the time since the last collision.
#
#   coll, a flag indicating whether a collision has been detected.  It starts
#   as "0", since we start the simulation 1000 time steps before the first
#   collision.
#
#   coll_counter, which will keep track of the total number of collisions that
#   occur.

E_counter = 0.0
t_counter = 0.0
t = 0.0
coll = 0
coll_counter = 0 # Start at zero since processing the current collision will
                 # increment it up one.
```

```
# Now, set up the output file, which will be sent the state of the system
# after each timestep, after collisions are detected but before they are
# processed.  (So, if a collision occurs, the collision flag will be set
# at that time step, but the pre-collision velocities and energies will be
# reported.)

output_csv = open(str(outputfile) + '.csv','w')

output_txt = open(str(outputfile) + '.txt','w')

# Begin by creating a header.

output_csv.write("Silicon mass in amu: " + str(M/amu) + "\n")
output_txt.write("Silicon mass in amu: " + str(M/amu) + "\n")

output_csv.write("Fluorine mass in amu: " + str(m/amu) + "\n")
output_txt.write("Fluorine mass in amu: " + str(m/amu) + "\n")

output_csv.write("Spring contant in N/m: " + str(K) + "\n")
output_txt.write("Spring contant in N/m: " + str(K) + "\n")

output_csv.write("Surface temperature in K: " + str(T) + "\n")
output_txt.write("Surface temperature in K: " + str(T) + "\n")

output_csv.write("Silicon thermal energy in kcal/mol: " + str(E*kcal) + "\n")
output_txt.write("Silicon thermal energy in kcal/mol: " + str(E*kcal) + "\n")

output_csv.write("Silicon amplitude at thermal equilibrium: " + str(X_max) + "\n")
output_txt.write("Silicon amplitude at thermal equilibrium: " + str(X_max) + "\n")

output_csv.write("\n")
output_txt.write("\n")

# Now put in initial conditions for the data table..

data = ["t (s)","x_f (m)","v_f (m/s)","e_f (kcal/mol)","X (m)","V (m/s)","E (kcal/mol)","c"]
output_csv.write('\t'.join(map(str,data)) + '\n')
output_txt.write('\t'.join(map(str,data)) + '\n')

output_txt.write("\n")

data = [t_counter+t,x_i,v_i,kcal*((.5)*m*v_i*v_i),
        X_i,V_i,kcal*(.5*M*V_i*V_i+.5*K*X_i*X_i),coll]

output_csv.write('\t'.join(map(str,data)) + '\n')
output_txt.write('\t'.join(map(str,data)) + '\n')
output_txt.write("\n")

x1 = x_i
v1 = v_i
X1 = X_i
V1 = V_i

x0 = x_i
v0 = v_i
X0 = X_i
V0 = V_i
```

```
# Now we can start the loop.

while True: # This while loop will continue running until the fluorine
            # escapes, at which point a break statement will kill it.
            #
            # While the system state is recorded after each timestep of
            # dt, integrations are carried out from the starting point
            # of the last collision, so x0, X0, v0, and V0 are not reset
            # except at a collision.

    # Begin by going forward one time step.

    t = t + dt

    # While we always step from the previous collision, we want to check for
    # collisions between runs of the loop (time differences of dt, not t),
    # so we create a set of _prev variables to hold the outcome of the last
    # cycle to be compared against.

    x_prev = x1
    X_prev = X1
    v_prev = v1
    V_prev = V1

    # Now we can increment the positions and velocities for the new value of t.

    x1 = step_x(x0,v0,t)
    v1 = step_v(x0,v0,t)

    # Stepping X and V is slightly more complicated.

    XV1 = step_XV(X0,V0,dt,t,M,K,Omega,C,E)

    # XV1 is a 2D array with each row containing values for X and Y at
    # values of time = {0, 0.1dt, 0.2dt, ... , t}.  We need the values from
    # the last row.  Conveniently, Python will allow us to index from the back
    # of the array, with the last row indexed as -1.

    X1 = XV1[-1,0]
    V1 = XV1[-1,1]

    # Now check to see if a collision has occured between t - dt and t by
    # comparing x_prev - X_prev to x1 - X1.  If there is a sign change, or
    # if x1 - X1 = 0, there is a collision.

    coll = collision(x_prev,x1,X_prev,X1)

    # Read the current system state to the output file.

    data = [t_counter + t, x1, v1, kcal*((.5)*m*v1*v1),
            X1, V1, kcal*((.5)*M*V1*V1 + (.5)*K*X1*X1), coll]

    output_csv.write('\t'.join(map(str,data)) + '\n')
```

```
# If there was no collision, X0, V0, x0, and v0 will remain unchanged and
# the loop will run again for t = t + dt.
#
# If there was a collision, things are more complicated.  A collision means
# that the particles have passed each other, which can't actually happen.
# So we reset the system to the t - dt state, the last time step before the
# collision, and evaluate the velocity and energy changes from the
# collision.  Then the collision flag is reset, the collision counter is
# incremented, at the system continues to evolve.
#
# In this case, we want the _prev variables to be the same as the 0
# variables: the state directly after the collision.

if coll == 1 :
    data = [t_counter + t - dt, x_prev, v_prev, kcal*((.5)*m*v_prev*v_prev),
            X_prev, V_prev,
            kcal*((.5)*M*V_prev*V_prev + (.5)*K*X_prev*X_prev), 0]
    output_txt.write('\t'.join(map(str,data)) + '\n')
    data = [t_counter + t, x1, v1, kcal*((.5)*m*v1*v1),
            X1, V1, kcal*((.5)*M*V1*V1 + (.5)*K*X1*X1), coll]
    output_txt.write('\t'.join(map(str,data)) + '\n')
    v0 = v1 = collision_v(v_prev,V_prev,m,M)
    V0 = V1 = collision_V(v_prev,V_prev,m,M)
    E_counter = E_counter + collision_trans(v_prev,v0,m)
    x0 = x1 = x_prev
    X0 = X1 = X_prev
    t_counter = t_counter + t
    t = dt
    coll = 0
    coll_counter = coll_counter + 1
    x1 = step_x(x0,v0,t)
    v1 = step_v(x0,v0,t)
    XV1 = step_XV(X0,V0,dt,t,M,K,Omega,C,E)
    X1 = XV1[-1,0]
    V1 = XV1[-1,1]
    data = [t_counter + t, x1, v1, kcal*((.5)*m*v1*v1),
            X1, V1, kcal*((.5)*M*V1*V1 + (.5)*K*X1*X1), coll]
    output_txt.write('\t'.join(map(str,data)) + '\n')
    output_csv.write('\t'.join(map(str,data)) + '\n')
    output_txt.write(str(kcal*collision_trans(v_prev,v0,m)) + ' kcal/mol transferred to
             surface.\n')
    output_txt.write('\n')
```

```
    # Now check to see if the fluorine is far enough from the surface that
    # further collisions are impossible.  If so, break the loop.  Otherwise,
    # cycle through again.  We need to require that v1 be negative as well,
    # which we didn't require in fluorine_8.py, because otherwise the initial
    # position will trigger this before any collisions have occured.

    if (x1 < x_escape) and (v1 < 0) :
        print "Fluorine escaped surface."
        output_txt.write('Fluorine escaped surface at t = ' + str(t_counter + t) + '\n')
        break

    if x1 > (-1*x_escape) :
        print "Fluorine fell through surface."
        break

output_csv.close()

print "Net energy transfered to surface, in kcal/mol: " + str(kcal*E_counter)
output_txt.write("Total energy transfered to surface, in kcal/mol: " + str(kcal*E_counter) +
                 "\n")

lattice = (0.5)*m*v_i*v_i + 0.5*M*V_i*V_i + (0.5)*K*X_i*X_i - (0.5)*m*v1*v1 - (0.5)*M*V1*V1 -
                 (0.5)*K*X1*X1
print "Total energy lost to lattice bath, in kcal/mol: " + str(kcal*lattice)
output_txt.write("Total energy lost to lattice bath, in kcal/mol: " + str(kcal*lattice) +
                 '\n')


print "Total number of collisions to occur: " + str(coll_counter)
output_txt.write("Total number of collisions to occur: " + str(coll_counter) + "\n")

output_txt.close()


#
#
# ***************
```

Appendix B: Curriculum Vitae

Daniel Walter Rowlands

EDUCATION

Massachusetts Institute of Technology (MIT) **Cambridge, MA**
- S.M. in Physical Chemistry September 2015
- Research Advisor: Professor Sylvia Ceyer GPA: 4.5/5.0
- Research Topic: etching and oxidation of Si crystals by molecular beams in ultra-high vacuum

California Institute of Technology (Caltech) **Pasadena, CA**
- B.S. with Honors in Chemistry with Minor in History June 2009
- Research Advisor: Professor Daniel Weitekamp GPA: 3.7/4.0
- Research Topic: NMR hyperpolarization

RESEARCH EXPERIENCE

Ceyer Lab, MIT Chemistry Department **Cambridge, MA**
Graduate Research Assistant *Jan 2010—Sep 2015*
- Repaired and operated an ultra-high vacuum molecular beam set-up, including rebuilding vacuum pumps, leak-checking the system, and aligning the molecular beams and instruments.
- Repaired and maintained electronics including heating power supplies, the RF source for a quadrupole mass spectromer.
- Rebuilt an Auger electron spectrometer and repaired its control electronics.
- Designed and programmed a classical dynamics simulation in Python to model the collision of gas molecules with a silicon surface.

Weitekamp Lab, Caltech Chemistry Department **Pasadena, CA**
Undergraduate Researcher *Jun 2007—Jun 2009*
- Designed an experiment to transfer NMR hyperpolarization from xenon to biomolecules.
- Constructed an experimental apparatus necessary to perform hyperpolarization transfer.
- Shimmed high-field NMR magnets.

Barton Lab, Caltech Chemistry Department **Pasadena, CA**
Undergraduate Researcher *Apr 2006—Aug 2006*
- Performed organic synthesis and thin film and high pressure liquid chromatography.
- Performed fluorescence experiments to evaluate several organometallic complexes as probes of DNA charge transport.

NASA Goddard Space Flight Center **Greenbelt, MD**
High School Researcher *Sep 2004—Jun 2005*
- Took spectra of the sky glow over several cities and spectra of various light pollution sources to identify the light sources responsible for the light pollution sky glow in different cities.
- Developed a set of scripts in Interactive Data Language (IDL) to analyze astronomical spectra and identify their components.

TEACHING EXPERIENCE

Cambridge School Volunteers, Inc. **Cambridge, MA**
Scientist Mentor for Cambridge Ringe and Latin School Science Olympiad Team *Nov 2014—Feb 2015*

- Tutored students in preparation for chemistry and timekeeping events at the state Science Olympiad.

MIT Educational Studies Program **Cambridge, MA**
Volunteer Teacher for Splash and Spark Programs *Feb 2010—Nov 2014*

- Designed and taught one-day courses for high and middle school students.
- Course topics included thermodynamics and statistical mechanics, evolutionary biology and paleontology, and American and Boston history.

MIT Chemistry Department **Cambridge, MA**
Graduate Teaching Assistant *Aug 2009—Dec 2012*

- TAed freshman chemistry (5.112) twice and undergraduate thermodynamics (5.60) once.
- Ran recitation sections, held office hours, helped write problem sets, and graded problem sets and exams.

LEADERSHIP EXPERIENCE

MIT Graduate Student Council (GSC) **Cambridge, MA**
General Council Representative and Member of the Funding Board *Oct 2013—Jan 2015*

- Represented the Chemistry Department and served on the GSC Housing and Community Affairs committee and the GSC Transportation subcommittee.
- Represented the GSC on the MIT Campus Activities Complex Advisory Board.
- Served as the General Council's representative on the six-member GSC Funding Board, which allocates $160,000 to graduate student groups each year.
- Consulted with the GSC Treasurer on the design of a new online funding application.

MIT Science Fiction Society **Cambridge, MA**
President, Vice President, and Secretary *Jan 2010—Jan 2015*

- Co-ordinated a major rearrangement of a 60,000-book library to increase shelf space with fixed floor space and improve the organization and navigability of the collection.
- Arranged author visits and talks and organized the annual post-elections retreat.

MIT Association of Student Activities (ASA) **Cambridge, MA**
Treasurer and Student Member at Large *Oct 2011—Oct 2013*

- Chaired the Large Events Fund and Cultural and Diversity Events Funding Board, and prepared allocations totaling $175,000 to student-run events over the course of one year.
- Served on all student group funding boards and represented the ASA to MIT administration.
- Served as the ASA's representative on the MIT Campus Activities Complex Advisory Board.
- Organized the reallocation of office space to student groups.
- Chaired the ASA committee in charge of recognizing new student groups.

SKILLS

- Proficient with Microsoft Word, Excel, and Powerpoint, and with GIMP (image editing).
- Proficient with IgorPro (data analysis and plotting); VectorWorks (computer-aided design).
- Programming in Labview, Matlab, and Python.
- Repair of ultra-high vacuum systems, including leak-checking and internal repairs.
- Repair and rebuilding of mechanical and ionization vacuum pumps, and some knowledge of oil diffusion pumps.
- Mass spectroscopy and time-of-flight mass spectroscopy and helium diffraction.
- Auger electron spectroscopy.
- Work with F_2, HF, cryogens, and in confined spaces.

PUBLICATIONS

- D. W. Rowlands, "Analysis of Light Pollution Spectra", *Eleanor Roosevelt High School (Greenbelt, Maryland) Senior Thesis*, (2005).
- D. W. Rowlands, "Producing Safe Spin-Polarized Metabolites for Magnetic Resonance Imaging", *Caltech Undergraduate Chemistry Senior Thesis*, (2009).
- D. W. Rowlands, M. R. Blair, J.-G. Lee, R. Hefty, & S. T. Ceyer, "Making F_2 Heavy: Activated Etching of Si by van der Waals Molecules", *Poster at Gordon Research Conference on Dynamics at Surfaces*, (2013).

AWARDS AND HONORS

- MIT Chemistry Department Outstanding Teaching Award (2012-2013)
- MIT Energy Initiative Fellowship (2010-2011)
- Dow-Corning Foundation Fellowship (2010)
- MIT Presidential Fellowship (2009-2010)
- Arthur A. Noyes Summer Research Fellowship, Caltech (2008)
- James A. Michener NASA College Scholarship (2006-2009)
- Robert and Phyllis Henigson Scholarship, Caltech (2006-2008)
- Vera Cope Weinbach Scholarship, City of New Carrollton, Maryland (2005)
- National Merit Scholarship Finalist (2004)
- Maryland Distinguished Scholar Finalist (2004)
- Caltech Signature Award for demonstrating creativity or innovation in the fields of mathematics and/or the sciences (2004)